CHARGE TRANSPORT IN POLYPYRROLE-BASED CONDUCTING POLYMERS

XIAOMING REN

Charge Transport in Polypyrrole-Based Conducting Polymers

By

Xiaoming Ren

A thesis submitted to the
School of Graduate Studies
in partial fulfilment of the
requirements for the degree of
Doctor of Philosophy in Chemistry

Department of Chemistry
Memorial University of Newfoundland

July 1993

St. John's Newfoundland

ISBN 0-315-91575-7

This thesis is devoted to my beloved wife and daughter

Beelan and Suelynn

Abstract

Impedance spectroscopy has been used to study polypyrrole/perchlorate (PPY/ClO_4^-), PPY/poly(styrene sulphonate) (PPY/PSS), poly-(3-methyl-pyrrole-4-carboxylic acid) (poly-MPCA), poly-[1-methyl-3-(pyrrol-1-ylmethyl)pyridinium] (poly-MPMP), bilayers of PPY/ClO_4^- and PPY/PSS, and polypyrrole formed in mixed perchlorate and poly(styrene sulphonate) (PPY/ClO_4^-+PSS) polymer films coated Pt electrodes in electrolyte solutions. All impedance responses can be modelled with a porous electrode theory to extract reliable electronic and ionic conductivities, which agree with the results of other independent measurements.

The impedances of PPY/ClO_4^- and PPY/PSS reveal dominant anion and cation transport, respectively, in these polymers. A strong interaction between the anions and the positive charges on the oxidized polypyrrole chains hinders anion movement in PPY/ClO_4^-. Absence of such an interaction for the mobile cations in PPY/PSS gives this polymer a *ca.* 20 times higher ionic conductivity than PPY/ClO_4^-.

Deviation from the ideal model impedance response occurs for poly-MPCA because of its non-uniform structure. Mixed ion conduction can cause another type

of deviation as shown by the impedance of PPY/ClO_4^-+PSS polymers and the simulated data. High frequency data for reduced films of PPY/PSS and poly-MPCA form a semicircle in the complex impedance plane. This semicircle is attributed to electron transfer at the Pt/polymer interface for PPY/PSS but ion transfer at the polymer/solution interface for poly-MPCA.

The impedances of the PPY/ClO_4^- and PPY/PSS bilayer films show that the location of the initial reaction induced by a potential perturbation for a highly conducting PPY film coated electrode is at the polymer/solution interface. The impedances of poly-MPMP and PPY/PSS show that the location of the initial reaction depends on the relative magnitudes of the film's electronic and ionic conductivities, as theoretically predicted.

Ionic conductivity measurements were used to probe polymer structure. Films of PPY/ClO_4^-, PPY/PSS and poly-MPCA all have a two phase structure, a polymer phase and a pore solution phase. Ionic conduction in the polymer phase occurs mainly through the movement of mobile counterions via an ion-exchanging process, while in the pore solution phase migration of both electrolyte cations and anions contributes to conduction.

Acknowledgements

My most sincere gratitude goes to my supervisor Dr. P. G. Pickup for his help, advice and encouragement throughout my Ph.D study. I am greatly benefited and influenced by his devout research attitude, critical judgement and boundless knowledge.

I am also very grateful to Dr. F. R. Smith, Dr. M. D. Mackey and Dr. R. A. Poirier, who have taught me through course studies. I would like also to thank Dr. S. Mandal for his great help and our fruitful collaboration.

I appreciate very much the friendly help received everyday from the staff of the Chemistry Department. Those people that I would specially like to mention are Ms. Marion Baggs and Dr. B. Gregory for operating the mass spectrometer, Ms. Nathalie Brunet and Dr. C. R. Jablonski for running NMR samples and Ms. Carolyn Emerson for her assistance in operating the SEM.

Financial support received in the form of Graduate Fellowships from the School of Graduate Studies, Teaching Assistantships provided by the Chemistry Department and supplements from my supervisor's NSERC grant are gratefully acknowledged.

Table of Contents

List of Tables

List of Figures

List of Abbreviations and Symbols Used

Symbol	Meaning	Dimensions	Section
A	electrode area	cm^2	2.3
c	$= c_O + c_R$	M	4.2.1
c_{Ion}	concentration of counterions in film	M	4.3.2
c_O	average concentration of oxidized sites	M	4.2.1
c_R	average concentration of reduced sites	M	4.2.1
C_{cv}	film capacitance from CV	F cm^{-2}	3.2
C_{dl}	double layer capacitance	F cm^{-2}	5.4
C_F	film capacitance from IS	F	4.2
$C_{V,ac}$	volumetric capacitance from IS	F cm^{-3}	5.1
$C_{V,cv}$	volumetric capacitance from CV	F cm^{-3}	5.1
C_Σ	combined capacitance	F	4.2
d	film thickness	μm	3.2
D	diffusion coefficient	$cm^2\ s^{-1}$	4.3
$E^{o'}$	formal potential	V	3.2
EDXA	energy dispersive x-ray analysis		2.4
E_{FWHM}	full width at half maximum	V	3.2
$E_{ox,m}$	oxidation potential of monomer	V	3.1.1
$E_{p,a}$	anodic peak potential	V	3.2
$E_{p,c}$	cathodic peak potential	V	3.2
ESR	electron spin resonance		1.2
F	faraday constant	C mol^{-1}	4.2.1
I	current vector	A	4.1
$I_{p,a}$	anodic peak current	mA cm^{-2}	3.2
$I_{p,c}$	cathodic peak current	mA cm^{-2}	3.2
IS	impedance spectroscopy		1.4
ITO	indium tin oxide coated glass plate		3.1.1
j	$(-1)^{½}$		4.2.1
MPCA	3-methyl-pyrrole-4-carboxylic acid		3.1
MPMP	1-methyl-3-(pyrrol-1-ylmethyl)pyridinium		3.2

Symbol	Meaning	Dimensions	Section
n	electrons per molecule oxidized or reduced		3.2
PCA	pyrrole-3-carboxylic acid		3.1
PSS	poly(styrene sulphonate)		3.2
Q_{ac}	charge calculated from ac capacitance	C	6.4
Q_{cv}	charge under cyclic voltammogram	C	3.4
Q_{prp}	polymerization charge	C	3.4
R	gas constant	J $mol^{-1}K^{-1}$	4.2.1
R_{appr}	apparent ionic resistance of polymer film	Ω	10.3
R_{ct}	charge transfer resistance	Ω	5.4
R_E	electronic resistance of polymer film	Ω	4.1
$R_{I,inner}$	ionic resistance of inner layer	Ω	9.3
$R_{I,outer}$	ionic resistance of outer layer	Ω	9.3
R_{Ion}	ionic resistance of polymer film	Ω	4.1
R_{low}	intercept of low frequency data on real axis minus R_s	Ω	4.2.1
RMS	root mean square (of a wave signal)		2.3
R_∞	intercept of high frequency data on real axis minus R_s	Ω	4.2.1
R_Σ	sum of R_E and R_{Ion}	Ω	4.2.1
R_s	uncompensated bulk solution resistance	Ω	4.1.1
SEM	scanning electron microscope		2.4
SSCE	sodium-saturated calomel electrode		2.3
XPS	x-ray photo electron spectroscopy		1.2
Z	impedance vector	Ω	4.1
Z′	real part of impedance	Ω	4.1
Z″	imaginary part of impedance	Ω	4.1
β	angle between Warburg-type line and real axis in complex impedance plane	degree	5.2.2
θ	phase angle between I and V	rad	4.2.1
σ_{Ion}	ionic conductivity	S cm^{-1}	4.3
σ_E	electronic conductivity	S cm^{-1}	4.3
ν	scan rate	mV s^{-1}	3.2
χ	oxidation level		6.2.4
ω	angular frequency of rotation	rad s^{-1}	4.2.1

Structures of Some Chemicals Used

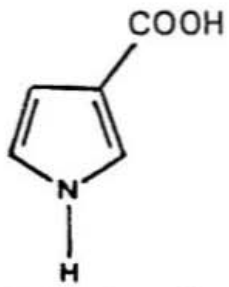

Pyrrole-3-carboxylic acid
(PCA)

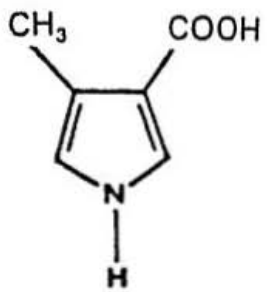

3-Methyl-pyrrole-4-carboxylic acid
(MPCA)

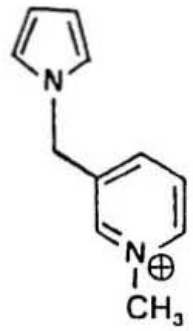

1-Methyl-3-(pyrrol-1-ylmethyl)pyridinium
(MPMP)

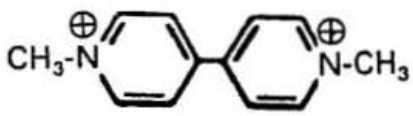

Methyl Viologen
(MV^{2+})

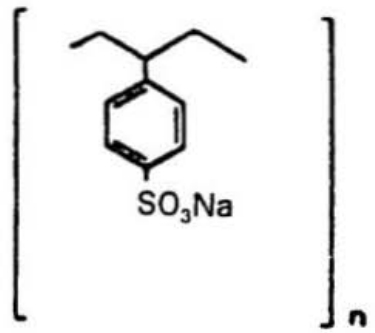

poly(styrene sulphonate)
(PSS)
M.W. ~ 70,000

Chapter 1

Polypyrroles

Most polymers, such as the common plastics. are well known electronic insulators with room temperature conductivity less than 10^{-10} S cm^{-1}. As engineering materials, plastics have other remarkable properties such as light weight, flexibility, high strength and good processibility. They have been used extensively as wire insulating materials and insulating parts in electronic equipment. As a matter of fact, we were so familiar with the insulating properties of these plastics that we did not expect to find conducting plastics. This view was changed when Walatka and coworkers[1] found in 1973 that polysulfurnitride $((SN)_x)$ has an electronic conductivity of 10^3 S cm^{-1} at room temperature. A study by Greene and coworkers[2] showed that this polymer becomes superconducting at about 0.3 K. Although the explosive nature of this material precluded virtually any practical usage, the discovery that some polymers can conduct electricity led researchers to look for other conducting polymers which may be processed using conventional plastics technology. Since then, a whole new class of polymers

including polyacetylenes[3,4], polyanilines[5,6], polypyrroles[7,8], polythiophenes[9] and poly(*p*-phenylenes)[10], has been discovered to have high electronic conductivity. Room temperature conductivity as high as 10^5 S cm^{-1} has been reported for polyacetylene[11], and $2x10^2$ S cm^{-1} for polypyrrole[12,13]. These polymers (so called conducting polymers) have attracted the attention of many researchers in a variety of fields. The extensive and intensive research effort has generated an astronomical amount of information from basic properties to new scientific concepts and technological applications. Many reviews of the field have appeared[14-30]. Today research on conducting polymers is one of the most dynamic areas in electrochemistry. As an introduction, the following discussion will be focused on polypyrrole based polymers which are the subject of this thesis.

1.1 Polymerization

1.1.1 Chemical and Electrochemical Polymerization

Polypyrrole can be formed by oxidizing pyrrole with an oxidizing agent[31-34] or at an electrode in a supporting electrolyte solution[7,8,35,36]. The former route is called chemical polymerization and the latter electrochemical polymerization. The

chemical polymerization of pyrrole was reported as early as 1916 by an Italian chemist Angeli[31], who discovered that oxidation of pyrrole forms a black conducting powder. The first electrochemical polymerization of pyrrole was reported in 1968 by Dall'Olio *et al*[35]. They found that when pyrrole was anodically oxidized in sulphuric acid a conducting polypyrrole film was formed on the electrode. However, it was not until Diaz and coworkers[7,8] showed that stable good quality polypyrrole films could be formed by electrochemical polymerization in acetonitrile containing 1 % water that full scale research activity on this and other conducting polymers was launched. Electrochemical polymerization is now regarded as a general method for forming the various conducting polymers, except polyacetylene.

Compared to chemical polymerization, the electrochemical route offers several advantages for electrochemical studies. Most chemical oxidations form polypyrrole powders. Although films can be prepared by oxidizing pyrrole at a solid or liquid interface[32,37,38], these films are of poor quality and sometimes even non-conductive[37]. In electrochemical polymerization, an adhering polymer film is formed on the electrode and is ready to be characterized with a variety of electrochemical techniques. For some of the applications, such as electrocatalysis[29,39] and electroanalysis[19,40,41], the formation of a thin film adhering

to the electrode is desirable.

Electrochemical methods give the researcher much better control over the polymerization process. The film thickness can be controlled by monitoring the charge density, and the electrode potential can be adjusted so that overoxidation[42-52] of the polymer film is kept to a minimum. To do this in chemical polymerization, the oxidizing agent has to be carefully chosen so that its formal potential matches the oxidation potential of the monomer. This sometimes requires the use of toxic compounds such as Br_2 and AsF_5[53]. Warren and coworkers[54] showed by x-ray diffraction that chemically polymerized polypyrroles have a higher degree of disorder than their electrochemically polymerized counterparts.

The electrochemical polymerization method also allows the formation of various polypyrrole/electrolyte anion composites by simply changing the electrolyte in the monomer solution. Since the formal potential of the polymer is lower than the oxidation potential of the monomer, the freshly formed polymer is in its oxidized state and electrolyte anions are incorporated to reach electroneutrality. Various electrolyte anions have been incorporated this way to allow researchers to systematically study the film's conductivity[12,54], morphology[12,55-57] and structure[55,56]. Applications such as controlled release of drugs which are incorporated in polypyrrole during polymerization have been anticipated[50,58-61].

1.1.2 Mechanism of Electrochemical Polymerization

The mechanism of electrochemical polymerization of pyrrole has been studied by many workers[46,62-67] but is still not fully understood. The first step certainly involves the oxidation of the monomer at the electrode to form a radical cation. However, there are two different views regarding the coupling of monomer units to form the dimer and propagation to form the polymer. Diaz *et al*[68,69] have found that the growth of polymer is terminated as soon as the electrode potential is lowered below the oxidation potential of the monomer. This, they suggested, indicates that the propagation occurs via addition of monomer radical cations to oxidized oligomer chains, since at the potential needed to oxidize the monomer, the dimer and higher oligomers would also be oxidized due to their greater π-orbital conjugation. They proposed a radical cation-radical cation coupling mechanism for the electrochemical polymerization. Inoue and Yamase[70] suggested that the strong coulombic repulsion between the monomer radical cations would prevent this direct dimerization step. They proposed a radical cation-monomer coupling mechanism. However, recent MO calculations[71] and experimental results[64,71] favour the radical cation-radical cation coupling mechanism. Formation of the trimer involves the oxidative coupling of the monomer with the dimer. Formation of the tetramer can involve either the coupling of the monomer with the

trimer or two dimers. As the size of the oligomer is increased, the number of possible combinations increases.

A study by John and Wallace[72] showed that polypyrrole is formed by the continual precipitation of oligomers on to the electrode surface and not by addition of pyrrole monomers to the ends of polymer chains in the growing film. Consequently, polypyrrole has a densely packed space filling appearance, and elongation of less than 1 % is sufficient to break the film[73]. Oligomers in solution have been detected with a rotating ring disc electrode by Raymond and Harrison[74,75], and with ultramicroelectrodes by Andrieux and coworkers[76,77]. A nucleation process has also been observed prior to the precipitation of oligomers during the polymerization of polypyrrole[78-81]. Despite the complicated steps involved, the current efficiency for polymerizing pyrrole has been reported to be near 100% in some cases[82,83].

The electrode potential has a profound affect on the quality of the final polymer obtained. In a study of the electrochemical polymerization of polythiophene, the molecular weight distribution has been found to be a function of the electrode potential[84]. This may also be true for polypyrrole. Also, since the oxidation potential of the monomer is much higher than the polymer redox potential, overoxidation[42-52] can easily occur during the polymerization process, especially in the presence of nucleophiles such as OH^-, CN^-, CH_3O^-, and Br^-.

Nucleophilic addition of such species to the pyrrole rings destroys the conjugated π-system of the formed polymer. These factors and others contribute to the complex nature of the electrochemical polymerization process.

1.2 Composition, Structure and Conductivity

Elemental analysis of polypyrrole chemically polymerized with H_2O_2 revealed an empirical composition of $C_{4.0\text{-}4.5}H_{3.0\text{-}4.5}N_{1.0}O_{1.0\text{-}1.5}$, indicating linked pyrrole units[85]. Since oxidative degradation of this polymer using $KMnO_4$ forms mainly pyrrole-2,5-dicarboxylic acid[85], the pyrrole units are linked at the α-α' positions. The composition of polypyrrole electrochemically polymerized in CH_3CN containing Et_4NBF_4 is approximately $C_4H_3N(BF_4)_{0.25}$, indicating that every four pyrrole rings carry one positive charge[86]. This is in agreement with the charge consumed during polymerization (2.2 to 2.4 per pyrrole ring) and the integrated anodic or cathodic charge in cyclic voltammograms. Linkage at the α-α' position for electrochemically polymerized polypyrrole is indicated by the fact that α-substituted pyrroles cannot be polymerized[87].

X-ray diffraction studies on the pyrrole dimer and trimer have shown that these oligomers are linear with all pyrrole units lying in a plane and the N-H

bonds on adjacent pyrrole rings orientated in opposite directions[88]. However, such an ideal structure has not been observed for polypyrrole. X-ray diffraction analysis of polypyrrole shows only very broad peaks, indicating an amorphous structure[55,56]. Short range structural order exists but is limited to within 10 to 20 Å[89]. Part of the structural disorder is caused by a significant number of α-β' linked pyrrole units as shown by x-ray photoelectron spectroscopy (XPS) results[90-94]. Linkage at the β positions can form a branched polymer chain and, consequently, decrease the conjugation length and thus the conductivity[88,95]. Increased structural ordering has been observed for poly-3,4-dimethylpyrrole by electron diffraction[96] and XPS[93,94] studies.

Neutral polypyrrole, like most plastics, has a filled valence band and is a poor conductor. When the polymer is oxidized (p-doped), electrons are withdrawn from the valence band and the polymer becomes conductive. Since the π-electrons have a low ionization potential due to the extended conjugated π-electron system along the chains, they can be relatively easily removed from the valence band to switch the polymer to the conducting state.

Early studies showed that oxidized polypyrrole has a strong electron spin resonance (ESR) signal[35], indicating the presence of unpaired electrons. Recent *in-situ* electrochemical e.s.r experiments reported by Genoud[97,98], Waller *et al*[99] and

Albery *et al*[100,101] show that there is a one-to-one relationship between electron withdrawn and the ESR signal in the early stages of oxidation. As the oxidation level is increased, the ESR signal passes through a maximum (at about one unpaired electron per six pyrrole rings[97-99]) and then starts to decrease.

Quantum chemical calculations have shown that significant geometric and electronic structure modification of the polymer occurs upon the removal of electrons from the conducting polymer chains[91,92,102-107]. At a low oxidation level, withdrawal of electrons creates paramagnetic (S=1/2) polarons. Fig. 1.1A shows a polaron spread over four pyrrole units. As the oxidation level increases, two adjacent polarons are converted to a spinless bipolaron (Fig. 1.1B). Electronic conduction occurs by movement of the charged polarons or bipolarons along (or hopping between) the polymer chains[102]. Optical absorption spectra of polypyrrole doped with ClO_4^- as a function of dopant concentration show three absorption bands below the band gap absorption for the polaron doping level and two absorption bands for the bipolaron doping level[108,109]. This result agrees with the band structure of a polymer chain containing polarons at a low oxidation level and bipolarons at a high oxidation level[102].

The conductivity of polypyrrole can be altered by changing the structure of the polymer, such as by introducing substituent groups at the nitrogen or β

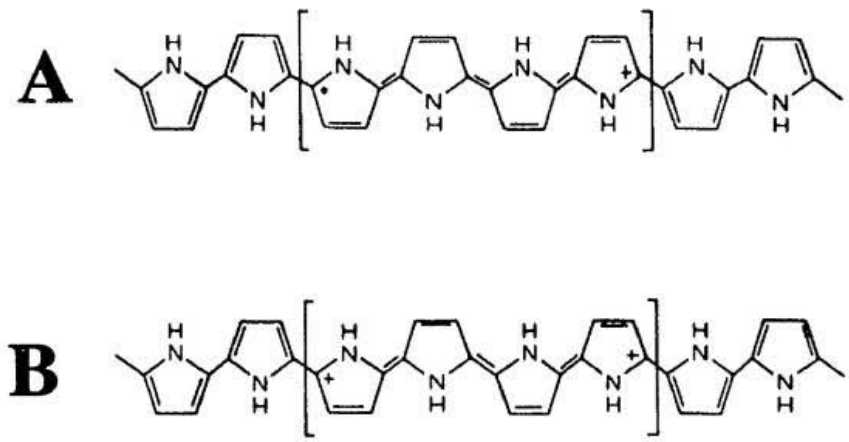

Fig. 1.2.1 Structural distortions of a polaron (A) and a bipolaron (B) over four pyrrole units.

positions of the pyrrole ring. Compared to polypyrrole, poly-N-methylpyrrole exhibits a conductivity decrease of over 5 orders of magnitude[73], while poly-3-methylpyrrole is less than 2 orders of magnitude less conductive than polypyrrole[73]. X-ray diffraction studies on the tetramer of N-methyl pyrrole indicate that the adjacent pyrrole ring planes are rotated almost 90° to each other[88]. The effect of torsion angle on a polymer's conductivity has been elucidated in a valence effective hamiltonian (VEH) study on poly-*p*-phenylene by Brédas and coworkers[110]. Their results indicate that a 90° orientation eliminates the possibility

of significant π-electron delocalization.

Changing the electrolyte anions can produce a variation of as much as 10^5 in the electronic conductivity of polypyrrole films[111], indicating some form of anion-induced localization of the radical cation (polaron) or dication (bipolaron) in the polymer structure[73]. Such interaction between the anions and cations on the polymer chains has also be shown to slow down anion movement[112,113]. X-ray photo emission[114] and Raman scattering[115] data clearly verified the above interaction in polypyrrole/doping anion materials. It may be expected that coupled transport of electrons and counterions occurs in certain types of experiments such as impedance measurements[116] where movement of both polarons/bipolarons and counterions occurs.

1.3 Redox Reaction and Ion Transport

One of the unique properties of conducting polymers is that they can be reversibly switched between insulating (neutral) and conducting (doped) states within a certain potential range[22,117]. This inherent electrochemical activity is due to electron withdrawal from, or addition to, the π-system of the polymer backbone. This differs from the electrochemical activity of redox polymers, such

as poly-vinylpyridine and vinylbipyridine complexes of ruthenium[118], which contain discrete redox centres attached to an electro-inactive polymer framework.

Since large changes in electronic conductivity, polymer ionic strength, polymer ion permeability and optical properties, *etc.*, accompany redox switching, conducting polymers are very promising materials for applications such as rechargeable battery electrodes[21,119,120], supercapacitors[21,121], electrochromic display materials[122-125], molecular electronic devices[124,126-128], electroanalysis[129-131] and electrocatalysis[25,29,132-134].

The oxidized (p-doped) polypyrrole chains are polycations. The positive charges on the chains are counterbalanced by anions (A^-), which are called the dopant anions or counterions, to preserve electroneutrality. Switching the polymer film between the doped and undoped states involves anion movement in or out of the polymer film. For polypyrrole, it has been found that ion movement in the polymer phase is the rate determining step in switching[12,135-137] and thus is the limiting factor for many practical applications. To enhance the ion transport rate in the polymer, ion-exchange centres have been introduced in the polypyrrole backbone[138-140]. Also, by forming polypyrrole on a nitrile butadiene rubber precoated electrode, Naoi and coworkers[141-143] have shown that the morphology of the polymer can be regulated with improved ion transport. Polymers exhibiting

self-doping, which will be discussed in the following section, also have enhanced ion transport rates.

1.3.1 Normally Doped Polypyrroles

In the normal doping process, the positive charges on the oxidized polymer chains are counterbalanced by anions from the electrolyte. Reduction of the polymer involves expulsion of these anions into the bulk electrolyte solution. In the reverse process, oxidation of the polymer causes anions from the electrolyte to be inserted. Polypyrroles prepared in electrolyte solutions containing small anions such ClO_4^-, Cl^- and BF_4^- exhibit this normal doping process.

1.3.2 Self-doped Polypyrroles

Although most conducting polymers involve the intercalation of anions into the polymer to maintain electroneutrality upon oxidation as discussed above, there is an important class of polymers in which cations are expelled upon p-doping. These so called self-doped polymers have permanent anionic sites fixed within the polymer matrix, and electroneutrality in the undoped form is maintained by mobile cations. There are of two types of self-doped polymers:

Type I: The conducting polymer is electrochemically polymerized in a monomer solution containing a polyanion electrolyte. Because of the physical size, and more

importantly, the entanglement of the two types of polymer chains, the polyanions are physically trapped in the polymer matrix. Thus instead of anion insertion, cations are expelled into the bulk electrolyte solution to maintain electroneutrality upon oxidation. Polypyrrole doped with polystyrene sulphonate is an example of a type I self-doped polymer. It has been studied extensively in literature[52,101,112,144-159] and in this work. Other polypyrrole/polyelectrolyte composite polymers include PPY/Kodak AQ[160], PPY/flavin-containing polyanion[161], PPY/sulphated poly(β-hydroxyethers)[162], PPY/sulphated poly(butadienes)[162]; PPY/sulphated poly(imides)[162], PPY/sulphated poly(methacrylates)[162], PPY/poly(p-phenyleneterephthalamide propane sulphonate)[158,163], PPY/poly(vinyl sulphate)[146.164,165], PPY/poly(vinylsulphonate)[147,148], poly(styrene-*co*-maleic acid)[55] and PPY/Nafion[150,165-172]. These polypyrrole composites are reported to have high tensile strength[173], high thermostability (>300 °C)[158], environmental stability[153,174] and excellent processing properties[162].

Type II: The conducting polymer is prepared from a monomer which contains an anionic substituent. The reduced polymer is in the acid or salt form. Self-doped conducting polymers of this type reported in the literature include polypyrroles with carboxylate[175,176], alkyl carboxylate[177] and alkylsulphonate[169,178-181] substituents

and polythiophene with alkylsulphonates[123,182-185] substituents.

There are several advantages to be gained from self-doping. In aqueous solution, the proton is the smallest and most mobile ion. Relatively rapid doping/undoping processes may be realized by utilizing proton movement. In aprotic solutions, Li salts have high solubility and the small light Li^+ ion should also speed up the doping/undoping processes. Our experimental results show that slow anion movement in the oxidized polymer is due to a strong interaction between the anions and diffuse positive charges (polarons/bipolarons) on the oxidized polymer chains[112,113]. In self-doped polymers the mobile cations and fixed anions can be selected to minimize ion pairing and so enhance the polymer's ionic conductivity.

The advantages of self-doped polymers are particularly important in lithium batteries because they can enhance the charging/discharging rate and charge density. During the discharging process, Li^+ is released from the Li anode into the bulk electrolyte solution and inserted into the polymer cathode. Because the two electrodes are the source and drain of Li^+ respectively, the concentration of the electrolyte solution does not change during the charge/discharge cycle. The volume of the electrolyte solution can be kept at a minimum level to make the battery light-weight and robust.

1.4 Scope of This Work

Since charge transport in conducting polymers is crucial to many of their applications, it has been the focus of intensive research. Cyclic voltammetry is the simplest and most commonly used technique[12,22,135,147,186,187]. Noticing that the shapes of cyclic voltammograms were sensitive to the counterions, Diaz and coworkers[12,135] predicted correctly that the ion movement in polypyrrole was the rate limiting charge transport step. Other techniques used include potentiostatic pulse transient experiments[69,188-190], galvanostatic pulse transient experiments[191-195] techniques involving dual working electrodes[196-199], rotating disc voltammetry[200,201], ionic conductivity measurements on polymer membranes[188,202] and impedance spectroscopy.

Impedance spectroscopy (IS) is one of the most powerful techniques available to electrochemist. It has been successfully applied in the study of many electrochemical systems, such as corrosion, batteries, coatings evaluation, electrodeposition, semiconductor electrochemistry and electro-organic synthesis. It can provide a wealth of kinetic and mechanistic information[203,204]. Bard and coworkers[205] first introduced IS in the study of conducting polymers (polypyrrole films on electrodes) in 1982. Since then, this method has been widely

used[112,116,156,199,206-219].

Unfortunately, the impedance responses of conducting polymers reported in the literature vary widely and there is so far no settled theory and equivalent circuit to model experimental impedance data. It was the purpose of this study to investigate the impedance responses of various conducting polymers under a wide variety of different conditions. To select the most appropriate model, measured experimental parameters, such as electronic and ionic conductivities, were compared with the results obtained from other independent measurements. The polymers studied in this work are poly-3-methyl-pyrrole-4-carboxylic acid (poly-MPCA), poly-pyrrole-3-carboxlic acid (poly-PCA), poly-[1-methyl-3-(pyrrol-1-ylmethyl)pyridinium] (poly-MPMP), polypyrrole/perchlorate (PPY/ClO_4^-) and polypyrrole/poly(styrene sulphonate) (PPY/PSS) composites. In Chapter 5, the impedance responses for these polymer film coated electrodes immersed in electrolyte solutions are analyzed to test various models discussed in Chapter 4. Deviations from the ideal model impedance were investigated. The film ionic conductivity extracted from impedance data was used to probe the polymer structure (Chapter 6 and 8), and interaction between the counterions and positive charges on oxidized polypyrrole chains (Chapter 7). The impedance responses of a self-doped conducting polymer film was shown for the first time to be different from that of a normally doped polymer film (Chapter 7). This difference was used

to locate the initial reaction layer in conducting polypyrrole film when subjected to a potential perturbation by studying the impedance responses of bilayer films (Chapter 9). A polypyrrole film which has both normal and self-doping properties can function as an ion-gate device which can be electrochemically switched between the anion exchanger state and cation exchanger state (Chapter 10). Some results of this work have already been published[112,116,156,199].

References

(1) Walatka, V.V.; Labes, M.M.; Perlstein, J.H. *Phys. Rev. Lett.* 1973,*31*,1139.

(2) Greene, R.L.; Street, G.B.; Suter, L.J. *Phys. Rev. Lett.* 1975,*34*,577.

(3) Shirakawa, H.; Louis, E.J.; MacDiarmid, A.G.; Chiang, C.K.; Heeger, A.J. *J. Chem. Soc., Chem. Commun.* 1977,,578.

(4) Chiang, C.K.; Park, Y.W.; Heeger, A.J.; Shirakawa, H.; Louis, E.J.; Macdiarmid *J. Chem. Phys.* 1978,*69*,5098.

(5) Langer, J. *Solid State Commun.* 1978,*26*,839.

(6) Diaz, A.; Logan, J.A. *J. Electroanal. Chem.* 1980,*111*,111.

(7) Diaz, A.F.; Kanazawa, K.K.; Gardini, G.P. *J. Chem. Soc., Chem. Commun.* 1979,,635.

(8) Kanazawa, K.K.; Diaz, A.F.; Geiss, R.H.; Gill, W.D.; Kwak, J.F.; Logan, J.A.; Rabolt, J.F.; Street, G.B. *J. Chem. Soc., Chem. Commun.* 1979,,854.

(9) Tourillon, G.; Garnier, F. *J. Electroanal. Chem.* 1982,*135*,173.

(10) Ivory, P.M.; Miller, G.G.; Sowa, J.M.; Shacklette, L.W.; Chance, R.R.; Baughman, R.H. *J. Chem. Phys.* 1979,*71*,1506.

(11) Tsukamot, J.; Takahashi, A.; Kawasaki, K. *Jpn. J. Appl. Phys.* 1990,*29*,125.

(12) Salmon, M.; Diaz, A.F.; Logan, A.J.; Krounbi, M.; Bargon, J. *Mol. Cryst. Liq. Cryst.* 1982,*83*,265.

(13) Diaz, A.F.; Castillo, J.; Kanazawa, K.K.; Logan, J.A.; Salmon, M.; Fajardo, O. *J. Electroanal. Chem.* 1982,*133*,233.

(14) Skotheim, T.A., Editor, *Handbook of Conducting Polymers*, Marcel Dekker: New York, Vol.1 and 2,1986.

(15) Waltman, R.J.; Bargon, J. *Can. J. Chem.* 1986,*64*,76.

(16) Heinze, J. *Synth. Met.* 1991,*41-43*,2805.

(17) Scrosati, B. *Mater. Sci. Eng., B* 1992,*B12*,369.

(18) Evans, G.P. in *Advances in Electrochemical Science and Engineering*, Gerischer, H.; Tobias, C.W. (Ed.),VCH: New York,1990, p.1

(19) Imisides, M.D.; John, R.; Riley, P.J.; Wallace, G.G. *Electroanalysis* 1991,*3*,879.

(20) Kanatzidis, M.G. *Chem. Eng. News* 1990,36.

(21) Techagumpuch, A.; Nalwa, H.S.; Miyata, S. in *Electroresponsive Molecular and Polymeric Systems*, Skotheim, T.A. (Ed.) Marcel Dekker: New York, 1991, p.257

(22) Heinze, J.in *Current Chemistry*, Springer-Verlag: Berlin,1990,p.1.

(23) Diaz, A.F.; Rubinson, J.F.; Mark, H.B., Jr. *Adv. Polym. Sci.*

1988,*84*,113.

(24) Kaneko, M.; Wohrle, D. *Adv. Polym. Sci.* 1988,*84*,141.

(25) Curran, D.; Grimshaw, J.; Perera, S.D. *Chem. Soc. Rev.* 1991,*20*,391.

(26) Naarmann, H.; Theophilou, N. in *Electroresponsive Molecular and Polymeric Systems*, Skotheim, T.A. (Ed.) Marcel Dekker: New York,1988,p.1.

(27) Krivoshei, I.V.; Skorobogatov, V.M. *Polyacetylene and Polyarylenes. Synthesis and Conductive Properties*, Gordon and Breach: Philadelphia,1991.

(28) Deronzier, A.; C. Moutet, J. *Acc. Chem. Res.* 1989,22,249.

(29) Deronzier, A. *J. Chim. Phys. Phys. Chim. Biol.* 1989,*86*,31.

(30) Reynolds, J.R.; Pomerantz, M. in *Electroresponsive Molecular and Polymeric Systems*, Skotheim, T.A. (Ed.), Marcel Dekker: New York,1991,p.187.

(31) Angeli, A. *Gazz. Chim. Ital.* 1916,*46 II*,279.

(32) Street, G.B.; Clarke, T.C.; Krounbi, M.; Kanazawa, K.; Lee, V.; Pfluger, P.; Scott, J.C.; Weiser, G. *Mol. Cryst. Liq. Cryst.* 1982,*83*,1285.

(33) Walker, J.A.; Warren, L.F.; Witucki, E.F. *Polym. Prepr. (Am. Chem. Soc., Div. Polym. Chem.)* 1987,*28*,256.

(34) Lei, J.T.; Cai, Z.H.; Martin, C.R. *Synth. Met.* 1992,*46*,53.

(35) Dall'Olio, A.; Dascola, Y.; Varacca, V.; Bocchi, V. *Comptes Rendus* 1968,*C267*,433.

(36) Myers, R.E. *J. Electronic Materials* 1985,*15*,61.

(37) Salmon, M.; Kanazawa, K.K.; Diaz, A.F.; Krounbi, M. *J. Polym. Sci.*

1982,*20*,187.

(38) Shimidzu, T.; Ohtani, A.; Iyoda, T.; Honda, K. *J. Chem. Soc., Chem. Commun.* 1986,,1414.

(39) Deronzier, A.; Moutet, J.C. *Acc. Chem. Res.* 1989,*22*,249.

(40) Murray, R.W.; Ewing, A.G.; Durst, R.A. *Anal. Chem.* 1987,*59*,379A.

(41) Barendrecht, E. *J. Appl. Electrochem.* 1990,*20*,175.

(42) Witkowski, A.; Brajter-Toth, A. *Anal. Chem.* 1992,*64*,635.

(43) Beck, F.; Braun, P.; Oberst, M. *Ber. Bunsenges. Phys. Chem.* 1987,*91*,967.

(44) Novak, P.; Vielstich, W. *J. Electrochem. Soc.* 1990,*137*,1681.

(45) Christensen, P.A.; Hamnett, A. *Electrochim. Acta* 1991,*36*,1263.

(46) Rosseinsky, D.R.; Morse, N.J.; Slade, R.C.T.; Hix, G.B.; Mortimer, R.J.; Walton, D.J. *Electrochim.. Acta* 1991,*36*,733.

(47) Beck, F.; Braun, P.; Oberst, M. *Ber. Bunsen Ges. Phys. Chem.* 1987,*91*,967.

(48) Lee, C.; Kwak, J.; Bard, A.J. *J. Electrochem. Soc.* 1989,*136*,3720.

(49) Schlenoff, J.B.; Xu, H. *J. Electrochem. Soc.* 1992,*139*,2397.

(50) Beck, F.; Braun, P.; Schloten *J. Electroanal. Chem.* 1989,*267*,141.

(51) Li, Y.F.; Qian, R.Y. *Synth. Met.* 1993,*53*,149.

(52) Wegner, G.; Wernet, W.; Glatzhofer, D.T.; Ulanski, J.; Kroehnke, C.; Mohammadi, M. *Synth. Met.* 1987,*18*,1.

(53) Gau, S.C.; Milliken, J.; Pron, A.; MacDiarmid, A.C.; Heeger, A.J. *J.*

Chem. Soc., Chem. Commun. 1979,,662.

(54) Warren, L.F.; Walker, J.A.; Anderson, D.P.; Rhodes, C.G.; Buckley, L.J. *J. Electrochem. Soc.* 1989,*136*,2286.

(55) Warren, L.F.; Anderson, D.P. *J. Electrochem. Soc.* 1987,*134*,101.

(56) Yoneyama, H.; Wakamoto, K.; Tamura, H. *Mater. Chem. Phys.* 1986,*15*,567.

(57) Ge, H.; Ashraf, S.A.; Gilmore, K.J.; Too, C.O.; Wallace, G.G. *J. Electroanal. Chem.* 1992,*340*,41.

(58) Zinger, B.; Miller, L.L. *J. Am. Chem. Soc.* 1984,*106*,6861.

(59) Zhou,Q.X.; Miller, L.L.; Valentine, J.R. *J. Electroanal. Chem.* 1989,*261*,147.

(60) Miller, L.L.; Zinger, B.; Zhou, Q.-X. *J. Am. Chem. Soc.* 1987,*109*,2267.

(61) Li, Y.J.; Dong, S.J. *J. Chem. Soc., Chem. Commun.* 1992,,827.

(62) Schlenoff, J.B.; Fong, Y.; Xu, H. *Polym. Mater. Sci. Eng.* 1990,*63*,411.

(63) Dong, S.; Ding, J. *Synth. Met.* 1987,*20*,119.

(64) Satoh, M.; Imanishi, K.; Yoshino, K. *J. Electroanal. Chem.* 1991,*317*,139.

(65) Yang, H.G.; Bard, A.J. *J. Electroanal. Chem.* 1991,*306*,87.

(66) Otero, T.F.; Santamaria, C. *Electrochim. Acta* 1992,*37*,297.

(67) Otero, T.F.; Angulo, E. *J. Appl. Electrochem.* 1992,*22*,369.

(68) Diaz, A. *Chem. Scr.* 1981,*17*,145.

(69) Genies, E.M.; Bidan, G.; Diaz, A.F. *J. Electroanal. Chem.* 1983,*149*,101.

(70) Inoue, T.; Yamase, T. *Bull. Chem. Soc. Jpn.* 1983,*56*,985.

(71) Andrieux, C.P.; Audebert, P.; Hapiot, P.; Saveant, J.M. *J. Phys. Chem.* 1991,*95*,10158.

(72) John, R.; Wallace, G.G. *J. Electroanal. Chem.* 1991,*306*,157.

(73) Diaz, A.F.; Kanazawa, K.K. in *Extended Linear Chain Compounds*, Miller, J.S. (Ed.) : 1982,p.417.

(74) Raymond, D.E.; Harrison, D.J. *J. Electroanal. Chem.* 1990,*296*,269.

(75) Beck, F.; Oberst, M. *J. Electroanal. Chem.* 1990,*285*,177.

(76) Andrieux, C.P.; Audebert, P.; Hapiot, P.; Saveant, J.M. *Synth. Met.* 1991,*43*,2877.

(77) Andrieux, C.P.; Grzeszczuk, M.; Saveant, J.M. *J. Electroanal. Chem.* 1991,*318*,369.

(78) Otero, T.F.; Tejada, R.; Elola, A.S. *Polymer* 1987,*28*,651.

(79) Fletcher, S.; Halliday, C.S.; Gates, D.; Westcott, M.; Lwin, T.; Nelson, G. *J. Electroanal. Chem.* 1983,*159*,267.

(80) Asavapiriyanont, S.; Chandler, G.K.; Gunawardena, G.A.; Pletcher, D. *J. Electroanal. Chem.* 1984,*177*,229.

(81) Downard, A.J.; Pletcher, D. *J. Electroanal. Chem.* 1986,*206*,147.

(82) Beck, F.; Oberst, M. *J. Appl. Electrochem.* 1992,*22*,332.

(83) Beck, F.; Oberst, M. *Makromol. Chem., Macromol. Symp.* 1987,*8*,97.

(84) Yen, W.; Jing, T. *Macromolecules* 1993,*26*,457.

(85) Gardini, G.P. *Adv Heterocyclic chem* 1973,*15*,67.

(86) Kanazawa, K.K.; Diaz, A.F.; Gill, W.D.; Grant, P.B.; Street, G.B.; Gardini, G.P.; Kwak, J.F. *Synth. Met.* 1980,*1*,329.

(87) Diaz, A.F.; Martinez, A.; Kanazawa, K.K.; Salmon, M. *J. Electroanal. Chem.* 1981,*130*,181.

(88) Street, G.B. in *Handbook of Conducting Polymers*, Skotheim, T.A.(Ed.), Marcel Dekker, Inc: New York,1985,p.265.

(89) Bott, D.V. in *Handbook of Conducting Polymers*, Skotheim, T.A. (Ed.), Marcel Dekker, Inc: New York,1985,p.1225.

(90) Pfluger, P.; Street, G.B. *Polym. Prepr. (Am. Chem. Soc., Div. Polym. Chem.)* 1982,*23*,122.

(91) Scott, J.C.; Bredas, J.L.; Yakushi, K.; Pfluger, P.; Street, G.B. *Synth. Met.* 1984,*9*,165.

(92) Pfluger, P.; Weiser, G.; Scott, J.C.; Street, G.B. in *Handbook of Conducting Polymers*, Skotheim, J.A.(Ed.), Marcel Dekker: New York,1986,p.1369.

(93) Pfluger, P.; Krounbi, M.; Street, G.B.; Weiser, G. *J. Chem. Phys., Part I* 1983,*78*,3212.

(94) Pfluger, P.; Street, G.B. *J. Chem. Phys.* 1984,*80*,544.

(95) Tourillon, G.; Garnier, F. *J. Phys. Chem.* 1983,*87*,2289.

(96) Geiss, R.H.; Economy, J.; Volksen, W. *IBM J. Res. Dev.* 1983,*27*,321.

(97) Genoud, F.; Guglielmi, M.; Nechtstein, M.; Genies, F.; Salmon, M. *Phys. Rev. B:. Condens. Matter.* 1985,*55*,148.

(98) Nechtstein, M.; Devreux, F.; Genoud, F.; Vieil, E.; Pernaut, J.M.; Genies, F. *Synth. Met.* 1986,*15*,59.

(99) Waller, A.M.; Compton, R.G. *J. Chem. Soc., Faraday. Trans. I* 1989,*85*,977.

(100) Albery, W.J.; Chen, Z.; Horrocks, B.R.; Mount, A.R.; Wilson, P.J.; Bloor, D.; Monkman, A.T.; Elliott, C.M. *Faraday. Discuss. Chem. Soc.* 1989,*88*,247.

(101) Li, F.; Albery, W.J. *J. Chem. Soc., Faraday. Trans.* 1991,*87*,2949.

(102) Bredas, J.L.; Street, G.B. *Acc. Chem. Res.* 1985,*18*,309.

(103) Bredas, J.L.; Scott, J.C.; Yakushi, K.; Street, G.B. *Phys. Rev. B:. Condens. Matter.* 1984,*30*,1023.

(104) Bredas, J.L.; Themans, B.; Andre, J.M. *Phys. Rev. B:. Condens. Matter.* 1983,*27*,7827.

(105) Bredas, J.L.; Themans, B.; Fripiat, J.G.; Andre, J.M.; Chance, R.R. *Phys. Rev. B:. Condens. Matter.* 1984,*29*,6761.

(106) Bredas, J.L. in *Handbook of Conducting Polymers*, Skotheim, T.A.(Ed.), Marcel Dekker: New York,1985,p859.

(107) Kaufman, J.H.; Colaneri, N.; Scott, J.C.; Street, G.B. *Phys. Rev. Lett.* 1984.*53*,1005.

(108) Yakushi, K.; Lauchlan, L.J.; Clarke, T.C.; Street, G.B. *J. Chem. Phys.* 1983,*79*,4774.

(109) Genies, E.M.; M. Pernaut, J. *J. Electroanal. Chem.* 1985,*191*,111.

(110) Bredas, J.L.; Chance, R.R.; Baughman, R.H.; Silbey, R. *J. Chem. Phys.* 1982,*76*,3673.

(111) Diaz, A. *Chem. Scr.* 1981,*17*,145.

(112) Ren, X.; Pickup, P.G. *J. Phys. Chem.* 1993,*97*,5356.

(113) Ren, X.; Pickup.PG *unpublished. results.* 1993.

(114) Atanasoska, L.; Naoi, K.; Smyrl, W.H. *Chemistry of Materials* 1992,*4*,988.

(115) Inoue, T.; Hosoya, I.; Yamase, T. *Chem. Lett.* 1987,563.

(116) Ren, X.; Pickup, P.G. *J. Chem. Soc., Faraday. Trans.* 1993,*89*,321.

(117) Diaz, A.F.; Castillo, J.I. *J. Chem. Soc., Chem. Commun.* 1980,,397.

(118) Abruna, H.D.; Denisevich, P.; Umana, M.; Meyer, T.J.; Murray, R.W. *J. Am. Chem. Soc.* 1981,*103*,1.

(199) Scrosati, B. *J. Electrochem. Soc.* 1989,*136*,2774.

(120) Naegele, D.; Bittihn, R. *Solid State Ionics* 1987,*28-30*,983.

(121) Naoi, K.; Oyama, N. in *Proc. - Electrochem. Soc.*, 92-15(Proc. Symp. High Power, Ambient Temp. Lithium Batteries, 1991),1992,187.

(122) Mastragostino, M.; Marinangeli, A.M.; Corradini, A.; Giacobbe, S. *Synth. Met.* 1989,*28*,C501.

(123) Ikenoue, Y.; Tomozawa, H.; Saida, Y.; Kira, M.; Yashima, H. *Synth. Met.* 1991,*40*,333.

(124) Baughman, R.H. *Makromol. Chem., Macromol. Symp.* 1991,*51*,193.

(125) Mastragostino, M.; Arbizzani, C.; Bongini, A.; Barbarella, G.; Zambianchi, M. *Electrochim. Acta* 1993,*38*,135.

(126) Thackeray, J.W.; White, H.S.; Wrighton, M.S. *J. Phys. Chem.* 1985,*89*,5133.

(127) Bauerle, P.; Wrighton, M.S.; Chyan, O.M.R.; Spangler, C.W. *Ber. Bunsenges. Phys. Chem.* 1987,*91*,889.

(128) Takashima, W.; Sasano, K.; Asano, T.; Kaneto, K. *Polymer International* 1992,*27*,249.

(129) O'Riordan, D.M.T.; Wallace, G.G. *Anal. Chem.* 1986,*58*,128.

(130) Zhi, W.; Galal, A.; Zimmer, H.; Mark, H.B. *Electroanalysis* 1992,*4*,77.

(131) Lyons, M.E.G.; Bartlett, P.N.; Lyons, C.H.; Breen, W.; Cassidy, J.F. *J. Electroanal. Chem.* 1991,*304*,1.

(132) Bedioui, F.; Granados, S.G.; Devynck, J.; Biedcharreton, C. *New J. Chem.* 1991,*15*,939.

(133) Haimerl, A.; Merz, A. *J. Electroanal. Chem.* 1987,*220*,55.

(134) Bose, C.S.C.; Rajeshwar, K. *J. Electroanal. Chem.* 1992,*333*,235.

(135) Diaz, A.F.; Castillo, J.I.; Logan, J.A.; Lee, W.-Y. *J. Electroanal. Chem.* 1981,*129*,115.

(136) Panero, S.; Prosperi, P.; Bonino, F.; Scrosati, B.; Corradini, A.; Mastragostino, M. *Electrochim. Acta* 1987,*32*,1007.

(137) Novak, P.; Inganas, O.; Bjorklund, R. *J. Power Sources* 1987,*21*,17.

(138) Cosnier, S.; Deronzier, A.; Moutet, J.C.; Roland, J.F. *J. Electroanal. Chem.* 1989,*271*,69.

(139) Mao, H.; Pickup, P.G. *Chem. Mater.* 1992,*4*,642.

(140) Mao, H.; Pickup, P.G. *J. Phys. Chem.* 1992,*96*,5604.

(141) Naoi, K.; Osaka, T. *J. Electrochem. Soc.* 1987,*134*,2479.

(142) Osaka, T.; Naoi, K.; Maeda, M.; Nakamura, S. *J. Electrochem. Soc.* 1989,*136*,1385.

(143) Van Dyke, L.S.; Martin, C.R. *Langmuir* 1990,*6*,1118.

(144) Shimidzu, T.; Ohtani, A.; Iyoda, T.; Honda, K. *J. Electroanal. Chem.* 1987,*224*,123.

(145) Shimidzu, T.; Ohtani, A.; Honda, K. *J. Electroanal. Chem.* 1988,*251*,323.

(146) Naoi, K.; Lien, M.; Smyrl, W.H. *J. Electrochem. Soc.* 1991,*138*,440.

(147) Shimidzu, T.; Ohtani, A.; Iyoda, T.; Honda, K. *J. Electroanal. Chem.* 1987,*224*,123.

(148) Iyoda, T.; Ohtani, A.; Shimidzu, T.; Honda, K. *Synth. Met.* 1987,*18*,747.

(149) Shimizu, A.; Yamataka, K.; Kohno, M. *Bull. Chem. Soc. Jpn.* 1988,*61*,4401.

(150) Valentine, J.R.; Miller, L.L. *Polym. Prepr. (Am. Chem. Soc., Div. Polym. Chem.)* 1988,*29*,446.

(151) Markham, G.; Obey, T.M.; Vincent, B. *Colloids Surf.* 1990,*51*,239.

(152) Prezyna, L.A.; Wnek, G.E.; Qiu, Y.J.; Reynolds, J.R. *Synth. Met.* 1991,*41*,979.

(153) Li, F.; Albery, W.J. *J. Chem. Soc., Faraday. Trans.* 1991,*87*,2949.

(154) Lien, M.; Smyrl, W.H.; Morita, M. *J. Electroanal. Chem.* 1991,*309*,333.

(155) Elliott, C.M.; Kopelove, A.B.; Albery, W.J.; Chen, Z. *J. Phys. Chem.* 1991,*95*,1743.

(156) Ren, X.; Pickup, P.G. *J. Phys. Chem.* 1993,*97*,3941.

(157) Baker, C.K.; Qiu, Y.J.; Reynolds, J.R. *J. Phys. Chem.* 1991,*95*,4446.

(158) Reynolds, J.R.; Baker, C.K.; Gieselman, M. *Polym. Prepr. (Am. Chem. Soc., Div. Polym. Chem.)* 1989,*30*,151.

(159) Ohtani, A.; Shimidzu, T. *Bull. Chem. Soc. Jpn.* 1989,*62*,234.

(160) Wang, J.; Sun, Z.; Lu, Z. *J. Electroanal. Chem.* 1991,*310*,269.

(161) Schoo, H.F.M.; Challa, G. *ACS Symp. Ser., 487,*(Biosens. Chem. Sens.), 1992,164.

(162) Wernet, W. *Synth. Met.* 1991,*41*,843.

(163) Gieselman, M.B.; Reynolds, J.R. *Macromolecules* 1990,*23*,3118.

(164) Bidan, G.; Genies, E.M.; Lapkowski, M. *J. Electroanal. Chem.* 1988,*251*,297.

(165) Noftle, R.E.; Pletcher, D. *J. Electroanal. Chem.* 1987,*227*,229.

(166) Fan, R.F.; Bard, A.J. *J. Electrochem. Soc.* 1986,*133*,301.

(167) Nagasubramanian, G.; Di Stefano, S.; Moacanin, J. *J. Phys. Chem.* 1986,*90*,4447.

(168) Morita, M.; Miyake, R.; Tsutsumi, H.; Matsuda, Y. *Chem. Express* 1990,*5*,985.

(169) Qiu, Y.-J.; Reynolds, J.R. *Polym. Eng. Sci.* 1991,*31*,417.

(170) Deoliveira, I.M.F.; Moutet, J.C.; Hamarthibault, S. *J. Mater. Chem.* 1992,*2*,167.

(171) Fan, F.-R.F.; Bard, A.J. *J. Electrochem. Soc.* 1986,*133*,301.

(172) Ye, S.Y.; Belanger, D. *J. Electroanal. Chem.* 1993,*344*,395.

(173) Iyoda, T.; Ohtani, A.; Shimidzu, T.; Honda, K. *Chem. Lett.* 1986,,687.

(174) Reynolds, J.R.; Gieselman, M.B.; Qiu, Y.J.; Pyo, M.H. *Polym. Mater. Sci. Eng.*, 1991,*64*,202.

(175) Pickup, P.G. *J. Electroanal. Chem.* 1987,*225*,273.

(176) Delabouglise, D. *Synth. Met.* 1992,*51*,321.

(177) Delabouglise, D.; Garnier, F. *New J. Chem.* 1991,*15*,233.

(178) Reynolds, J.R.; Sundaresan, N.S.; Pomerantz, M.; Basak, S.; Baker, C.K. *J. Electroanal. Chem.* 1988,*250*,355.

(179) Sundaresan, N.S.; Basak, S.; Pomerantz, M.; Reynolds, J.R. *J. Chem. Soc., Chem. Commun.* 1987,,621.

(180) Collard, D.M.; Fox, M.A. *J. Am. Chem. Soc.* 1991,*113*,9414.

(181) Reynolds, J.R.; Sundaresan, N.S.; Pomerantz, M.; Basak, S.; Baker, C.K. *J. Electroanal. Chem.* 1988,*250*,355.

(182) Patil, A.O.; Ikenoue, Y.; Wudl, F.; Heeger, A.J. *J. Am. Chem. Soc.* 1987,*109*,1858.

(183) Patil, A.O.; Ikenoue, Y.; Basescu, N.; Colaneri, N.; Chen, J.; Wudl, F.; Heeger, A.J. *Synth. Met.* 1987,*20*,151.

(184) Ikenoue, Y.; Chiang, J.; Patil, A.O.; Wudl, F.; Heeger, A.J. *J. Am. Chem. Soc.* 1988,*110*,2983.

(185) Ikenoue, Y.; Chiang, J.; Patil, A.O.; Wudl, F.; Heeger, A.J. *J. Am. Chem. Soc.* 1988,*110*,2983.

(186) Marque, P.; Roncali, J.; Garnier, F. *J. Electroanal. Chem.* 1987,*218*,107.

(187) Walton, D.J.; Hall, C.E.; Chyla, A. *Analyst* 1992,*117*,1305.

(188) Paulse, C.D.; Pickup, P.G. *J. Phys. Chem.* 1988,*92*,7002.

(189) Kalaji, M.; Nyholm, L.; Peter, L.M. *J. Electroanal. Chem.* 1992,*325*,269.

(190) Vieil, E.; Oudard, J.F.; Servagent, S. *Synth. Met.* 1989,*28*,C599.

(191) Will, F.G. *J. Electrochem. Soc.* 1985,*132*,2093.

(192) Penner, R.M.; Van Dyke, L.S.; Martin, C.R. *J. Phys. Chem.* 1988,*92*,5274.

(193) Cai, Z.; Martin, C.R. *J. Electroanal. Chem. Interfac. Electrochem.* 1991,*300*,35.

(194) Denuault, G.; Mirkin, M., V; Bard, A.J. *J. Electroanal. Chem.* 1991,*308*,27.

(195) Aoki, K.; Tezuka, Y. *J. Electroanal. Chem.* 1989,*267*,55.

(196) Kittlesen, G.P.; White, H.S.; Wrighton, M.S. *J. Am. Chem. Soc.* 1984,*106*,7389.

(197) Feldman, B.J.; Burgmayer, P.; Murray, R.W. *J. Am. Chem. Soc.* 1985,*107*,872.

(198) Focke, W.W.; Wnek, G.E.; Wei, Y. *J. Phys. Chem.* 1987,*91*,5813.

(199) Ren, X.; Pickup, P.G. *J. Electrochem. Soc.* 1992,*139*,2097.

(200) Mao, H.; Pickup, P.G. *J. Am. Chem. Soc.* 1990,*112*,1776.

(201) Mao, H.; Pickup, P.G. *J. Phys. Chem.* 1989,*93*,6480.

(202) Burgmayer, P.; Murray, R.W. *J. Phys. Chem.* 1984,*88*,2515.

(203) Macdonald, J.R. *Impedance Spectroscopy*,;Wiley: New York,1987;

(204) Macdonald, J.R.E. *Electrochim. Acta* 1990,*35*,.

(205) Bull, R.A.; Fan, F.R.F.; Bard, A.J. *J. Electrochem. Soc.* 1982,*129*,1009.

(206) Pickup, P.G. *J. Chem. Soc., Faraday. Trans.* 1990,*86*,3631.

(207) Duffitt, G.L.; Pickup, P.G. *J. Phys. Chem.* 1991,*95*,9634.

(208) Panero, S.; Prosperi, P.; Zane, D.; Scrosati, B. *J. Appl. Electrochem.*

1992,*22*,189.

(209) Miller, D.L.; Bockris, J.O. *J. Electrochem. Soc.* 1992,*139*,967.

(210) West, K.; Zachauchristiansen, B.; Jacobsen, T.; Skaarup, S. *Materials Science and Engineering B Solid State Materials for Advanced Technology* 1992,*13*,229.

(211) Tanguy, J.; Baudoin, J.L.; Chao, F.; Costa, M. *Electrochim. Acta* 1992,*37*,1417.

(212) Tanguy, J.; Hoclet, M. *Synth. Met.* 1991,*43*,2995.

(213) Penner, R.M.; Martin, C.R. *J. Phys. Chem.* 1989,*93*,984.

(214) Musiani, M.M. *Electrochim. Acta* 1990,*35*,1665.

(215) Naoi, K.; Lien, M.M.; Smyrl, W.H.; Owens, B.B. *Appl. Phys. Commun.* 1989,*9*,147.

(216) Tanguy, J.; Slama, M.; Hoclet, M.; Baudouin, J.L. *Synth. Met.* 1989,*28*,C145.

(217) Amemiya, T.; Hashimoto, K.; Fujishima, A. *J. Phys. Chem.* 1993,*97*,4187.

(218) Amemiya, T.; Hashimoto, K.; Fujishima, A. *J. Phys. Chem.* 1993,*97*,4192.

(219) Tanguy, J.; Slama, M.; Hoclet, M.; Baudoin, J.L. *Synth. Met.* 1989,*28*,C145.

Chapter 2

Experimental

2.1 Synthesis of Monomers

3-methyl-pyrrole-4-carboxylic acid (MPCA) and pyrrole-3-carboxylic acid (PCA) were synthesized by a literature method[1], which can be used to prepare various pyrroles substituted at the β-positions. In this type of reaction, tosylmethylisocyanide (TosMIC) reacts under basic conditions with an α,β-unsaturated ester to give a 3-methoxycarbonyl-4-alkylpyrrole with concomitant loss of β-toluenesulphonic acid.

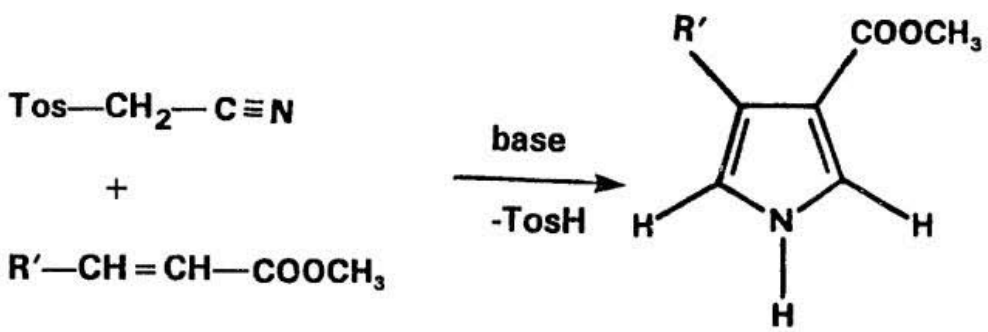

Where: R′ = H, CH_3

To prepare MPCA, a solution of 4 mmol TosMIC (Aldrich) and 4 mmol methyl crotonate (Aldrich) in 90 mL Et_2O/DMSO (2:1) was added slowly to 7 mmol NaH in 40 mL Et_2O under N_2. After the reaction mixture was stirred for 2 hours at 50 °C, the reaction was stopped by adding 50 g of ice. The reaction mixture was then neutralized with concentrated HCl. 3-methoxycarbonyl-4-methylpyrrole (MMP) was extracted into dichloroethane. The extract was washed three times with water (15 mL each), and dried with $MgSO_4$ overnight. Crude product was obtained by removing the solvent under reduced pressure. Recrystallization from petroleum ether (b.p. 30 -40 °C) gave white needle shaped crystals.

The MMP was then hydrolysed in 1 M KOH over a steam bath for 10 min. The solution was cooled to room temperature and neutralized with concentrated HCl. MPCA was obtained as a precipitate after cooling at -20 °C overnight.

To prepare PCA, methyl acrylate (Aldrich) was used instead of methyl crotonate. The overall yields for MPCA and PCA were 40% and 25% respectively.

Mass spectra of MPCA and PCA were obtained with electron impact ionization (70 eV). The molecular ion and other major ionic fragments correspond to the expected structures.

MPCA: m.p. *ca.* 200 °C; H^1 NMR(DMSO-d_6) 11.5 (s,1H), 11.0(b,1H),

7.2(s,1H), 6.6(s,1H) and 2.2(s,3H). MS:(m/z) M^+ (125); -OH (108); -COOH (80).

PCA: m.p. *ca.* 152 °C; H^1 NMR(DMSO-d_6) 11.7 (s,1H), 11.3(b,1H), 7.3(s,1H), 6.8(s,1H) and 6.4(s,1H). MS:(m/z) M^+ (111); -OH (94); -COOH (66).

2.2 Chemicals

Tetrabutylammonium perchlorate (electrochemical grade, Fluka), NaCl (certified ACS, BDH Inc), HCl (certified ACS, Fisher Scientific). Poly (4-styrene sulphonate) sodium salt (NaPSS) (Aldrich, M.W. ~ 70,000), methyl viologen dichloride hydrate (Aldrich), acetonitrile (Fisher, HPLC grade), (±)-propylene carbonate (Aldrich, 99+%, water<0.005%) were used as received.

Pyrrole (Aldrich) was purified by passing through a dry aluminium oxide column followed by distillation under N_2.

$LiClO_4$ and $NaClO_4$ (both from Fluka) were vacuum dried at 100 °C for 24 hours. Tetraethylammonium perchlorate (Et_4NClO_4) was prepared by reacting tetraethylammonium chloride (Et_4NCl) with perchloric acid (70-72%). The precipitate of Et_4NClO_4 was collected by filtration, washed with water, recrystallized twice from water, and dried under vacuum at 100 °C for 24 hours before use.

1-Methyl-3-(pyrrol-1-ylmethyl)pyridinium (MPMP) was synthesized by Mao[2] and used here without further purification.

In the early stages of this study, MPCA was purchased from Aldrich as a rare chemical. Due to lack of supply, sufficient MPCA was later synthesized by a literature method[1](Section 2.1).

2.3 Electrodes, Cells and Electrochemical Instrumentation

Oxygen is an important yet often overlooked factor that affects the electrochemistry of most conducting polymers. Diaz and coworkers[3] have found that oxygen can irreversibly oxidize a neutral polypyrrole film. An optical study of polypyrrole/perchlorate by Street and coworkers[4] has shown that this irreversible oxidation occurs for both the oxidized and neutral films. In this study, the electrolyte solutions were purged with argon to avoid the interference of dissolved oxygen. A sheath of argon gas was then allowed to flow above the electrolyte solution to prevent oxygen re-entering the solution during the

experiments.

For experiments using non-aqueous solutions (Chapters 3, 6 and 7), an aqueous sodium chloride saturated calomel electrode (SSCE, Fisher), which has a potential of 0.212 V *vs.* SHE, was used as the reference electrode. In other chapters when aqueous electrolyte solutions were used, a Ag/AgCl electrode in 0.1 M NaCl(aq) solution, which has potential 0.223 V *vs.* SHE, was used as the reference electrode. Potentials are quoted with respect to either the SSCE or Ag/AgCl. Other electrodes were a large surface area Pt wire ($\sim$ 0.6 cm^2) as counter electrode and the polymer film coated support electrode as working electrode. The support electrodes are further described as follows:

1. Small Platinum Disc Electrode. These electrodes are prepared by sealing a piece of platinum wire (Aldrich) in a soft glass tube and consisted of 0.0045 cm^2 exposed platinum disc. Most of the cyclic voltammetry and all of the impedance measurements were carried out using this type of support electrode.

2. Large Platinum Disc Electrode. This electrode was manufactured by Pine Instrument Co by sealing a platinum disc in polytetrafluoroethylene (PTFE). The exposed platinum disc has an area of 0.458 cm^2.

3. Glassy Carbon Electrode. These electrodes were prepared by sealing a piece of Glassy carbon rod (Electrosynthesis Co) in a glass tube with epoxy. The exposed glassy carbon disc has an area of 0.0707 cm^2.

4. Indium/Tin Oxide (ITO) Coated Glass Electrodes. These electrodes were made with a piece of indium/tin oxide coated glass plate (NESATRON glass, 20 ohm/sq, PPG Industries Inc.). These electrodes were used to study the cross sections of polymer films with scanning electron microscopy and observe the electrochromic effect of polymer layers.

5. Dual Pt Disc Electrode. This electrode assembly was used for *in situ* measurement of the polymer film electronic conductivities[5,6], and consisted of two small Pt disc electrodes (area = 1.3×10^{-4} cm^2) sealed in glass. The polymer film is deposited on one Pt disc electrode. A thin porous gold film is then coated over the whole electrode assembly surface (Edwards Pirani Penning (model 4) vacuum coating unit). The gold film provides an electrical contact between the outside of the polymer film and the second Pt disc electrode. With the twin electrode immersed in an electrolyte solution in an electrochemical cell, a potential ramp is applied to the two electrodes such that a constant 20 mV potential difference is maintained between the two sides of the polymer film. The current flow between the two electrodes is used to determine the film's electronic resistance at each applied potential using Ohm's Law.

All electrochemical experiments were carried out in the conventional three compartment glass cells. The electrochemical cell has a Luggin capillary tip positioned close to the working electrode to control precisely the electrode

potential. Before the experiment, the platinum electrode was polished with 0.3 μm Linde A alumina paste (Micro Metallurgical Ltd) on a flannel cloth, then washed with water and wiped clean with acetone moistened Kimwipes tissue.

To preliminarily characterize the polymer film coated electrodes, cyclic voltammetry was performed using a HA-301 Potentiostat/Galvanostat with a HB-104 Function Generator (both from HOKUTO DENKO Ltd.) and a SE780 BBC XY recorder (GOERZ METRAWATT). For dual electrode voltammetry a RDE 4 Potentiostat (Pine Instrument Company) was used. Polymer films were prepared with the HA-301 Potentiostat/Galvanostat in galvanostat mode.

Impedance measurements were carried out with a Solartron Frequency Response Analyzer (Model 1250) coupled to a Solartron Electrochemical Interface (Model 1286). The instruments were regularly checked with a 12861 ECI Test Module to assure the accuracy of measured impedances. In the impedance study of conducting polymers, the polymer film coated electrode was polarized by a dc potential bias to various redox states. Upon the dc potential a sinusoidal wave potential perturbation of 5 mV root mean square (RMS) amplitude was used. The frequency of potential perturbation was usually in the range of 65 kHz - 0.005 Hz. All the data were collected and analyzed using a Laser 286/2 microcomputer and ZPLOT software (Scribner Associates Inc.). Fig.2.3.1 shows a schematic diagram of the measuring system.

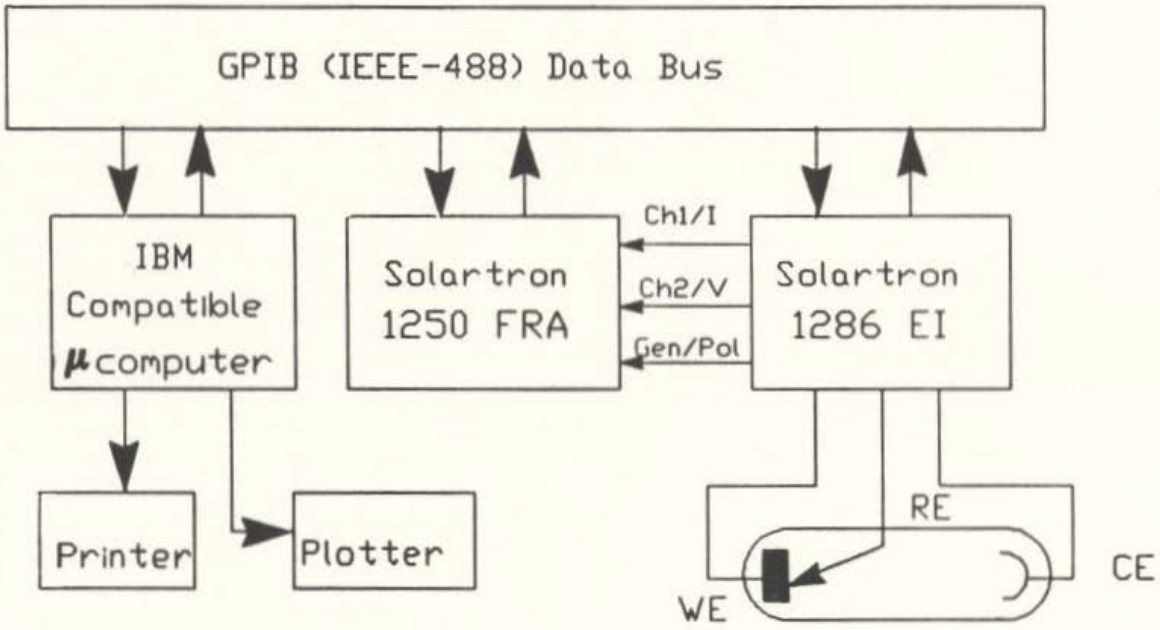

Figure 2.3.1 Schematic diagram of instrumental set-up for impedance spectroscopy.

2.4 Scanning Electron Microscopy and Energy Dispersive X-ray Analyses

The thickness and morphology of polymer films were directly observed with a Hitachi S-570 Scanning Electron Microscope (SEM). To examine the cross section of a polymer film, the polymer was electrochemically deposited on an ITO glass plate electrode, which was then broken to expose a cross section of the polymer film. Since polymer morphology may change with the nature of the support electrode, polymer layers deposited on Pt electrodes were also examined by tearing part of the films away with a scalpel.

An Energy Dispersive X-ray Analyzer (EDXA. Tracor-Northern 5500) equipped with a Microtrace 70152 silicon detector was used for semi-quantitative elemental analysis of Cl, K, Na, S in free standing films peeled from the electrode. Relative elemental concentrations were calculated from the x-ray emission counts using Tracor Northern's Standardless Quantitative Analysis (SQ) software. However, to obtain reliable results a standard that closely matches the compositions and matrix of the samples is required. In this study (Chapter 10),

polypyrrole/4-chlorobenzene sulphonate films were used as a standard for Cl and S molar ratios and PPY/PSS films fully reduced in 0.05 M $KClO_4$(aq) as a standard for K and S molar ratios.

2.5 Reproducibility of Experimental Results

The true thickness of a conducting polymer film soaked in an electrolyte solution may be considerably different from the dry film thickness determined using SEM, due to the unknown degree of film swelling by solvent molecules. All conductivity results are reported based on the dry film thickness.

High precision impedance measurements can easily be obtained with a properly calibrated system and with sufficiently long periods of signal integration. Since the electrochemical polymerization process is very complicated and difficult to control, the impedance results are more reproducible when the measurements are performed on the same film than on different films.

Potential cycling of a polymer film can cause considerable variation in the results of the subsequent impedance measurements[7]. In this study it has been observed that newly prepared polypyrrole films are shiny, brittle and difficult to

remove from the electrode. After only one potential cycle, the polymer film becomes less shiny and more flexible and can be easily removed from the electrode. Compared to a newly formed polymer, a cycled polymer has much higher ionic conductivity. This phenomena has long been known as the "break-in" effect observed both in some redox polymers[8] and conducting polymers[7]. Hillman and Bruckenstein[9] attributed this effect of film history on the redox switching kinetics of electroactive films to pseudo-equilibrium states of the polymer films. Clearly, a polymer film that has been subjected to different potential cycling conditions may show variable results. In this study, all polymer films were subjected to the minimum number of potential scans necessary to produce a reproducible cyclic voltammogram before the impedance measurements. For poly-MPCA, and poly-MPMP the potential cycling had no noticeable effect on the impedance results. Unless indicated, curves and tabulated data are from a single measurement only.

All electrochemical experiments in this work were carried out at room temperature (23 $\pm$ 2 °C).

References

(1) van Leusen, A.M.; Siderius, H.; Hoogenboom, B.E.; van Leusen, D. *Tetrahedron Lett.* 1972,*52*,5337.

(2) Mao, H.; Pickup, P.G. *J. Electroanal. Chem.* 1989,*265*,127.

(3) Diaz, A.F.; Castillo, J.I.; Logan, J.A.; Lee, W.-Y. *J. Electroanal. Chem.* 1981,*129*,115.

(4) Street, G.B.; Clarke, T.C.; Krounbi, M.; Kanazawa, K.; Lee, V.; Pfluger, P.; Scott, J.C.; Weiser, G. *Mol. Cryst. Liq. Cryst.* 1982,*83*,1285.

(5) Pickup, P.G.; Kutner, W.; Leidner, C.R.; Murray, R.W. *J. Am. Chem. Soc.* 1984,*106*,1991.

(6) Mao, H.; Pickup, P.G. *Chem. Mater.* 1992,*4*,642.

(7) Duffitt, G.L.; Pickup, P.G. *J. Chem. Soc., Faraday. Trans.* 1992,*88*,1417.

(8) Denisevich, P.; Abruna, H.D.; Leidner, C.R.; Meyer, T.J.; Murray, R.W. *Inorg. chem.* 1982,*21*,2153.

(9) Hillman, A.R.; Bruckenstein, S. *J. Chem. Soc., Faraday. Trans.* 1993,*89*,339.

Chapter 3

Electrochemical Polymerization and Preliminary Characterization of Polymer Films

The polymers studied in this work were all electrochemically polymerized by oxidizing their monomer in an electrolyte solution. The resulting polymers were formed as films adhering to the support electrode due to their insolubility in the solvent used. Various electrochemical methods can be used to prepare the polymer, such as potential cycling, potentiostatic and constant current methods. Unsuitable polymerization conditions can produce a polymer of poor quality as well as irreproducible or controversial results. For example, Casas *et al*[1] have reported that MPCA can not be polymerized from acetonitrile containing tetraethylammonium *p*-toluenesulphonate. This result contradicts a previous study on this monomer[2].

The effects of the polymerization method and various experimental parameters on the quality of a polymer film were investigated for poly-(3-methyl-pyrrole-4-carboxylic acid) (poly-MPCA) and poly 3-(pyrrole-carboxylic acid) (poly-PCA). Optimal polymerization conditions were strictly controlled later to

prepare poly-MPCA, polypyrrole (PPY)/ClO_4^-, polypyrrole/poly(styrene sulphonate) (PPY/PSS), and poly-[1-methyl-3-(pyrrol-1-ylmethyl)pyridinium] (poly-MPMP).

3.1 Polymerization Methods

3.1.1 Polymerization by Potential Cycling

Fig. 3.1.1 shows voltammograms recorded during the polymerization of MPCA using the potential cycling method. The first forward scan exhibits a low background current up to about 1.20 V, where the current starts to increase sharply. The monomer oxidation potential ($E_{ox,m}$) is estimated by extrapolating the most rapidly increasing part of the current response to the potential axis. On the reverse scan, the anodic current is higher than it was on the forward scan in the potential region 1.22 → 1.05 V. This shows that the monomer oxidation, which continues at potentials above 1.05 V, is catalysed by the previously formed oxidation products. This type of voltammetric behaviour indicates that the polymerization follows a nucleation mechanism[3-5]. During the second forward scan, the current starts to increase rapidly at a much lower potential (ca. 1.05 V), confirming that the polymer film already deposited catalyses the oxidation of the

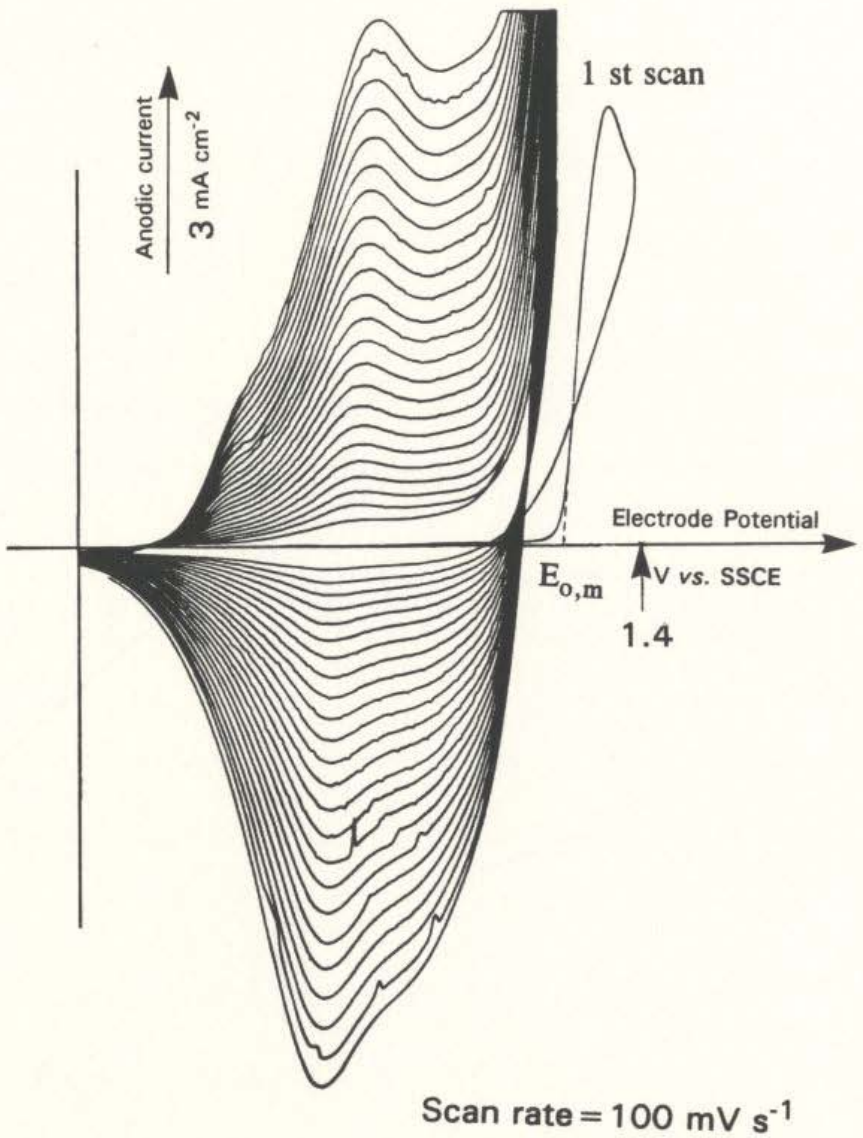

Figure 3.1.1 Cyclic voltammograms for MPCA polymerization on a small Pt electrode by potential cycling in a 0.01 M MPCA-acetonitrile solution containing 0.1 M Et_4NClO_4.

monomer. The electrochemical reaction of the polymer film growing on the electrode is responsible for the reversible redox waves that develop at a formal potential (E°') of 0.58 V.

Similar voltammetric behaviours are observed when polymerizing poly-PCA as shown in Fig. 3.1.2. Table 3.1.1 lists $E_{ox,m}$ values for the two monomers on various electrode materials.

Table 3.1.1 Monomer oxidation potentials on various electrode materials (V *vs.* SSCE).

Monomer[a]	ITO[b]	Pt	Glassy carbon	Own polymer
MPCA	1.31	1.20	1.16	1.06
PCA	1.37	1.28	1.26	1.17

a. In all cases, the monomer solution was 0.01 M in acetonitrile containing 0.1 M Et_4NClO_4.
b. Indium Tin Oxide coated glass plate electrode.

It is interesting to note that the oxidation potential of MPCA is lower than that of PCA. This can be attributed to the electron donating effect of the methyl group of MPCA. Similar results have been reported for other β-substituted polypyrroles[1] and polythiophenes[6,7]. The oxidation potentials of the monomers decrease when electron-donating substituents are present.

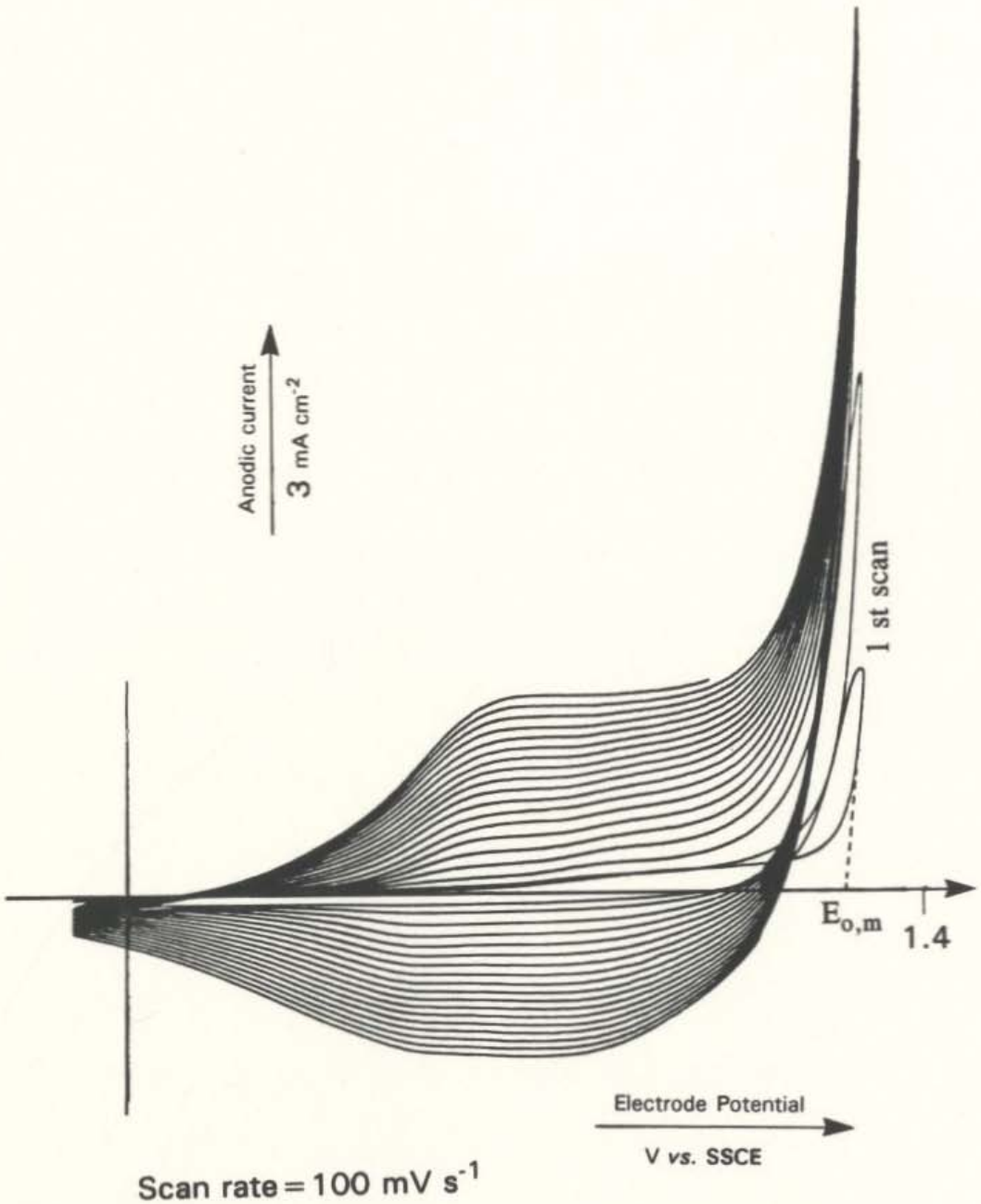

Figure 3.1.2 Cyclic voltammograms for PCA polymerization on a glassy carbon electrode by potential cycling in a 0.01 M PCA-acetonitrile solution containing 0.1 M Et_4NClO_4.

In choosing an electrode material for support of the polymer film, criteria that are usually considered include electronic conductivity and electrochemical stability over the applied potential range. However, the observed change of the monomer oxidation potential with the nature of the electrode material indicates that the electrode's catalytic effect towards the oxidation of the monomer and/or nucleation of the polymer are also important factors. It has been observed that some properties of the polymer, such as conductivity and morphology[8], can be affected by the electrode material especially during the early stages of polymer formation. The lowest monomer oxidation potential is found on its own polymer and is independent of the nature of the electrode material underneath the polymer film.

3.1.2 Polymerization at Constant Current

In this method, a polymer film with acceptable electroactivity is formed only over a certain range of current density. Fig. 3.1.3 shows typical traces of the electrode potential during the polymerization. The initially high electrode potential reflects the difficulty of oxidizing the monomer on the bare support electrode. As polymer is deposited, the potential decreases rapidly. An influence of the nature of the electrode material on the electrode potential is again observed in this experiment. Oxidation of the monomer at the indium/tin oxide (ITO) electrode

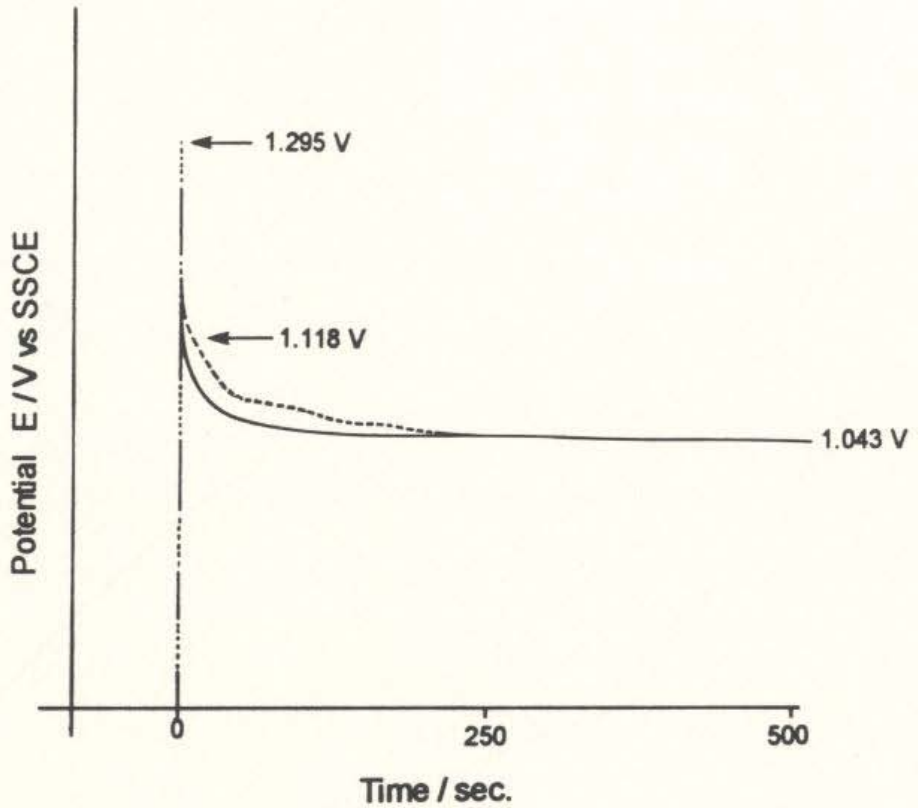

Figure 3.1.3 Electrode potential traces recorded during polymerization of MPCA at a constant current density of 0.45 mA cm^{-2} from a 0.01 M MPCA-acetonitrile solution containing 0.1 M Et_4NClO_4 on **Pt (———) and ITO (·····)**.

requires a higher electrode potential than at Pt. However, the electrode potential at long times (>300 s in this case) is independent of the electrode material. This potential is similar to the monomer oxidation potential on its own polymer found in the potential cycling experiment (Table 3.1.1).

The obvious disadvantage of using a low polymerization current is the long polymerization time. Other considerations may also discourage the use of a low current density. According to the polymerization mechanism discussed in Section 1.1 the polymer film is deposited by the precipitation of the oligomers formed close to the electrode[9-13]. If the oligomer formation rates are low relative to their rates of diffusing away from the electrode, no precipitation occurs since the oligomer concentration remains low. Thus decreasing the current density decreases the current efficiency of polymerization. It has been observed in this work that polymer films formed at low current densities (< 0.05 mA cm^{-2}) exhibit a low total cycling charge compared to films prepared under optimal conditions.

When the current density is too high, the electrode potential increases continuously during the polymerization. Eventually the deposited film becomes overoxidized and non-conductive, which causes the termination of polymerization. In this case, a thin insulating film is found on the electrode. Since the monomer is a competitive reactant, increasing the monomer concentration increases the upper limit of the allowable polymerization current density. Table 3.1.2 shows the

effects of the current density and monomer concentration on the near-constant electrode potential (at polymerization time > 300 s). Here, the potential is used as an indicator for the quality of the deposited polymer film. Based on potentiostatic experiments (Section 3.1.3), the polymer film suffers an insignificant amount of overoxidation as long as the near-constant electrode potential at long times is no higher than 1.20 V. According to the data in Table 3.1.2, the best ratio of current density to monomer concentration is *ca.* 0.044 mA cm^{-2} mM^{-1}.

Table 3.1.2 Near-constant electrode potentials at long times (> 300 s) during the formation of poly-MPCA as a function of the current density and the monomer concentration.

Monomer concentration mM	Current density mA cm^{-2}	Electrode potential V *vs.* SSCE
1.25	0.109	1.24
2.50	0.109	1.09
10.0	0.444	1.04

3.1.3 Potentiostatic Polymerization

Figs. 3.1.4 and 3.1.5 show traces of the anodic current during the polymerization of MPCA at various constant potentials in 1.25 and 2.50 mM MPCA solution respectively. The current-potential transients are characterized by

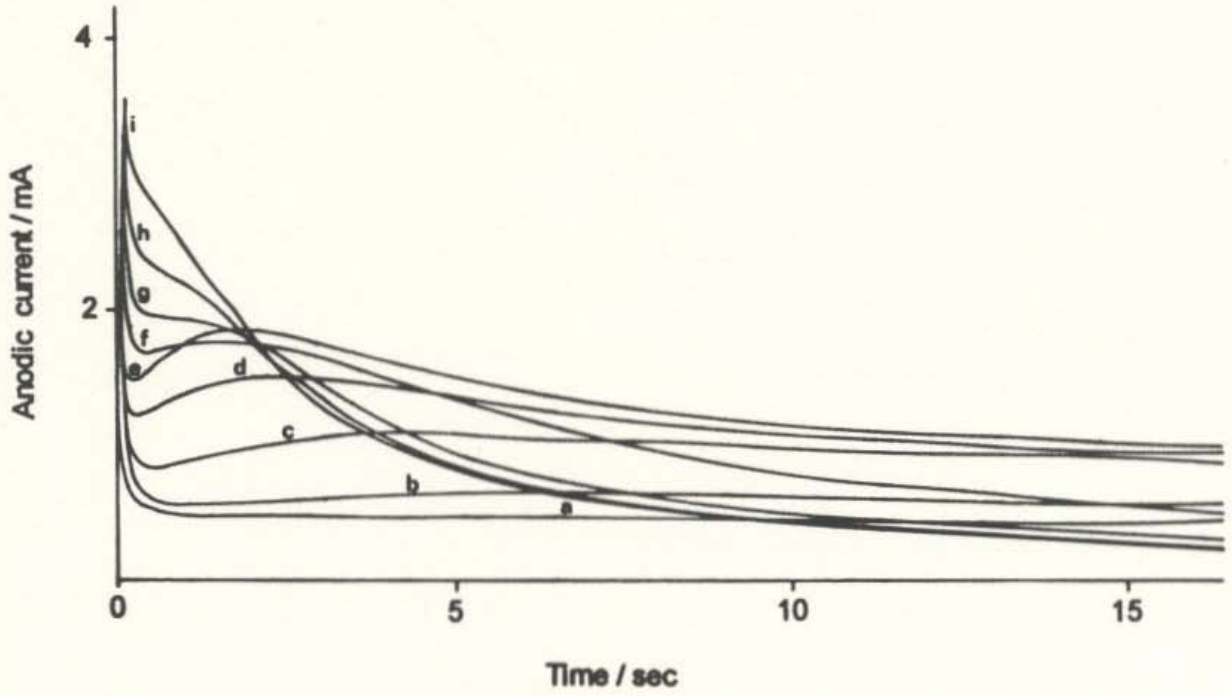

Figure 3.1.4 Anodic current transients for polymerization of MPCA from a 1.25 mM MPCA-acetonitrile solution containing 0.1 M Et_4NClO_4 at a Pt electrode (0.458 cm^2) at constant potentials of 1.235(a), 1.255(b), 1.275(c), 1.295(d), 1.305(e), 1.315(f), 1.325 (g) and 1.335 V (h).

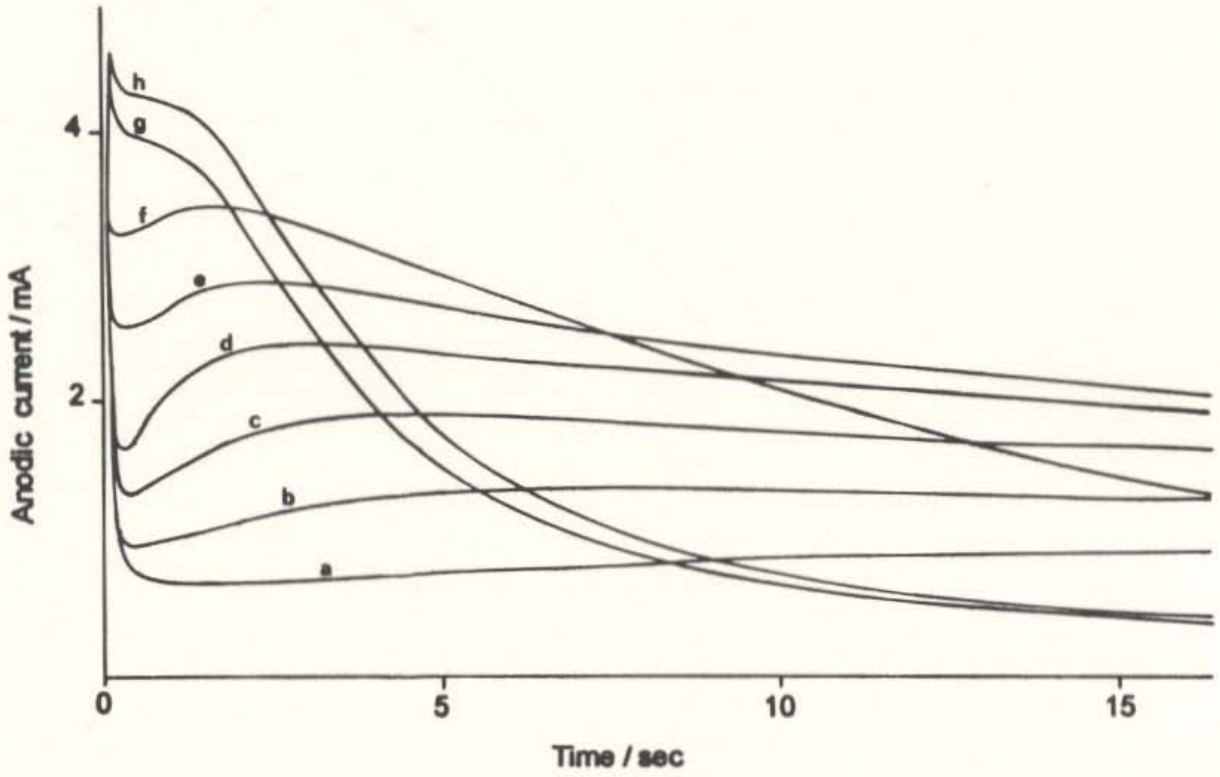

Figure 3.1.5 Anodic current transients for polymerization of MPCA from 2.50 mM MPCA-acetonitrile solution containing 0.1 M Et_4NClO_4 at a Pt electrode (0.458 cm^2) at constant potentials of 1.215(a), 1.235(b), 1.255(c), 1.275(d), 1.295(e), 1.315(f), 1.335 (g) and 1.345 V (h).

a current spike at short times; followed by a period of rising current at intermediate times and a gradually decreasing current at long times. At potentials less than 1.20 V (the minimum potential for the oxidation of the monomer at platinum, Table 3.1.1), there is only a small current spike at short times. This current is due to charging the double layer at the electrode/solution interface when the electrode potential is changed. As the potential is increased above 1.20 V, the amount of charge passed in a given period of time (15 s for example) increases dramatically, indicating the occurrence of a sustained oxidation reaction at the electrode. At a very high potential (1.325 to 1.345 V), there is a large initial current followed by a sharp decrease.

The charge passed in the first 15 s was calculated by evaluating the area under the current-time curve, and plotted in Fig. 3.1.6 as a function of the applied potential. When the concentration of the monomer is doubled, the polymerization charge is doubled in nearly the whole potential range studied. However this does not imply that the polymerization rate is controlled by the diffusion rate of the monomer molecules to the electrode, since increasing the electrode potential also increases the polymerization charge.

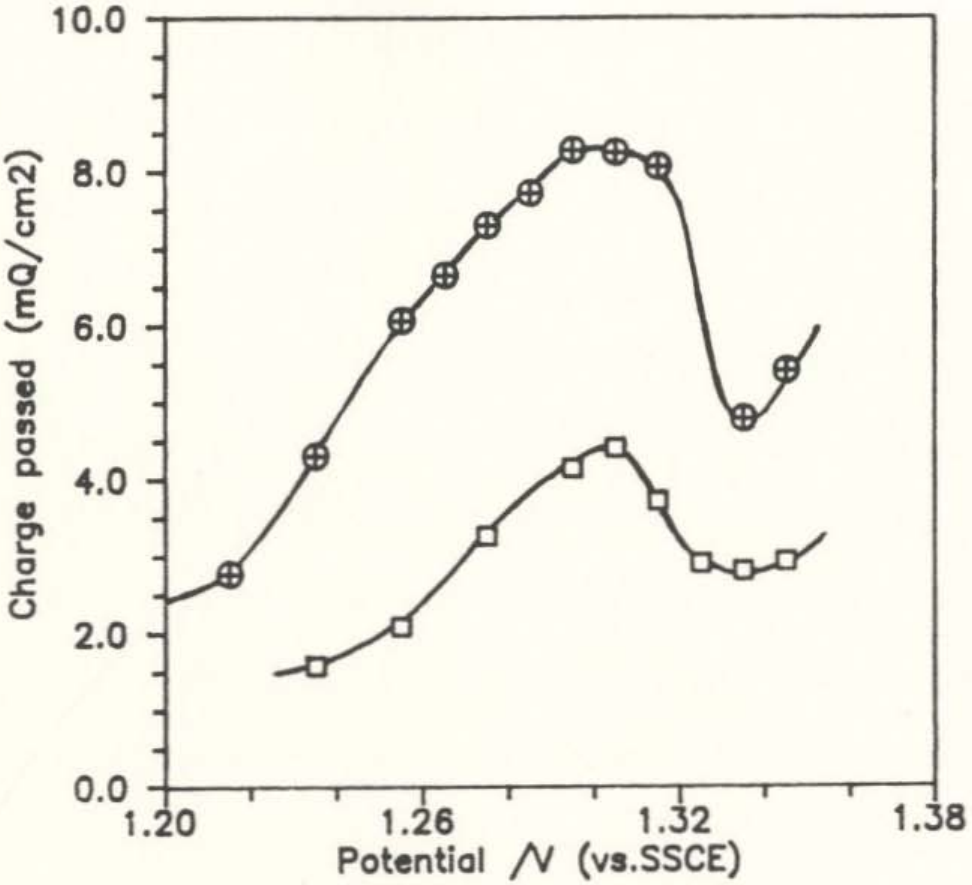

Figure 3.1.6 Charge passed during the first 15 s of the potentiostatic polymerization of MPCA, calculated from Figs.3.1.4 and 3.1.5. The monomer solutions are acetonitrile containing 0.1 M Et_4NClO_4 and 1.25 mM (□) or 2.50 mM (⊕) MPCA.

In studying the potentiostatic polymerization of polypyrrole, Asavapiriyanont and coworkers[4] analyzed the rising current portion of the transient at the intermediate times by plotting I *vs.* t^2. Their results fit the model of three dimensional film growth with instantaneous nucleation[4]. Such a mode of polymer formation is consistent with the space filling appearance of the polypyrrole film[14,15] and its amorphous structure indicated by X-ray diffraction experiments[16-18].

Scharifker *et al*[19] have suggested that in spite of the positive potential imposed on the electrode during polymerization, polypyrrole is formed essentially in its reduced state (during growth) and exhibits a conductivity several orders of magnitude lower than that attained after polymerization is terminated. They therefore attribute the current decrease at long times to an ohmic potential drop across the film. However, the assumption that the growing polymer is in its reduced state is not acceptable. As shown in Figs. 3.1.1 and 3.1.2, there is a reduction wave in each cathodic potential scan following the polymer forming anodic potential scan. Also, in constant current experiments, the electrode potential does not increase at long deposition times at a suitable current density (Fig. 3.1.3) as would otherwise be expected if the growing film was poorly conductive. On the contrary, all the experimental results indicate that a normally growing film is in the oxidized state and exhibits high electronic conductivity.

A decrease in the polymer's conductivity due to overoxidation at too high an electrode potential may cause the potentiostatic current to decrease at long times as observed in Figs. 3.1.4 and 3.1.5. According to Table 3.1.2 for the 2.5 mM MPCA monomer solution, the best current density to use for constant current polymerization is about 0.11 mA cm^{-2}, which corresponds to 1.67 mC cm^{-2} of charge density in the first 15 seconds. Now referring to Fig. 3.1.6, this charge will correspond to a polymerization potential of less than 1.20 V *vs.* SSCE if the polymerization could be carried out potentiostatically. As shown in Fig. 3.1.4 there is no current decrease at long times when the applied potential step is less than 1.235 V. This implies that as long as the electrode potential is less than 1.235 V there will be no significant overoxidation of the film during its preparation. Increasing the potential step above 1.235 V will cause overoxidation of the polymer and thus a decrease in current at long times.

3.1.4. Conclusions

The electrochemical polymerization is a complicated process and can be affected by many factors. The difficulty in preparing reproducible and defect free polymer films may account for the widely different and sometimes contradictory results found in the literature. However, with the polymerization conditions strictly controlled, the quality of the polymer as well as the experimental reproducibility

can be considerably improved.

The oxidation potential of the monomer is related to its structure and can be affected by the surface conditions of the electrode materials, which can exhibit a catalytic affect on the formation of the polymer.

Of the three polymerization methods studied, the potential cycling method is the simplest and is especially useful to test whether a new monomer can be polymerized. The formation of a conducting polymer film is clearly indicated by monotonically increasing redox peaks due to the electroactive polymer film accumulating on the support electrode during potential cycling. The number of potential cycles can be used as a rough control of the thickness of the polymer film. The oxidation potentials of the monomer and the formal potential of the polymer can be estimated from the cyclic voltammograms.

At a given monomer concentration, there is an optimal current density for formation of the polymer at constant current. Too small a current density lowers the polymerization efficiency, while too large a current density causes the polymer to be overoxidized. Overoxidation occurs when the electrode potential rises too high, and consequently the polymer becomes non-conductive. In extreme cases, overoxidation terminates the polymerization process. To prevent overoxidation, a safe upper limit for the electrode potential was determined by examining current-time transients for various potential steps in potentiostatic experiments. The current

decreases at long times due to overoxidation if the applied potential is too high.

Since the monomer can usually be oxidized at a lower electrode potential on its own polymer than on a support electrode material, maintaining a high electrode potential which is necessary for the initial oxidation of the monomer on the bare support electrode renders the polymer vulnerable to overoxidation. This disadvantage of potentiostatic polymerization is overcome in the constant current method, where the electrode potential automatically adjusted favourably as the polymerisation proceeds. An additional advantage of the constant current method is that the coverage of the polymer on the electrode is proportional to the deposition time, which can be used as a convenient way to control the film thickness. In the subsequent studies, the polymer films were all prepared at constant current. Fresh monomer solution was used each time since it was found that an aged monomer solution produces polymer films of poor quality. An aged monomer solution contains soluble oligomeric species which may be responsible for the poor quality of the polymer[20].

3.2 Poly-(3-methyl-pyrrole-4-carboxylic acid)

MPCA was polymerized from 0.01 M solution in acetonitrile containing 0.1

M Et_4NClO_4 at a constant current density of 0.44 mA cm^{-2}. Scanning electron microscopy revealed that deposition of 1 μm of poly-MPCA film requires a polymerization charge of *ca.* 0.3 C cm^{-2}. Although there is considerable uncertainty ($\pm$50%) in the absolute thickness of poly-MPCA films, relative thicknesses (up to 0.6 μm) can be quite precisely controlled by the polymerization charge. A charge to thickness conversion factor of 0.34 C cm^{-2} per micron is used to obtain the quoted thicknesses.

Cyclic voltammetry is a convenient method for the preliminary characterization of a newly prepared polymer film adhering to the electrode. Figs. 3.2.1A and B show cyclic voltammograms of a 0.7 μm poly-MPCA film in acetonitrile and propylene carbonate electrolyte solutions, respectively. The cycling charge ($Q_{cv.} = \int I/\nu \, dV$, where ν is the scan rate) from the slow scan in propylene carbonate (Fig. 3.2.1B, 20 mV s^{-1}) is presented in Fig. 3.2.2. There is a hysteresis in the cycling charge as generally observed for conducting polymers[21-23]. Table 3.2.1 lists some cyclic voltammetric data for poly-MPCA films in acetonitrile containing 0.1 M $LiClO_4$. Data for this polymer in acetonitrile containing 0.1 M Et_4NClO_4 are very similar to those listed in Table 3.2.1.

The cyclic voltammetric charge (Q_{cv}) in Table 3.3.1 is obtained by

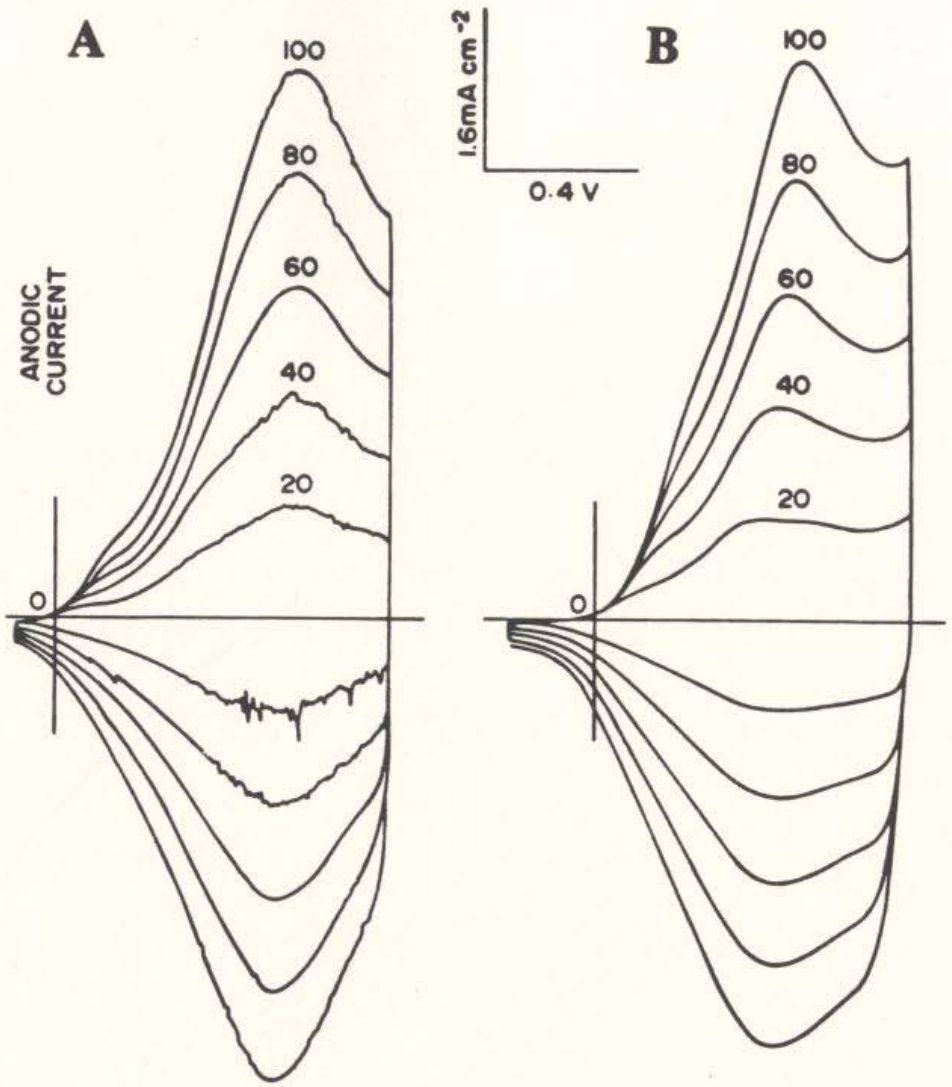

Figure 3.2.1 Cyclic voltammograms of a 0.7 μm poly-MPCA film on a Pt electrode in: (a) acetonitrile containing 0.4 M $LiClO_4$ and (b) propylene carbonate containing 0.8 M $LiClO_4$. The scan rates (mV s^{-1}) are indicated.

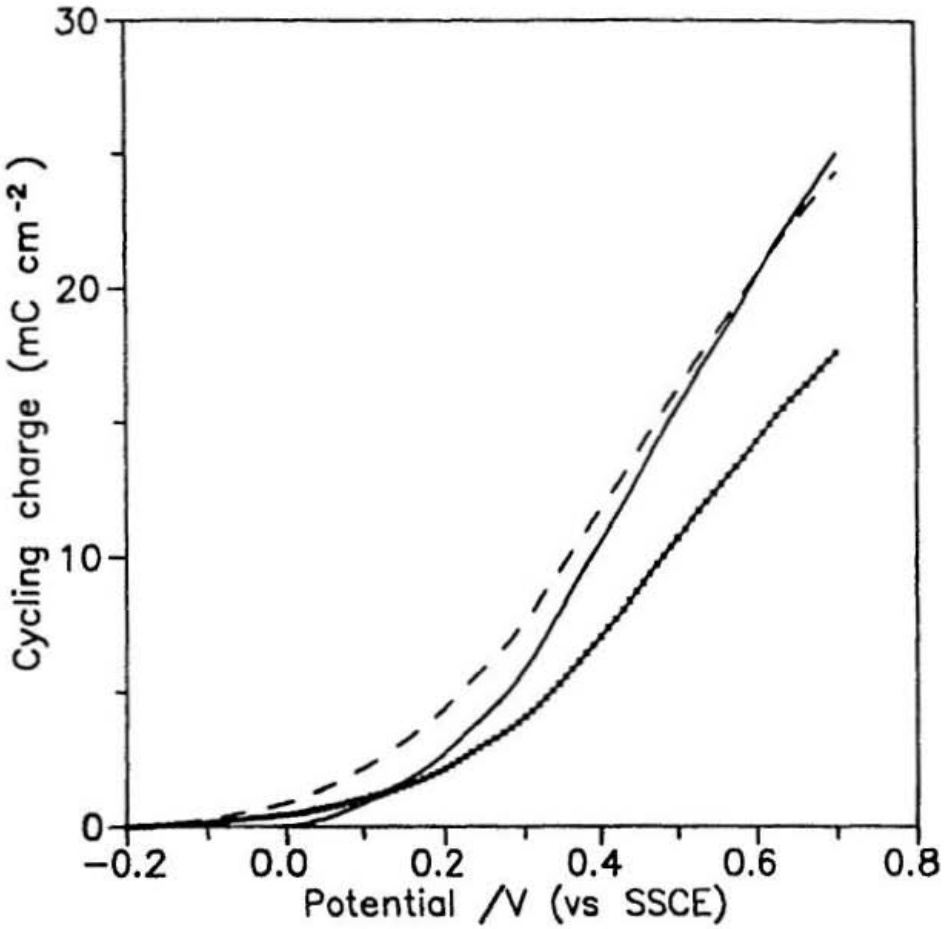

Figure 3.2.2 Plots of cycling charge *vs.* electrode potential for a 0.7 μm poly-MPCA film constructed from the 20 mV s^{-1} voltammetric data in Fig.3.2.1B (——— anodic scan; - - - cathodic scan) and from the capacitance data from impedance spectroscopy in Fig.6.2.8 (+++++).

integrating the anodic current below 0.9 V *vs.* SSCE. There is a linear relationship between the preparation charge (Q_{prp}) and Q_{cv} as shown by the near constant ratio of these two values. The formal potential ($E^{\circ\prime}$) of the polymer redox reaction is obtained by averaging the anodic and cathodic peak potentials. As the film thickness increases, the peak potential separation (E_{pa}-E_{pc}) increases and the formal potential ($E^{\circ\prime}=(E_{pa}+E_{pc})/2$) shifts anodically. Both the anodic peak current (I_{pa}) and the cathodic current (I_{pc}) increase with increasing film thickness, and the ratio of I_{pa}/I_{pc} is nearly constant. The voltammetric capacitances ($C_{V,cv}$) (obtained as $C_{V,cv} = (I_a+I_c)/2\nu d$) at 0.8 V of thin films are small relative to those of thicker films. Similar results have been observed in the values of ac capacitances ($C_{V,ac}$) from impedance measurements and the possible cause is discussed in section 6.2.1.

A polymer film of poor quality can be identified by the irregular shape of its cyclic voltammogram (*e.g.* $Q_{cv}/Q_{prp} < 0.12$ and $I_{pa}/I_{pc} > 1.4$) and thus is rejected. Table 3.2.2 lists peak currents and peak potentials for a 0.7 μm poly-MPCA films on a Pt electrode in acetonitrile containing 0.1 M Et_4NClO_4. The anodic peak current increases linearly with the scan rate up to at least 400 mV s^{-1} while the cathodic peak current shows a linear response to only *ca.* 200 mV s^{-1} as shown in Fig. 3.2.3. Increasing scan rate increases the peak potential separation as shown in Fig. 3.2.4. However, even at very low scan rates (*e.g.* 1 mV s^{-1})

there is still a significant peak potential separation of *ca.* 50 mV.

Table 3.2.1 Cyclic voltammetric data for poly-MPCA film coated Pt electrodes in acetonitrile containing 0.1 M $LiClO_4$ at a scan rate of 60 mV s^{-1}.

Thickness /μm	0.14	0.28	0.42	0.56	0.70	0.98	1.30
Q_{cv} /mC cm^{-2}	6.91	14.0	20.2	25.2	34.1	46.7	63.9
Q_{cv}/Q_{prp}	0.144	0.146	0.140	0.131	0.142	0.139	0.144
I_{pa}/ mA cm^{-2}	0.53	1.19	1.64	2.42	2.80	4.31	5.67
I_{pc}/ mA cm^{-2}	0.40	0.97	1.37	1.73	2.22	3.42	4.61
I_{pa}/I_{pc}	1.33	1.23	1.20	1.29	1.26	1.26	1.23
$C_{V,cv}$/ F cm^{-3}	320	369	407	429	415	433	450
E_{pa}/ V	0.605	0.615	0.630	0.650	0.660	0.680	0.655
E_{pc}/ V	0.535	0.555	0.555	0.545	0.540	0.555	0.555
E°/ V	0.57	0.59	0.59	0.60	0.60	0.62	0.61
E_{pa}-E_{pc}/ mV	70	60	75	105	120	125	100

For an immobilized electroactive thin film of Nernstian behaviour, the full peak width at half maximum (E_{FWHM}) of the cyclic voltammogram peaks is 90.6/n mV and the peak potential separation is zero[24,25]. The non-zero peak potential separation (Table 3.2.1) suggests that the redox reaction produces conformation changes in the polymer[21,26,27]. The broad peak shown in Fig. 3.2.1 has a value of

E_{FWHM} at least 200 mV. The broadening may be due to repulsive interactions between the electroactive sites[25,28] and/or the distribution of polymer formal potentials[28-32] as have been discussed in the literature for redox polymers.

Table 3.2.2 Cyclic voltammetric data for a 1.0 μm poly-MPCA film coated Pt electrode in acetonitrile containing 0.1 M Et_4NClO_4.

Scan rate mV s^{-1}	I_{pa} mA cm^{-2}	I_{pc} mA cm^{-2}	E_{pa} V	E_{pc} V
1	0.07	0.07	0.645	0.655
3	0.21	0.18	0.640	0.600
5	0.34	0.32	0.640	0.585
10	0.69	0.63	0.640	0.580
20	1.34	1.20	0.650	0.570
40	2.71	2.38	0.665	0.565
60	4.12	3.47	0.680	0.560
80	5.49	4.68	0.685	0.560
100	6.69	5.84	0.700	0.550
200	13.4	11.4	0.735	0.520
300	20.1	16.7	0.770	0.500
400	26.5	21.6	0.800	0.475

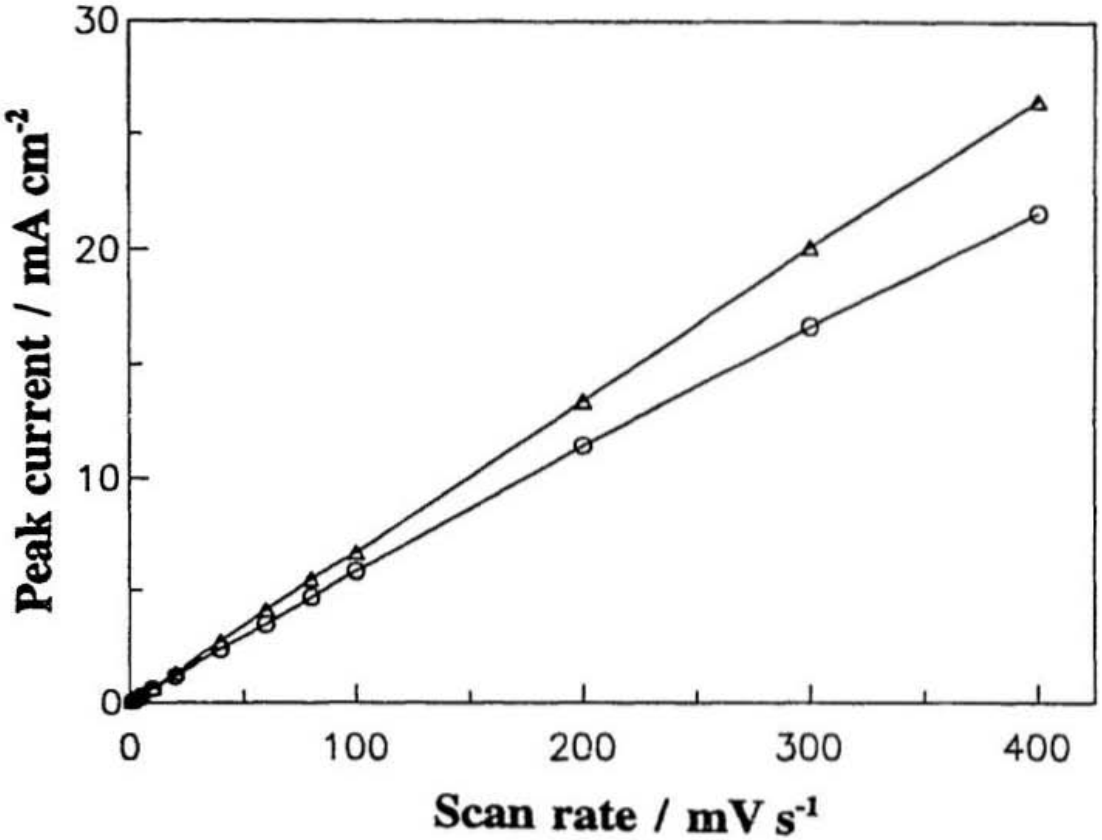

Figure 3.2.3 Plot of anodic (△) and cathodic (○) peak currents *vs.* potential scan rates for a 0.7 μm poly-MPCA film coated Pt electrode in 0.1 M Et_4NClO_4 acetonitrile solution.

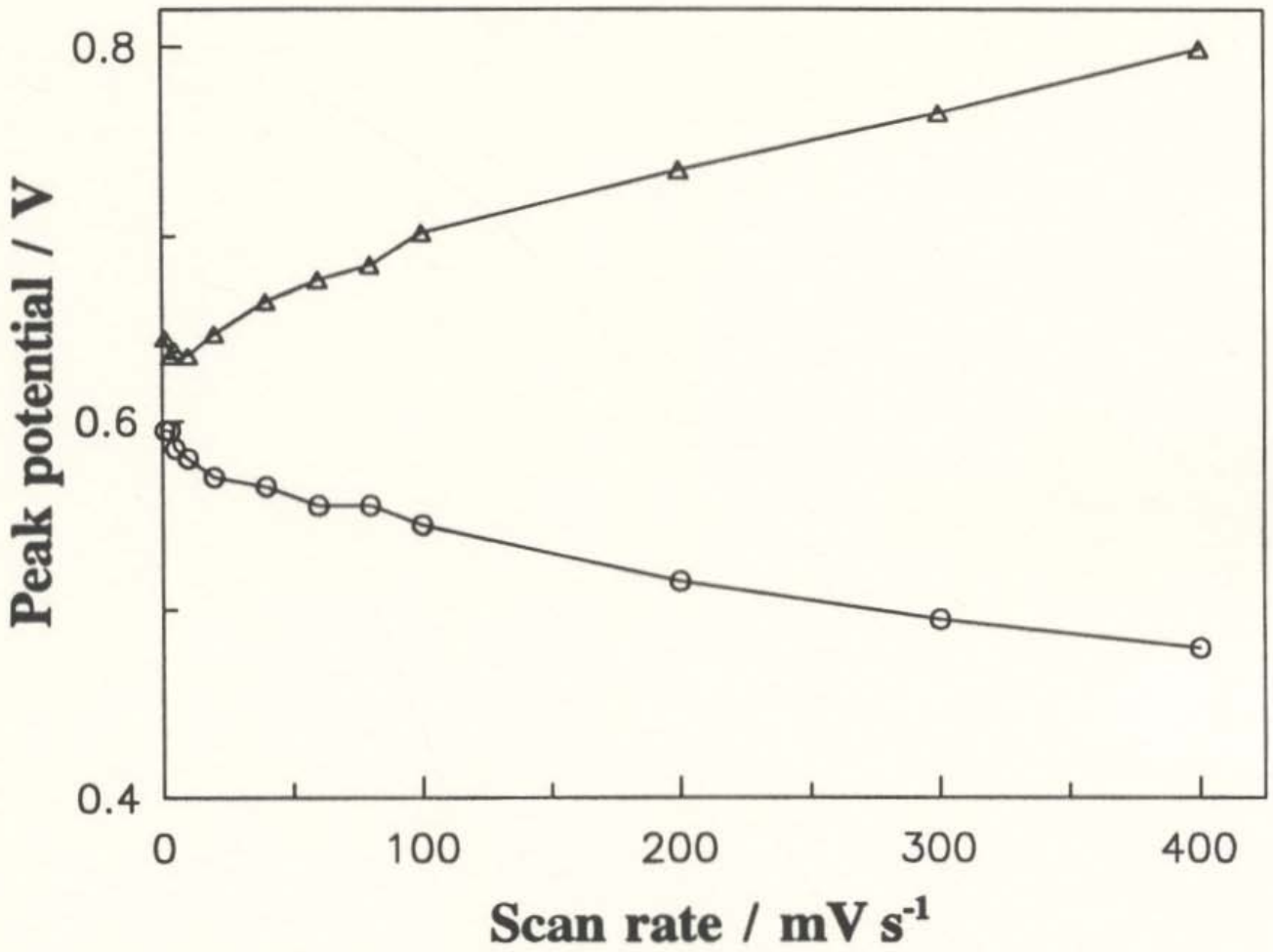

Figure 3.2.4 Plot of anodic (△) and cathodic (○) peak potentials *vs.* potential scan rates for a 0.7 μm poly-MPCA film coated Pt electrode in 0.1 M Et_4NClO_4 acetonitrile solution.

3.3 Polypyrrole/perchlorate and Polypyrrole/poly(styrene sulphonate)

The polymer films were prepared from aqueous solutions containing 0.5 M pyrrole and 0.5 M supporting electrolyte ($NaClO_4$ or NaPSS) using a constant anodic current density of 0.88 mA cm^{-2}. The concentration of poly(sodium 4-styrene sulphonate) was calculated based on the sulphonate unit. The electrode potential during polymerization remained steady at *ca.* 0.47 V *vs.* Ag/AgCl in both electrolytes.

PPY/ClO_4^- and PPY/PSS both had similar compact and homogeneous morphology when observed using the scanning electron microscope (SEM). A linear relationship between thickness and deposition charge was found for PPY/PSS films up to 3 μm (Fig. 3.3.1). Deposition of 2 μm PPY/ClO_4^- or PPY/PSS requires *ca.* 0.48 C cm^{-2}.

The composition of PPY/PSS films was determined by quantitative IR absorbance measurements. In these experiments, the polymer film was prepared on a 0.456 cm^2 Pt disc electrode using a charge of 0.6 C. Since *ca.* 2.25 electrons are required to polymerize each pyrrole unit, the mass of polypyrrole in each film

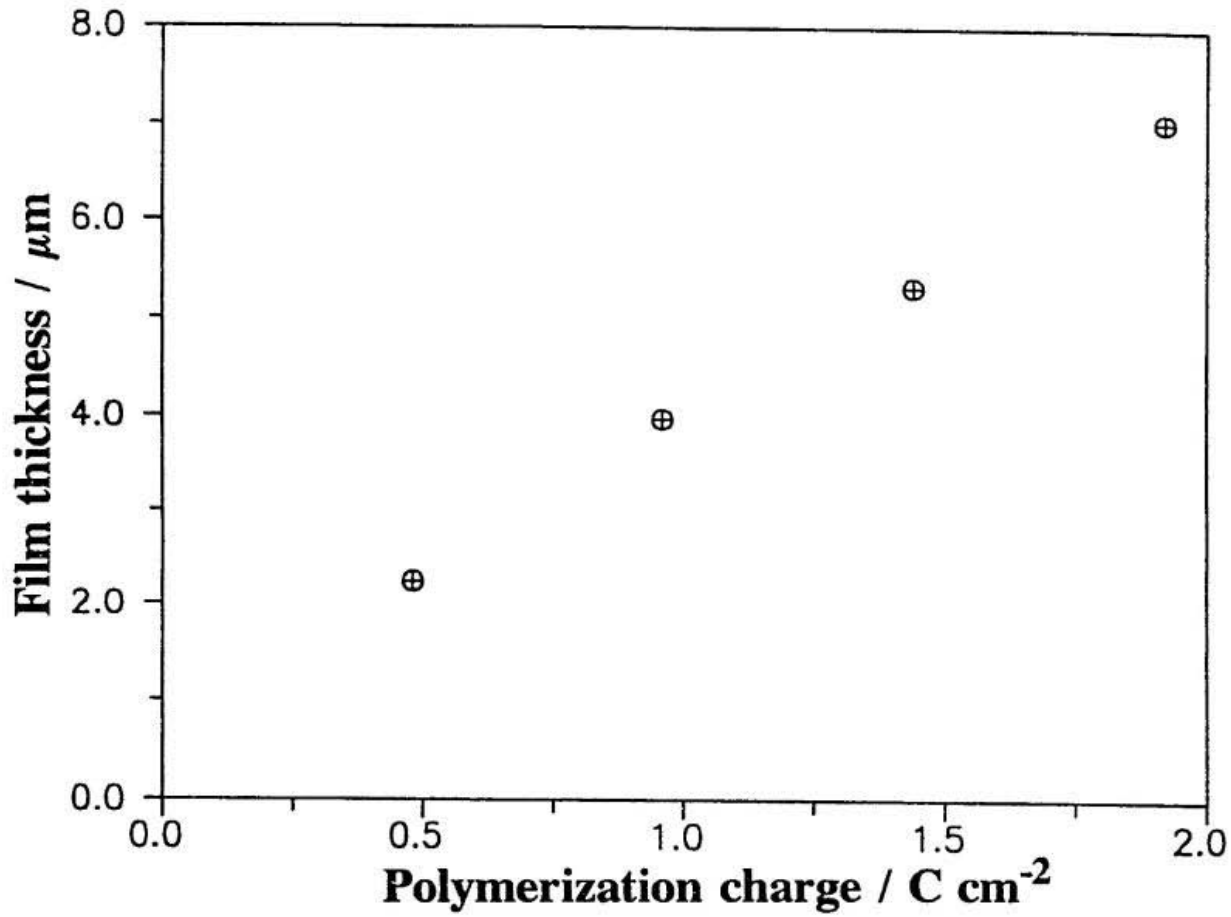

Figure 3.3.1 Plot of PPY/PSS film thickness *vs.* deposition charge.

should have been 0.18 mg. Prior to removal from the monomer solution, each film was reduced at -0.9 V for 5 min in 0.2 M $NaClO_4$ (aq). Then, after rinsing with water and acetone, and drying in air, it was peeled from the electrode and weighed. From three films, a reproducible mass of 0.37 mg per film was obtained.

The content of NaPSS in each PPY/PSS film was determined by using quantitative IR analysis. Each polymer film (0.37 mg) was ground with 150 mg KBr (Infrared Grade, Spectrex LTD) and pressed under vacuum into a transparent pellet of 1 cm in diameter. Three NaPSS standards and one neat KBr pellet were prepared similarly. IR spectra were collected using a Mattson Polaris FTIR spectrometer at 2 cm^{-1} intervals and averaged for 300 scans. After subtracting the background absorbance of the neat KBr pellet, the peak height of the characteristic SO_3^{-1} band at 1200 cm^{-1} was used as the analytical signal. It was found that each PPY/PSS film contained 0.14 mg NaPSS. Combining this result with the expected mass of polypyrrole, it can be concluded that the molar ratio of pyrrole:sulphonate in the PPY/PSS composite is 4:1. There is a discrepancy between the measured (0.37 mg) and expected (0.32 mg) masses. This is presumably due to water remaining in the air-dried polymer films. Based on chemical analysis of the nitrogen to sulphur ratio for the PPY/PSS composite, Shimidzu and co-workers[33] have found that there is approximately one sulphonate anion incorporated into the composite for every four to five pyrrole units.

3.4 Poly-[1-methyl-3-(pyrrol-1-ylmethyl)pyridinium]

Poly-MPMP thin films were polymerized on to Pt electrodes from a 20 mM monomer solution in acetonitrile containing 0.1 M Et_4NClO_4 at an anodic current density of 0.44 mA cm^{-2}. The electrode potential remained at about 1.08 V vs SSCE with little variation during polymerization. Polymer film thickness was estimated from the deposition charge using the relationship (150 mC cm^{-2} per micron) reported by Mao and Pickup[34]. The polymer films were preliminarily characterized by cyclic voltammetry after the polymer electrode was removed from the monomer solution and washed with the test electrolyte solution. In the case of propylene carbonate solution a special procedure was followed. After the electrode was removed from the monomer solution, the film was washed with acetone, allowed to dry in air for 5 min. and then soaked in propylene carbonate electrolyte solution for about 4 hours.

Fig. 3.5.1 shows cyclic voltammograms of a poly-MPMP film coated Pt electrode in water + 0.1 M $NaClO_4$, acetonitrile + 0.1 M Et_4NClO_4 and propylene carbonate + 1.6 M $LiClO_4$. In all three solutions, the cyclic

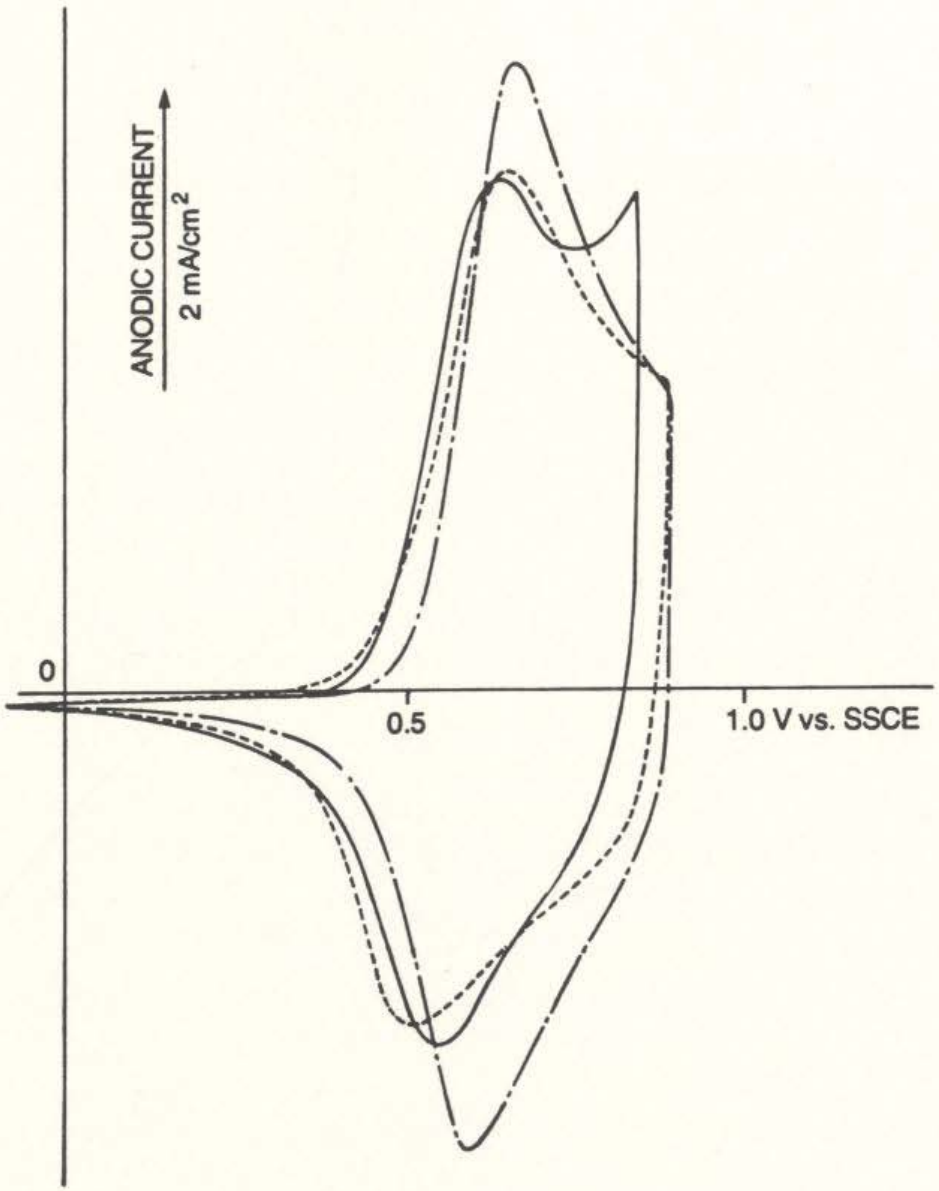

Figure 3.4.1 Cyclic voltammograms of 1.6 μm poly-MPMP film coated Pt electrode in acetonitrile + 0.1 M Et_4NClO_4 (——), water + 0.1 M $NaClO_4$ (- -) and propylene carbonate + 1.6 M $LiClO_4$ (·····). The scan rate is 60 mV s^{-1}.

voltammograms exhibit very symmetrical waves with small peak potential separations as compared with the cyclic voltammograms of PPY/ClO_4^- (Fig. 7.3.1A). The cyclic voltammograms of poly-MPMP in acetonitrile and propylene carbonate solutions are similar in shape as well as size. However, changes occur in aqueous solution as shown by the increased peak currents and anodic shift of both peak potentials. The peak potential separations in the three solvents decrease in the order of propylene carbonate (*ca.* 140 mV), acetonitrile (*ca.* 100 mV), and water(*ca.* 70 mV). This order parallels the decreasing ionic conductivity of the polymer (section 5.3) in these solvents.

References

(1) Casas, R.; Dicko, A.; Ribo, J.M.; Valles, M.A.; Ferrer-Anglada, N.; Bonnett, R.; Hanly, N.; Bloor, D. *Synth. Met.* 1990,*39*,275.

(2) Pickup, P.G. *J. Electroanal. Chem.* 1987,*225*,273.

(3) Fletcher, S.; Halliday, C.S.; Gates, D.; Westcott, M.; Lwin, T.; Nelson, G. *J. Electroanal. Chem.* 1983,*159*,267.

(4) Asavapiriyanont, S.; Chandler, G.K.; Gunawardena, G.A.; Pletcher, D. *J. Electroanal. Chem.* 1984,*177*,229.

(5) Downard, A.J.; Pletcher, D. *J. Electroanal. Chem.* 1986,*206*,147.

(6) Tourillon, G.; Garnier, F. *J. Electroanal. Chem.* 1984,*161*,51.

(7) Ferraris, J.P.; Newton, M.D. *Polymer* 1992,*33*,391.

(8) Witkowski, A.; Freund, M.S.; Brajter-Toth, A. *Anal. Chem.* 1991,*63*,622.

(9) John, R.; Wallace, G.G. *J. Electroanal. Chem.* 1991,*306*,157.

(10) Raymond, D.E.; Harrison, D.J. *J. Electroanal. Chem.* 1990,*296*,269.

(11) Beck, F.; Oberst, M. *J. Electroanal. Chem.* 1990,*285*,177.

(12) Andrieux, C.P.; Grzeszczuk, M.; Saveant, J.M. *J. Electroanal. Chem.* 1991,*318*,369.

(13) Andrieux, C.P.; Audebert, P.; Hapiot, P.; Saveant, J.M. *Synth. Met.* 1991,*43*,2877.

(14) Diaz, A.F.; Kanazawa, K.K.; Gardini, G.P. *J. Chem. Soc., Chem. Commun.* 1979,,635.

(15) Kanazawa, K.K.; Diaz, A.F.; Geiss, R.H.; Gill, W.D.; Kwak, J.F.; Logan, J.A.; Rabolt, J.F.; Street, G.B. *J. Chem. Soc., Chem. Commun.* 1979,,854.

(16) Kanazawa, K.K.; Diaz, A.F.; Gill, W.D.; Grant, P.B.; Street, G.B.; Gardini, G.P.; Kwak, J.F. *Synth. Met.* 1980,*1*,329.

(17) Warren, L.F.; Anderson, D.P. *J. Electrochem. Soc.* 1987,*134*,101.

(18) Warren, L.F.; Walker, J.A.; Anderson, D.P.; Rhodes, C.G.; Buckley, L.J. *J. Electrochem. Soc.* 1989,*136*,2286.

(19) Scharifker, B.R.; Garciapastoriza, E.; Marino, W. *J. Electroanal. Chem.* 1991,*300*,85.

(20) Satoh, M.; Imanishi, K.; Yoshino, K. *J. Electroanal. Chem.* 1991,*317*,139.

(21) Heinze, J.; Bilger, R.; Meerholz, K. *Ber. Bunsenges. Phys. Chem.* 1988,*92*,1266.

(22) Feldberg, S.W.; Rubinstein, I. *J. Electroanal. Chem.* 1988,*240*,1.

(23) Kalaji, M.; Peter, L.M. *J. Chem. Soc., Faraday. Trans.* 1991,*87*,853.

(24) Hubbard, A.T.; Anson, F.C. *Electroanal. Chem.* 1970,*4*,129.

(25) Brown, A.P.; Anson, F.C. *Anal. Chem.* 1977,*49*,1589.

(26) Diaz, A.F.; Crowley, J.; Bargon, J.; Gardini, G.P.; Torrance, J.B. *J. Electroanal. Chem.* 1981,*121*,355.

(27) Meerholz, K.; Heinze, J. *Ange. Chem.* 1990,*29*,692.

(28) Smith, D.F.; Willman, K.; Kuo, K.; Murray, R.W. *J. Electroanal. Chem.* 1979,*95*,217.

(29) Laviron, E. *J. Electroanal. Chem.* 1979,*100*,263.

(30) Laviron, E. *J. Electroanal. Chem.* 1979,*105*,25.

(31) Laviron, E. *J. Electroanal. Chem.* 1979,*105*,35.

(32) Lennox, J.C.; Murray, R.W. *J. Am. Chem. Soc.* 1978,*100*,3710.

(33) Shimidzu, T.; Ohtani, A.; Iyoda, T.; Honda, K. *J. Electroanal. Chem.* 1987,*224*,123.

(34) Mao, H.; Pickup, P.G. *J. Electroanal. Chem.* 1989,*265*,127.

Chapter 4

Impedance Spectroscopy of Electroactive Films

4.1 Introduction

Many applications of conducting polymers arise from their reversible switching between the doped and undoped states[1-4]. During switching, both electron and ion transport occur within the polymer film which is generally immersed in an electrolyte solution. Because the mass and charge transport processes accompanying switching are directly related to fundamental properties, such as electronic and ionic conductivity[5] and ionic permeability[6,7], and are crucial to the applications, they have been the focus of intensive research.

Compared to cyclic voltammetry and other techniques involving a large potential perturbation, impedance spectroscopy (IS) has the advantage of perturbing the system only slightly from its equilibrium state with 5-10 mV peak-to-peak sinusoidal signals[8,9]. This is particularly important in the study of conducting polymers, since large perturbations cause structural/morphological changes in the polymer[10-13] and may induce an inhomogeneous state[14]. Using a small potential

perturbation also reduces the measurement error caused by the technique itself, since in large potential perturbation experiments measurement errors can occur due to inadequate control of the electrode potential. An additional benefit of using a low amplitude perturbation is that the response can be assumed to follow a linear current-potential characteristic, which simplifies the theoretical treatment[15].

In impedance measurements, a sinusoidal stimulating signal (it can either be current or voltage, but in this thesis only potential perturbation was used) of constant amplitude and known frequency is applied to the working electrode, which is usually held at a steady state by a dc-bias potential. The phase and the magnitude of the system response (current) are determined. The impedance (Z) is defined as the ratio of the ac input voltage (V) against the ac current (I) of the system response. For convenient mathematical manipulation, the impedance can be expressed as a complex number:

$$Z=Z'+jZ'' \qquad [4.1.1]$$

which is denoted by a point (Z',Z") in the complex impedance plane, where Z' and Z" are the real (in phase) and imaginary (90° out of phase) components of the impedance, respectively. With measurements made over a wide-enough frequency range, various processes, such as interfacial charge transfer and bulk charge

transport during the redox switching of a conducting polymer, may be separated through the difference in their time constants. Often these time constants are also a function of the electrode potential and the properties of the bathing electrolyte solution. Therefore, changing these experimental conditions can cause additional separation. In contrast, the system response in pulse transient experiments is observed in the time domain, and decoupling the overlapping responses is usually difficult.

High precision measurements are usually obtained with the impedance methods because the system response is intrinsically stable and the signal at each frequency can be averaged over a unlimited period of time. Indeed, the reproducibility of the impedance measurements in this study was found to be limited mainly by the reproducibility of the electrochemical polymerization of the polymer films. With precaution to prevent deterioration of the polymer film at extreme dc bias potentials and to avoid changes in the concentration of the electrolyte solution due to solvent evaporation during the experiments, measurements on a single polymer film can be remarkably reproducible (relative standard deviation $< 5\%$).

To understand electrochemical processes, the system impedance response is analyzed according to an equivalent circuit which contains circuit elements such as resistors, capacitors and sometimes inductors. Unfortunately, a circuit which

can reproduce a given system's impedance response is not unique. The best equivalent circuit should contain the least number of circuit elements[15], and more importantly each circuit element must have a defined physical meaning. The objectives of an impedance experiment are thus to find the most appropriate equivalent circuit to represent the electrochemical system under study and to determine the value of each circuit element from the experimental data to quantify the electrochemical parameters.

The complex phenomena involved in the electrochemistry of conducting polymers have rendered it difficult to extract unambiguous information from impedance data, and even to select an appropriate kinetic model. Some authors[9,16-20] have used the model proposed for redox polymers[21] and metal oxide electrodes[22] to explain their impedance data. In their treatment, the movement of charge balancing ions is assumed to be a diffusion process driven by concentration gradients. Others[23-33] believe that the polymer film behaves like a porous electrode[34-36], where ion movement within the polymer matrix is due to migration and is driven by a potential gradient. Discrepancies often arise when results from the two different models are compared[23,37]. Additional complications arise due to individual habits in preparing and handling the polymers. The complex electrochemical polymerization processes often leaves the researcher with less than complete control over the quality of the final polymers. Overoxidation of the

polymer film can easily occur during the electrochemical polymerization step (section 3.1). Such difficulty in preparing a typical and defect free polymer accounts partly for the widely varied impedance data reported for conducting polymers. For example, some authors have reported a high frequency semicircle in complex plane impedance plots for oxidized polypyrrole films[14,16,26,38] which have not been observed by others[9,18,27,39,40]. In many cases the origin of this semicircle is not well understood. A variety of temporary explanations have appeared such as a charge transfer resistance in parallel with the double layer capacitance of the underlying electrode[16], the polymer's electronic resistance in parallel with its bulk capacitance[26], an ion transfer resistance in parallel with the polymer's double layer capacitance[41,42], or some other parallel resistance-capacitance combination[38]. Obviously, different types of polymers or the same type of polymer but handled differently may require different models to describe their impedance responses. Furthermore, equivalent circuits which incorporate different opinions and assumptions can also provide far different results from the same set of experimental impedance data.

4.2 Models of Electroactive Polymer Film Electrodes

Current theories of charge transport in electroactive polymer film coated electrodes can be divided into three groups, the redox layer model, the porous electrode model and the metal oxide electrode model. The metal oxide electrode model was deduced by Ho and coworkers[22] in studying lithium (a neutral electroactive species) insertion in tungsten trioxide (conducting and electroactive) thin film electrodes. They treated the insertion of lithium into the electrode as driven by diffusion, not by migration. Since this model is inappropriate for the insertion of ions into a conducting polymer, only the redox layer model and the porous electrode model will be discussed in this section.

4.2.1 Redox Layer Model

This type of theory has been used to describe the impedance responses of redox polymer modified electrodes. In these systems an oxidized or reduced species is generated at the electrode/thin layer interface, and its movement through the film is diffusion controlled, but restricted to the thin layer. Gabrielli *et al*[21,43] proposed a model which includes the interfacial kinetics and charge transport for

a reversible redox polymer film. They treated charge transport in the polymer film as a diffusion process, which occurs through a bimolecular self-exchange reaction between adjacent oxidized and reduced sites. A simpler model with no interfacial process can be derived under the following assumptions:

1. Counterion movement is facile and does not limit electron hopping rate;
2. Electron transport within the film obeys Fick's second law;
3. Electron movement is blocked at the polymer/solution interface;
4. Electron transfer at the electrode/polymer interface is fast so that Nernstian equilibrium is always maintained there.

The general impedance response of the polymer coated electrode according to this model would be:

$$Z = \frac{r \coth(d\, s')}{s'} \qquad [4.2.1]$$

where:

$$r = \frac{R\ T}{F^2\, A\, D\, \frac{\overline{c_O}\ \overline{c_R}}{c}}$$

and

$$s' = \sqrt{\frac{j\omega}{D}}$$

$\overline{c}_O$ and $\overline{c}_R$ are the average concentrations of oxidized and reduced sites respectively, ω is the angular frequency of rotation. D is the diffusion coefficient for the electron hopping process, d the film thickness and A the electrode area. The

symbols R, T, and F have their usual meanings. The parameter r has the dimensions of Ω cm^{-1}, and thus represents the resistance per unit film thickness.

The mathematical form of eq. [4.2.1] is exactly the one that describes the impedance of the transmission line[44,45] shown in Fig. 4.2.1, which may therefore be considered as a possible electrical equivalent circuit.

Simplified forms of eq.[4.2.1] can be obtained for two extreme cases. First, consider the impedance at the high frequency limit: As $\omega \rightarrow \infty$,

$$Z_{\omega \rightarrow \infty} = \sqrt{\frac{D}{\omega}}\, r\,(1 - j) \qquad [4.2.2]$$

which corresponds to a Warburg impedance (Z_w)[46]. The real component (Z') of the impedance equals the imaginary component (Z''), and varies with frequency as $\omega^{-1/2}$:

$$|Z'_w| = |Z''_w| = \sqrt{\frac{D}{\omega}}\, r \qquad [4.2.3]$$

The Warburg impedance (Z_w) is independent of the film thickness (d) in this high frequency range. That is, the restricting effect of the finite film thickness is not felt and the film appears infinitely thick to the potential perturbation. The phase angle (θ) between the ac current and potential perturbation is:

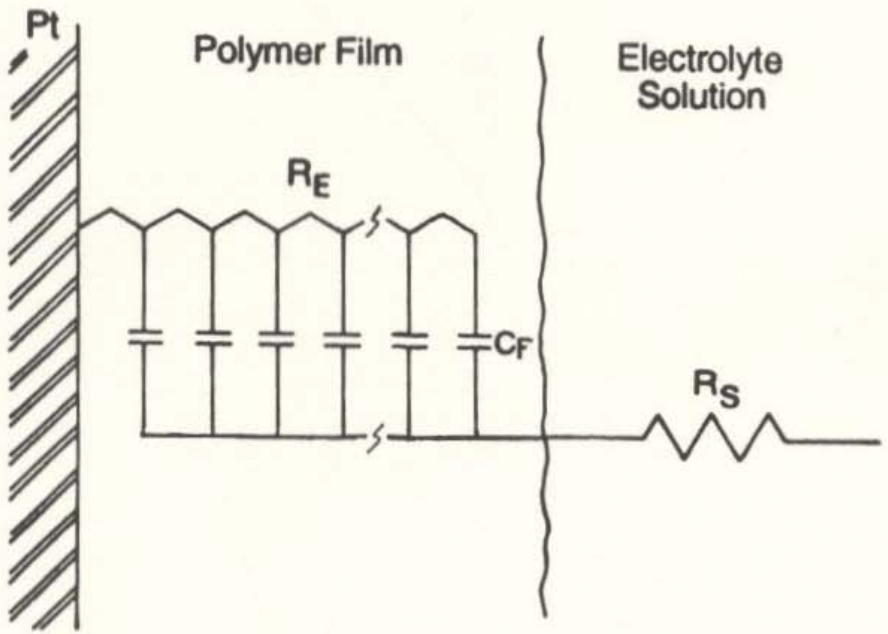

Figure 4.2.1 Equivalent circuit for slow electron hopping. The uncompensated bulk electrolyte solution resistance (R_s) which is not included in theoretical equations is added.

$$\theta = \arctan\left(\frac{|Z''_w|}{|Z'_w|}\right) = \arctan(1) = \frac{\pi}{4} \qquad [4.2.4]$$

and is independent of the frequency.

The other simplified case occurs at the low frequency limit:

As $\omega \rightarrow 0$,

$$Z_F(\omega \rightarrow 0) \sim \frac{r\,d}{3} + \frac{r\,D}{j\,\omega\,d} \qquad [4.2.5]$$

which corresponds to the impedance of a resistor (R_{lf}) and capacitor (C_{lf}) in series, where;

$$R_{lf} = \frac{r\,d}{3} \qquad [4.2.6]$$

$$C_{lf} = \frac{d}{r\,D} \qquad [4.2.7]$$

Therefore the low frequency data form a vertical line in the complex impedance plane. The projected length of the 45° Warburg line on the real axis is one third of the total resistance of the transmission line (rd).

According to the first assumption above, the resistive rail of the

transmission line circuit shown in Fig. 4.2.1 represents the slow election hopping process while the fast counterion movement is represented by the zero resistance rail. The distributed capacitance represents the redox reaction involved in the impedance measurement.

Limitation of charge transport in a redox polymer by the movement of counterions has been encountered in a number of experiments[47-51]. This coupled electron and ion movement has been treated theoretically by Savéant and coworkers[52-57], and by Buck and coworkers[45,58-61]. They have derived modified diffusion/migration equations to describe electron transport between fixed sites.

Mathias and Haas[62] have proposed an impedance model for redox polymer coated electrodes using the modified diffusion/migration equation for electron hopping and the standard Nernst-Planck equations for counterion movement. They have assumed that the redox reaction of the polymer layer starts at the electrode/polymer interface.

Albery and coworkers[63] have also proposed an impedance model for modified electrodes and thin layer cells. From the fundamental transport equations, they[63] related electron and counterion charge transport to a novel transmission line circuit similar to that shown in Fig. 4.2.2, where R_E and R_{Ion} are the distributed polymer electronic and ionic resistances, respectively, across the polymer thickness.

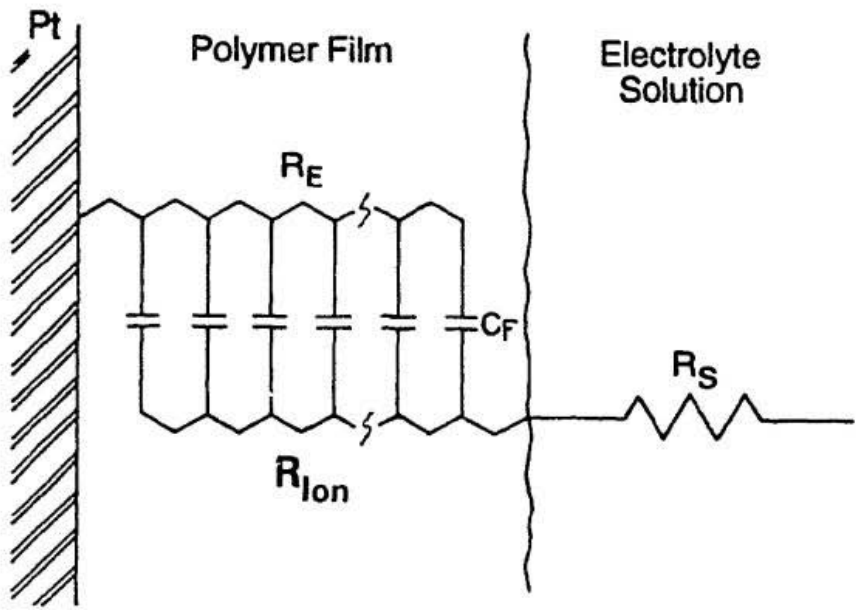

Figure 4.2.2 Albery's dual rail transmission line circuit. R_s which is not included in theoretical equations is added.

The polymer's capacitance (C_F), which is also distributed uniformly across the film, has been described by Feldberg[64] as an indistinguishable combination of a faradaic pseudo capacitance and a double layer capacitance. The current flows across the electrode/polymer interface through the metallic contact only and the polymer/solution interface through the ionic contact only. Albery's model differs from previous work in that the potentials that drive the current through the polymer rail and solution rail of the transmission line are the modified Nernst potential and modified Donnan potential respectively.

Since the experimental results of this work can be best analyzed with Albery's model, a detailed discussion of the model's equations and method of experimental data analysis is given here. The impedance is[14]

$$Z/R_{\Sigma} = \rho + \frac{2\rho}{s^{1/2}\sinh(s)^{1/2}} + \frac{1-2\rho}{s^{1/2}\tanh(s)^{1/2}} \qquad [4.2.8]$$

where

$$\rho = \frac{R_E R_{Ion}}{R_{\Sigma}^2}$$

$$s = j\ \omega\ R_{\Sigma}\ C_{\Sigma}$$

The C_{Σ} is the combined capacitance defined in eq. 11 of Ref. 19 and equals approximately C_F. By plotting the imaginary impedance at low frequency vs. 1/frequency, C_F is calculated from the slope of the linear plot ($C_F = 1/(2\pi$ slope)). R_{Σ} is the sum of R_E and R_{Ion}.

The film electronic and ionic resistances can be obtained from measurements of the impedance plotted in the complex impedance plane, using the following two equations[14].

$$\frac{1}{R_{\infty}} = \frac{1}{R_E} + \frac{1}{R_{Ion}} \qquad [4.2.9]$$

$$R_{\Sigma} = R_E + R_{Ion} \qquad [4.2.10]$$

where R_{∞} is the high frequency intercept of the 45° Warburg-type region in the complex plane impedance plot minus the uncompensated solution resistance (R_s),

and $R_\Sigma/3$ is the theoretically constant real impedance at low frequency minus R_s. However, in almost all reported impedance experiments on conducting polymers, instead of the ideal vertical line for an ideal capacitance response at low frequency a slightly titled line has been obtained. The value of $(R_s + R_\Sigma/3)$ is thus obtained by extrapolating the experimental data at low frequency to the real axis. Since the impedance data form a characteristic shape in the complex impedance plane, most of the data has been analyzed using the above method in this thesis.

R_E and R_{Ion} can also be obtained by analyzing the high frequency data on the Warburg-type line. For this region, plots of $|Z - R_\infty - R_s|^2$ *vs.* $1/\omega$ form a straight line as predicted by eq, [4.2.11], which is derived from eq. [4.2.8][65]

$$|Z - R_\infty - R_s|^2 = \frac{R_\Sigma (1 - 2\rho)^2}{\omega C_F} \qquad [4.2.11]$$

When R_E and R_{Ion} are very different, Eq. [4.2.11] is reduced to the form given by Jakobs and coworkers[27].

4.2.2 Porous Electrode Theory

The impedance response of a porous carbon electrode in a sulphuric acid

solution[34] can be described using the simple model of a single uniform pore. The mathematic form of the impedance response is[34]:

$$Z = \sqrt{\frac{R_{Ion}}{j\omega\ C}}\ \coth\sqrt{j\omega\ R_{Ion}\ C} \qquad [4.2.12]$$

where R_{Ion} is the total ionic resistance in the pore and C the total distributed interfacial capacitance of the pore. The equivalent circuit for this impedance is the simple transmission line shown in Fig. 4.2.3. The resistive path here represents the slow migration of ions in the pore solution and the zero resistance rail the fast electron transport in the electronically conducting electrode material.

Further extensions of the porous electrode model include the electrode rail resistance (R_E) and an electrochemical reaction at the electrode/pore solution interface. The equivalent circuit is then the same as shown in Fig. 4.2.2[28,29,35] and the values of R_E, R_{Ion} and C_F can be derived from the experimental impedance data in the same way as for Albery's redox model. It is at this point that Albery's redox model derived from a microscopic point of view agrees with the porous electrode model derived from a macroscopic point of view.

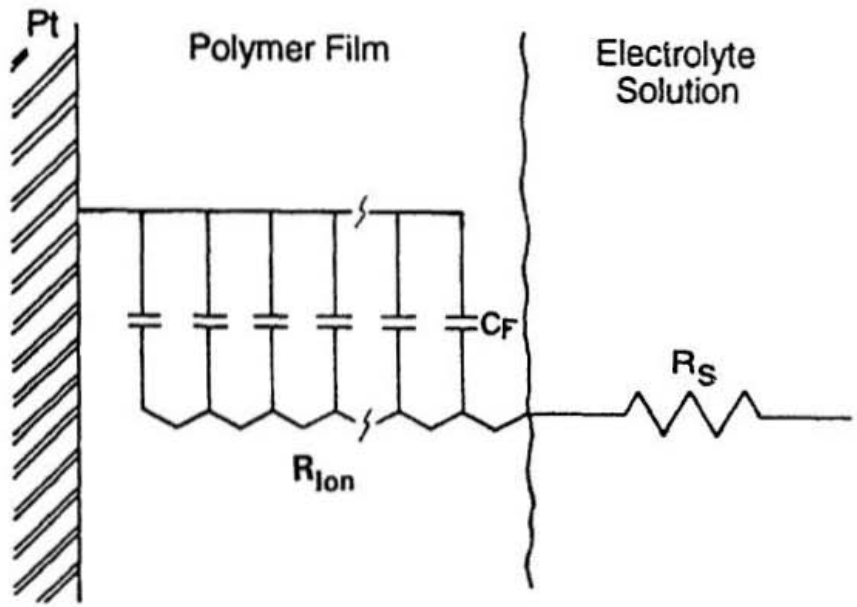

Figure 4.2.3 Equivalent circuit for polymer film-coated electrode according to the porous metal electrode model. R_s which is not included in theoretical equations is added.

4.3 Discussion

The impedance responses of conducting polymer coated electrodes can be modelled based on the transmission line circuits shown in Figs. 4.2.1,4.2.2 and 4.2.3. The experimental impedance responses can be categorized into the following three cases; $R_E >> R_{Ion}$, $R_E << R_{Ion}$, and $R_E \approx R_{Ion}$.

4.3.1 $R_E >> R_{Ion}$

The equivalent circuit representing this case is shown in Fig. 4.2.1. At very high frequency, the (near) zero resistance rail allows ionic current to pass through the polymer layer and the charging/discharging begins at the support electrode (Pt)/polymer interface[65]. Therefore, the polymer electrode exhibits an additional uncompensated resistance (R_{Ion}) compared to the bare Pt electrode[31,65]. As the frequency is decreased, the redox reaction layer grows outwards toward the polymer/solution interface. The impedance data in this frequency range forms a 45° Warburg line, which characterizes the slow electron hopping in the polymer. The projected length of the Warburg line on the real axis equals $R_E/3$. The

diffusion coefficient of the electron hopping process (D_E) can be calculated using the Nernst-Einstein relationship[21,63]:

$$D_E = \sigma_E \frac{R\ T}{F^2 \frac{\overline{c_O}\ \overline{c_R}}{c}}$$

[4.3.1]

In this case, the conducting polymer behaves like a redox polymer. This has been shown to be correct for lightly doped polypyrrole by small step chronoamperometry studies[8,66] and by a rotating disc voltammetry study[67]. Therefore the redox model derived by Gabrielli *et al*[21] can be used to derive the diffusion coefficient for the electron hopping process from the experimental impedance data. Under the assumption that $R_E >> R_{ion}$, Albery's model[14] is reduced to the Gabrielli's model[21].

Gabrielli's[21] and Ho's[22] models have been incorrectly used to derive the ion diffusion coefficient (so called apparent diffusion coefficient) by some authors[9,17,18]. They may be perfectly correct in stating that the rate limiting step is the slow ion movement for their cases, but do not realize that Fick's diffusion equations are no longer valid. Instead, the modified Nernst/Planck equation for coupled migration/diffusion charge transport should be used and the impedance data should

be modeled with Albery's model or the porous electrode model.

4.3.2 $R_E << R_{Ion}$

The equivalent circuit representing this case is shown in Fig. 4.2.3. In this case, the polymer coated electrode behaves like a porous metal electrode. This has been recognized by Bull *et al*[25], Burgmayer *et al*[68,69], Jakobs *et al*[27], Waller *et al*[26] and Pickup *et al*[23,24,70] for oxidized polypyrrole films. At very high frequency, both the polymer coated Pt electrode and the bare Pt electrode have real impedances equal to the uncompensated bulk solution resistance (R_s)[9,30]. The redox reaction of the polymer induced by the ac potential perturbation starts at polymer/electrolyte solution interface. As the frequency is decreased, the redox layer grows inwards to the Pt/polymer interface. This prediction has been recently proven by Ren and Pickup using a conducting polypyrrole bilayer electrode[40] (Chapter 9). The projected length of the 45° Warburg-type line characterizes the slow ion migration process in the pore solution and equals $R_{Ion}/3$. The diffusion coefficient for the counterion in the polymer phase can be calculated using the Nernst-Einstein relationship[21,63]:

$$D_{Ion} = \sigma_{Ion} \frac{R\ T}{F^2\ c_{Ion}} \qquad [4.3.2]$$

4.3.3 $R_E \approx R_{Ion}$

The equivalent circuit representing this case is shown in Fig. 4.2.2. This is the case of coupled electron hopping and counterion migration treated in Albery's model. At very high frequency, the transmission line has the resistance of a parallel combination of R_E and R_{Ion}. The polymer redox reaction layer induced by the ac potential perturbation starts at both interfaces and grows towards the centre as the frequency is reduced. Solving the simultaneous eqs. [4.2.9] and [4.2.10] gives two values for the resistances, but to assign them to R_E and R_{Ion} requires additional information, such as an independent measurement of R_E or R_{Ion}. The diffusion coefficients for electron hopping and ion migration can be calculated using eqs. [4.3.1] and [4.3.2] respectively.

4.4 Conclusion

The simple redox model of Gabrielli *et al*[21] can be used to derive the diffusion coefficient for electron hopping when it is slow relative to counterion

movement. When charge transport in the polymer film is limited by counterion movement, modified diffusion/migration equations must be used to describe electron hopping and the coupled counterion movement. In this case, the impedance data should be modelled with Albery's model[63]. When $R_E >> R_{ion}$, the polymer behaves like a porous metal electrode and the impedance can be modelled with a simple transmission line circuit. The dual transmission line circuit, which can either be viewed as the equivalent circuit for Albery's model or an extension from the porous metal electrode model, can be used to model both types of charge transport in a conducting polymer.

References

(1) Scrosati, B. *J. Electrochem. Soc.* 1989,*136*,2774.

(2) Naegele, D.; Bittihn, R. *Solid State Ionics* 1987,*28-30*,983.

(3) Yu, L.; Chen, M.; Dalton, L.R. *Chem. Mater.* 1990,*2*,649.

(4) Techagumpuch, A.; Nalwa, H.S.; Miyata, S. in *Electroresponsive Molecular and Polymeric Systems*, Skotheim, T.A.(Ed.), Marcel Dekker: New York,1991, p.257.

(5) Ofer, D.; Crooks, R.M.; Wrighton, M.S. *J. Am. Chem. Soc.* 1990,*112*,7869.

(6) Chiu, H.T.; Lin, J.S.; Shiau, J.N. *J. Appl. Electrochem.* 1992,*22*,522.

(7) Buvet, R.; Messina, R. in *Electr. Phenom. Biol. Membr. Level, Proc.* Int. Meet. Soc. Chim. Phys., 29th, Meeting Date 1976, Roux, E.(Ed.), Elsevier: Amsterdam, Neth,1976, p.431.

(8) Penner, R.M.; Van Dyke, L.S.; Martin, C.R. *J. Phys. Chem.* 1988,*92*,5274.

(9) Penner, R.M.; Martin, C.R. *J. Phys. Chem.* 1989,*93*,984.

(10) Heinze, J.; Bilger, R.; Meerholz, K. *Ber. Bunsenges. Phys. Chem.* 1988,*92*,1266.

(11) Heinze, J.; Storzbach, M.; Mortensen, J. *Ber. Bunsenges. Phys. Chem.* 1987,*91*,960.

(12) Heinze, J.; Mortensen, J.; Hinkelmann, K. *Synth. Met.* 1987,*21*,209.

(13) Heinze, J. *Synth. Met.* 1991,*41-43*,2805.

(14) Albery, W.J.; Chen, Z.; Horrocks, B.R.; Mount, A.R.; Wilson, P.J.; Bloor, D.; Monkman, A.T.; Elliott, C.M. *Faraday. Discuss. Chem. Soc.* 1989,*88*,247.

(15) Macdonald, J.R. *Impedance Spectroscopy*, Wiley: New York,1987;

(16) Panero, S.; Prosperi, S.; Passerini, S.; Scrosati, B.; Perlmutter, D.D. *J. Electrochem. Soc.* 1989,*136*,3729.

(17) Amemiya, T.; Hashimoto, K.; Fujishima, A. *J. Phys. Chem.* 1993,*97*,4192.

(18) Amemiya, T.; Hashimoto, K.; Fujishima, A. *J. Phys. Chem.* 1993,*97*,4187.

(19) Tanguy, J.; Baudoin, J.L.; Chao, F.; Costa, M. *Electrochim. Acta* 1992,*37*,1417.

(20) Rubinstein, I.; Sabatani, E.; Rishpon, J. *J. Electrochem. Soc.* 1987,*134*,3078.

(21) Gabrielli, C.; Haas, O.; Takenouti, H. *J. Appl. Electrochem.* 1987,*17*,82.

(22) Ho, C.; Raistrick, I.D.; Huggins, R.A. *J. Electrochem. Soc.* 1980,*127*,343.

(23) Paulse, C.D.; Pickup, P.G. *J. Phys. Chem.* 1988,*92*,7002.

(24) Mao, H.; Ochmanska, J.; Paulse, C.D.; Pickup, P.G. *Faraday. Discuss. Chem. Soc.* 1989,*88*,165.

(25) Bull, R.A.; Fan, F.R.F.; Bard, A.J. *J. Electrochem. Soc.* 1982,*129*,1009.

(26) Waller, A.M.; Compton, R.G. *J. Chem. Soc., Faraday. Trans. I* 1989,*85*,977.

(27) Jakobs, R.C.M.; Janssen, L.J.J.; Barendrecht, E. *Recl. J. R. Netherlands. Chem. Soc.* 1984,*103*,275.

(28) Fletcher, S. *J. Electroanal. Chem.* 1992,*337*,127.

(29) Fletcher, S. *J. Chem. Soc., Faraday. Trans.* 1993,*89*,311.

(30) Ren, X.; Pickup, P.G. *J. Electrochem. Soc.* 1992,*139*,2097.

(31) Pickup, P.G. *J. Chem. Soc., Faraday. Trans.* 1990,*86*,3631.

(32) Sunde, S.; Hagen, G.; Odegard, R. *J. Electroanal. Chem.* 1993,*345*,43.

(33) Sunde, S.; Hagen, G.; Odegard, R. *J. Electroanal. Chem.* 1993,*345*,59.

(34) Johnson, A.M.; Newman, J. *J. Electrochem. Soc.* 1971,*118*,510.

(35) DeLevie, R.; in *Advances in Electrochemistry and Electrochemical Engineering*, Delahay, P.; Tobias, C.W. (Eds.), Vol.6, John-wiley & Sons: New York,1967;p329.

(36) Raistrick, I.D. *Electrochim. Acta* 1990,*35*,1579.

(37) Elliott, C.M.; Redepenning, J.G.; Balk, E.M. *J. Am. Chem. Soc.* 1985,*107*,8302.

(38) Duffitt, G.L.; Pickup, P.G. *J. Chem. Soc., Faraday. Trans.* 1992,*88*,1417.

(39) Ren, X.; Pickup, P.G. *J. Phys. Chem.* 1993,*97*,5356.

(40) Ren, X.; Pickup, P.G. *J. Phys. Chem.* 1993,*97*,3941.

(41) Albery, W.J.; Mount, A.R. *Abstracts 671, p.965, The Electrochemicall Society Extended Abstracts,* Washington, DC,1991, May 5-10.

(42) Albery, W.J. *personal. communication.* 1993.

(43) Gabrielli, C.; Takenouti, H.; Haas, O.; Tsukada, A. *J. Electroanal. Chem.* 1991,*302*,59.

(44) Glarum, S.H.; Marshall, J.H. *J. Electrochem. Soc.* 1980,*127*,1467.

(45) Buck, R.P. *J. Electroanal. Chem.* 1986,*210*,1.

(46) Bard, A.J.; Faulkner, L.R. *Electrochemical Methods, Fundamentals and Applications*, John Wiley & Sons, Inc: New York,1980.

(47) Chambers, J.Q.; Kaufman, F.B.; Nichols, K.H. *J. Electroanal. Chem.* 1982,*142*,277.

(48) Inzelt, G.; Szabo, L.; Chambers, J.Q.; Day, R.W. *J. Electroanal. Chem.* 1988,*242*,265.

(49) Forster, R.J.; Vos, J.G.; Lyons, M.E.G. *J. Chem. Soc., Faraday. Trans.* 1991,*87*,3761.

(50) Oh, S.M.; Faulkner, L.R. *J. Electroanal. Chem.* 1989,*269*,88.

(51) Ren, X.; Pickup, P.G. *J. Electroanal. Chem.* 1993, submitted.

(52) Saveant, J.M. *J. Electroanal. Chem.* 1986,*201*,211.

(53) Saveant, J.M. *J. Electroanal. Chem.* 1986,*238*,1.

(54) Saveant, J.M. *J. Electroanal. Chem.* 1988,*242*,1.

(55) Saveant, J.M. *J. Electroanal. Chem.* 1987,*238*,1.

(56) Andrieux, C.P.; Saveant, J.M. *J. Phys. Chem.* 1988,*92*,6761.

(57) Saveant, J.-M. *J. Phys. Chem.* 1988,*92*,1011.

(58) Buck, R.P. *J. Electroanal. Chem.* 1987,*219*,23.

(59) Buck, R.P. *J. Electroanal. Chem.* 1989,*258*,1.

(60) Buck, R.P. *J. Phys. Chem.* 1989,*93*,6212.

(61) Buck, R.P.; Vanysek, P. *J. Electroanal. Chem.* 1990,*292*,73.

(62) Mathias, M.F.; Haas, O. *J. Phys. Chem.* 1992,*96*,3174.

(63) Albery, W.J.; Elliott, C.M.; Mount, A.R. *J. Electroanal. Chem.* 1990,*288*,15.

(64) Feldberg, S.W. *J. Am. Chem. Soc.* 1984,*106*,4671.

(65) Ren, X.; Pickup, P.G. *J. Chem. Soc., Faraday. Trans.* 1993,*89*,321.

(66) Cai, Z.H.; Martin, C.R. *Synth. Met.* 1992,*46*,165.

(67) Mao, H.; Pickup, P.G. *J. Am. Chem. Soc.* 1990,*112*,1776.

(68) Marque, P.; Roncali, J.; Garnier, F. *J. Electroanal. Chem.* 1987,*218*,107.

(69) Burgmayer, P.; Murray, R.W. *J. Phys. Chem.* 1984,*88*,2515.

(70) Pickup, P.G.; Murray, R.W. *J. Electrochem. Soc.* 1984,*131*,833.

Chapter 5

Experimental and Simulated Impedance Responses of Polymers

Since oxidized polypyrrole has a much higher electronic conductivity than its ionic conductivity, a polypyrrole film coated electrode can be treated as a porous metal electrode as discussed in Section 4.3.2. In this chapter experimental impedance data for a variety of polymers are compared with the simulated data from this and other models.

The impedance response of polypyrrole doped with perchlorate (PPY/ClO_4^-) is presented in section 5.1. Complex plane impedance plots for this polymer are very close to the porous metal electrode model's impedance response due to its uniform structure. An oxidized poly-MPCA film coated electrode can also be treated as a porous metal electrode. However, the morphology of this polymer differs from that of polypyrrole. A dense bottom layer and dendritic top layer have been observed by SEM for poly-MPCA films. Due to this non-uniform structure, the polymer film's impedance response deviates from the ideal one. Various impedance responses are simulated by linearly varying the distributed ionic

resistance and film capacitance in the transmission line circuit shown in Fig. 4.2.3.

As discussed in Chapter 4, Albery *et al* have recently proposed a new transmission line model for electroactive polymers[1,2]. In this model, two rails of distributed resistances are used to model charge transport in the polymer phase and the pore solution respectively. They have applied this model to study the impedance responses of poly(vinylferrocene)-modified electrodes[3] and polypyrrole coated electrodes[1,4]. In section 5.3, Albery's model is thoroughly tested with the impedance response of poly-[1-methyl-3-(pyrrol-1-ylmethyl)pyridinium] (poly-MPMP) over a wide potential range. There were two reasons for choosing this polymer for this study. Firstly, poly-MPMP is an anion exchange polymer, which contains about 5-6 M of anion exchange sites[5]. It is permselective[6] and its ionic conductivity is dominated by the mobile counter anions[7]. Therefore, unlike other conducting polymers such as polypyrrole[8] and poly-3-methyl-pyrrole-4-carboxylic acid[9], the ionic conductivity of poly-MPMP does not vary greatly with the oxidation level of the polymer film[6]. This property provides the opportunity to study the impedance response of a conducting polymer which has various relative levels of ionic and electronic conductivities, since the latter can be easily changed by varying the electrode potential while the former shows much less change with potential. Secondly, both the electronic[10] and ionic[7] conductivities of this polymer

have been measured by various other independent methods. The correct transport mode of charge carriers within the polymer film can be identified by comparison with these experimental results.

The electronic and ionic resistances of polypyrrole (PPY) doped with perchlorate anions increase as the electrode potential is decreased[8]. The low mobilities of both charge carriers at low electrode potentials make the Warburg-type line extend to very high resistance, which requires using very low frequency potential perturbations to determine the limiting low frequency capacitance and resistance. Consequently, these measurements are both time consuming and inaccurate.

The potential dependence of the ionic conductivity of PPY doped with poly(styrene sulphonate) (PSS) is different from that of PPY/ClO_4^-. For PPY/PSS films, decreasing the electrode potential decreases the polymer's ionic resistance[8] and increases its electronic resistance. Changing the polymer film's oxidation state by varying the electrode potential from a highly oxidized state to the near neutral state produces three different types of impedance responses, corresponding to the three situations $\sigma_{Ion} < \sigma_E$, $\sigma_{Ion} \approx \sigma_E$ and $\sigma_{Ion} > \sigma_E$. At very low electrode potentials ($<$-0.73 V *vs.* Ag/AgCl), the high frequency impedance data also form a well defined semicircle in the complex impedance plane. It is one of the purposes of this study to investigate the origin of this semicircle.

5.1 Polypyrrole/perchlorate

A complex plane impedance plot for a 2 μm PPY/ClO_4^- coated Pt electrode in 0.2 M NaCl(aq) at 0.0 V *vs.* Ag/AgCl is shown in Fig. 5.1.1A. The real axis intercept at high frequency coincides with the uncompensated resistance of the bulk electrolyte solution (R_s = 311 Ω, determined with the bare Pt electrode). Thus according to the dual transmission line circuit (Fig. 4.2.2), either the ionic or the electronic resistance of the polymer is negligible when compared to the other. Based on the known high electronic conductivity of polypyrrole when it is even slightly oxidized[11-13], it can be concluded that the electronic resistance of the polymer film is negligible in the case treated here (*i.e.* electron transport is very fast). The redox reaction induced by the ac potential wave at high frequency therefore starts at the polymer/solution interface[14,15] (a more detailed discussion on this topic is given in Chapter 9). As the frequency is decreased, the redox reaction layer expands inwards from the polymer/solution interface, and the corresponding impedance data forms a 45° Warburg-type line which is characteristic of the slow

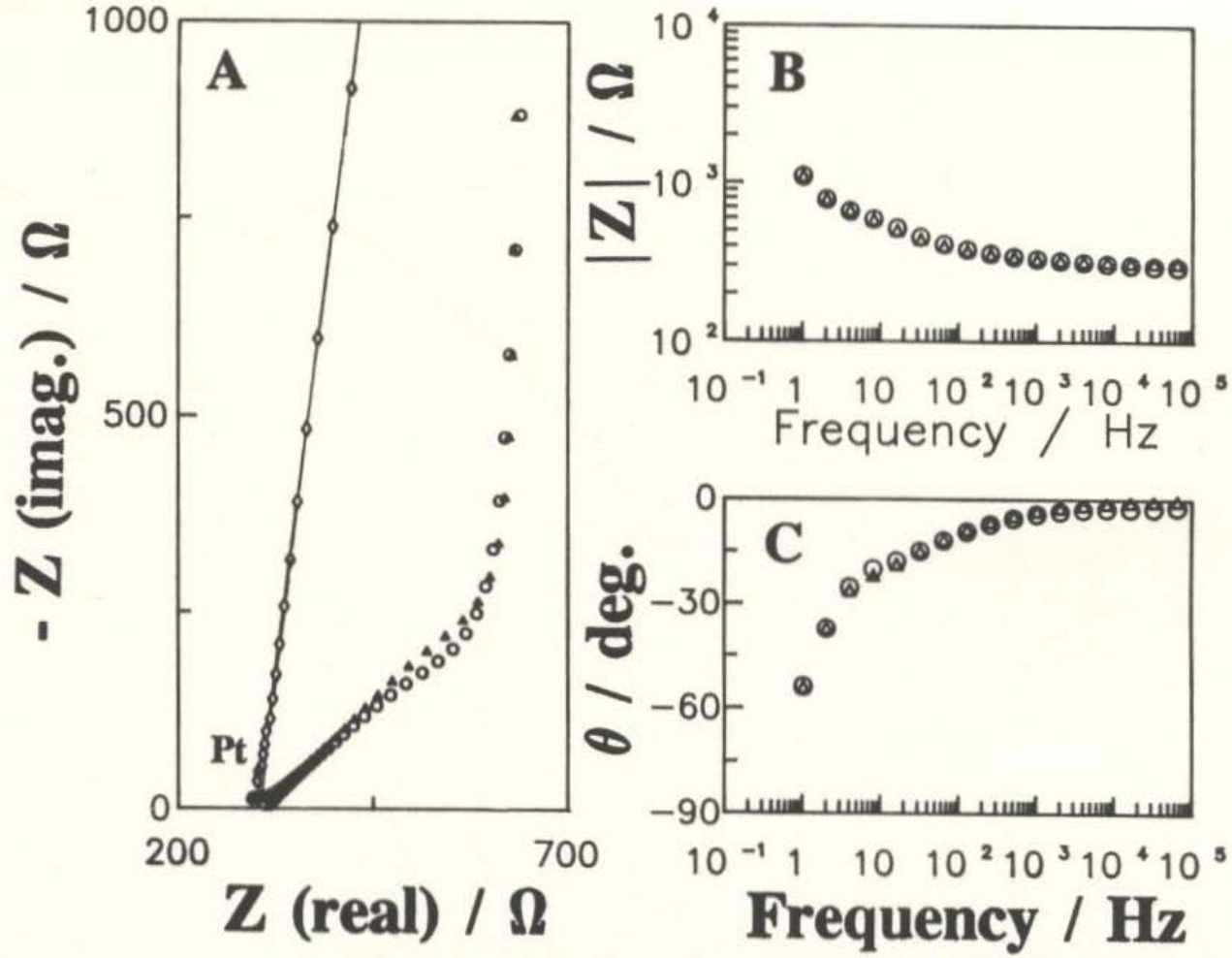

Figure 5.1.1 **A;** Complex plane impedance plots for a 2 μm PPY/ClO_4^- in 0.2 M NaCl (aq) at 0.0 V *vs.* Ag/AgCl (○) and simulated data (△) from the classical transmission line circuit shown in Fig.4.2.3 with R_s =311 Ω, R_{ion}=972 Ω and C_F=18.1 mF. **B** and **C**; Comparisons of the magnitude (|Z|) and phase angle (θ) of the impedance respectively for the experimental (○) and simulated data (△).

ion transport in the film. At low frequency, the redox reaction layer encompasses the whole polymer film which therefore remains in equilibrium with the changing potential. Under these conditions the polymer coated electrode behaves like a simple capacitor and the complex plane impedance plot becomes a vertical line. The polymer's impedance response can be modelled with a finite transmission line circuit (Fig. 4.2.3). The ionic resistance R_{Ion} of the polymer film is given by: $R_{Ion} = 3\ R_{low}$, where R_{low} is the real axis intercept of the (almost) vertical low frequency region of the complex plane impedance plot minus the solution resistance. The ionic conductivity of the film (σ_{Ion}) is calculated by $\sigma_{Ion} = d/(R_{Ion} A)$, where A is the geometric area of the electrode and d the dry film thickness. From Fig. 5.1.1A, R_{Ion} equals 971 Ω and the film ionic conductivity is 15.3 μS cm^{-1}.

Fig. 5.1.2 shows a plot of the imaginary impedance (Z″) *vs.* 1/frequency for the low frequency data. The film capacitance (C_P) calculated from the slope ($C_P = 1/(2\pi$ slope)) is 1.81×10^{-4} F, the volumetric capacitance ($C_{V,ac} = C_P/(A\ d)$) is 201 F cm^{-3}.

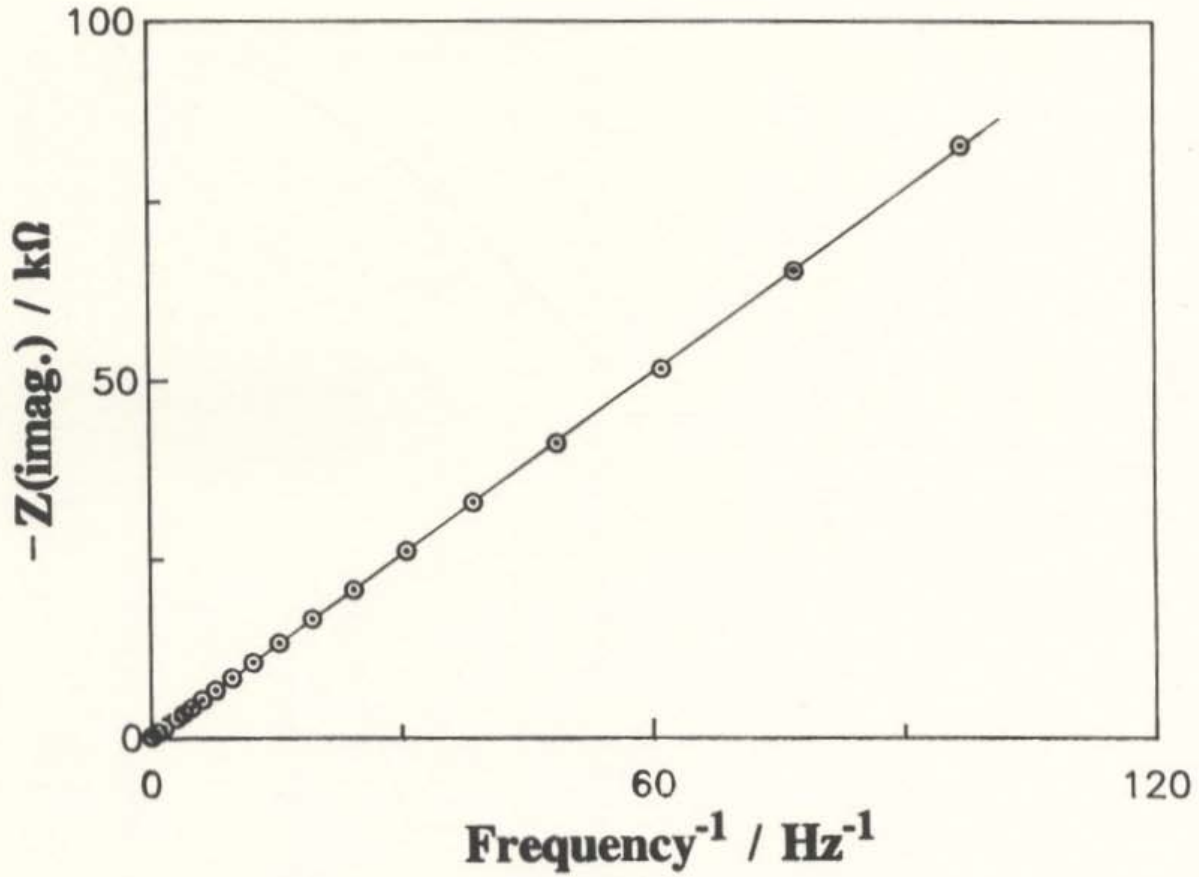

Figure 5.1.2 Plot of imaginary impedance *vs.* 1/frequency for the experimental data shown in Fig. 5.1.1.

5.2 Poly-(3-methyl-pyrrole-4-carboxylic acid) and Simulated Impedance Responses

5.2.1 Poly-(3-methyl-pyrrole-4-carboxylic acid)

The impedance response of a typical oxidized poly-MPCA film is shown in Fig. 5.2.1 in the complex plane. The real axis intercept of the high frequency data coincides with the uncompensated resistance of the bulk electrolyte solution (R_s = 670 Ω) measured with the bare Pt electrode. This value does not change with the thickness of the polymer film on the electrode nor with the electrode potential. Thus either the ionic or the electronic resistance of the polymer is negligible when compared with the other. Independent measurements of the film electronic conductivity with dual electrode voltammetry (Table 6.2.1) confirm that R_E is less than 2 Ω and is thus negligible. The polymer's impedance response was modelled with the classical transmission line circuit (Fig. 4.2.3) with the resistive path representing the slow ion transport across the polymer film thickness. From Fig. 5.2.1, R_{Ion} (*ca.* 540 Ω) equals three times the projected length of the Warburg-type line on the real axis and the film ionic conductivity is 9.6 μS cm^{-1}.

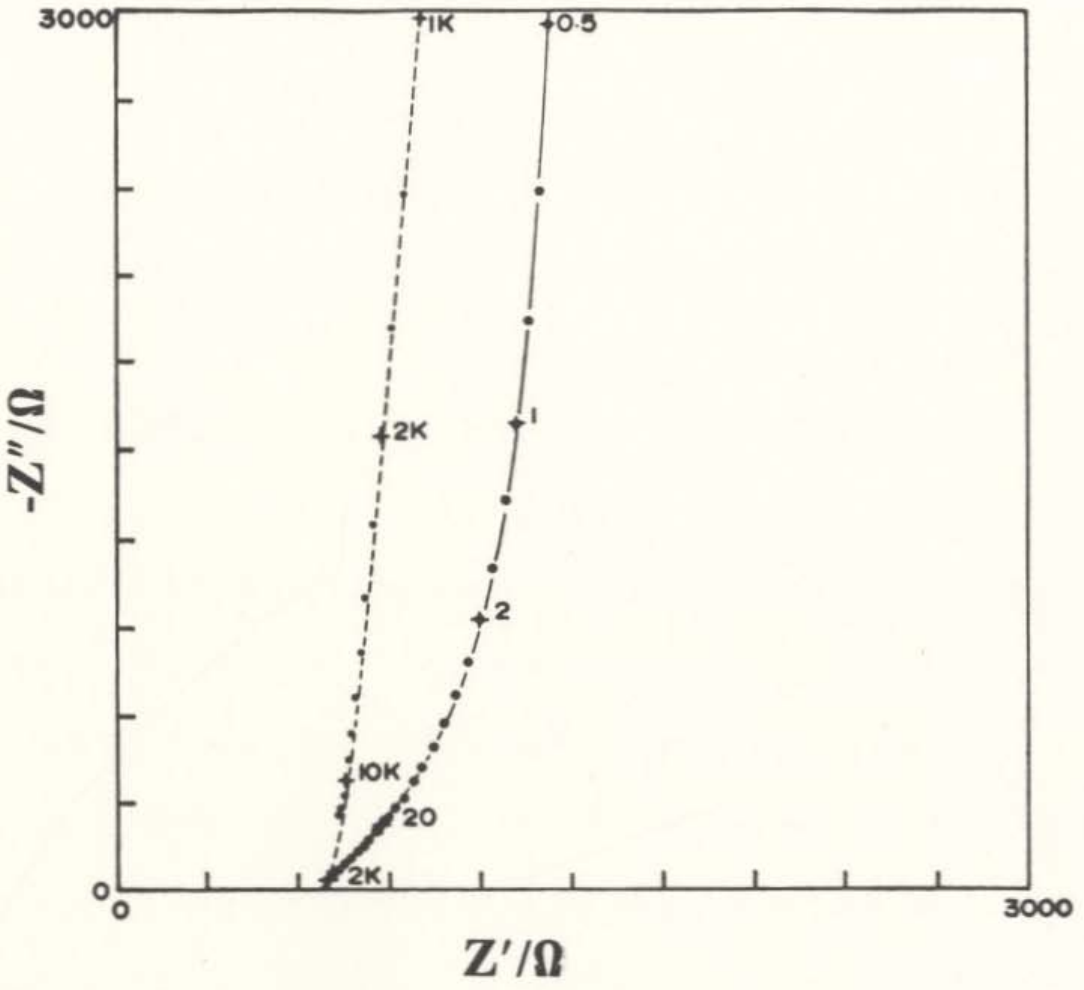

Figure 5.2.1 Complex plane impedance plots for a 0.7 μm poly-MPCA film coated Pt electrode at 0.8 V *vs.* SSCE (———), and for the bare Pt electrode (— — —), both in acetonitrile containing 0.1 M $LiClO_4$. Frequencies in Hz are indicated for selected points.

A plot of the imaginary impedance (Z″) *vs.* 1/frequency for the low frequency data forms a straight line. The film capacitance (C_F) calculated from the slope ($C_F = 1/(2\pi \text{ slope})$) is 1.1×10^{-4} F and the volumetric capacitance ($C_{V,*}$) is 352 F cm^{-3}. The deviation from the ideal vertical line at low frequency is similar to that observed in Fig. 5.1.1A for PPY/ClO_4^-.

The complex plane impedance plot for poly-MPCA also differs from the ideal response of the classical transmission line circuit (Fig. 4.2.3) in that the Warburg-type line has a angle to the real axis of *ca.* 55° instead of 45° and the transition from the Warburg-type line to the vertical line (finite film thickness-limited charging/discharging region) is less distinct. In comparison, the impedance response for PPY/ClO_4^- is closer to the ideal response (Fig. 5.1.1A). The differences in the polymer film impedance response between PPY/ClO_4^- and poly-MPCA can be related to their difference in film morphology observed by scanning electron microscopy (SEM). Fig. 5.2.2A shows the cross section of a PPY/ClO_4^- film deposited on an indium/tin oxide (ITO) coated glass plate electrode. The uniform appearance of this polymer justifies the use of the classical transmission line circuit which has uniformly distributed resistances and capacitances to model the experimental impedance response. In contrast, the morphology of poly-MPCA shown in Fig. 5.2.2B, C and D is clearly different. Two types of polymer

structures can be easily identified. The polymer layer formed at the beginning of the electrochemical polymerization (less than 0.6 μm thick) has a uniform appearance while the polymer deposited at later stages assumes a more open dendritic structure. Clearly, the ionic resistivity of the polymer layer will decrease from the Pt/polymer interface outward. The capacitance per unit film thickness also decreases across the polymer film thickness as the polymer structure becomes more open. For poly-MPCA it is therefore necessary to vary the distributions of resistors and capacitors in the modelling circuit accordingly.

5.2.2 Simulation with a Transmission Line Circuit

For the majority of cases studied in this work, the electronic conductivity of the polymer film is much larger than its ionic conductivity. A transmission line with a zero resistance wire representing the fast electron transport and a resistive rail representing the slow ion transport is therefore sufficient to model the experimental impedance response. In the classical transmission line circuit shown in Fig. 4.2.3, the capacitance and resistance are uniformly distributed across the polymer film thickness. At the electrode/polymer interface only electrons carry the current and at the polymer/solution interface only ions carry the current. Since the transmission line can be described as a two-port cascaded network, network

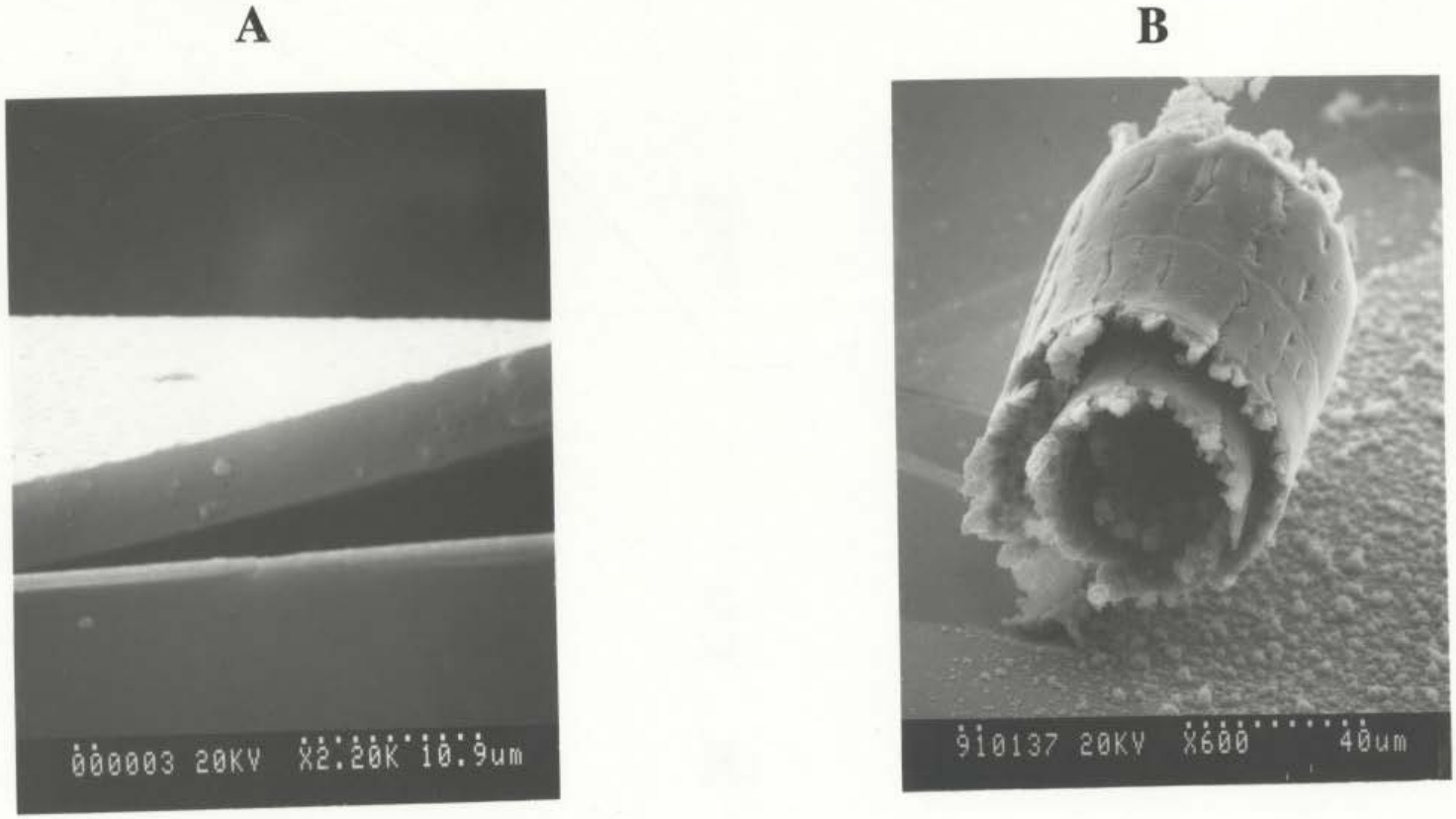

Figure 5.2.2 A & B Scanning electron micrographs of an across section of 5.3 μm PPY/ClO_4^- film on ITO electrode (A), and a 1.3 μm poly-MPCA film deposited on a Pt electrode after peeled off the electrode with a scalpel for comparison of the top and bottom morphologies (B).

C

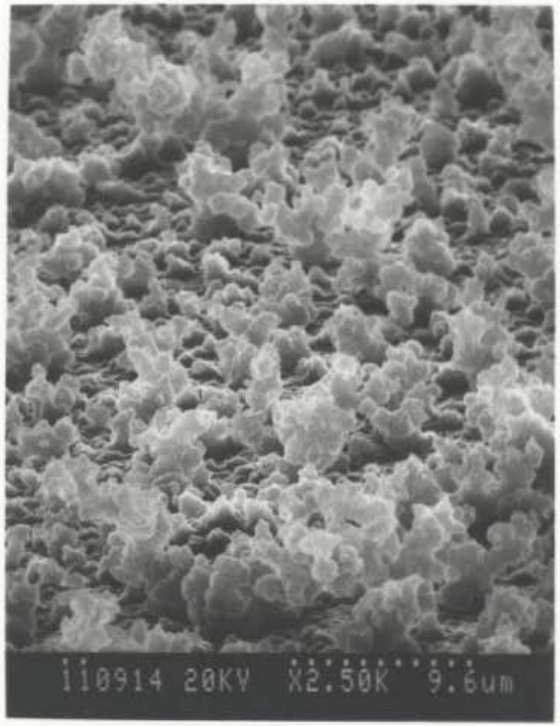

D

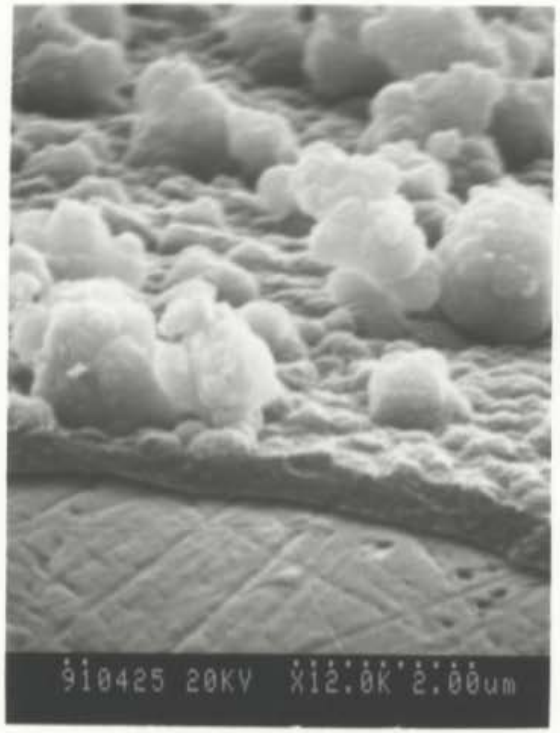

Figure 5.2.2 C & D Scanning electron micrographs of side view (C) and an across section revealed after part of the film torn away with a scalpel (D) for a 1.3 μm poly-MPCA film deposited on a Pt electrode.

theory[16-18] can be used to calculate the impedance response of such a circuit. However, the calculation can be greatly simplified by making use of the zero resistance wire to redraw the network as shown in Fig. 5.2.3. The circuit is merely a repetition of a capacitor and a resistor in series combination which then parallels with the next capacitor. The impedance can be calculated by using a successive reduction method[19]. Starting from the electrode/polymer interface the total impedance from the electrode (plane 0) to plane k+1 is calculated from the total impedance to plane k using the following iterative equation.

$$Z_{k+1}=R_{k+1}+\frac{1}{\frac{1}{Z_k}+\frac{1}{j\omega C_{k+1}}} \qquad [5.2.1]$$

Since only electrons can pass through the electrode/polymer interface, the resistor R_0 is infinite for such an open circuit point. Therefore Z_1 is calculated from eq. [5.2.1] with $1/Z_0 = 0$.

For the simulation of the experimental impedance response using the classical transmission line circuit, the film ionic resistance and capacitance were divided among 2000 equal resistors and 2000 equal capacitors respectively, distributed according to the circuit in Fig. 4.2.3. Fig. 5.1.1A shows a comparison

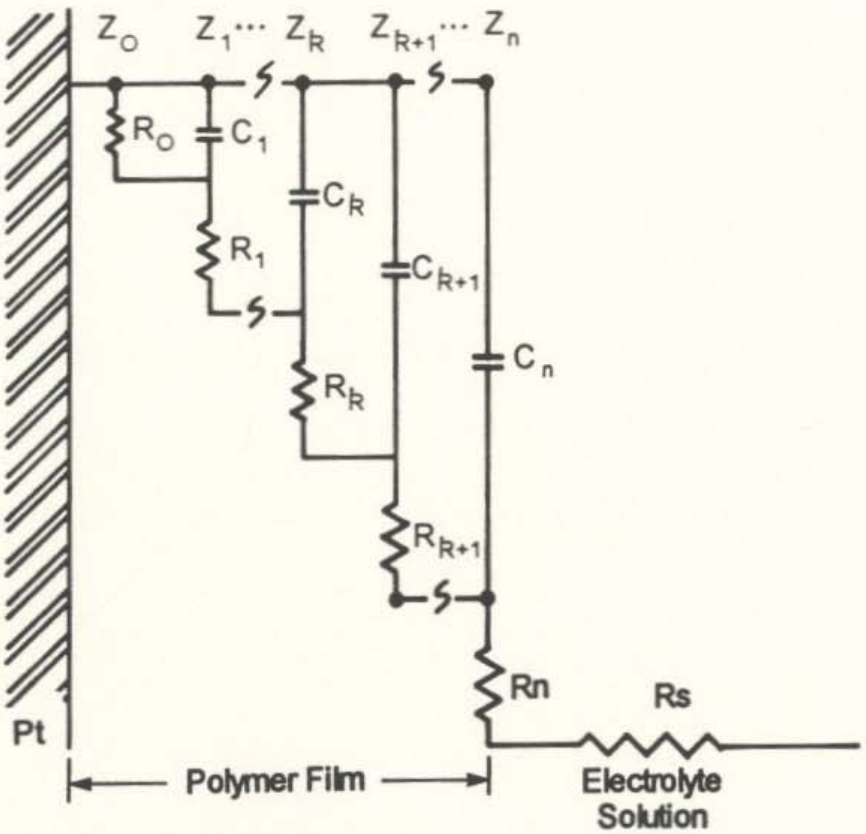

Figure 5.2.3 An alternate representation of the transmission line circuit shown in Fig.4.2.3.

of the simulated and experimental impedance data for PPY/ClO_4^- in the complex impedance plane. The magnitude ($|Z|$) and phase angle (θ) of the impedance as a function of frequency are compared in Figs. 5.1.1B and 5.1.1C respectively for the simulated and experimental data. Clearly, there is a very good agreement between the experimental and simulated data except that the experimental data shown in Fig. 5.1.1A deviate from the ideal vertical line at low frequency. Such deviation has been observed in all impedance studies of conducting polymers. Possible reasons, such as non-uniform film thickness[20-22] and distribution of diffusion coefficients[20], have been discussed in the literature. In addition, the various pathways for ion transport across the film may contribute to this deviation[9]. Detailed discussion of this topic is given in Chapter 10.

To simulate the experimental impedance response of a non-uniform polymer film like poly-MPCA, the film ionic resistance and capacitance were both decreased linearly with distance from the Pt/polymer interface as shown in Fig. 5.2.4. Since the variations of film ionic resistance and capacitance are assumed to be symmetrical about the half film thickness plane, the distribution can be defined with a single parameter (s_C or s_R), which is the ratio of the value at the polymer/electrolyte interface (C(d) or R(d)) against the average value across the film thickness ($\overline{C}$ or $\overline{R}$). The classical transmission line circuit can be regarded as a special case when both s_C and s_R are unity.

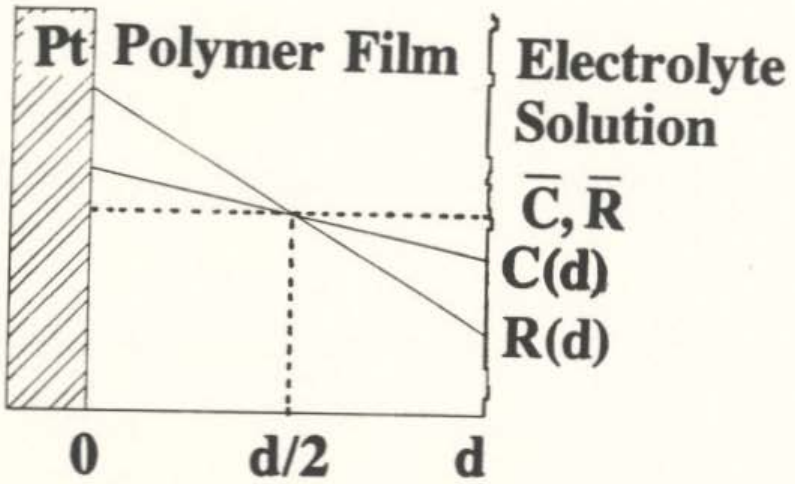

$$s_C = C(d) / \bar{C}$$

$$s_R = R(d) / \bar{R}$$

Figure 5.2.4 A schematic diagram showing uniform and linearly varying distributions of film ionic resistance and capacitance across the film thickness.

Complex impedance plots of simulated impedance responses of the transmission line circuit with linear film ionic resistance and capacitance distributions are shown in Fig. 5.2.5. Table 5.2.1 summarizes the characteristic shapes of the simulated complex plane impedance plots for various combinations of s_R and s_C. The angle between the high frequency Warburg-type line and real axis is denoted by β, and $(Z'/R_{ion})_{\omega \to 0}$ is the constant value of the real impedance for the low frequency data on the vertical line divided by the film ionic resistance (R_{ion}).

It is surprising to notice that even for a non-uniform film it is possible to have the ideal impedance response as long as both s_R and s_C are the same. When $s_R < s_C$, the Warburg-type line at high frequency has an angle (β) larger than 45° to the real axis and the transition from the Warburg-type region to the capacitance region is less distinct. On the other hand, when $s_R > s_C$ the Warburg-type line at high frequency has an angle (β) smaller than 45° to the real axis and the transition from the Warburg-type region to the capacitance region becomes more abrupt.

The experimental impedance response of poly-MPCA can thus be modelled with $s_R < s_C$, *i.e.*, the decrease in film ionic resistance towards the polymer/solution interface is more rapid than the decrease in capacitance (*e.g.* $s_R = 0$ and $s_C = 0.5$). This result corresponds qualitatively with the observed morphology of this polymer.

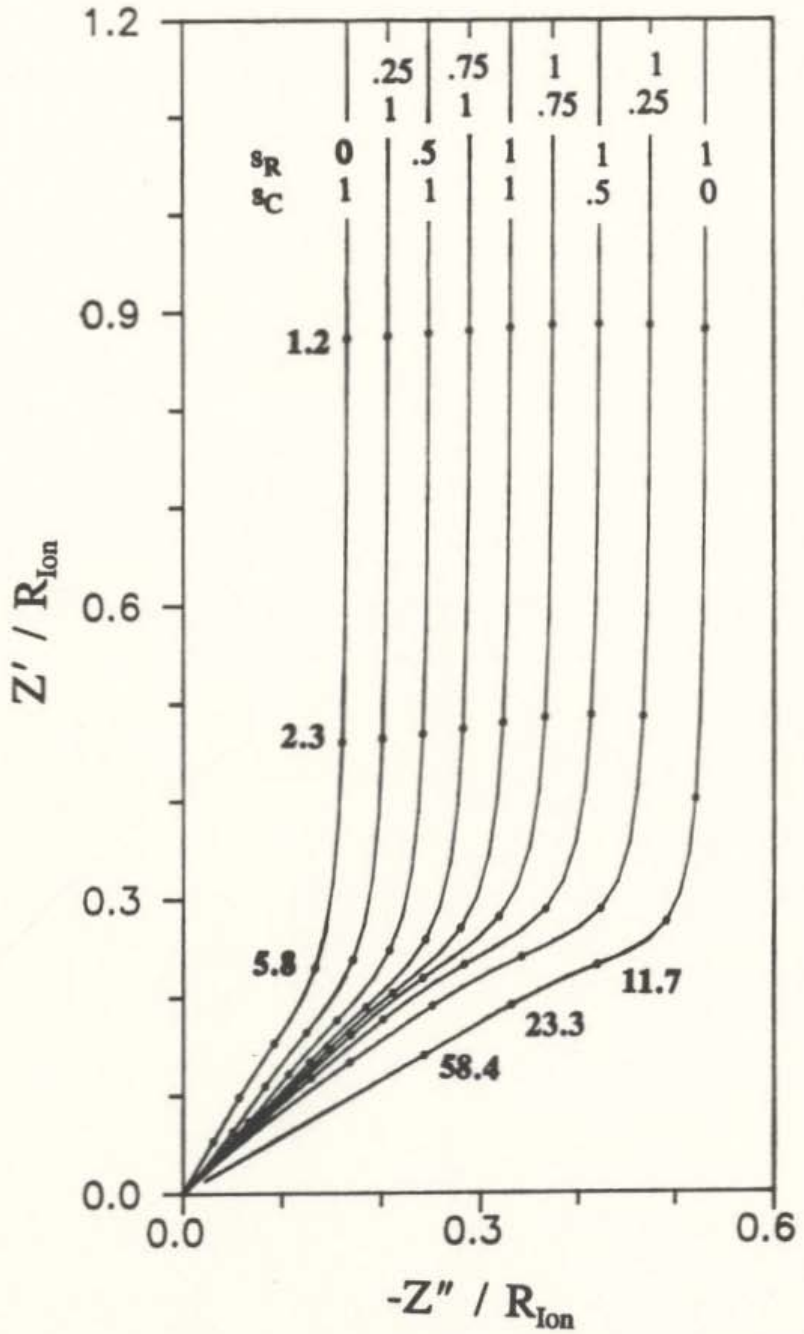

Figure 5.2.5 Complex plane impedance plots for the simulated impedance response of linearly distributed transmission line circuit. Normalised frequencies ($\omega R_{Ion} C_F$) are marked for selected points.

Table 5.2.1 Characteristics of simulated complex plane impedance plots

s_C	s_R	β/deg.	$(Z'/R_{I\infty})_{\omega\to 0}$
1.00	1.00	45.0	0.3338
1.00	0.00	60.0	0.1675
1.00	0.25	53.0	0.2091
1.00	0.50	48.9	0.2507
1.00	0.75	46.2	0.2923
0.75	1.00	43.6	0.3777
0.75	0.75	45.0	0.3338
0.75	0.50	47.4	0.2903
0.75	0.25	51.3	0.2466
0.75	0.00	58.1	0.2029
0.50	1.00	41.5	0.4255
0.50	0.75	42.8	0.3798
0.50	0.50	45.0	0.3338
0.50	0.25	48.9	0.2883
0.50	0.00	55.2	0.2426
0.25	1.00	36.7	0.4776
0.25	0.75	39.1	0.4298
0.25	0.50	41.2	0.3820
0.25	0.25	45.0	0.3338
0.25	0.00	52.0	0.2864
0.00	1.00	30.0	0.5337
0.00	0.75	31.6	0.4838
0.00	0.50	34.3	0.4340
0.00	0.25	38.3	0.3841
0.00	0.00	45.0	0.3338

5.3 Poly-[1-methyl-3-(pyrrol-1-ylmethyl)pyridinium]

5.3.1 Impedance of Poly-[1-methyl-3-(pyrrol-1 -ylmethyl)pyridinium]

Fig. 5.3.1 shows a comparison of an experimental impedance plot for a poly-MPMP film coated Pt electrode with that calculated from the dual transmission line circuit shown in Fig. 4.2.2 using eq. [4.2.8]. The value of C_F used in the calculation was obtained from the slope ($=1/C_F$) of an imaginary impedance (Z″) *vs.* 1/frequency ($1/\omega$) plot for the low frequency experimental data. The values of R_s and R_s+R_Σ were obtained by extrapolating the low frequency data on the near vertical lines for the bare Pt electrode and the polymer film coated Pt electrode to the real axis respectively, and the value of R_∞ by extrapolating the high frequency data on the 45° Warburg-type line to the real axis.

Impedance data for ⊿ 1.6 μm poly-MPMP coated Pt electrode at various potentials in water containing 0.1 M $NaClO_4$, acetonitrile containing 0.1 M Et_4NClO_4 and propylene carbonate containing 1.6 M $LiClO_4$ are shown in the complex impedance plane in Figs. 5.3.2, 5.3.3 and 5.3.4, respectively. Figs. 5.3.5, 5.3.6 and 5.3.7 are the plots of the electronic and ionic conductivities,

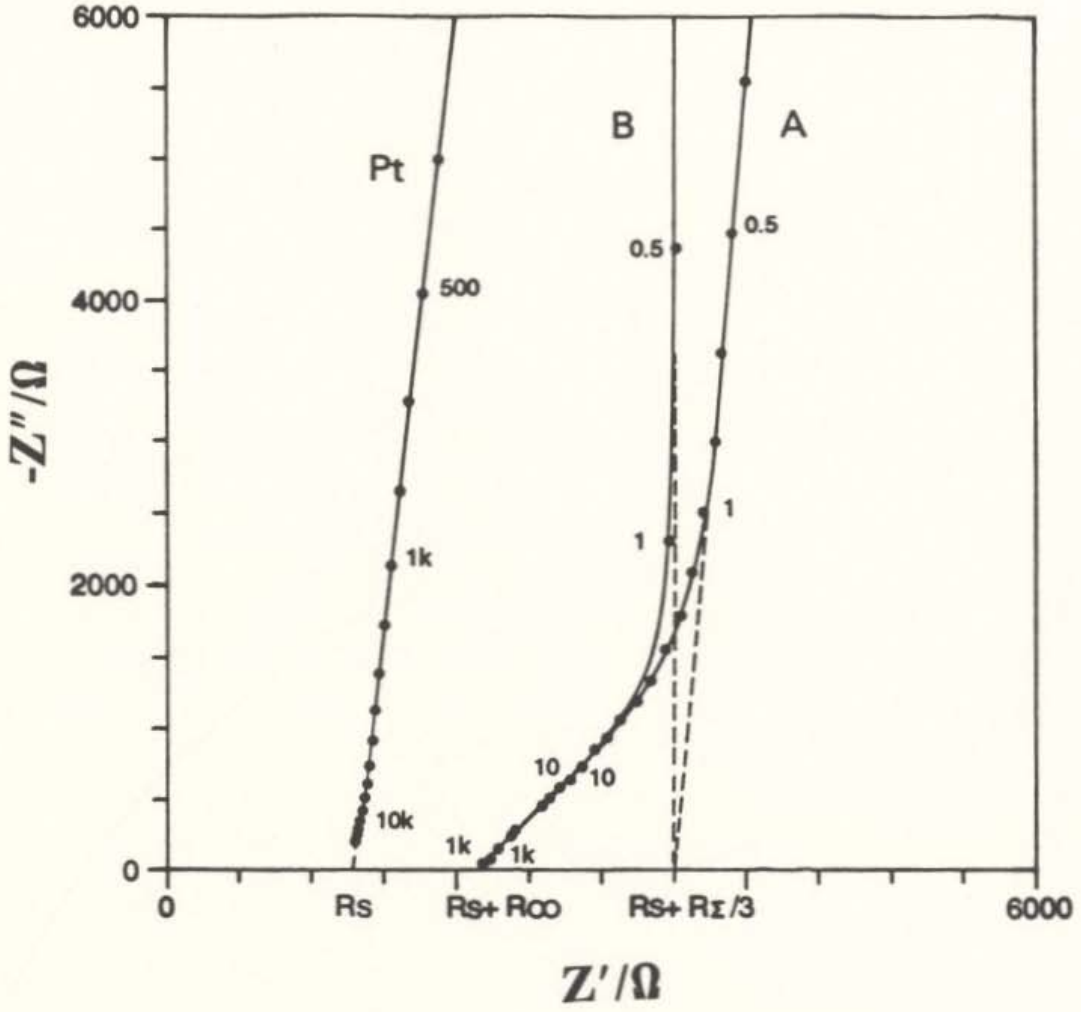

Figure 5.3.1 Experimental impedance plot for a 1.6 μm poly-MPMP film at 0.86 V in propylene carbonate + 1.6 M $LiClO_4$ (A) and simulated impedance plot based on the circuit shown in Fig.4.2.2 (B). The plot marked Pt is for the bare Pt electrode at open circuit. Frequencies of selected points are indicated in Hz.

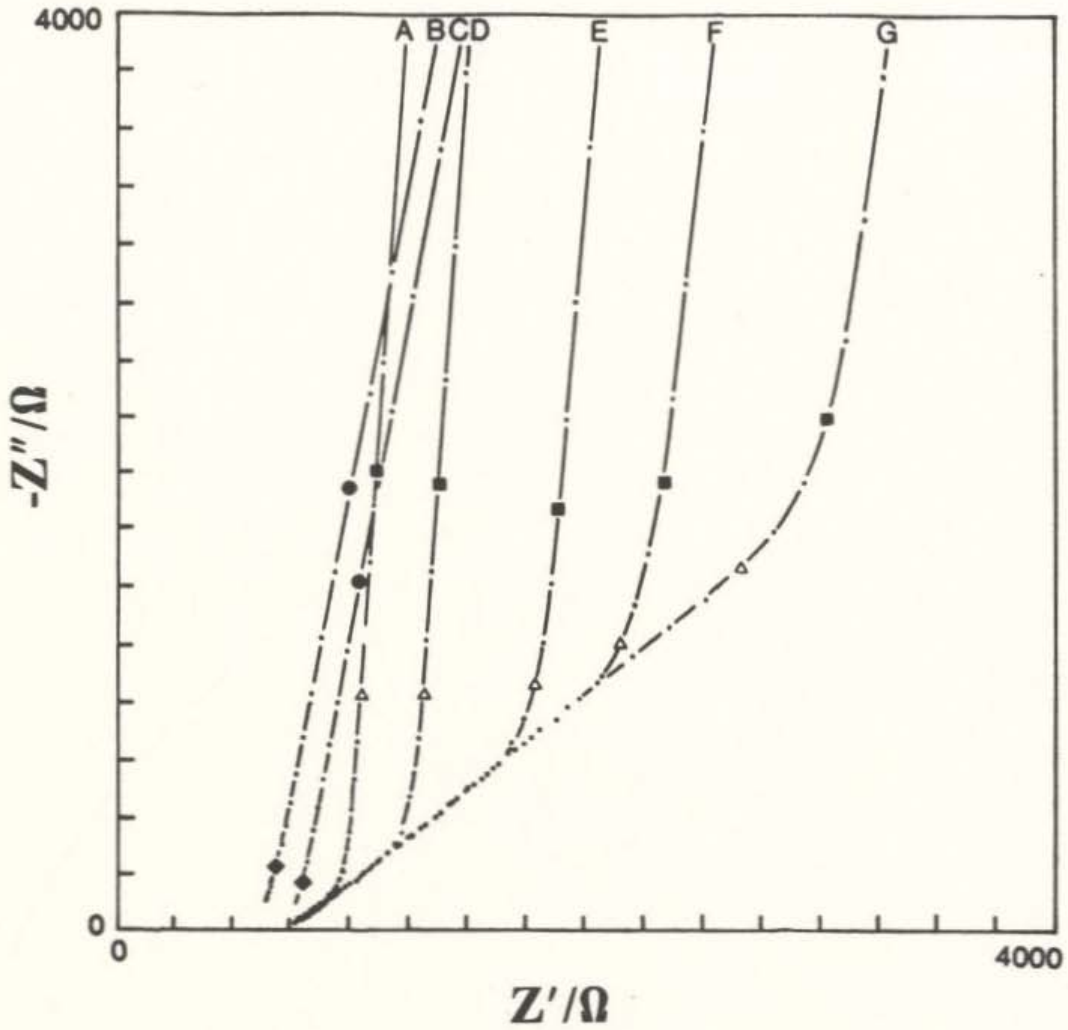

Figure 5.3.2 Complex plane impedance plots for a 1.6 μm poly-MPMP film on a Pt electrode at potentials of 0.70(A), 0.00(C), 0.63(D), 0.57(E), 0.55(F), and 0.53(G) V in 0.1 M $NaClO_4$(aq) solution. Plot (B) is for the bare Pt electrode at open circuit. Marked points correspond to frequencies of 10^4(◆), 10^3(●), 2(▵) and 1(■) Hz.

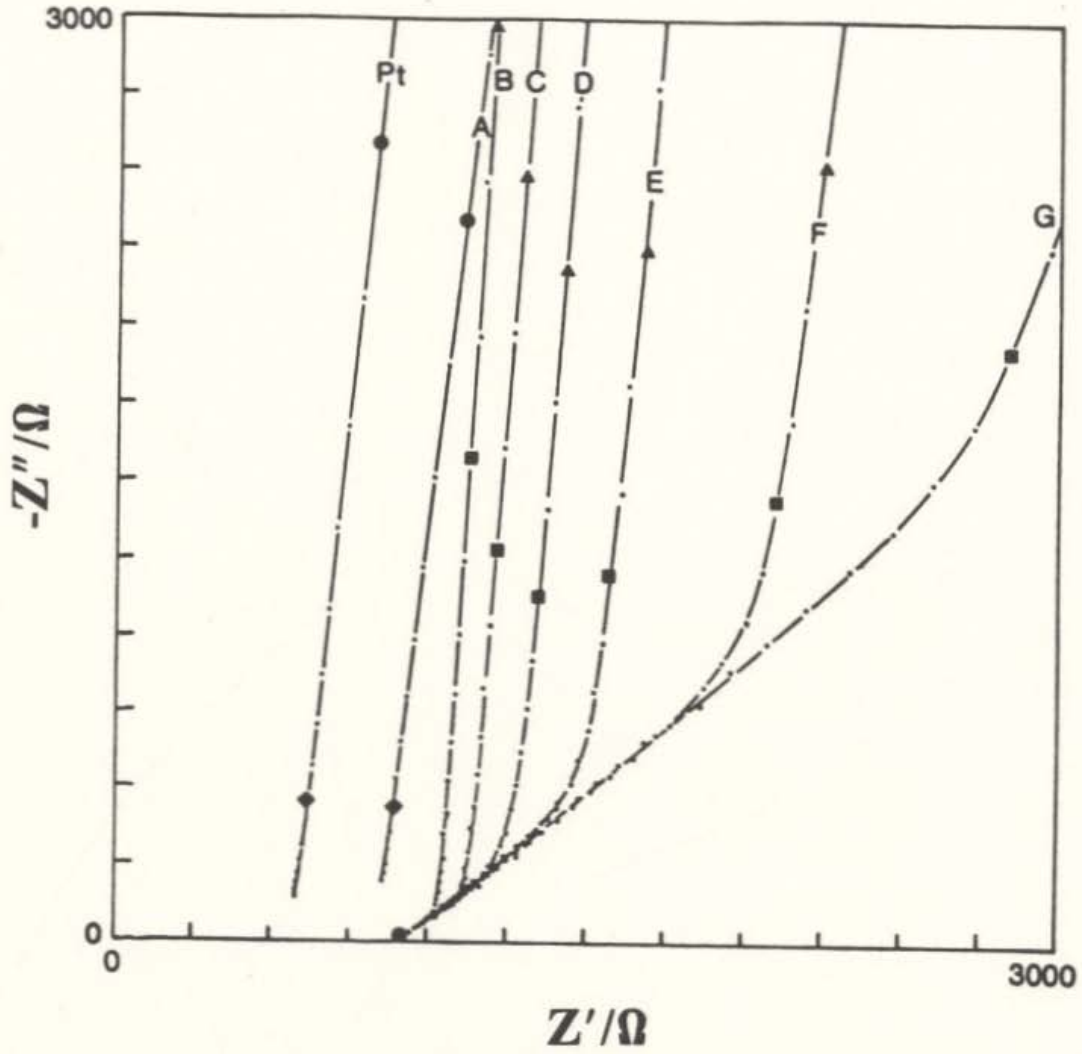

Figure 5.3.3 Complex plane impedance plots for a 1.6 μm poly-MPMP film on a Pt electrode at potentials of 0.00(A), 0.82(B), 0.74(C), 0.70(D), 0.68(E) and 0.66(F), and 0.64(G) V in acetonitrile containing 0.1 M Et_4NClO_4. The plot marked Pt is for the bare Pt electrode at open circuit. Marked points correspond to frequencies of 10^4(◆), 10^3(●), 1(■) and 0.5(▲) Hz.

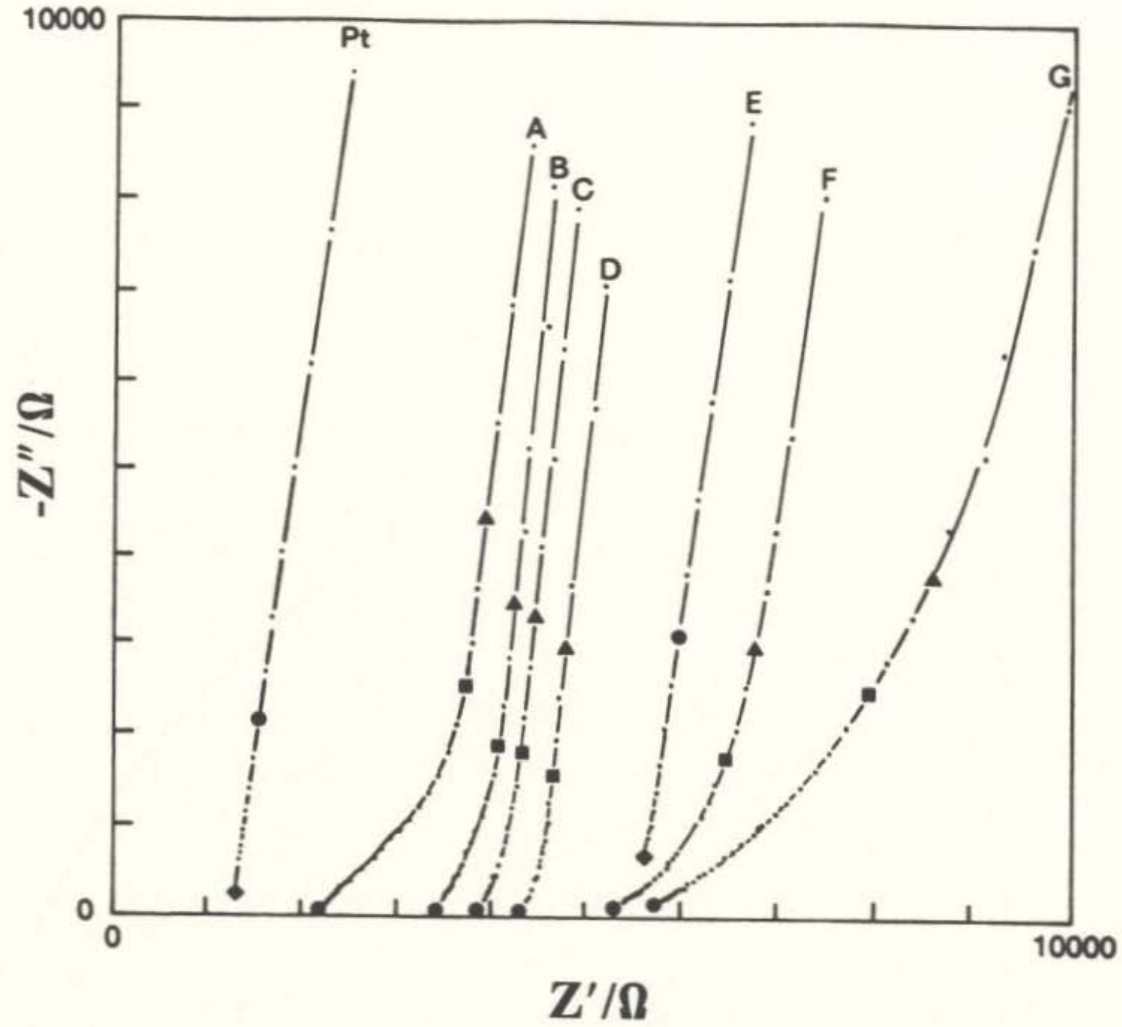

Figure 5.3.4A Complex plane impedance plots for a 1.6 μm poly-MPMP film on a Pt electrode at potentials of 0.85(A), 0.65(B), 0.63(C), 0.59(D), 0.00(E), 0.53(F), and 0.51(G) V, in propylene carbonate containing 1.6 M $LiClO_4$. The plot marked Pt is for the bare Pt electrode at open circuit. Marked points correspond to frequencies of 10^4(◆), 10^3(●), 100(○), 1(■), 0.5(▲) and 0.1(□) Hz.

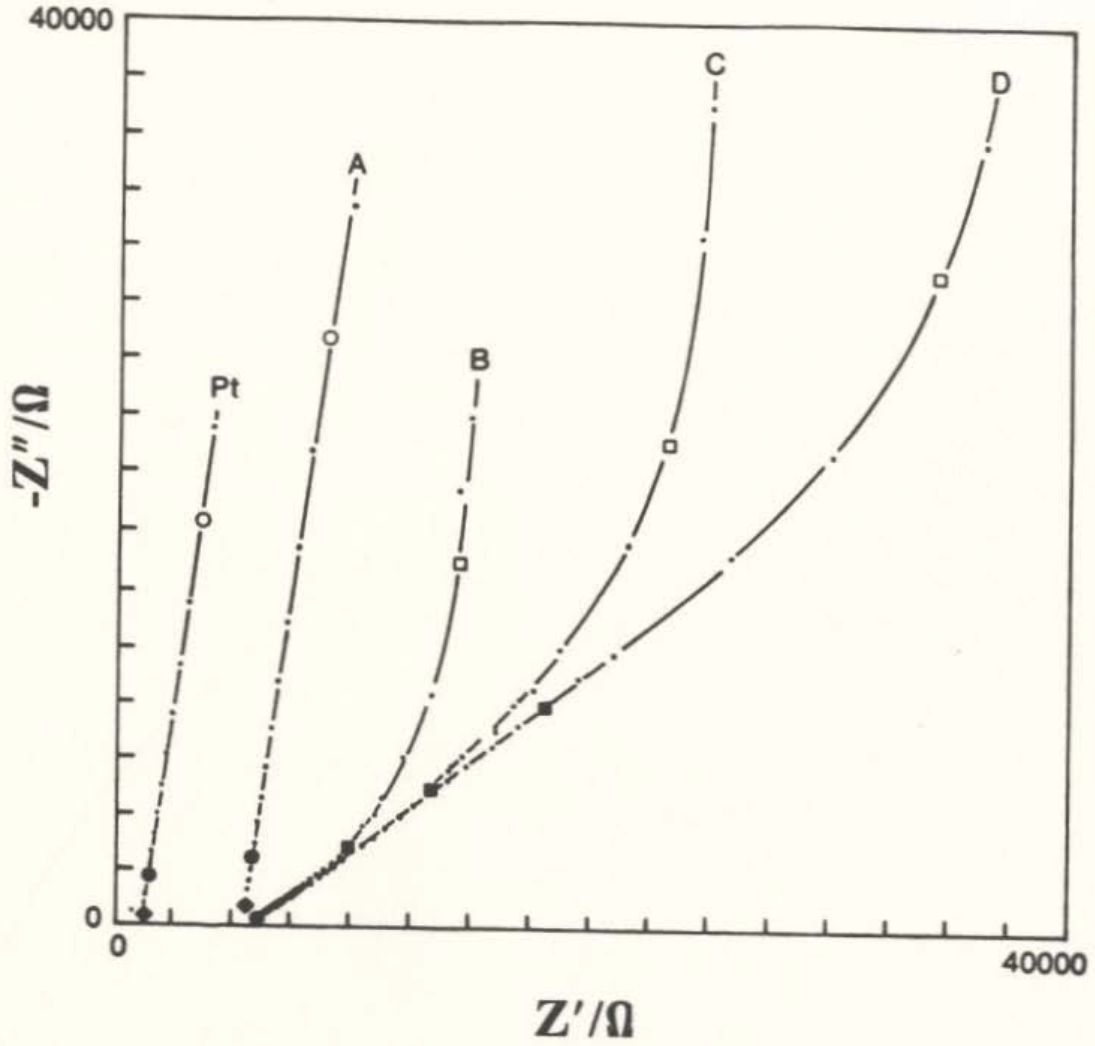

Figure 5.3.4B Complex plane impedance plots for a 1.6 μm poly-MPMP film on a Pt electrode at potentials of 0.00(A),0.49(B), 0.47(C) and 0.45(D) V, in propylene carbonate containing 1.6 M $LiClO_4$. The plot marked Pt is for the bare Pt electrode at open circuit. Marked points correspond to frequencies of 10^4(◆), 10^3(●), 100(○), 1(■), 0.5(▲) and 0.1(□) Hz.

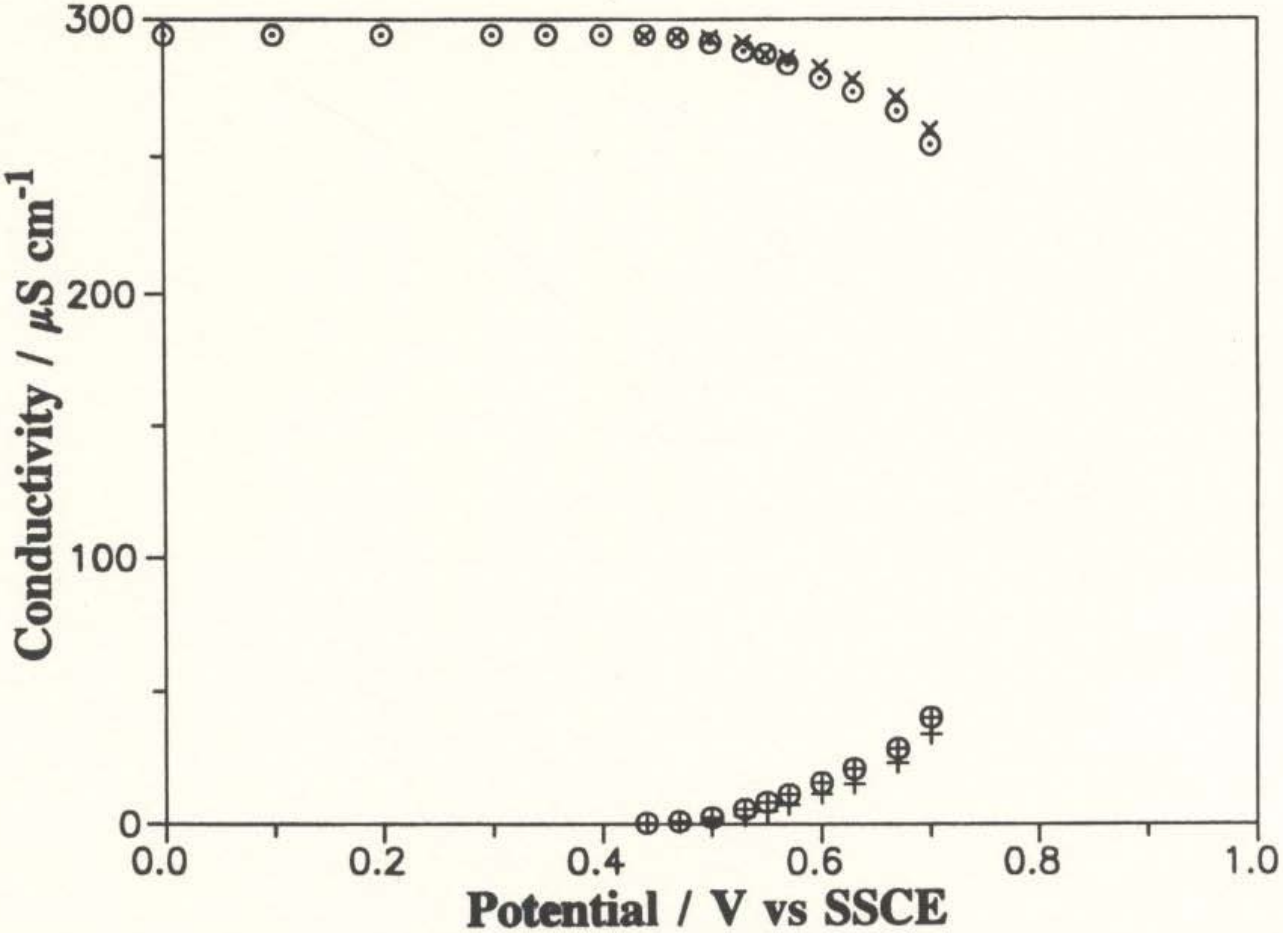

Figure 5.3.5 Electronic ($\oplus, +$) and ionic ($\odot, \times$) conductivities from the impedance data shown in Fig. 5.3.2(plus additional data) for poly-MPMP in 0.1 M aqueous $NaClO_4$. Circled points were obtained using low-frequency data while the others were obtained using data from the Warburg-type region.

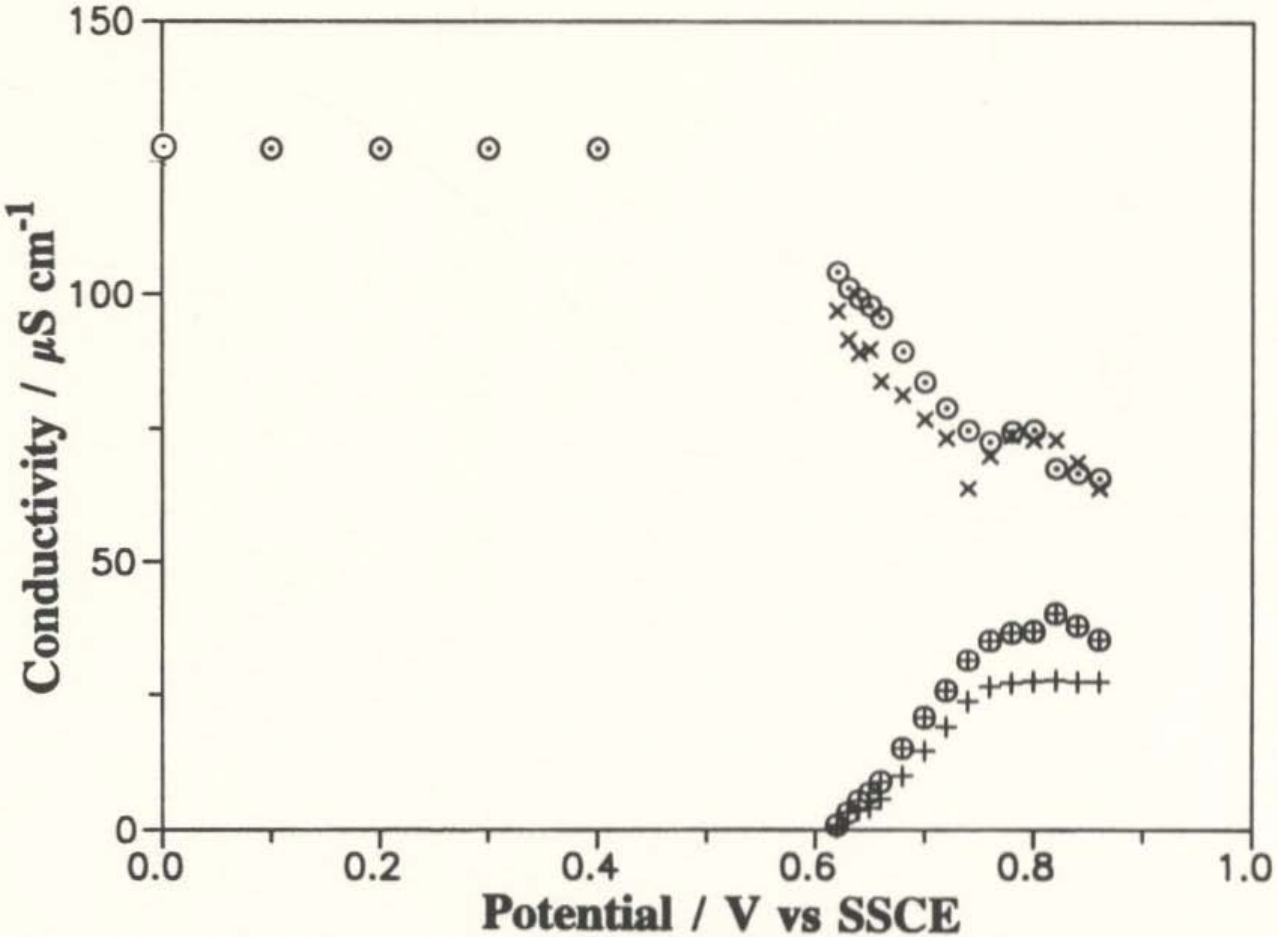

Figure 5.3.6 Electronic (⊕, +) and ionic (⊙, ×) conductivities from the impedance data shown in Fig. 5.3.3 (plus additional data) for poly-MPMP in acetonitrile containing 0.1 M Et_4NClO_4. Circled points were obtained using low-frequency data while the others were obtained using data from the Warburg-type region.

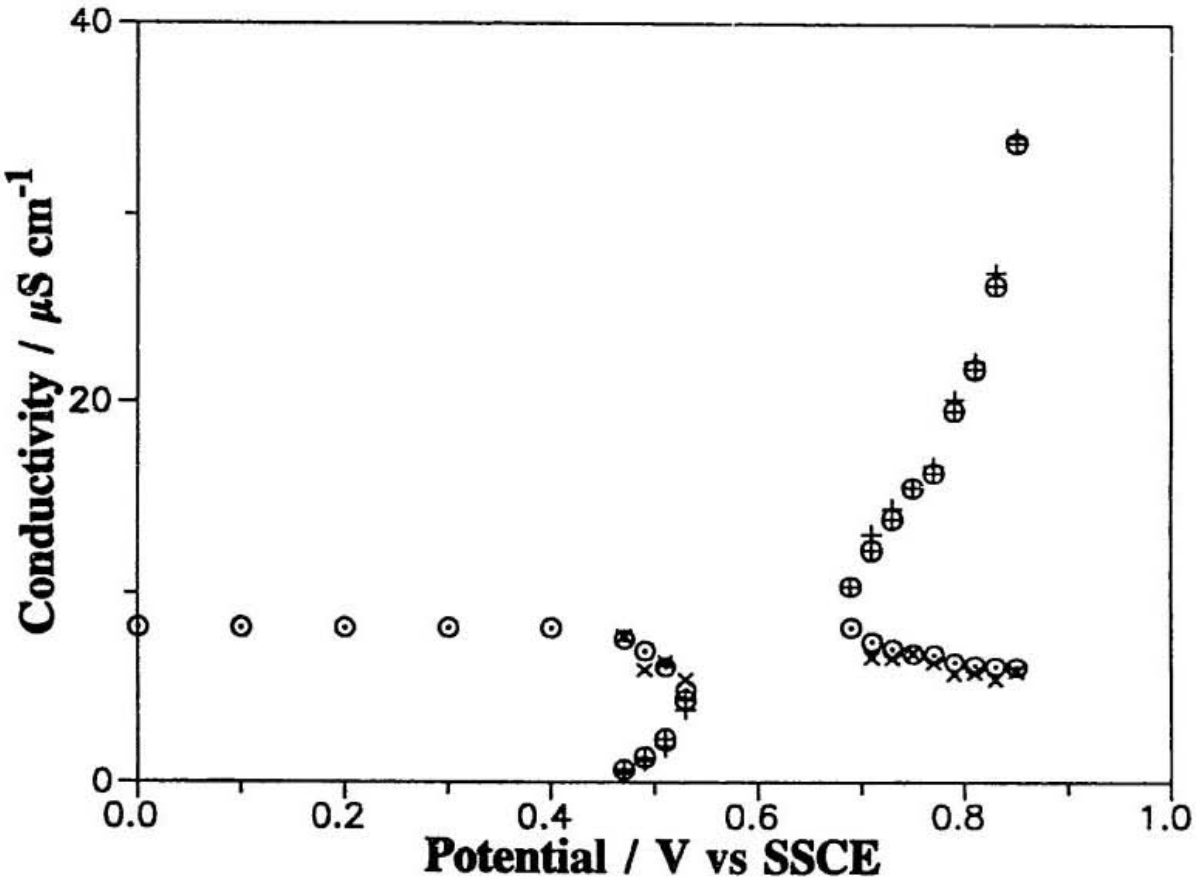

Figure 5.3.7 Electronic (⊕, +) and ionic (⊙, ×) conductivities from the impedance data shown in Fig. 5.3.4(plus additional data) for poly-MPMP in propylene carbonate containing 1.6 M $LiClO_4$. Circled points were obtained using low-frequency data while the others were obtained using data from the Warburg-type region.

obtained by solving eqs. [4.2.9] and [4.2.10], as a function of the electrode potential for the three electrolyte solutions. The conductivity which shows the least variation with electrode potential and is closest to the value of the film ionic conductivity measured for the reduced state (*e.g.* at 0.0 V *vs.* SSCE, see below) is assigned as the ionic conductivity.

5.3.2 Conductivity of Reduced Films

The impedance responses of reduced poly-MPMP (*e.g.* at 0.0 V) films shown in Fig. 5.3.2 curve C, Fig. 5.3.3 curve A and Fig. 5.3.4A curve E are almost the same as those of the bare Pt electrode; the only significant difference being a shift along the real impedance (Z′) axis. The similar values of the capacitance for the reduced film coated Pt electrodes and the bare Pt electrode (Table 5.3.1) indicate that no Faradaic processes (charging/discharging) of the polymer film occur during the impedance measurement. The very high electronic resistance of the reduced film prevents substantial electronic current (Faradaic current) to flow into the polymer. However its ionic conductivity allows the charging/discharging of the Pt/polymer interface. In this case the ionic current travels through the bulk electrolyte solution and across the polymer film to reach the underlying Pt electrode. The measured resistance for a reduced film coated Pt electrode is therefore the sum of the uncompensated solution resistance, which is measured with the bare Pt electrode, and the film's ionic resistance. Tables 5.3.2

and 5.3.3 list the ionic conductivities of reduced poly-MPMP films in various electrolyte solutions.

Table 5.3.1 Capacitances of poly-MPMP film coated Pt electrodes at 0.0 V and the bare Pt electrode at the open circuit potential in various electrolyte solutions.

Electrolyte solutions	Poly-MPMP		Pt
	Thickness μm	Capacitance μF cm^{-2}	Capacitance μF cm^{-2}
Water + 0.1 M $NaClO_4$	1.6	24.4	20.1
	3.2	25.3	21.7
CH_3CN + 0.1 M Et_4NClO_4	1.6	9.9 ± 0.1	8.3 ± 0.6
Propylene carbonate + 1.6 M $LiClO_4$	0.4	12.9 ± 0.1	16.1 ± 0.5
	0.8	13.4 ± 0.7	13.8 ± 0.6
	1.6	12.6 ± 0.1	15.0 ± 1.9
	4.0	15.0	16.7
Propylene carbonate+ 0.4 M $LiClO_4$	1.6	11.6 ± 0.1	14.9 ± 0.5

The average and standard deviation are for four measurements on the same film.

This interpretation of the impedance response of reduced poly-MPMP has been previously discussed by Pickup and shown to be correct[6]. The ionic conductivities of reduced poly-MPMP in 0.1 M KCl and KI (Table 5.3.3) are in

reasonable agreement with the values of 2.8 mS cm^{-1} and 1.2 mS cm^{-1} respectively determined by d.c. conductivity measurements on free-standing films[7].

Table 5.3.2 Ionic conductivities of reduced poly-MPMP films in various electrolyte solutions.

Electrolyte solutions	Film thickness μm	Conductivity $\mu S\ cm^{-1}$
Water + 0.1 M $NaClO_4$	1.6	312 ± 21
	3.2	384
Propylene carbonate + 1.6 M $LiClO_4$	0.4	20.2
	0.8	11.4
	1.6	7.97 ± 0.78
	3.2	7.61
	4.0	8.23
Acetonitrile + 0.1 M Et_4NClO_4	1.6	95.1 ± 13.0
	3.2	107

The average and standard deviation are for measurements on the three films.

5.3.3 $\sigma_{Ion} > \sigma_E$

Poly-MPMP films have a much higher ionic conductivity in aqueous solutions than in acetonitrile and propylene carbonate solutions due to a much larger swelling factor in water. In both aqueous and acetonitrile solutions, poly-

MPMP films have a higher ionic conductivity than electronic conductivity over the whole potential range studied. Thus in both solvents (Fig. 5.3.2 and Fig. 5.3.3) the high frequency end of the Warburg-type line in the complex plane impedance plot starts near the real axis intercept for the reduced polymer film. These experimental results show that the polymer resistance at high frequency is dominated by the low resistive path for ion transport. The polymer redox reaction starts at the Pt/polymer interface at high frequency and spreads to the polymer/electrolyte interface as the frequency is decreased.

Table 5.3.3 Ionic conductivities of a reduced 1.6 μm poly-MPMP film in various electrolyte solutions.

Electrolyte solution	Ionic conductivity $\mu S\ cm^{-1}$
Water + 0.1M KCl	1.61×10^{3}
Water + 0.1M KBr	1.01×10^{3}
Water + 0.1M KI	9.66×10^{2}
Acetonitrile + 0.1M Et_4NCl	9.21
Acetonitrile + 0.1M Et_4NBr	8.30×10^{-1}
Acetonitrile + 0.1M Tetrapropyl ammonium bromide	7.70×10^{-1}
Acetonitrile + 0.1M Tetraethyl ammonium toluene sulphonate	1.24

5.3.4 $\sigma_{Ion} < \sigma_E$

In the very viscous propylene carbonate solution, poly-MPMP exhibits the lowest ionic conductivity among the three solvents studied. Fig. 5.3.4A curve A shows a complex plane impedance plot for a highly oxidized film. The high frequency end of the Warburg-type line starts near the real axis intercept for the bare Pt electrode, indicating that charge transport in the oxidized polymer film at high frequency is dominated by electron transport, which is now the lower resistance rail in the transmission line (Fig. 4.2.2). In this case, the polymer redox reaction induced by the potential perturbation starts near the polymer/electrolyte interface at high frequency and spreads inwards to the Pt/polymer interface as the frequency is decreased.

For Poly-MPMP, decreasing the electrode potential decreases its electronic conductivity. At electrode potentials lower than 0.51 V *vs.* SSCE, the electronic conductivity of the polymer film is lower than its ionic conductivity, and the complex plane impedance plots (Fig. 5.3.4B) are similar to those for the aqueous and acetonitrile solutions.

5.3.5 $\sigma_{Ion} \approx \sigma_E$

The movement of charge carriers within the polymer film can be described by the classical transmission line circuit (Figs. 4.2.1 and 4.2.3) when the electronic and ionic conductivities are very unequal, and the impedance plot in the complex plane has a well defined 45° Warburg-type region. However, as the two conductivities approach each other, the Warburg-type region becomes steeper and shorter as shown in Fig. 5.3.4A curve C and D, and eventually eqs. [4.2.9] and [4.2.10] offer no real solutions. For these equations to have a real solution, the length of the Warburg-type region (projected onto the real axis) must be at least 33% of R_∞ (*i.e.* R_Σ must at least $4R_\infty$). Similar situations were encountered for thicker films as well (Table 5.3.4). Fig. 5.3.8 shows a comparison of the complex plane impedance plots for a poly-MPMP film in propylene carbonate at 0.59 V *vs.* SSCE (previously shown as curve D in Fig. 5.3.4A) with the simulated data from the model circuit (Fig. 4.2.2) using $R_E = R_{Ion} = R_\infty/2$. Clearly the Warburg-type region for the experimental data is too short.

Table 5.3.4 Electronic and ionic conductivities ($\mu S\ cm^{-1}$) for Poly-MPMP films in propylene carbonate containing 1.6 M $LiClO_4$.

Electrode Potential V	1.6 μm		3.2 μm		4.0 μm	
	σ_E	σ_{Ion}	σ_E	σ_{Ion}	σ_E	σ_{Ion}
0.85	33.8	6.11	38.2	4.10	23.0	5.04
0.83	26.2	6.15	30.0	4.23	19.3	5.19
0.81	21.8	6.22	25.8	4.32	17.4	5.28
0.79	19.6	6.39	23.8	4.28	16.3	5.35
0.77	16.3	6.80	21.3	4.26	15.4	5.36
0.75	15.5	6.82	20.4	4.25	14.4	5.77
0.73	13.9	7.10	15.8	4.45	13.3	5.71
0.71	12.3	7.48	14.7	4.49	12.5	5.77
0.69	10.4	8.25	13.6	4.60	11.3	5.98
0.67	-[a]	-[a]	12.3	4.77	9.90	6.29
0.65	-[a]	-[a]	11.2	4.67	-[a]	-[a]
0.63	-[a]	-[a]	9.20	4.85	-[a]	-[a]
0.61	-[a]	-[a]	7.40	5.53	-[a]	-[a]
0.59	-[a]	-[a]	-[a]	-[a]	-[a]	-[a]
0.57	-[a]	-[a]	-[a]	-[a]	-[a]	-[a]
0.55	-[a]	-[a]	-[a]	-[a]	-[a]	-[a]
0.53	4.32	4.84	3.64	4.57	3.08	6.14
0.51	2.20	6.10	2.06	5.31	2.17	6.64
0.49	1.31	6.98	1.51	5.86	1.70	7.00
0.47	0.68	7.61	1.05	5.73	1.29	7.40

[a] -- No real solutions for the eqs. [4.2.9] and [4.2.10].

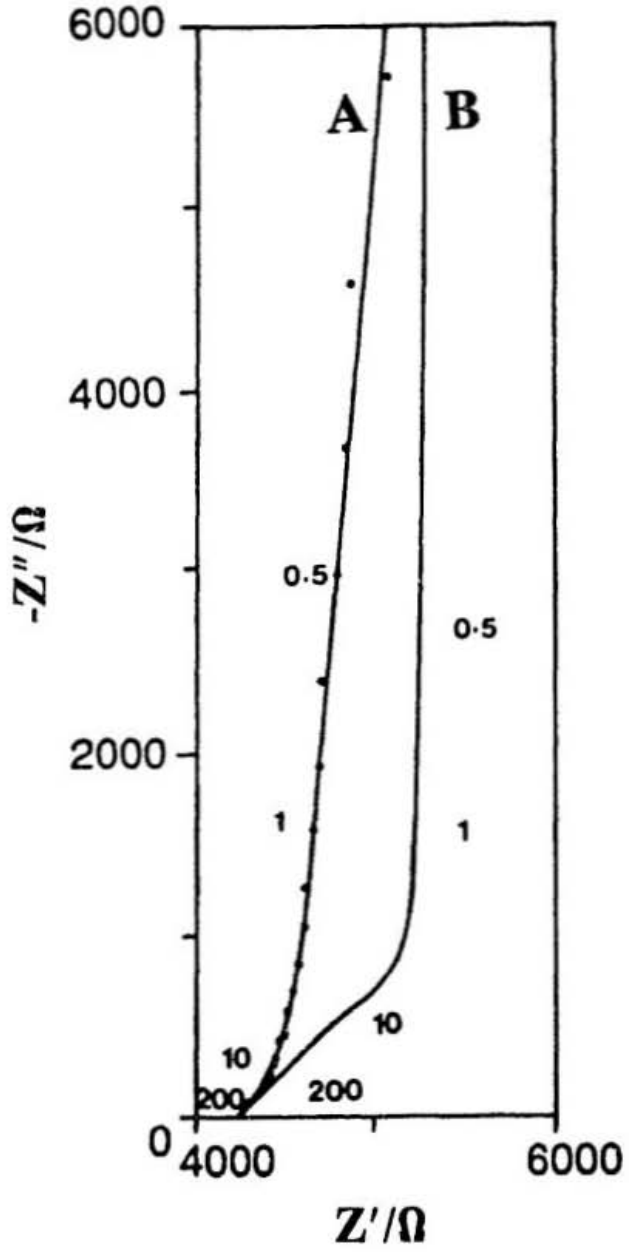

Figure 5.3.8 Experimental impedance plot (A) for a 1.6 μm poly-MPMP film at 0.59 V in propylene carbonate + 1.6 M $LiClO_4$ and (B) simulated impedance plot based on the circuit shown in Fig.4.2.3 when $R_{ion}=R_E$. Frequencies of selected points are indicated in Hz.

The decreasing ionic conductivity with increasing potential observed in Figs. 5.3.5, 5.3.6 and 5.3.7 is anomalous since the increasing concentration of counter ions in the polymer as it is oxidized should lead to an increase in ionic conductivity. Extrapolation of the sloped low-frequency region of the impedance plot will presumably underestimate R_Σ. However the low experimental ionic conductivity results indicate that R_Σ is overestimated. To investigate the significance of this error, R_E and R_{ion} were also estimated from data in the Warburg-type region. Plotting $|Z - R_\infty - R_s|^2$ *vs.* $1/\omega$ for these data forms a straight line (Fig. 5.3.9) as predicted by eq. [4.2.11]. R_E and R_{ion} values were obtained from the slopes of such plots and R_∞ (eq. [4.2.9]). Conductivities obtained in this way are not significantly different from those obtained using the low-frequency data (Figs. 5.3.5, 5.3.6 and 5.3.7). This confirms that the ionic conductivity of the polymer indeed decreases as it is oxidized. Similarly, there are no solutions for eqs. [4.2.9] and [4.2.10] for the data in curves B to D in Fig. 5.3.4A using this alternative data analysis method. Since all deviations from the transmission line model are centered at a potential where the film exhibits equal electronic and ionic conductivities, a coupling of ion and electron transport may be responsible. Further discussion of the coupling of ion and electron transport can be found in a published paper[23].

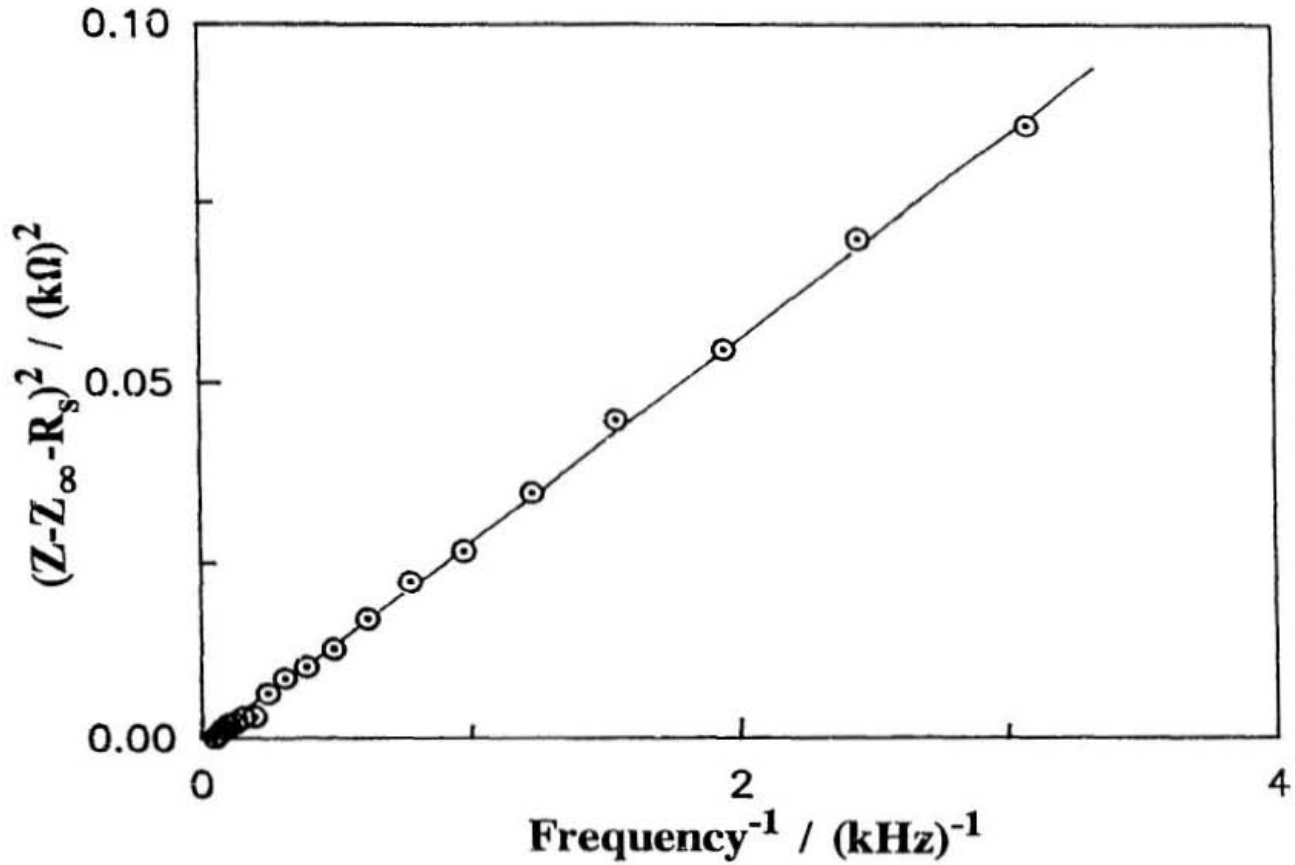

Figure 5.3.9 Plot of $(Z\text{-}Z_\infty\text{-}R_s)^2$ *vs.* 1/frequency for the high frequency data on the Warburg-type line for curve A shown in Figure 5.3.5A.

5.3.6 Discussion

Since one of the major purposes of this study was to examine the applicability of the dual rail transmission line model in analyzing the impedance data of conducting polymers, it is essential to compare the derived electronic and ionic conductivities of poly-MPMP with previously reported data[6,7,10]. The accuracy of the electronic conductivities can be seen by comparison with results from independent methods[10] as shown in Fig. 5.3.10. The impedance results agree well with results from rotating-disc voltammetry and dual electrode voltammetry. The discrepancy at higher potentials has been attributed to the coupling of ion and electron transport[23]. Ion and electron transports are involved simultaneously in impedance spectroscopy but not in the other two methods, and the coupling effect becomes more pronounced at potentials where both conductivities approach each other (Fig. 5.3.4).

The accuracy of the ionic conductivities can be assessed from the data in Figs. 5.3.5, 5.3.6 and 5.3.7 by comparing the values for the oxidized polymer (E > 0.4 V) with those for the reduced polymer. The determination of the reduced polymer ionic conductivity by impedance spectroscopy is effectively an independent method and there is no doubt that the values obtained are accurate.

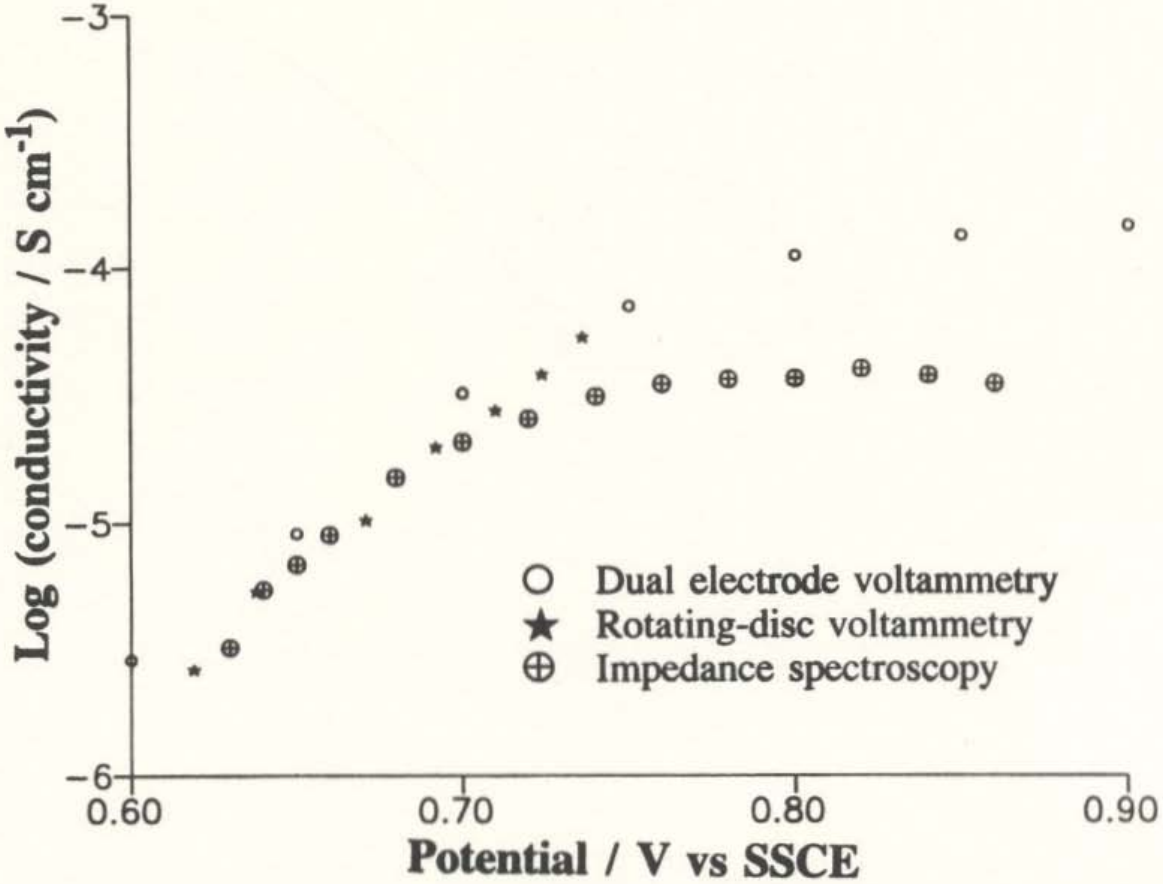

Figure 5.3.10 Comparison of electronic conductivities for poly-MPMP in acetonitrile from impedance spectroscopy (⊕ this work) with reported values (Ref. 10) from dual electrode voltammetry (○) and rotating-disc voltammetry (★).

Since poly-MPMP contains 5.6 M of cation exchange sites and oxidation adds at most 20% more cationic sites located on the polypyrrole backbone[5], it is expected that the ionic conductivities of the oxidized states are not significantly different from that of the reduced state. The discrepancies in Figs. 5.3.5, 5.3.6 and 5.3.7 are at most *ca.* 50%. This is remarkably good agreement given the difference in the electrochemistry involved in the polymer film during impedance measurements on the oxidized and reduced states. For the reduced polymer, only the Pt double layer is charged/discharged and the polymer film merely acts as a barrier to ion transport between the bulk electrolyte solution and the Pt surface. For oxidized films, a redox reaction occurs in the polymer layer and at low frequency the whole film is charged/discharged during each cycle of the potential perturbation.

5.4 Polypyrrole/poly(styrene sulphonate)

Complex plane impedance plots covering three different electrode potential ranges for a 2 μm PPY/PSS coated Pt electrode in a saturated $NaClO_4$(aq) solution are shown in Figs. 5.4.1A , B and C. A saturated solution was used in these

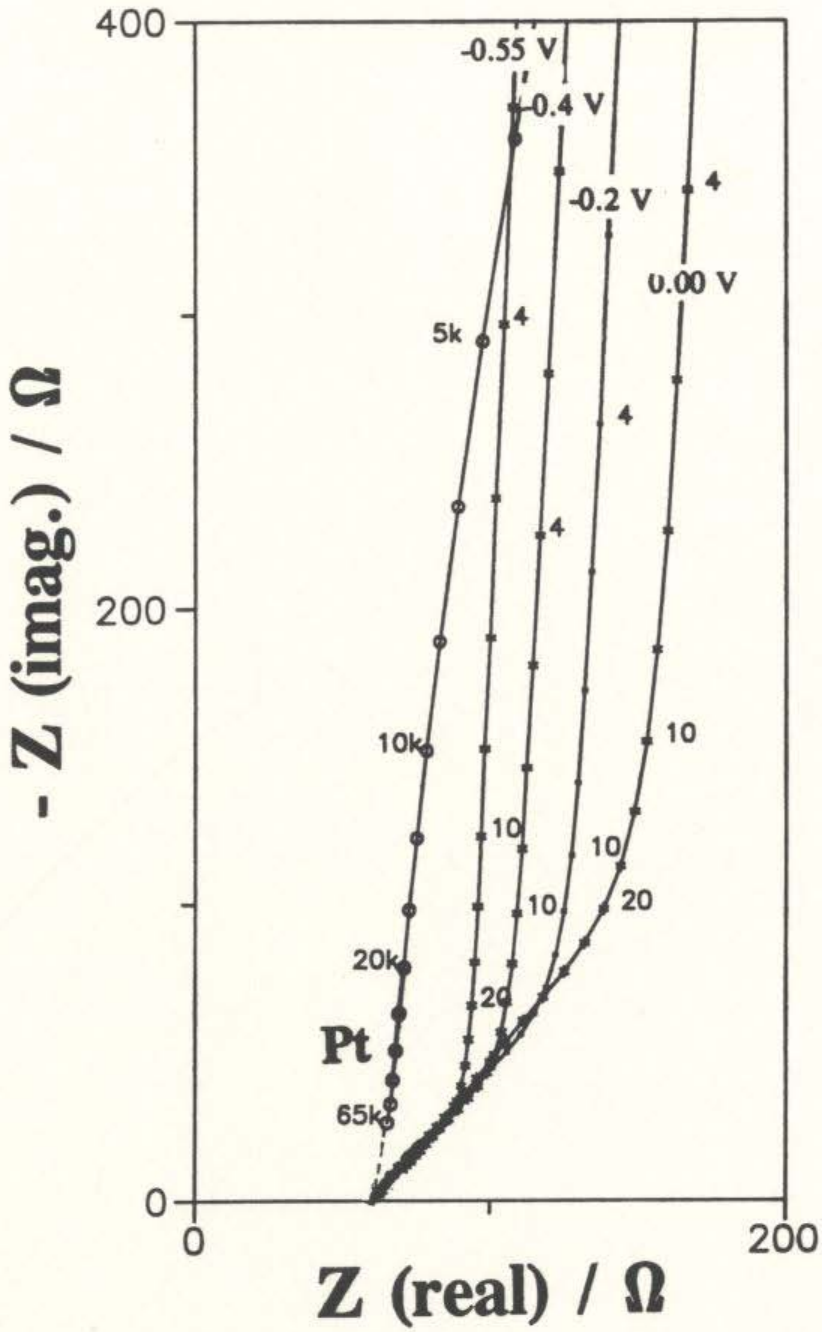

Figure 5.4.1A Complex plane impedance plots for a 2.0 μm PPY/PSS film on a Pt electrode in saturated aqueous $NaClO_4$. Electrode potentials are indicated in V *vs.* Ag/AgCl. The plot marked Pt is for the bare Pt electrode at open circuit. Frequencies in Hz are marked for selected points.

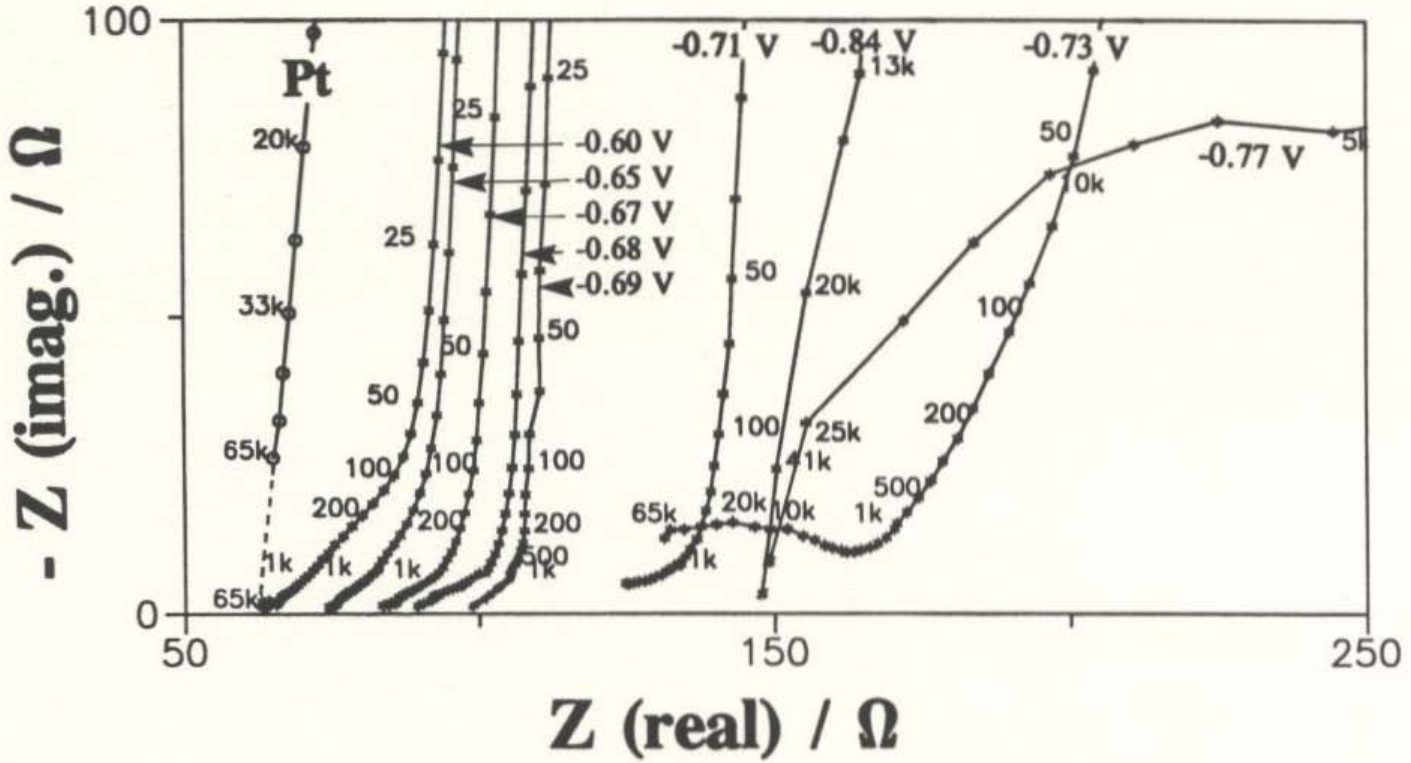

Figure 5.4.1B Complex plane impedance plots for a 2.0 μm PPY/PSS film on a Pt electrode in saturated aqueous $NaClO_4$. Electrode potentials are indicated in V *vs.* Ag/AgCl. The plot marked Pt is for the bare Pt electrode at open circuit. Frequencies in Hz are marked for selected points.

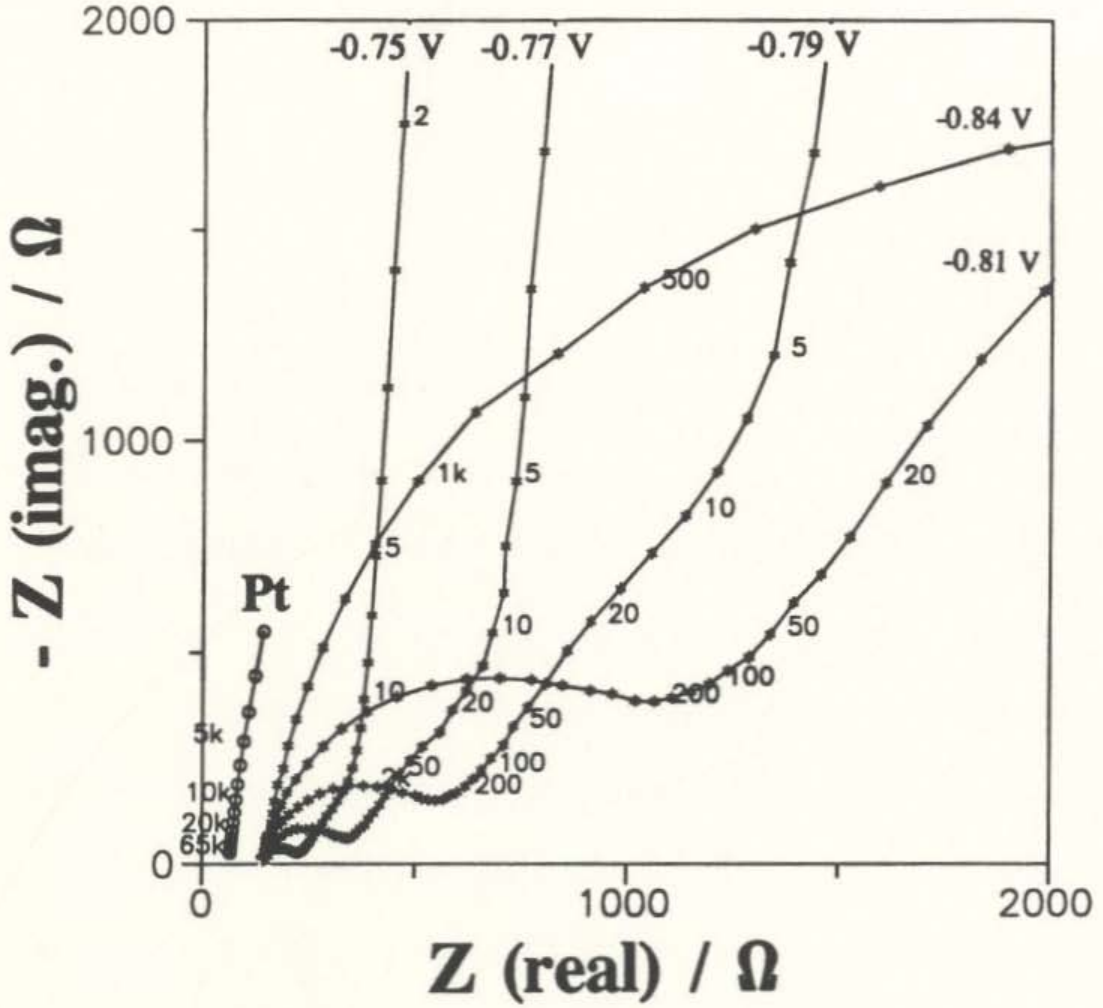

Figure 5.4.1C Complex plane impedance plots for a 2.0 μm PPY/PSS film on a Pt electrode in saturated aqueous $NaClO_4$. Electrode potentials are indicated in V *vs.* Ag/AgCl. The plot marked Pt is for the bare Pt electrode at open circuit. Frequencies in Hz are marked for selected points.

experiments to minimize the degree of polymer film swelling by water. The polymer films exhibited high stability in this solution. Consequently, very reproducible measurements (within 6 % at the same potential) were obtained either for a single film over a period of 24 hours or for different films prepared under the same conditions.

For the potential range covered by Fig. 5.4.1A, the electronic conductivity of the polymer film is much larger than its ionic conductivity. The impedance responses were therefore modelled with the classic transmission line circuit (Fig. 4.2.3) to extract ionic resistances for the polymer film. Table 5.4.1 lists the film ionic conductivities measured in this potential range.

The complex plane impedance plots shown in Fig. 5.4.1B are characterized by a shift of the real impedance intercept of the high frequency data for the polymer electrode away from that for the bare Pt electrode, indicating that the electronic resistance of the film has become comparable with its ionic resistance. To model these impedance data and extract the polymer's electronic and ionic resistances it is necessary to invoke the dual rail transmission line circuit (Fig. 4.2.2). The film electronic and ionic conductivities are also listed in Table 5.4.1. It is interesting to notice that for this polymer eqs. [4.2.9] and [4.2.10] offer no real solutions for the impedance data at -0.69 V because the Warburg-type region is too short.

Table 5.4.1 Electronic and ionic conductivities for a 2 μm PPY/PSS film coated Pt electrode in saturated $NaClO_4$ (aq).

E V	R_{high} Ω	R_{low} Ω	σ_{Ion} $\mu S\ cm^{-1}$	σ_E $\mu S\ cm^{-1}$	C_F [d] $mF\ cm^{-2}$
0.00	60.6	149	168	-[a]	28.1
-0.10	60.5	137	194	-[a]	31.3
-0.20	60.5	125	230	-[a]	37.0
-0.30	60.8	111	294	-[a]	41.4
-0.40	60.8	104	341	-[a]	43.2
-0.50	60.6	94.4	438	-[a]	38.7
-0.55	60.6	88.7	527	-[a]	32.8
-0.60	63.1	89.6	526	$1.73x10^4$	27.1
-0.63	68.0	91.3	529	$5.48x10^3$	24.0
-0.65	73.1	93.6	527	$3.03x10^3$	21.8
-0.67	83.4	100	506	$1.44x10^3$	19.5
-0.68	89.4	105	492	$1.05x10^3$	18.2
-0.69	96.7	107	-[b]	-[b]	17.9
-0.70	109	126	517	401	15.1
-0.71	-[c]	140	-[c]	-[c]	14.9
-0.72	-[c]	166	-[c]	-[c]	13.5

[a] The electronic conductivity of the polymer is very high, and the impedance response is modelled with a classical transmission line circuit (Fig. 4.2.3).

[b] No real solutions for the equations from Albery's dual rail transmission line model.

[c] R_{high} can not be accurately determined due to the ill-defined emerging semicircle at high frequency in the complex plane impedance plots.

[d] Capacitances were obtained from the slope ($=1/C_F$) of an imaginary impedance (Z'') *vs.* 1/frequency ($1/\omega$) plots for low frequency data.

Fig. 5.4.1C shows the impedance responses for PPY/PSS as the electrode potential is further decreased. Now the film's electronic resistance becomes much larger than its ionic resistance. In this potential range, the high frequency data form a distinct semicircle in the complex impedance plane. As the frequency is decreased, the semicircle merges with the 45° Warburg-type line. At very low frequencies the impedance data form a nearly vertical line.

Based on the same argument used for the reduced poly-MPMP film coated Pt electrode in section 5.3, the ionic resistance of reduced PPY/PSS film can be accurately and independently determined by the real impedance shift between the bare Pt and the polymer coated electrode at very high frequencies. It was found that the film ionic resistance in the potential range from -0.75 to -0.86 V is nearly constant at *ca.* 509 μS cm^{-1}. This value is remarkably close to the values (526 to 492 μS cm^{-1}) obtained using the dual rail transmission line circuit (Fig. 4.2.2) for electrode potentials from -0.6 to -0.7 V, and the value (527 μS cm^{-1}) obtained using the classical transmission line circuit (Fig. 4.2.3) for the data at -0.55 V. Thus varying the electrode potential between -0.55 V and -0.86 V does not appear to change significantly the number of mobile Na^+ ions in the polymer film. This conclusion is consistent with cyclic voltammograms of the polymer (Fig. 7.2.1B), which show little anodic current over this range.

The high frequency real axis intercepts of the semicircles in Fig. 5.4.1C correspond to the uncompensated bulk solution resistance plus the film ionic resistance. This suggests that the semicircles originate from a process at the polymer/Pt interface, where electron transfer occurs. However, an ionic double layer at the polymer/solution interface in parallel with an ion transfer resistance across the polymer/solution interface is also a possibility. In this case, the redox reaction of the reduced PPY/PSS film would still start at the Pt/polymer interface. Oxidation of the polymer would involve the transport of Na^+ ions towards the polymer/solution interface. It is possible that there is a kinetic barrier which hinders the Na^+ ions crossing the polymer/solution interface. Charge balance may be more easily achieved by bringing the electrolyte anions from the bulk solution to the polymer surface to form an ionic double layer at the polymer/solution interface. The equivalent circuits that describe the two kinds of interfacial charge transfer process discussed above are shown in Figs. 5.4.2A and 5.4.2B respectively.

Starting from the fundamental kinetic equations, it has been predicted by Albery[24] that the charge transfer resistance (R_{ct}) for electron transfer at the Pt/Polymer interface will increase as the electrode potential is shifted away from the polymer's formal potential. For a polymer film such as PPY/PSS which

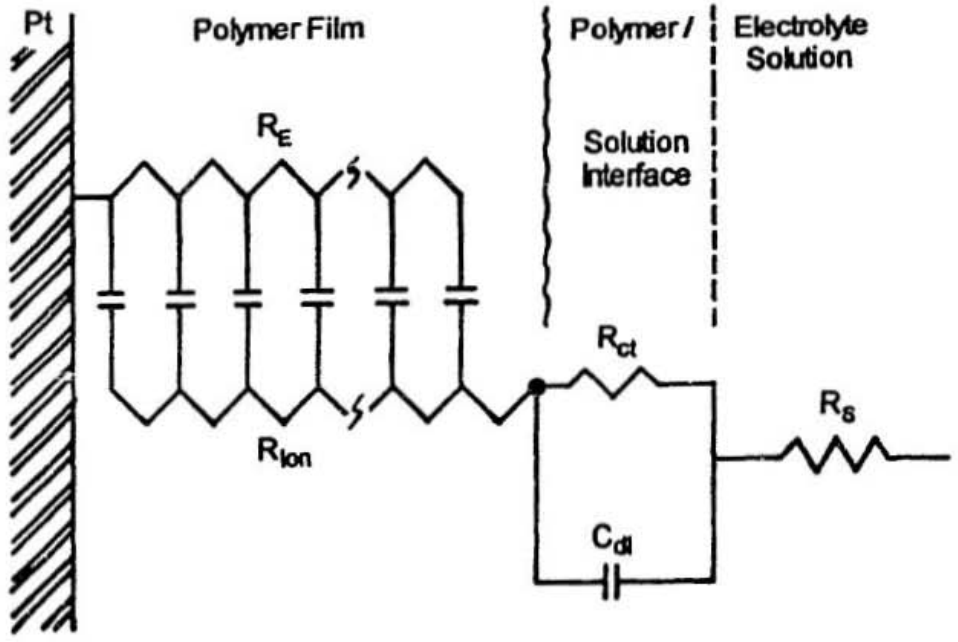

Figure 5.4.2B Modified transmission line circuit containing a R_{ct} and C_{dl} element at the polymer/solution interface.

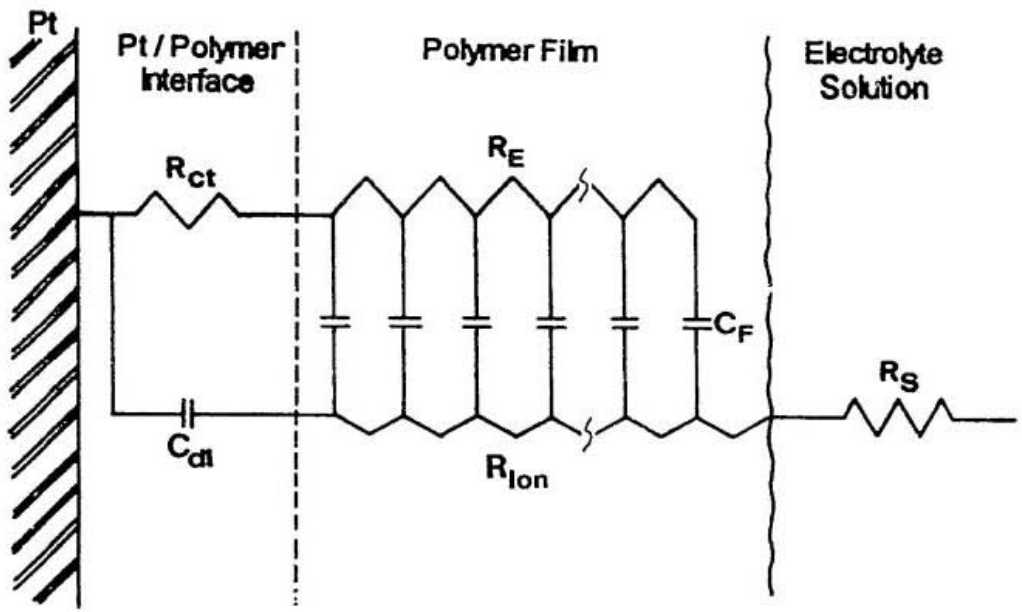

Figure 5.4.2A Modified transmission line circuit containing a R_{ct} and C_{dl} element at the electrode/polymer interface.

contains mobile cations as the ionic charge carriers, decreasing the electrode potential will decrease R_{ct} for ion transfer at the polymer/solution interface; while for a polymer film such as PPY/ClO_4^- which contains mobile anions as the ionic charge carriers, decreasing the electrode potential will increase R_{ct} for ion transfer at the polymer/solution interface. Therefore the observation of the potential dependence of R_{ct} for PPY/PSS (Fig. 5.4.1C) quickly confirms that the semicircle is due to electron transfer at the Pt/polymer interface. Discrimination between the two charge transfer processes for PPY/ClO_4^- requires additional information such as the electrolyte concentration dependence of R_{ct}[24], since R_{ct} values for both interfacial processes will increase with decreasing electrode potential.

The equivalent circuit shown in Fig. 5.4.2A can describe the impedance response of PPY/PSS at all potentials. For oxidized PPY/PSS film, R_{ct} is negligible. The small capacitance of C_{dl} in parallel with the large capacitance of the polymer layer is also negligible. In this situation, the equivalent circuit is reduced to the dual rail transmission line circuit (Fig. 4.2.2).

Table 5.4.2 lists the parameters obtained by fitting the experimental impedance data in the potential range from -0.73 to -0.86 V to the equivalent circuit shown in Fig. 5.4.2A with a complex non-linear least square fitting program (ZSIM/CNLS, Scribner Associates, Inc). Fig. 5.4 3 shows an example

Table 5.4.2 Fitting results for the impedance data shown in Fig.5.4.1C to the equivalent circuit shown in Fig. 5.4.2B. (R_{Ion} is 88.1 Ω at all potentials)

E V	C_{dl} $\mu F\ cm^{-2}$	R_{ct} Ω	R_E Ω	C_F [a] $mF\ cm^{-2}$	C_F [b] $mF\ cm^{-2}$	σ_E $\mu S\ cm^{-1}$
-0.73	42.6	26.4	158.3	10.7	13.2	281
-0.74	37.4	43.1	295.6	10.1	11.5	150
-0.75	36.4	62.0	516.7	9.27	11.0	86.0
-0.76	36.5	85.1	782.7	8.81	9.96	56.8
-0.77	35.4	126	$1.31x10^3$	7.97	9.65	34.1
-0.78	38.5	169	$2.02x10^3$	7.62	8.55	22.1
-0.79	43.9	227	$3.20x10^3$	7.28	8.13	13.9
-0.80	46.8	343	$4.81x10^3$	6.67	7.48	9.23
-0.81	49.6	516	$7.65x10^3$	6.20	6.74	5.81
-0.82	52.9	782	$1.21x10^3$	5.70	6.36	3.67
-0.83	59.8	$1.15x10^3$	$1.78x10^3$	5.44	5.92	2.50
-0.84	59.6	$1.91x10^3$	$2.94x10^3$	4.71	5.03	1.51
-0.85	63.1	$2.99x10^3$	$4.48x10^3$	4.29	4.81	0.99
-0.86	67.3	$4.48x10^3$	$6.95x10^3$	4.01	4.64	0.64

[a] From the best fit time constants ($\tau = C_F x R_E$) of the transmission line.
[b] From the slopes ($=1/C_F$) of imaginary impedance (Z'') *vs.* 1/frequency ($1/\omega$) plots for low frequency data.

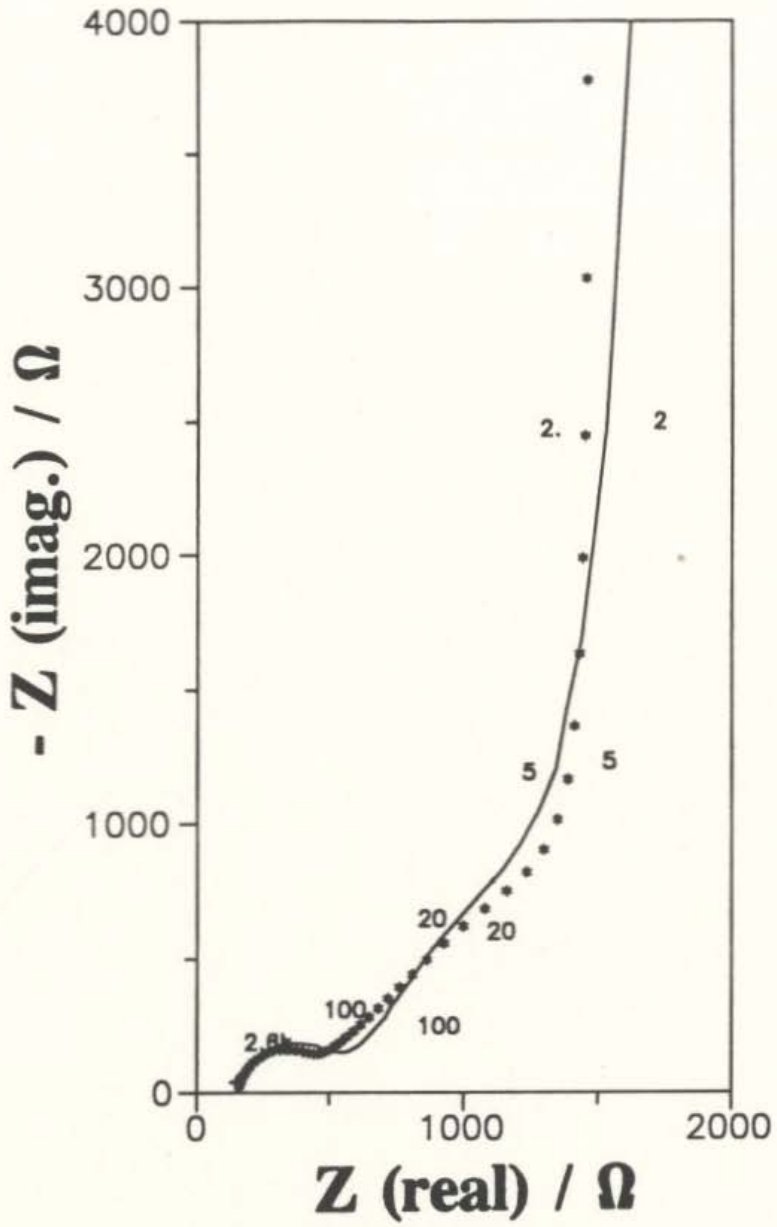

Figure 5.4.3 Complex plane impedance plots of the experimental data (curve for -0.79 V in Fig. 5.4.1C) and its fitted data to the circuit shown in Fig. 5.4.2A.

of the fitted data as compared to the experimental data in the complex impedance plane. The double layer capacitance of the polymer coated electrode is close to that for the bare Pt electrode (34.6 μF cm^{-2}) in the same electrolyte solution. Plotting $\log R_{\alpha}$ *vs.* electrode potential forms a straight line (Fig. 5.4.4) with a slope of -60 $\pm$ 1 mV (average for three films) per decade. Such super-Nearstian behaviour of the polypyrrole film is due to a very high self-exchange rate for the charge transfer process at the Pt/polymer interface so that the equilibrium state is always maintained with the changing potential.

The film electronic and ionic conductivities are plotted in Fig 5.4.5 as a function of electrode potential. The relative values of the electronic and ionic conductivities in the three potential regions discussed above are clearly presented in this figure. A plot of the film electronic conductivity *vs.* electrode potential forms a straight line with a slope of 60 mV /per decade (Fig. 5.4.6). The film electronic conductivities derived using the dual rail transmission line (Fig. 4.2.2) in the potential range -0.6 to -0.7 V are consistent with those obtained by fitting the experimental data to the equivalent circuit shown in Fig. 5.4.2A.

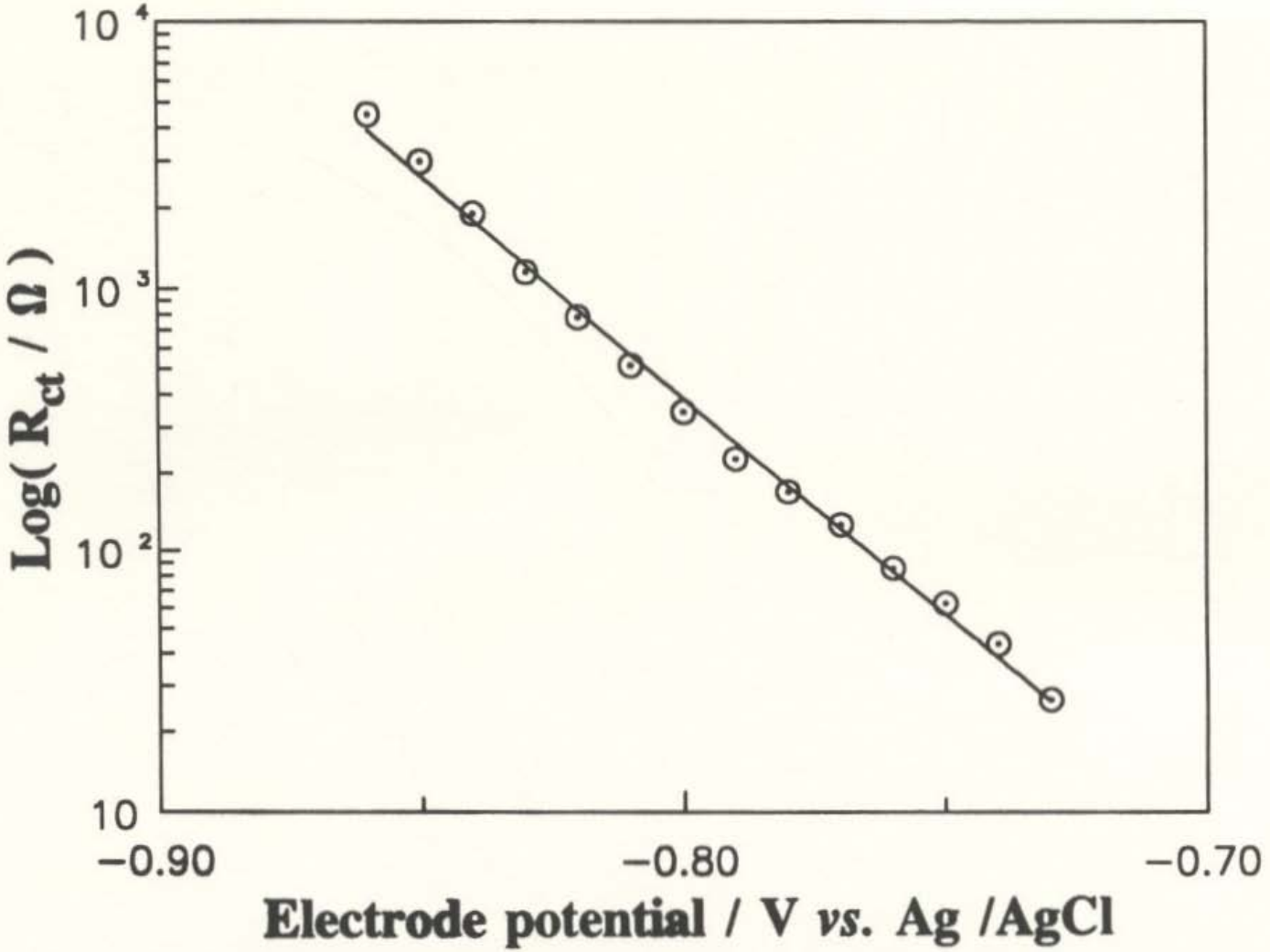

Figure 5.4.4 Plot of Log (charge transfer resistance) *vs.* electrode potential for a PPY/PSS film coated electrode. The best fit line has a slope of -60 mV /decade.

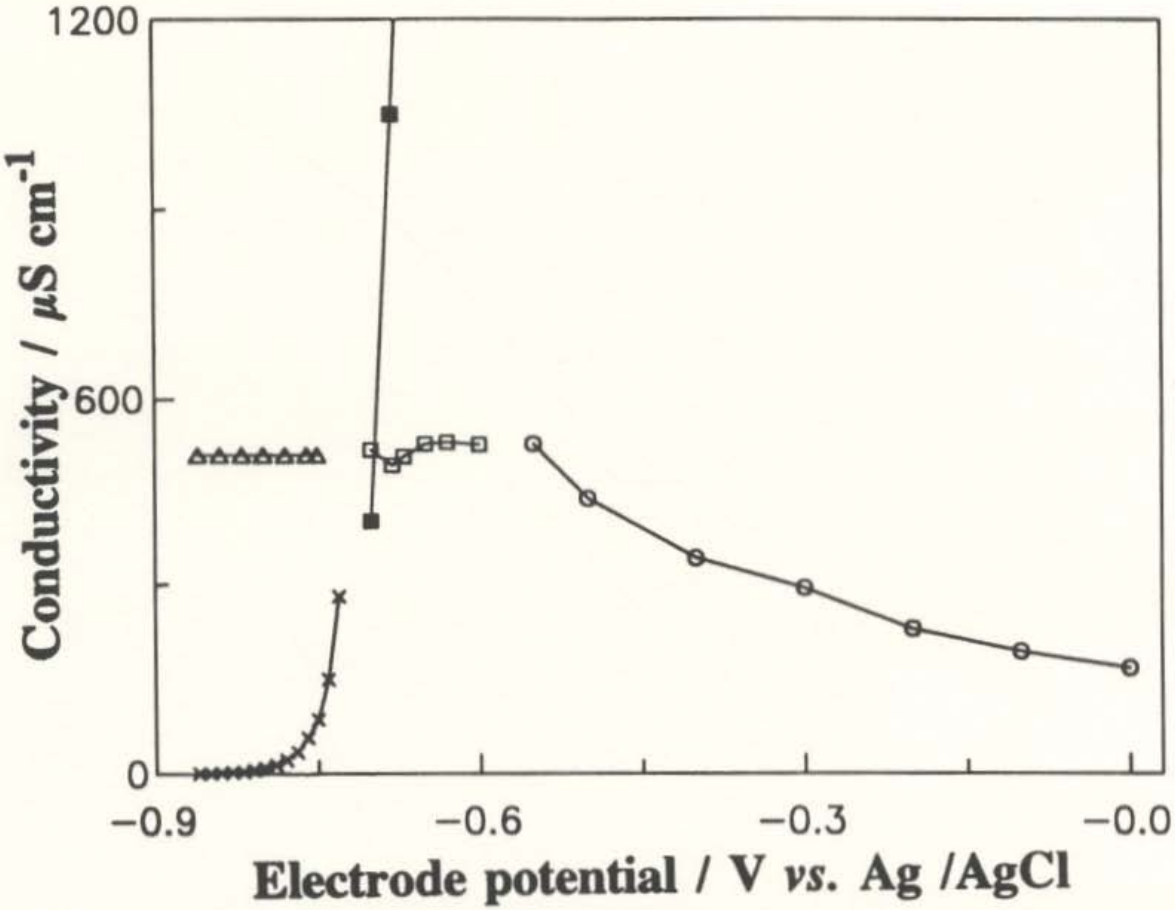

Figure 5.4.5 Electronic (× and ■) and ionic (△, □ and ○) conductivities from the impedance data shown in Fig.5.4.1 (plus additional data) for PPY/PSS in saturated aqueous $NaClO_4$. Circled points were extracted using the classic transmission line circuit shown in Fig.4.2.3 and squared points using the dual rail transmission line circuit shown in Fig.4.2.2. Crossed points and triangular points were obtained by fitting the experimental data to the circuit shown in Fig.5.4.2A.

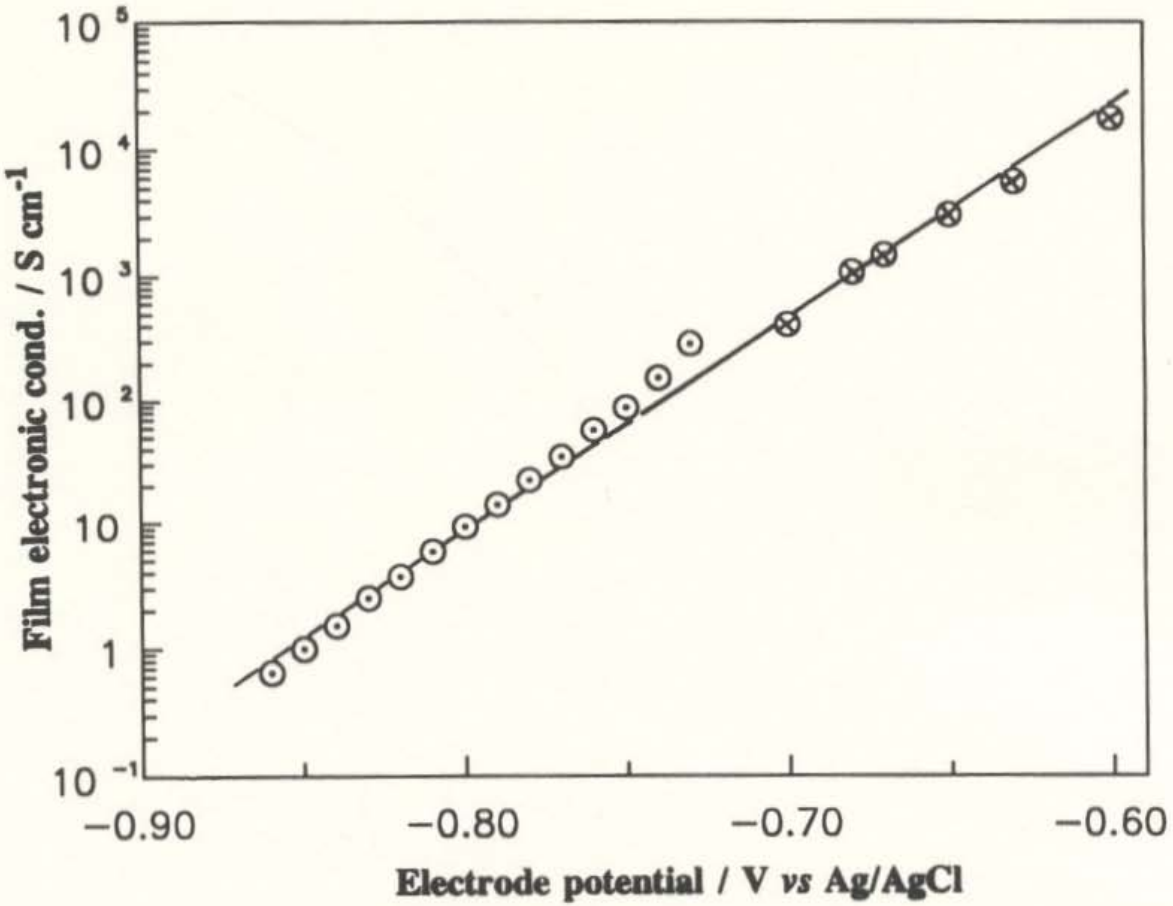

Figure 5.4.6 Plot of Log (electronic conductivity) *vs.* electrode potential for a PPY/PSS film coated electrode. Circled points were obtained by fitting the experimental data to the circuit shown in Fig.5.4.2A and crossed points were extracted using the dual rail transmission line circuit shown in Fig.4.2.2. The best fit line has a slope of **60** mV /decade.

5.5 Conclusions

The impedance response of oxidized PPY/ClO_4^- film on a Pt electrode is very close to the ideal impedance response of the classical transmission line circuit shown in Fig. 4.2.3. The high electronic conductivity of this film relative to its ionic conductivity and the uniform film morphology allow the use of the classical transmission line circuit to extract the film ionic resistance from experimental impedance data. The projected length of the Warburg-type line on the real axis equals one third of the film ionic resistance.

The high frequency Warburg-type line for poly-MPCA deviates from the ideal response. This has been shown to be related to the non-uniform structure of this polymer. Plots of simulated impedance responses obtained by linearly varying film ionic resistance and capacitance distribution across the film thickness can be used to characterize the experimental impedance data for films that have a non-uniform structure.

Overall, the experimental impedance data of poly-MPMP fit the dual rail transmission line circuit (Fig. 4.2.2) and the extracted film ionic and electronic

conductivities under a variety of conditions agree with independent measurements. This anion exchange polymer exhibits a nearly constant ionic conductivity over the electrode potential range studied. The ionic conductivity of the polymer film changes with the solvent used to prepare the electrolyte solution, from about 3.1×10^2 μS cm^{-1} in water to 8.0 μS cm^{-1} in propylene carbonate, while the maximum electronic conductivity of the oxidized polymer is almost constant at *ca.* 38 μS cm^{-1}. In propylene carbonate electrolyte solution, the oxidized polymer has a higher electronic conductivity than its ionic conductivity, and the reduced polymer has higher ionic conductivity than its electronic conductivity. As the electrode potential is changed, the whole spectrum of impedance responses for a conducting polymer has been observed. The experimental results generally support Albery's dual rail transmission line model, where the mobilities of charge carriers in the polymer phase and in the pore solution phase are each modelled with a uniformly distributed resistance rail. When either the electronic or ionic resistance is much larger than the other, the complex plane impedance plots exhibit a well defined 45° Warburg-type region. As the two resistances approach each other, the length of the Warburg-type region decreases and the polymer reaches the finite thickness limited charging/discharging region at a higher frequency than predicted by Albery's model. Although there are no real solutions for eqs. [4.2.9] and [4.2.10] when the two resistances are very similar, the Warburg-type region is still

observed. The unexpected changes of ionic conductivity of poly-MPMP with electrode potential suggest that electron transport in the polymer phase is coupled with the dopant ion transport in the solution phase.

The impedance response of PPY/PSS can be modelled with a modified dual transmission line circuit (Fig. 5.4.2A) which includes a parallel R_{ct} and C_{dl} element to represent the electron transfer process at the Pt/polymer interface. As the electrode potential is decreased from the highly oxidized state to the near neutral state, three types of impedance responses have been observed. For a conducting film (potential $>$-0.55 V), the classical transmission line circuit (Fig. 4.2.3) is sufficient to extract the ionic resistance, which equals three times the projected length of the Warburg-type line on the real axis. At intermediate potentials (-0.6 to -0.7 V), the electronic resistance of the polymer film becomes comparable with its ionic resistance and the dual rail transmission line circuit (Fig. 4.2.2) is required to model the impedance data. Abnormal behaviours similar to those observed for poly-MPMP have also been observed for PPY/PSS when the electronic and ionic conductivities are very similar. As the electrode potential is further decreased, the electronic resistance becomes much larger than the ionic resistance. Ideally, the classical transmission line (Fig. 4.2.1) can be used to extract the film's electronic resistance from the projected length of the Warburg-type line on the real axis. However, in this potential range the high frequency data

form a semicircle in the complex plane impedance plots. A better data analysis method is to fit the experimental data to the modified transmission line circuit (Fig. 5.4.2A). The ionic resistances obtained for the above three potential regions agree reasonably well with each other.

References

(1) Albery, W.J.; Chen, Z.; Horrocks, B.R.; Mount, A.R.; Wilson, P.J.; Bloor, D.; Monkman, A.T.; Elliott, C.M. *Faraday. Discuss. Chem. Soc.* 1989,*88*,247.

(2) Albery, W.J.; Elliott, C.M.; Mount, A.R. *J. Electroanal. Chem.* 1990,*288*,15.

(3) Albery, W.J.; Mount, A.R. *J. Chem. Soc., Faraday. Trans.* 1993,*89*,327.

(4) Elliott, C.M.; Kopelove, A.B.; Albery, W.J.; Chen, Z. *J. Phys. Chem.* 1991,*95*,1743.

(5) Mao, H.; Pickup, P.G. *J. Electroanal. Chem.* 1989,*265*,127.

(6) Pickup, P.G. *J. Chem. Soc., Faraday. Trans.* 1990,*86*,3631.

(7) Mao, H.; Pickup, P.G. *J. Phys. Chem.* 1989,*93*,6480.

(8) Ren, X.; Pickup, P.G. *J. Phys. Chem.* 1993,*97*,5356.

(9) Ren, X.; Pickup, P.G. *J. Electrochem. Soc.* 1992,*139*,2097.

(10) Mao, H.; Pickup, P.G. *Chem. Mater.* 1992,*4*,642.

(11) Mao, H.; Ochmanska, J.; Paulse, C.D.; Pickup, P.G. *Faraday. Discuss. Chem. Soc.* 1989,*88*,165.

(12) Mao, H.; Pickup, P.G. *J. Am. Chem. Soc.* 1990,*112*,1776.

(13) Zhang, W.B.; Dong, S.J. *Electrochim. Acta* 1993,*38*,441.

(14) Ren, X.; Pickup, P.G. *J. Phys. Chem.* 1993,*97*,3941.

(15) Lee, C.; Kwak, J.; Bard, A.J. *J. Electrochem. Soc.* 1989,*136*,3720.

(16) DeLevie, R.; in *Advances in Electrochemistry and Electrochemical Engineering*, Delahay, P.; Tobias, C.W. (Eds.); Vol.6, John-wiley & Sons: New York,1967;p.329.

(17) Fletcher, S. *J. Electroanal. Chem.* 1992,*337*,127.

(18) Fletcher, S. *J. Chem. Soc., Faraday. Trans.* 1993,*89*,311.

(19) Suchanski, M.R. *J. Electrochem. Soc.* 1985,*132*,2059.

(20) Rubinstein, I.; Rishpon, J.; Gottesfeld, S. *J. Electrochem. Soc.* 1986,*133*,729.

(21) Hunter, T.B.; Tyler, P.S.; Smyrl, W.H.; White, H.S. *J. Electrochem. Soc.* 1987,*134*,2198.

(22) Lang, G.; Inzelt, G. *Electrochim. Acta* 1991,*36*,847.

(23) Ren, X.; Pickup, P.G. *J. Chem. Soc., Faraday. Trans.* 1993,*89*,321.

(24) Albery, W.J. *personal. communication.* 1993.

Chapter 6

Ionic and Electronic Conductivity of Poly-(3-methyl-pyrrole-4-carboxylic acid)

Poly-(3-methyl-pyrrole-4-carboxylic acid) (poly-MPCA) was first reported as a conducting polymer by Pickup[1]. This polymer shows interesting self-doping[2-6] properties in aqueous solution[1,7,8] and has many potential applications, particularly as a battery cathode material. Here its electronic and ionic conductivity are measured *in situ* by dual electrode voltammetry and impedance spectroscopy, respectively, in aprotic solvents (acetonitrile and propylene carbonate), which are appropriate for applications in lithium batteries[9,10].

6.1 Dual electrode voltammetry

Fig. 6.1.1 shows a dual electrode voltammogram for a 3.0 μm poly-MPCA film in acetonitrile containing 0.1 M $LiClO_4$. The recorded current has been directly converted to the polymer's electronic conductivity. The contribution of ionic conductivity to this measurement is negligible because under the steady-state

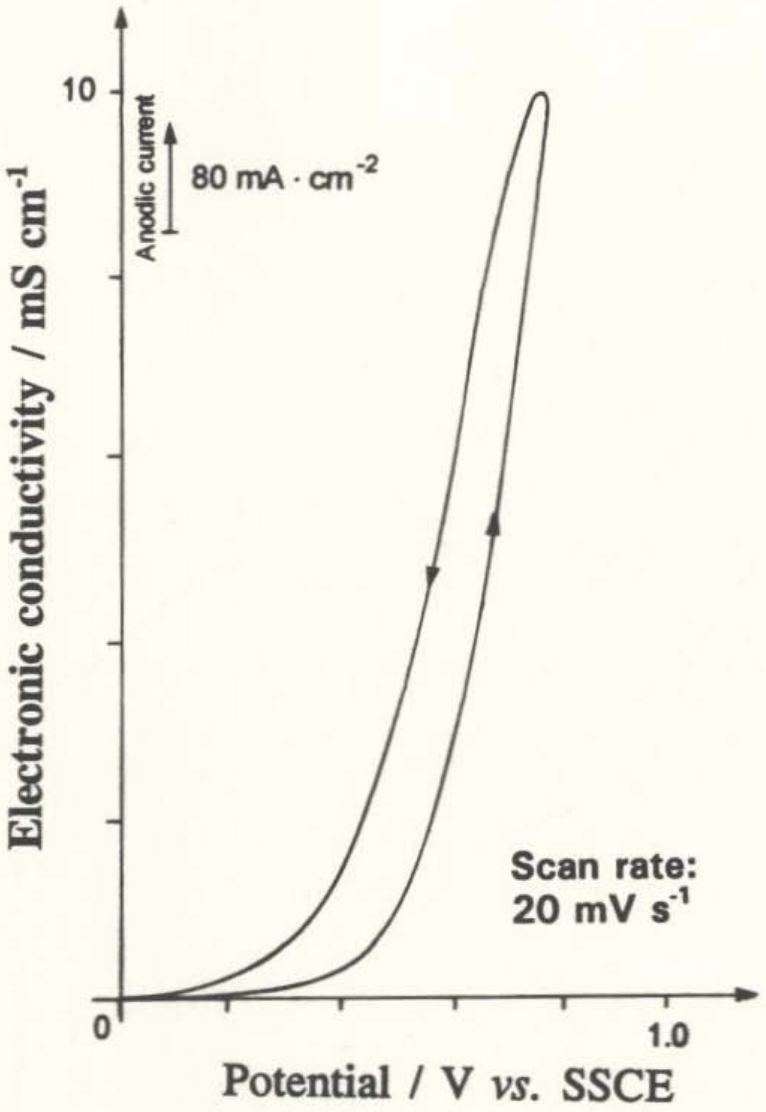

Figure 6.1.1 Dual electrode voltammogram for a 3.0 μm poly-MPCA film in acetonitrile containing 0.1 M $LiClO_4$.

dc conditions used the solution/conductor interfaces are fully polarized. The polymer acquires a higher electronic conductivity during the cathodic scan than during the anodic scan. This hysteresis increases as the scan rate and the potential difference between the two sides of the polymer film are increased, and parallels the hysteresis in the cycling charge (Fig. 3.2.2). Table 6.1.1 lists electronic conductivities measured at 0.8 V for films of various thickness. There is no significant dependence on film thickness. The electronic conductivity of poly-MPCA at 0.8 V in acetonitrile containing 0.1 M Et_4NClO_4 is therefore calculated to be 9.1 $\pm$ 2.1 mS cm^{-1}. Conductivities measured in acetonitrile containing 0.1 M $LiClO_4$ were not significantly different.

Table 6.1.1 Electronic conductivities of poly-MPCA films at 0.8 V in acetonitrile + 0.1 M Et_4NClO_4.

Film thickness μm	Electronic conductivity mS cm^{-1}
1.9	7.9
3.0	9.9
4.0	6.3
4.8	11
5.0	10.2
Average:	9.1
Standard deviation:	2.1

6.2 Impedance studies

To derive information about the mobility of charge carriers in a conducting polymer, the experimental impedance response is modelled with an electrical circuit containing a transmission line element (Fig. 4.2.3). The assumption in using this circuit is justified by the high electronic conductivity of poly-MPCA compared to its ionic conductivity. The film ionic resistance (R_{ion}) is estimated by extrapolating the low frequency part of the complex plane impedance plot to the real axis, as shown in section 5.2. Similar results are obtained by analyzing the Warburg-type region according to the equation: $Z^2 = R_{ion}/(\omega C_F)$[11].

The following sections present the effects of the main experimental variables on ion transport in poly-MPCA, as revealed by impedance spectroscopy.

6.2.1 Film Thickness

Table 6.2.1 lists film ionic conductivities obtained from impedance measurements on poly-MPCA films of various thickness. The variation for films of the same thickness is due primarily to the difficulty in controlling the electrochemical polymerization. Factors such as electrode preparation,

temperature[12,13] monomer concentration[13-15] changes due to solvent evaporation, and water content[16,17] may all influence the morphology, and hence the conductivity, of the polymer.

Table 6.2.1 Film ionic conductivities and volumetric capacitances from impedance measurements on poly-MPCA films at 0.8 V in acetonitrile + 0.1M $LiClO_4$.

Film thickness μm	Film ionic conductivity μS cm^{-1}	$C_{v,ac}$ F cm^{-3}
0.14	5.1	294
0.28	8.5	359
0.42	10	353
0.56	8.4	351
0.70	11 $\pm$ 1[a]	370 $\pm$ 8.4[a]
0.98	22	386
1.30	48	407
3.90	560	434

[a] Results calculated from 8 films

Over the thickness range 0.28 to 0.70 μm the ionic conductivity of poly-MPCA is approximately constant at 10 $\pm$ 1 μS cm^{-1}. However, for thicker films, the apparent film ionic conductivity increases rapidly with increasing film thickness. The cause of this increased conductivity is apparent from the morphology changes seen with scanning electron microscopy (Fig. 5.2.2B, C and

D). The polymer deposits as a dense film with no observable pores up to a film thickness of about 0.5 μm. As polymerization continues, clumps are formed and surrounded by electrolyte solution. The formation of clumps is perhaps due to a non-uniform current density distribution across the surface of the polymer film covered electrode. Rapid precipitation occurs near a projected polymer tip, where a higher than average current density increases the local polymerization rate. Once the polymer begins to deposit in this more open structure its effective thickness in terms of its ac response becomes the average radii of the clumps, since the polymer's ionic conductivity is about three orders of magnitude lower than that of the electrolyte solution surrounding the polymer clumps. The average radius of the clumps is similar to the thickness of the underlying dense film (0.5 to 1 μm). The surface area of the film increases due to an increase in surface roughness and an increase in geometric area due to lateral growth. Thus the film's ionic resistance begins to decrease as it becomes thicker. Clearly, ionic conductivities calculated for films thicker than 0.7 μm overestimate the conductivity of the polymer phase. However, they do provide an estimate of the conductivity of the thick poly-MPCA films that would be used in lithium batteries, and in this respect they are very encouraging.

The thinnest film studied here appears to be anomalous both in its low ionic conductivity and low volumetric capacitance (Tables 6.2.1 and 3.2.1). This may

be a result of the high initial potential during the constant current polymerization (Fig. 3.1.3). Thus thin films will contain a higher proportion of overoxidized sites[18-20]. The lower value of the volumetric capacitance ($C_{V,cv}$) for the thinner film (Table 3.2.1) agrees with the lower concentration of intact redox centres.

In view of the results discussed in this section, results for films in the thickness range of *ca.* 0.2 to 0.8 μm provide the best estimate of the ionic conductivity of poly-MPCA. Therefore only films within this thickness range are considered in the remaining sections.

6.2.2 Solvent and Electrolyte Concentration

Figs. 6.2.1 and 6.2.2 show complex plane impedance plots for a 0.7 μm film at 0.70 V in propylene carbonate and acetonitrile electrolyte solutions, respectively. In these experiments, the same film was used and the electrolyte concentration was changed from low to high, and before each impedance measurement, the polymer film was cycled between the oxidized and reduced states (1.0 to -0.1 V) at 60 mV s^{-1} until no further change was observed. Voltammograms are almost independent of electrolyte concentration at concentrations above 0.1 M, but at lower concentrations, the redox peaks become more separated and less cycling charge is obtained in the doping/undoping of the polymer.

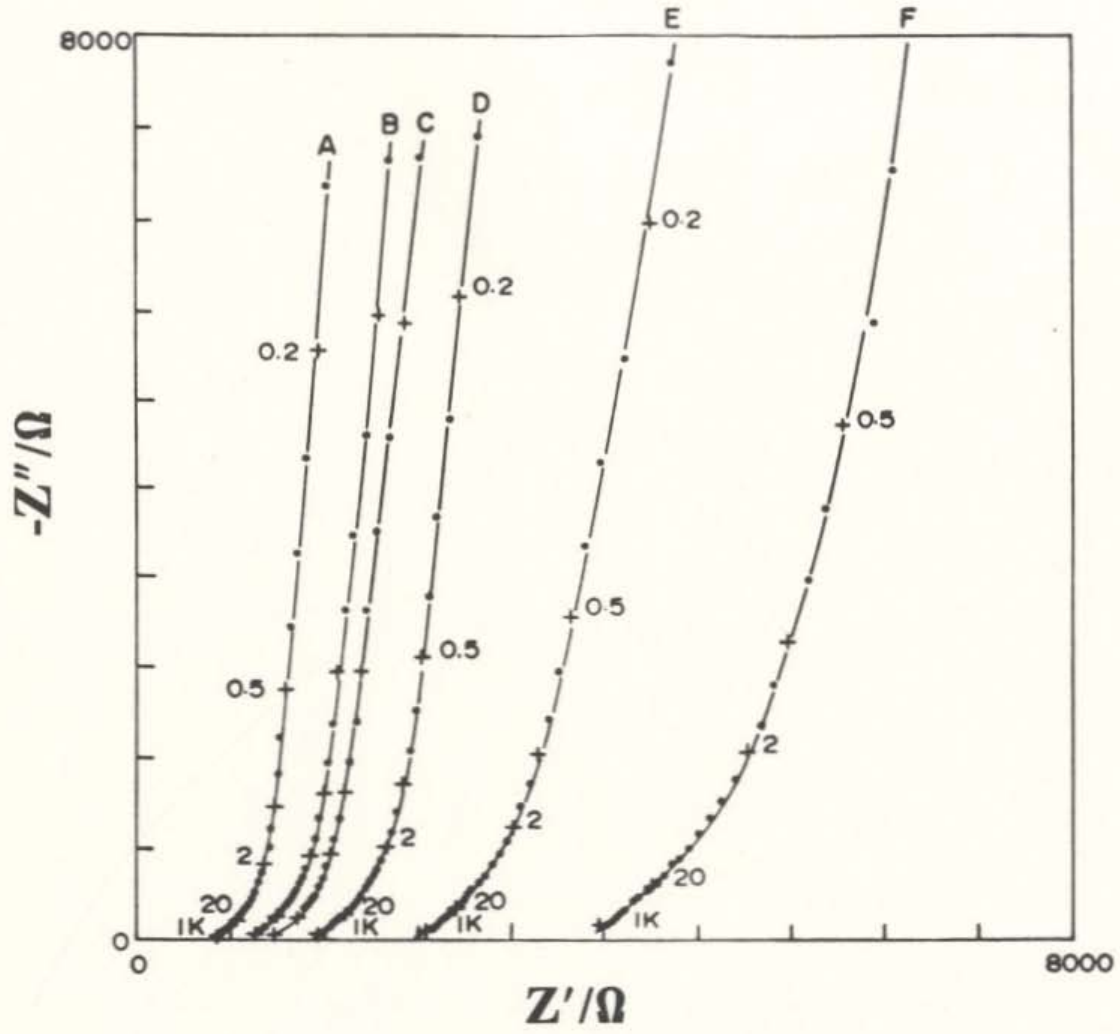

Figure 6.2.1 Complex plane impedance plots for a 0.7 μm poly-MPCA film at 0.80 V in $LiClO_4$ propylene carbonate solutions. Electrolyte concentrations: 1.6 M (A), 0.8 M (B), 0.6 M (C), 0.4 M (D) 0.2 M (E) and 0.1 M (F). Frequencies in Hz are indicated for selected points.

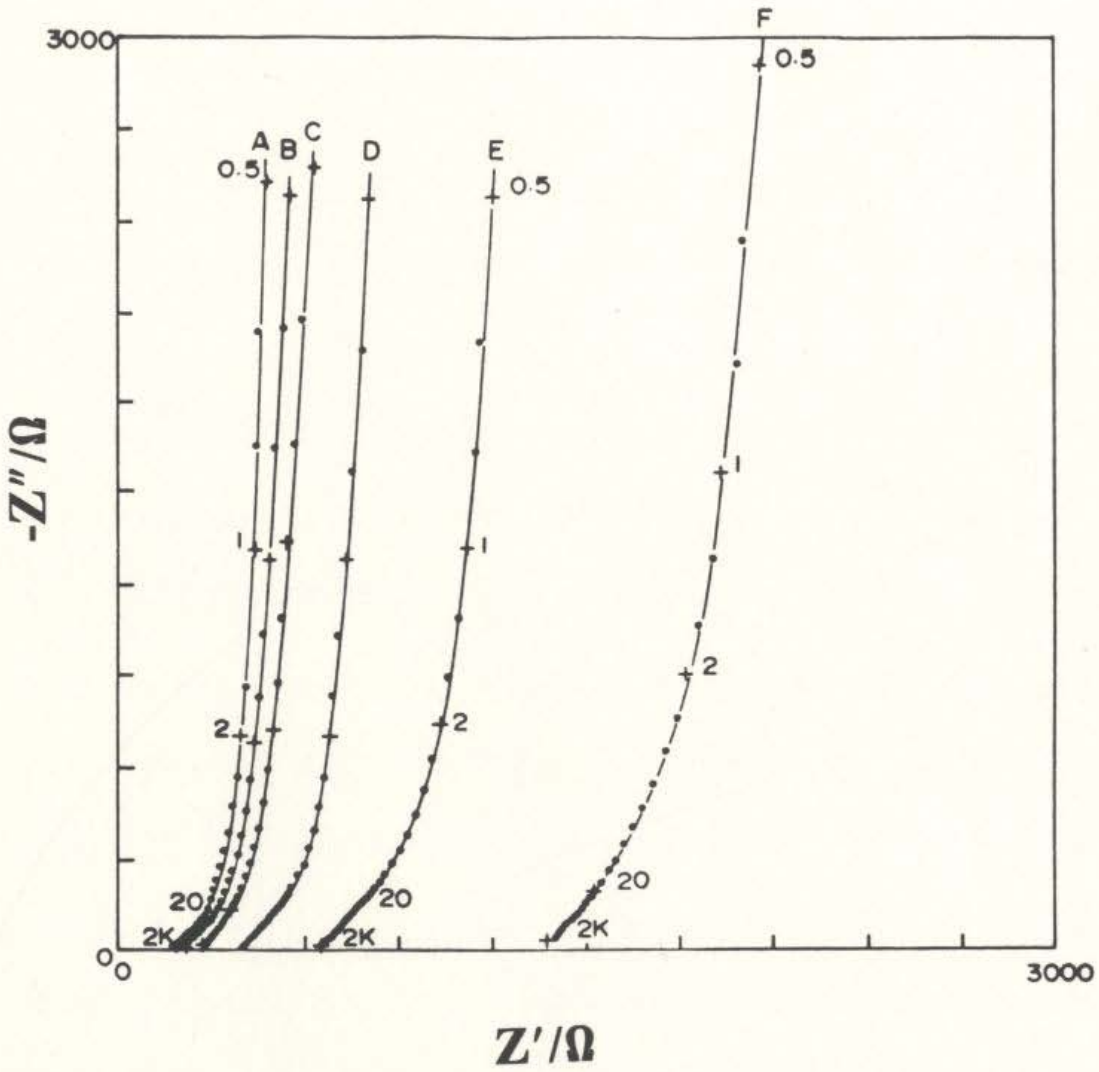

Figure 6.2.2 Complex plane impedance plots for a 0.7 μm poly-MPCA film at 0.80 V in $LiClO_4$ acetonitrile solutions. Electrolyte concentrations: 0.8 M (A), 0.6 M (B), 0.4 M (C), 0.2 M (D) 0.1 M (E) and 0.05 M (F). Frequencies in Hz are indicated for selected points.

The ionic conductivity of poly-MPCA is found to increase as the concentration of the electrolyte solution is increased and as the viscosity of the solvent is decreased. The high viscosity of propylene carbonate lowers ion mobility in both the bulk electrolyte solution and the polymer film, indicating that the film contains solvent. However, in solutions of similar conductivity, the film ionic conductivity is almost identical in the two solvents (Fig. 6.2.3). As the solution conductivity approaches zero, the film ionic conductivity becomes very low. On the other hand, as the solution conductivity is increased, the film ionic conductivity tends towards a maximum value. In between, the film ionic conductivity increases almost linearly with the solution conductivity.

6.2.3 Electrolyte Cation

Table 6.2.2 lists average ionic conductivities from impedance measurements made on three poly-MPCA films (0.28, 0.42, and 0.70 μm) in various electrolyte solutions containing three different cations. Measurements were made in a random order among the various solutions for each film. When the solution was changed, the polymer electrode was first rinsed with acetonitrile and then cycled between the oxidized and reduced states (1.0 to -0.1 V) at 60 mV s^{-1} until no further change was observed. Under the experimental conditions used, the polymer film showed no deterioration and repeated impedance measurements were reproducible.

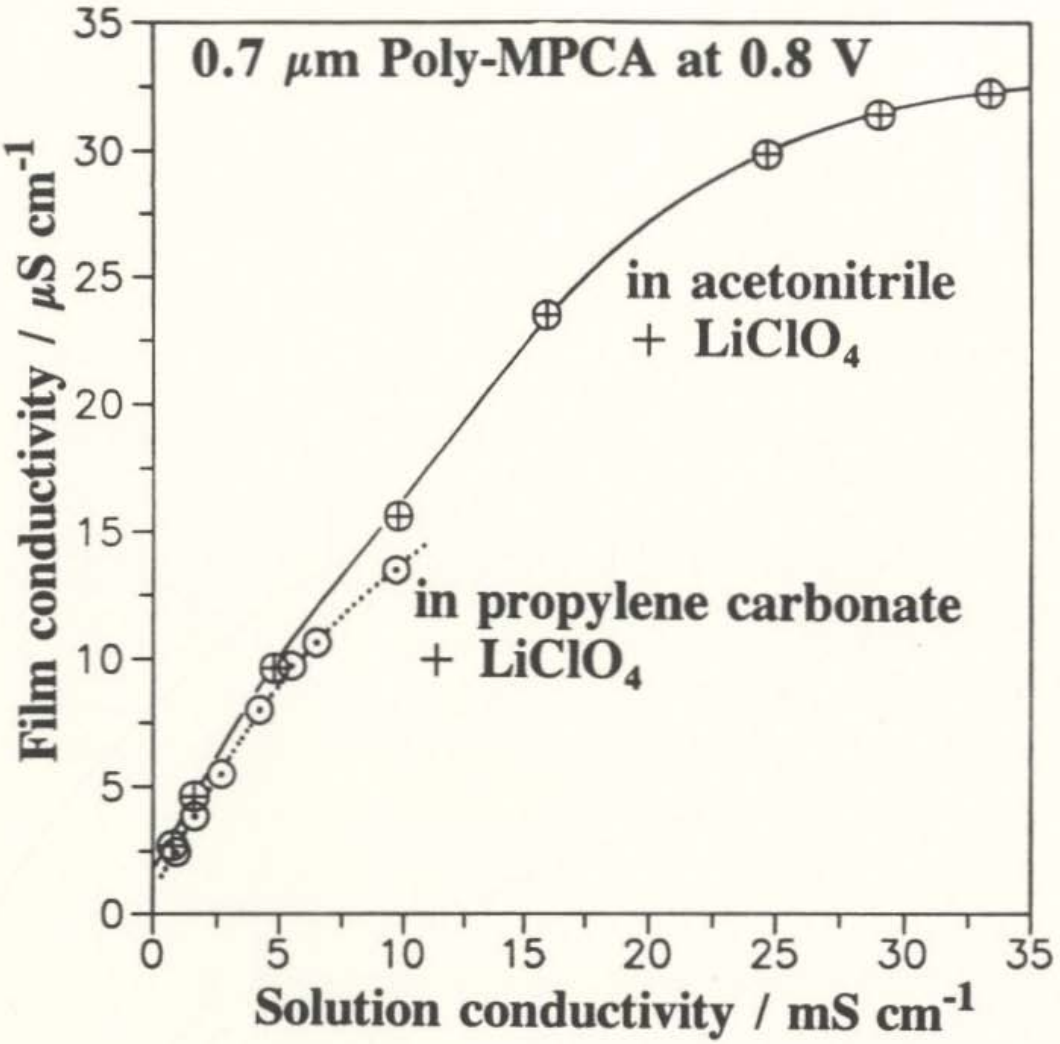

Figure 6.2.3 Plots of film ionic conductivity *vs.* electrolyte solution conductivity for a 0.7μm poly-MPCA film at 0.80 V in acetonitrile(⊕) and propylene carbonate (⊙) containing $LiClO_4$.

Table 6.2.2 Solution and film conductivities from impedance measurements on poly-MPCA films at 0.8 V in acetonitrile + electrolyte.

Acetonitrile + electrolyte	Sol. cond. mS cm^{-1}	Film cond. μS cm^{-1}	Cv F cm^{-3}
0.1M $LiClO_4$	8.4 ± 0.1	11.0 ± 0.1	360 ± 14
0.1 M Et_4NClO_4	12.0 ± 0.1	10.0 ± 0.5	368 ± 12
0.1 M But_4NClO_4	10 ± 0.1	8.3 ± 0.4	374 ± 17
0.05 M $LiClO_4$	4.8 ± 0.0	8.1 ± 0.5	366 ± 15
0.05 M Et_4NClO_4	6.9 ± 0.0	8.2 ± 0.5	367 ± 11
0.05 M But_4NClO_4	6.1 ± 0.0	7.1 ± 0.5	372 ± 12
0.01 M $LiClO_4$	1.2 ± 0.0	3.4 ± 0.9	362 ± 17
0.01 M Et_4NClO_4	2.3 ± 0.0	4.4 ± 0.9	370 ± 14
0.01 M But_4NClO_4	1.5 ± 0.0	3.4 ± 0.6	364 ± 7

averages and standard deviations for the measurements on films of thickness 0.28, 0.42 and 0.70 μm.

Although the film conductivities in Table 6.2.2 do not exhibit a very significant dependence on cation size they do show a distinctly different trend than the solution conductivities. This is important because it has been shown in the previous section that for $LiClO_4$ solutions there is a strong correlation between film and solution conductivities. The influence of cation size can best be observed by comparing plots of film ionic conductivity against solution conductivity for each

of the three electrolytes, as shown in Fig. 6.2.4. The film ionic conductivity follows the order $LiClO_4$ > Et_4NClO_4 > But_4NClO_4 at the same solution conductivity. These differences are especially pronounced in the more concentrated electrolyte solutions while film ionic conductivity is almost independent of cation size at low electrolyte concentration.

6.2.4 Electrode Potential

Figs. 6.2.5 and 6.2.6 show complex plane impedance plots for a 0.7 μm poly-MPCA film at different electrode potentials in acetonitrile containing 0.1 M $LiClO_4$. The solution resistance observed at frequencies above 1 kHz is independent of the electrode potential as expected. However, the film ionic conductivity decreases dramatically as the film is reduced. At 0.2 V, ion movement within the polymer is so slow that the film still appears infinitely thick at 1 Hz. Since the Warburg-type region continues to intersect the real axis at the solution resistance, the film's electronic resistance remains insignificant. This is again in agreement with the dual electrode results (Fig. 6.1.1). At lower potentials (*e.g.* 0 V), a distinct semicircle appears in the medium frequency range (1 to 2 kHz). Similar results were obtained in propylene carbonate electrolyte solution. Table 6.2.3 lists film ionic conductivities at several electrode potentials and $LiClO_4$ concentrations in this solvent.

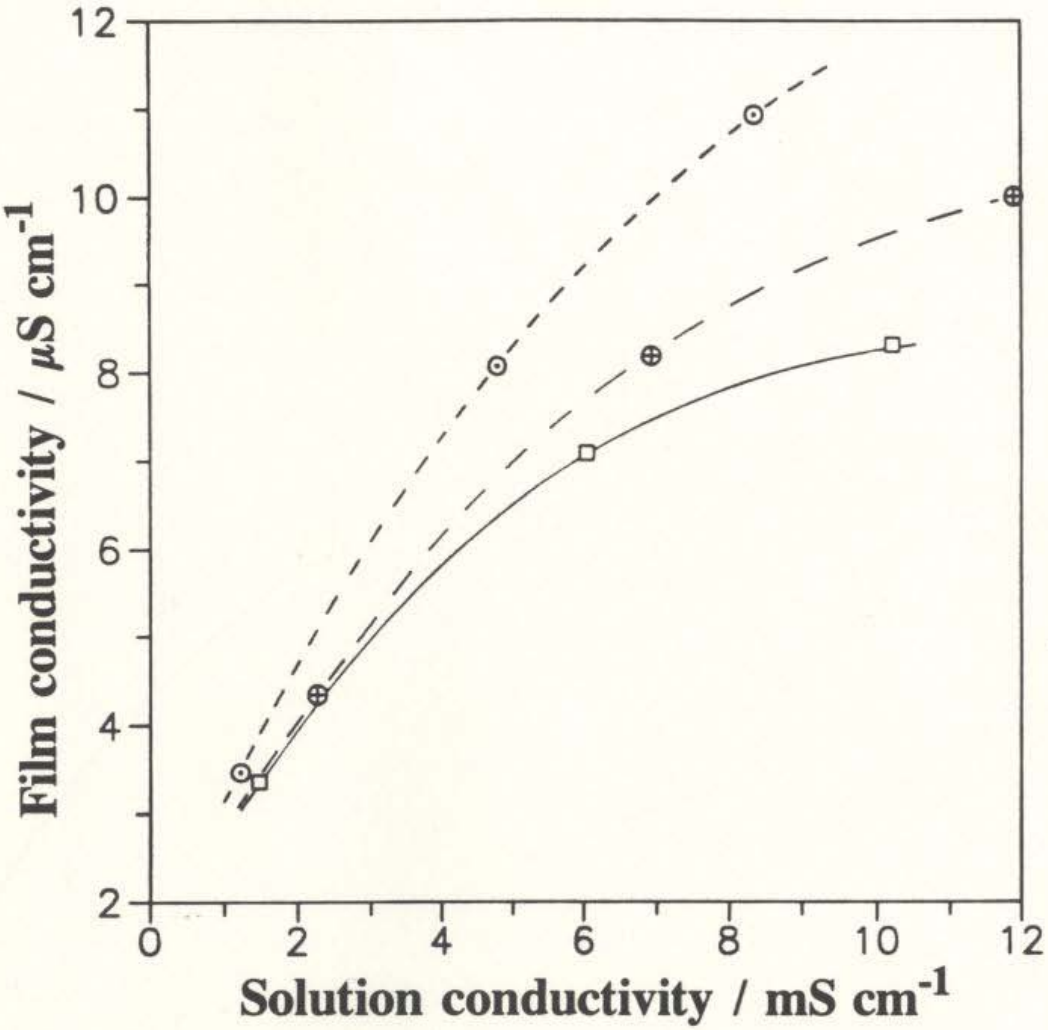

Figure 6.2.4 Plots of film ionic conductivity *vs.* solution conductivity for poly-MPCA films at 0.80 V in acetonitrile containing $LiClO_4$ (⊙), Et_4NClO_4 (⊕) and But_4NClO_4 (□).

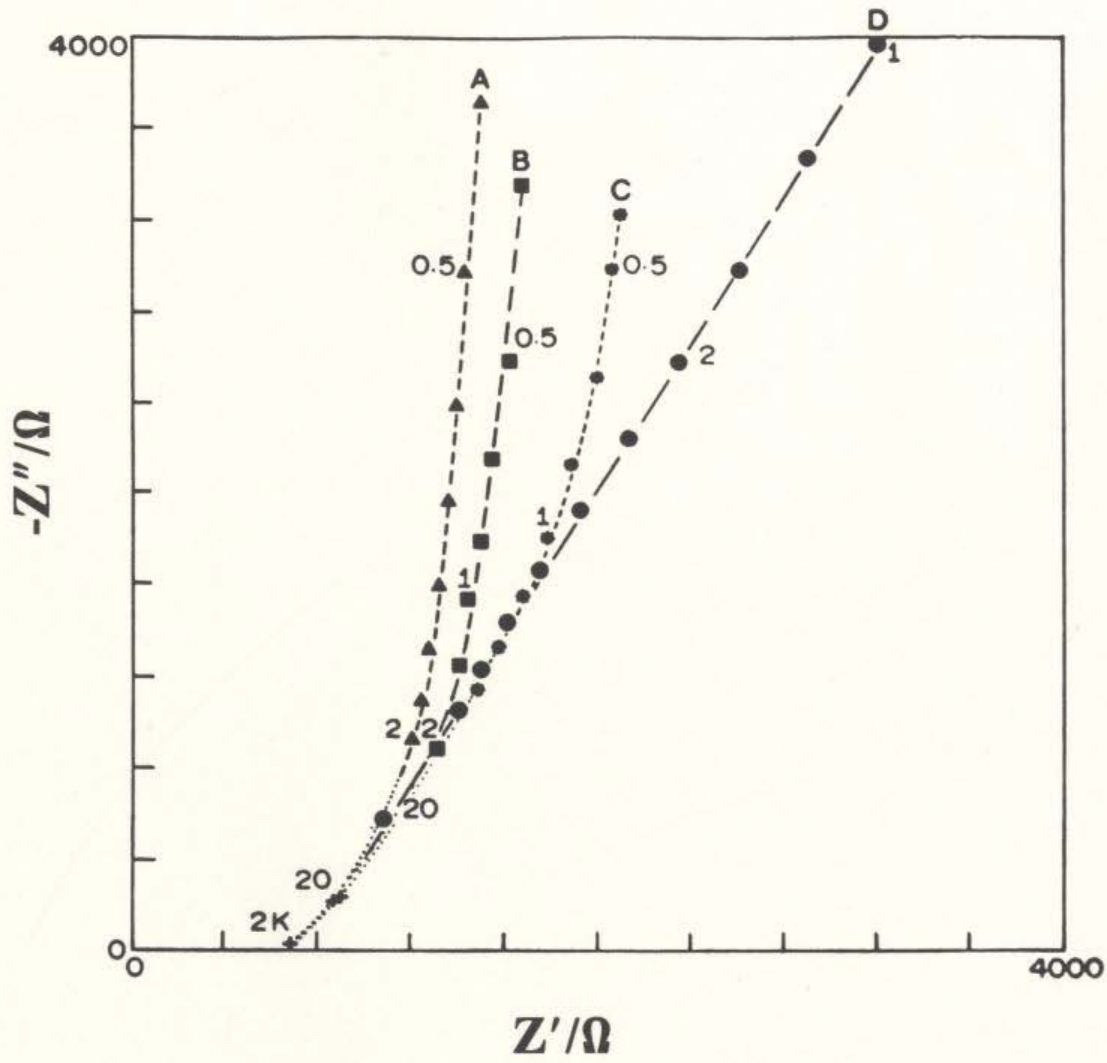

Figure 6.2.5 Complex plane impedance plots for a 0.7 μm poly-MPCA film at 0.80 V (A), 0.60 V (B), 0.50 V (C), 0.30 V (D) in acetonitrile containing 0.1 M $LiClO_4$.

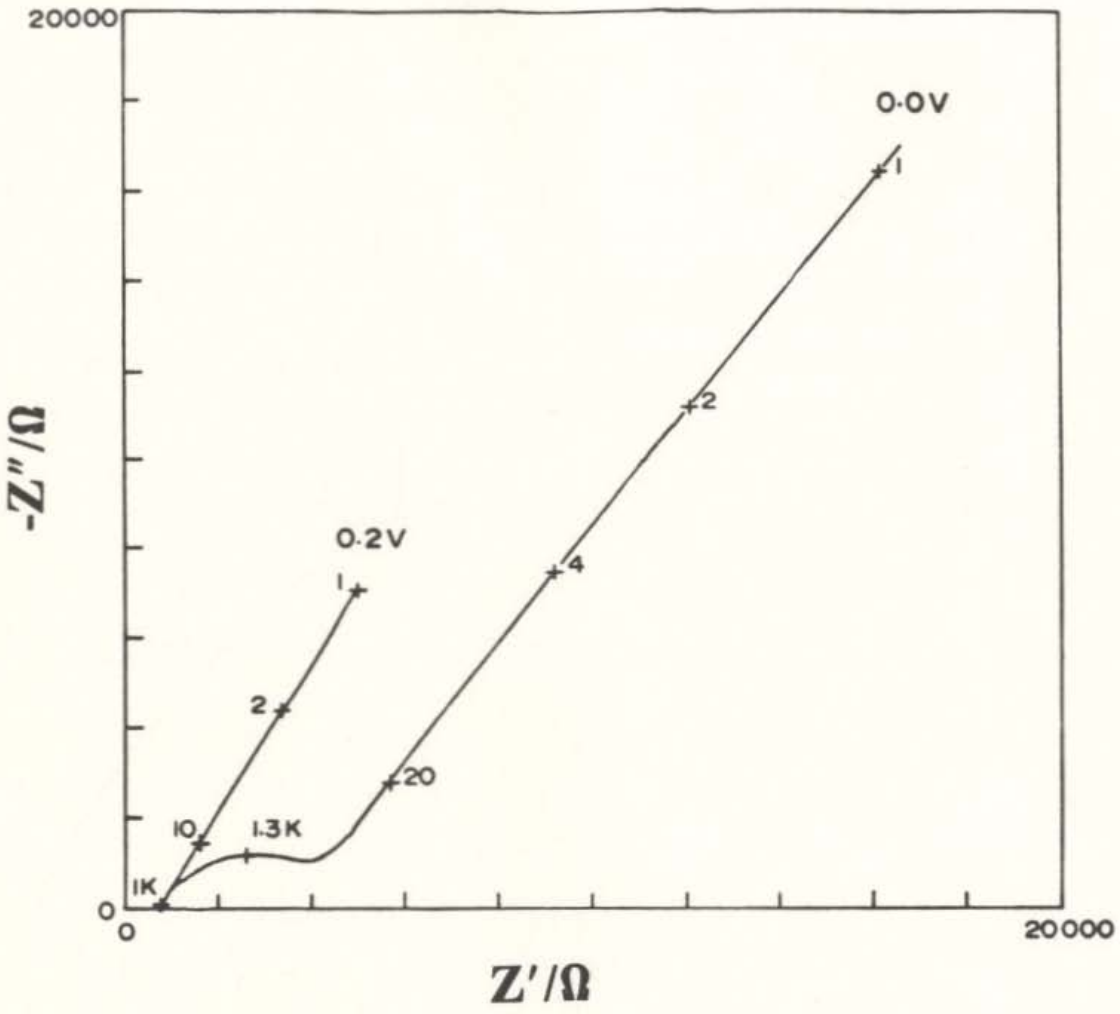

Figure 6.2.6 Complex plane impedance plots for a 0.7 μm poly-MPCA film at 0.20 V and 0.0 V in acetonitrile containing 0.1 M $LiClO_4$.

Table 6.2.3 Film ionic conductivities from impedance measurements on a 0.70 μm poly-MPCA film in propylene carbonate containing various $LiClO_4$.

$LiClO_4$ conc. (M)	Film ionic conductivity / μS cm^{-1} at electrode potential *vs.* SSCE				
	0.30 V	0.40 V	0.50 V	0.60 V	0.70 V
0.40	1.5	2.9	4.7	6.4	7.8
0.80	1.9	3.6	6.2	8.1	10
1.6	2.8	5.1	7.9	10	13

The number of electrons removed from the fully reduced polymer per pyrrole ring (degree of oxidation, χ) at each electrode potential is calculated from the cycling charge (Q_{cv}) of a slow scan cyclic voltammogram to that potential, and from the polymer preparation charge (Q_{prp}).

$$\chi = \frac{2.3\ Q_{cv}}{Q_{prp}} \qquad [6.2.1]$$

Although eq. [6.2.1] is approximate in that it assumes a polymerization efficiency of 100% and a degree of oxidation of 0.3 for the freshly formed polymer, it does provide a good estimate of relative values of χ. As shown in Fig. 6.2.7, there is

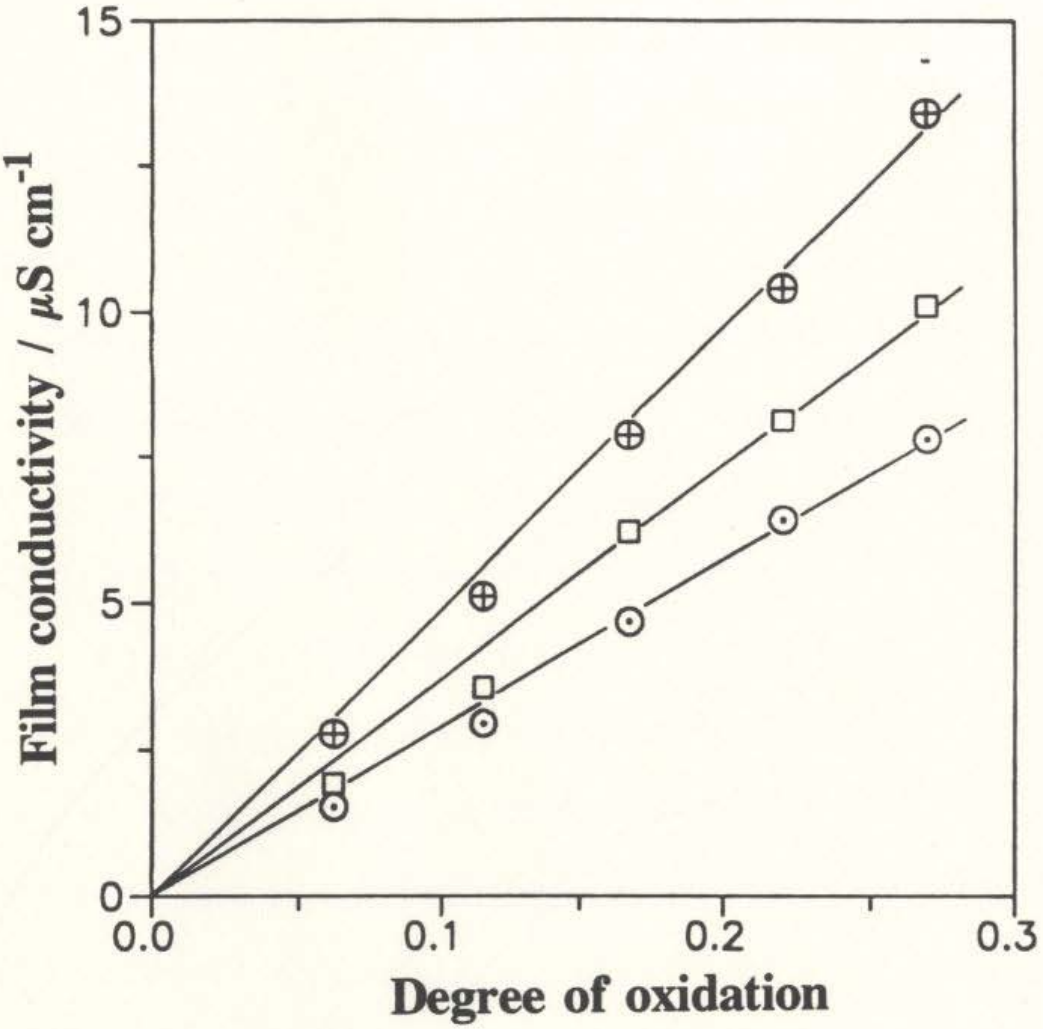

Figure 6.2.7 Plots of film ionic conductivity *vs.* degree of oxidation for a 0.7μm poly-MPCA film in propylene carbonate containing 1.6 M (⊙), 0.8 M (□) and 0.4 M (⊙) $LiClO_4$.

a linear relationship between the film ionic conductivity and the degree of oxidation. A linear relationship between polymer conductivity (ionic and electronic) and charge injection has also been reported for polypyrrole[21-23].

6.3 Discussion

The main purpose of this study was to determine the factors that control ion transport in poly-MPCA and to find an appropriate model of ion transport in this polymer. Detailed discussion can be found in a published paper[24], so only the major points are summarized here.

A novel two-phase model is proposed to explain the following observations:

1. The ionic conductivity of poly-MPCA changes with the viscosity of the solvent and the concentration of supporting electrolyte. The ionic conductivity of the electrolyte solution also changes with the above two factors and there is a strong correlation between the ionic conductivities of the polymer and the electrolyte solution.

2. At high electrolyte concentration the ionic conductivity of the polymer approaches a maximum value, and is independent of electrolyte solution conductivity.

3. There is a weak dependence of polymer ionic conductivity on the size of the electrolyte cations.

4. The ionic conductivity of the polymer is strongly dependent on its degree of oxidation.

In this model, ion transport in the polymer film is assumed to be due to counterions in one phase (the polymer phase) and excess electrolyte in the other phase (the pore solution). The conductivity of the polymer phase is dependent on potential but independent of solution conductivity (it appears to be permselective), and that of the pores is dependent on solution conductivity but independent of potential. The experimental results show that when the conductivity of either phase becomes small, the film ionic conductivity is small. This implies that neither phase alone can provide a low resistance pathway for ion transport through the film. Charge must pass through both phases and their resistances appear in series as the measured ionic resistance.

The two phase structure implied by the ion transport results can be explained as follows. There is good evidence that the deposition of polypyrrole occurs by the precipitation of oligomers formed by electrochemical polymerization in solution[25-27]. Such a mechanism should produce films consisting of randomly packed polymer aggregates enclosing pores filled with the electrolyte solution. Interconnections between the pores may be constricted due to continued

polymerization within the pores. The electron micrographs shown in Fig. 5.2.2B, C and D suggest that poly-MPCA is deposited with this type of structure, presumably by a similar mechanism. Ions will follow pathways across the polymer film that have minimum resistance. Such pathways may include more pores than polymer aggregates because the pore solution will generally have a higher ionic conductivity than the polymer aggregates. However, a redox reaction of the polymer aggregates occurs in impedance measurements. As the frequency of the potential perturbation is decreased, the reaction layer spreads inward from the polymer aggregate's surface. This forces the ionic current to go through part of the polymer aggregate at low frequency. Therefore, the total film ionic resistance (R_T) measured here is the sum of the ionic resistances across the polymer aggregate (R_{aggr}) and the pores (R_{pore}). The ionic resistance rail in the transmission line (Fig. 4.2.2) is then an combination of R_{aggr} and R_{pore}.

The pore solution composition appears to be similar to that of the bulk electrolyte solution, since film conductivity tracks with solution conductivity despite differences in solvent viscosity (Fig. 6.1.3). When the pore solution conductivity approaches zero, the film ionic conductivity becomes very small because of poor ionic interconnection between aggregates. On the other hand, a high solution conductivity can make R_{pore} much smaller than R_{aggr}. In this case, the total film ionic conductivity will approach the constant value determined by the

ionic conductivity of the polymer aggregates at the measured potential.

The ionic conductivity of the polymer aggregates is increased as the concentration of oxidized sites increases because of the increased concentration of counterions. Each oxidized site on the polymer chain creates one anion-exchange site and an associated mobile anion in the polymer aggregate (in the absence of self-doping). Thus, like polypyrrole in aqueous media[28] the ionic conductivity of the polymer aggregates is dependent on potential and should be affected by the characteristic size of the counterion.

The observed effect of cation size on the ionic conductivity of poly-MPCA may be related to the involvement of cations in the doping/undoping process. By plotting film conductivity *vs.* solution conductivity in Fig. 6.2.4, the effect of the bulk electrolyte solution on R_{pore} is separated and differences in cation movement in the polymer aggregates can be compared. Because R_{aggr} is important only when R_{pore} is small, the cation dependence becomes most apparent in the higher conductivity electrolyte solutions (Fig. 6.2.4). The observed R_{aggr} increases with the size of the cation in the order $Li^+ < Et_4N^+ < But_4N^+$ as expected. However, the involvement of cations in the doping/undoping reactions cannot be clearly established from the present data. The weak cation effect observed for poly-MPCA may be due to some subtle changes of the polymer when in contact with the

different electrolyte solutions.

The low frequency capacitances (C_F) for three films of different thickness are plotted against electrode potential in Fig. 6.3.1. The potential of maximum capacitance coincides with the polymer's formal potential (E°') of 0.60 V (Fig. 3.2.1). For each curve integration to the potential of maximum capacitance accounts for 50 to 55% of the total area under the curve (up to 1.0 V). The cycling charge based on these impedance measurements ($Q_{ac.} = \int C_{ac}\, dV$) is presented in Fig. 3.2.2 as a function of electrode potential for comparison with the data from cyclic voltammetry. There is a large discrepancy between these two charges and the reason for such discrepancy has been discussed[29].

The high frequency semicircle shown in Fig. 6.2.6 must be due to an interfacial charge transfer process. Since the real axis intercept of the high frequency data on the semicircle coincides with that for the bare platinum, it can be concluded that the electrochemical process does not involve ion transport through the polymer layer, otherwise a large film ionic resistance (at -0.3 V, R_{Ion} is already > 6.4 kΩ, Table 6.2.3) would be clearly visible. Fig. 6.3.2 shows an equivalent circuit that can describe the experimental impedance response in the whole potential range. The double layer capacitance (C_{dl}) and charge transfer resistance (R_{ct}) parallel combination represents a kinetic barrier for ion transport across the polymer/solution interface.

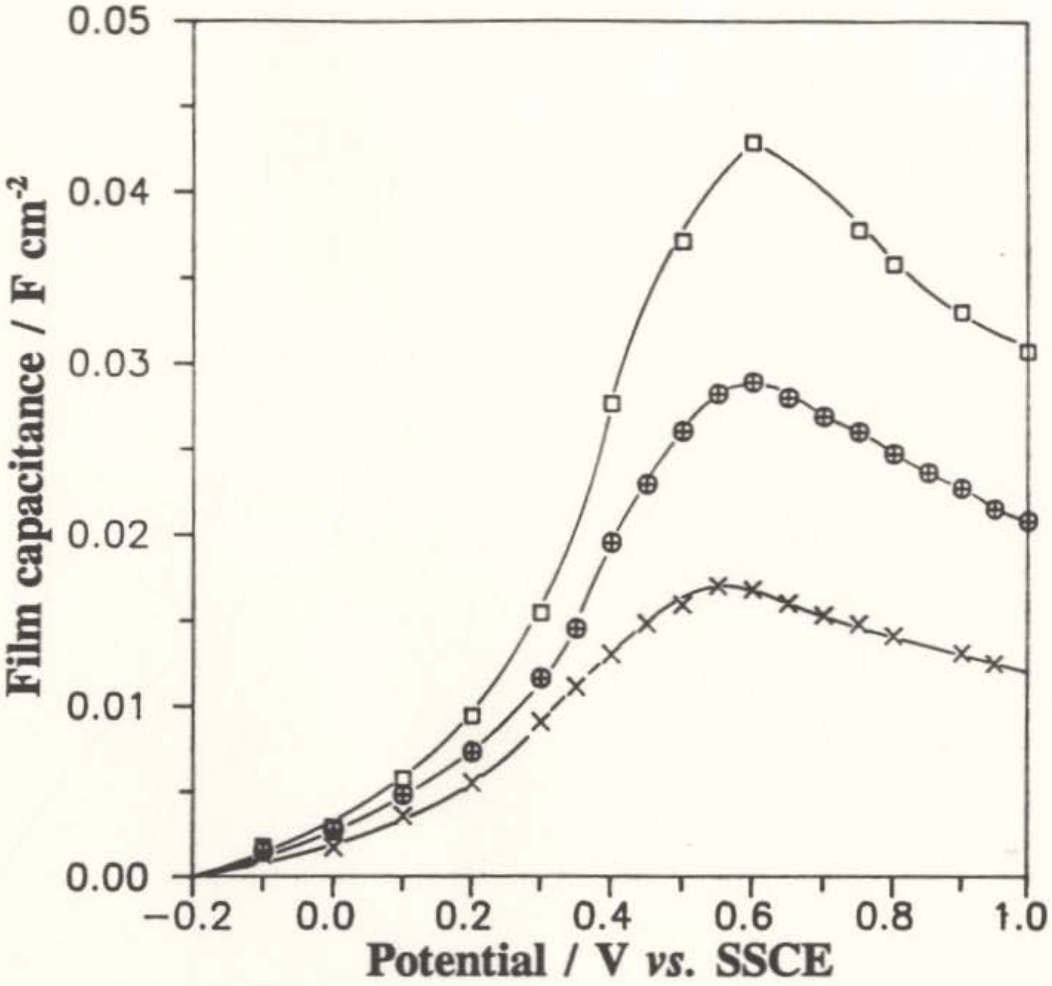

Figure 6.3.1 Plots of low frequency capacitance *vs*. electrode potential for poly-MPCA films in acetonitrile containing 0.1 M $LiClO_4$. Film thicknesses: 0.98 μm (□), 0.70 μm (⊗) and 0.28 μm (×).

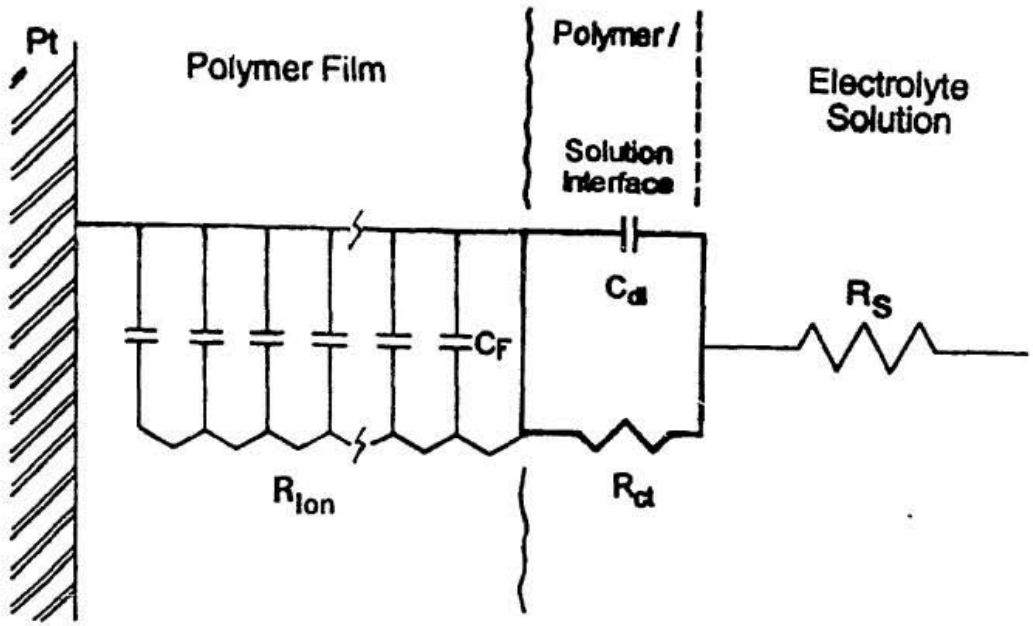

Figure 6.3.2 Modified transmission line circuit containing a R_{ct} and C_{dl} element at the polymer/solution interface.

From the diameter of the semicircle (= R_{ct} = 2.9 kΩ) and the characteristic relaxation frequency f_c (1.3 kHz), the double layer capacitance (C_{dl}) was calculated from:

$$f_c = \frac{1}{R_{ct} C_{dl}} \qquad [6.3.1]$$

to be 67 μF cm^{-2}. Penner *et al*[30] have obtained the double layer capacitance C_{dl} for reduced polypyrrole films on a Pt substrate electrode using current-step experiments to be 35 to 54 μF cm^{-2}.

In this study, the double layer capacitance of the bare Pt substrate electrode in acetonitrile containing 0.1 M $LiClO_4$ was found to be 17 μF cm^{-2}. According to Mermilloid *et al*[31] the ratio of effective area to geometrical area can been found by comparing C_{dl} of the polymer electrode with that of bare Pt electrode. This assumes the unit area capacitance for Pt is the same as that for the polymer. With this assumption, the poly-MPCA film exhibits an effective area about 3.5 times its geometrical area. The higher value of the effective area presumably arises from the roughness of the film surface since the same value of solution resistance was obtained for both the bare Pt and a polymer film coated Pt electrode.

6.4 Conclusions

Dual electrode voltammetry and impedance spectroscopy have shown that the rate of charge transport in poly-MPCA is limited by ion mobility. The ionic conductivity of the polymer is related to both its degree of oxidation and the conductivity of the electrolyte solution. This could only be explained by proposing a two phase model in which the ionic current must pass through both polymer aggregates and enclosed pores containing electrolyte solution. Some evidence is obtained for cation transport in the polymer aggregates. This result combined with the high ionic and electronic conductivities of thick poly-MPCA films supports the idea[32] that poly-MPCA is an attractive cathode material for secondary lithium batteries.

The high frequency semicircle observed for a reduced poly-MPCA is attributed to a kinetic barrier for ion transport across the polymer/solution interface. The effective polymer surface area corresponds well with the roughness of the polymer film as observed with SEM. A modified transmission line circuit can describe the observed impedance response of poly-MPCA in the whole potential range.

References

(1) Pickup, P.G. *J. Electroanal. Chem.* 1987,*225*,273.

(2) Sundaresan, N.S.; Basak, S.; Pomerantz, M.; Reynolds, J.R. *J. Chem. Soc., Chem. Commun.* 1987,,621.

(3) Patil, A.O.; Ikenoue, Y.; Wudl, F.; Heeger, A.J. *J. Am. Chem. Soc.* 1987,*109*,1858.

(4) Patil, A.O.; Ikenoue, Y.; Basescu, N.; Colaneri, N.; Chen, J.; Wudl, F.; Heeger, A.J. *Synth. Met.* 1987,*20*,151.

(5) Reynolds, J.R.; Sundaresan, N.S.; Pomerantz, M.; Basak, S.; Baker, C.K. *J. Electroanal. Chem.* 1988,*250*,355.

(6) Ikenoue, Y.; Chiang, J.; Patil, A.O.; Wudl, F.; Heeger, A.J. *J. Am. Chem. Soc.* 1988,*110*,2983.

(7) Delabouglise, D.; Garnier, F. *New J. Chem.* 1991,*15*,233.

(8) Ren, X.; Pickup, P.G. *unpublished. results.* 1993.

(9) Scrosati, B. *J. Electrochem. Soc.* 1989,*136*,2774.

(10) Naegele, D.; Bittihn, R. *Solid State Ionics* 1987,*28-30*,983.

(11) Jakobs, R.C.M.; Janssen, L.J.J.; Barendrecht, E. *Recl. J. R. Netherlands. Chem. Soc.* 1984,*103*,275.

(12) Tanaka, K.; Shichiri, T.; Yamabe, T. *Synth. Met.* 1986,*16*,207.

(13) Otero, T.F.; Santamaria, C. *Electrochim. Acta* 1992,*37*,297.

(14) Lei, J.T.; Cai, Z.H.; Martin, C.R. *Synth. Met.* 1992,*46*,53.

(15) Walton, D.J.; Hall, C.E.; Chyla, A. *Analyst* 1992,*117*,1305.

(16) Zotti, G.; Schiavon, G.; Berlin, A.; Pagani, G. *Electrochim. Acta* 1989,*34*,881.

(17) Otero, T.F.; Angulo, E. *J. Appl. Electrochem.* 1992,*22*,369.

(18) Heinze, J. *Synth. Met.* 1991,*41-43*,2805.

(19) Beck, F.; Braun, P.; Oberst, M. *Ber. Bunsen Ges. Phys. Chem.* 1987,*91*,967.

(20) Rosseinsky, D.R.; Morse, N.J.; Slade, R.C.T.; Hix, G.B.; Mortimer, R.J.; Walton, D.J. *Electrochim. Acta* 1991,*36*,733.

(21) Feldman, B.J.; Burgmayer, P.; Murray, R.W. *J. Am. Chem. Soc.* 1985,*107*,872.

(22) Waller, A.M.; Compton, R.G. *J. Chem. Soc., Faraday. Trans. I* 1989,*85*,977.

(23) Albery, W.J.; Chen, Z.; Horrocks, B.R.; Mount, A.R.; Wilson, P.J.; Bloor, D.; Monkman, A.T.; Elliott, C.M. *Faraday. Discuss. Chem. Soc.* 1989,*88*,247.

(24) Ren, X.; Pickup, P.G. *J. Electrochem. Soc.* 1992,*139*,2097.

(25) John, R.; Wallace, G.G. *J. Electroanal. Chem.* 1991,*306*,157.

(26) Raymond, D.E.; Harrison, D.J. *J. Electroanal. Chem.* 1990,*296*,269.

(27) Beck, F.; Oberst, M. *J. Electroanal. Chem.* 1990,*285*,177.

(28) Burgmayer, P.; Murray, R.W. *J. Phys. Chem.* 1984,*88*,2515.

(29) Ren, X.; Pickup, P.G. *J. Electroanal. Chem.* 1993, submitted.

(30) Penner, R.M.; Van Dyke, L.S.; Martin, C.R. *J. Phys. Chem.* 1988,*92*,5274.

(31) Mermilliod, N.; Tanguy, J.; Petiot, F. *J. Electrochem. Soc.* 1986,*133*,1073.

(32) Ren, X.; Pickup, P.G. Abstract 803, p.1144, *The Electrochem. Soc. Extended Abstracts*, Vol. 91-1, Washington, DC, May 5-10, 1991.

Chapter 7

Ionic Transport in Polypyrrole and a Polypyrrole/poly-anion Composite

7.1 Introduction

Since Shimidzu and coworkers reported that the redox processes of polypyrrole can be greatly influenced by the size of the incorporated anions[1-4], there has been great interest in the electrochemical polymerization of pyrrole in polyanionic electrolyte solutions[5-16]. The polyelectrolyte anions become trapped within the polypyrrole matrix due to their large size and, perhaps more importantly, their entanglement with the polypyrrole chains. In addition to increased stability and mechanical strength, the composite materials have been shown to be self-doped, *i.e.*, the positive charges on the polypyrrole chains formed upon oxidation are compensated by the trapped polyanions with the concurrent expulsion of the cations. This has been confirmed by elemental analysis of the polymer films in different oxidation states[2], measurements of membrane potentials[2], observation of the polymer's cation exchange properties[5] and *in situ*

monitoring of the mass change during electrochemical switching, using a quartz crystal microbalance[8,16].

The ion transport properties of polypyrrole/polyanion composites are clearly very different from those of polypyrrole doped with a small anion. Documentation and explanation of these differences are important to the understanding of ion transport in conducting polymers. To this end, there have been a number of studies of ion transport rates in polypyrrole/polyanion composite films. In a cyclic voltammetric study, Shimidzu *et al* found that the electrochemical switching of polypyrrole/poly(vinylsulphonate) composites was as fast as for polypyrrole doped with chloride[2]. Transport of cations (Na^+ or K^+) between the electrolyte solution and the composite was proposed as the charge compensating mechanism facilitating rapid switching. Chronocoulometry of polypyrrole/Nafion composite revealed a dependence on the cation in solution[17], supporting the view that the rate of cation transport in the film determines the switching rate. Chronocoulometry[8,10] and chronogravimetry[8] have been used to measure apparent diffusion coefficients in polypyrrole/poly(styrene sulphonate) (PPY/PSS) composites in aqueous media. Values ranging from *ca.* 10^{-10} to 10^{-8} cm^2 s^{-1} were reported. Apparent diffusion coefficients for the release of protonated dimethyldopamine from poly(N-methylpyrrole)/PSS composites have been determined by chronoabsorptometry[7].

Elliott and coworkers have recently reported an impedance study on

PPY/PSS in acetonitrile[11]. Their results show that for oxidized films the ionic resistance increases slightly with increasing potential and is almost independent of cation size. Upon reduction, the ionic resistance increases considerably and becomes strongly dependent on cation size. These results were interpreted in terms of a model involving coupling of ion and polymer chain motions. However, the reported impedance spectra are complicated in the high frequency region by a semi-circle, which obscures the ideal transmission line response and could make the experimental results difficult to interpret.

In this chapter, a comparative study of PPY/ClO_4^-, PPY/PSS and PPY/PSS/MV^{2+} (MV^{2+} = methyl viologen dication) in aqueous $NaClO_4$ solution using cyclic voltammetry and impedance spectroscopy is presented. The impedance spectra are simple and ionic conductivities are obtained from impedance data using the classical transmission line circuit (Fig. 4.2.2). The results are correlated with cyclic voltammetry to elucidate the charge transport mechanism for each material. The PPY/PSS/MV^{2+} is formed simply by immersing the reduced PPY/PSS film into an aqueous $NaClO_4$ solution containing methyl viologen dichloride. The MV^{2+} is strongly bound by the composite, presumably by ion pairing with the sulphonate groups. Its influence on ion transport in the composite provides valuable insight into the factors determining charge compensating mechanisms in polypyrrole electrochemistry.

7.2 Results

7.2.1 Preliminary Characterization of Polymer Films

The electrochemical properties of the three types of polypyrrole coated electrodes were preliminarily studied using cyclic voltammetry (Figs. 7.2.1 and 7.2.2). The two main peaks for PPY/ClO_4^- are centred at *ca.* -0.2 V. A second cathodic peak appears at *ca.* -0.9 V and becomes more pronounced with increasing scan rate. This peak is presumably associated with transient cation insertion[18,19]. The main redox waves for PPY/PSS are at slightly lower potentials than those for PPY/ClO_4^-. Transient anion insertion, which has been observed for PPY/PSS in a quartz crystal microbalance study by Lien and coworkers[20], may account for the small shoulder on the anodic branch for this polymer film.

When a PPY/PSS composite is cycled in a solution containing methyl viologen dichloride new redox waves appears in the -0.4 to -1.0 V region (Fig. 7.2.2). These can be attributed to the electrochemistry of MV^{2+} in the film. The incorporation of MV^{2+} in the PPY/PSS film enhances substantially the peak current for the MV^{2+}/MV^{+} couple relative to that at the bare Pt electrode. The favourable partitioning of MV^{2+} into the polymer film over that of the electrolyte cation (Na^+) must be due to a stronger interaction, such as ion-pairing, between

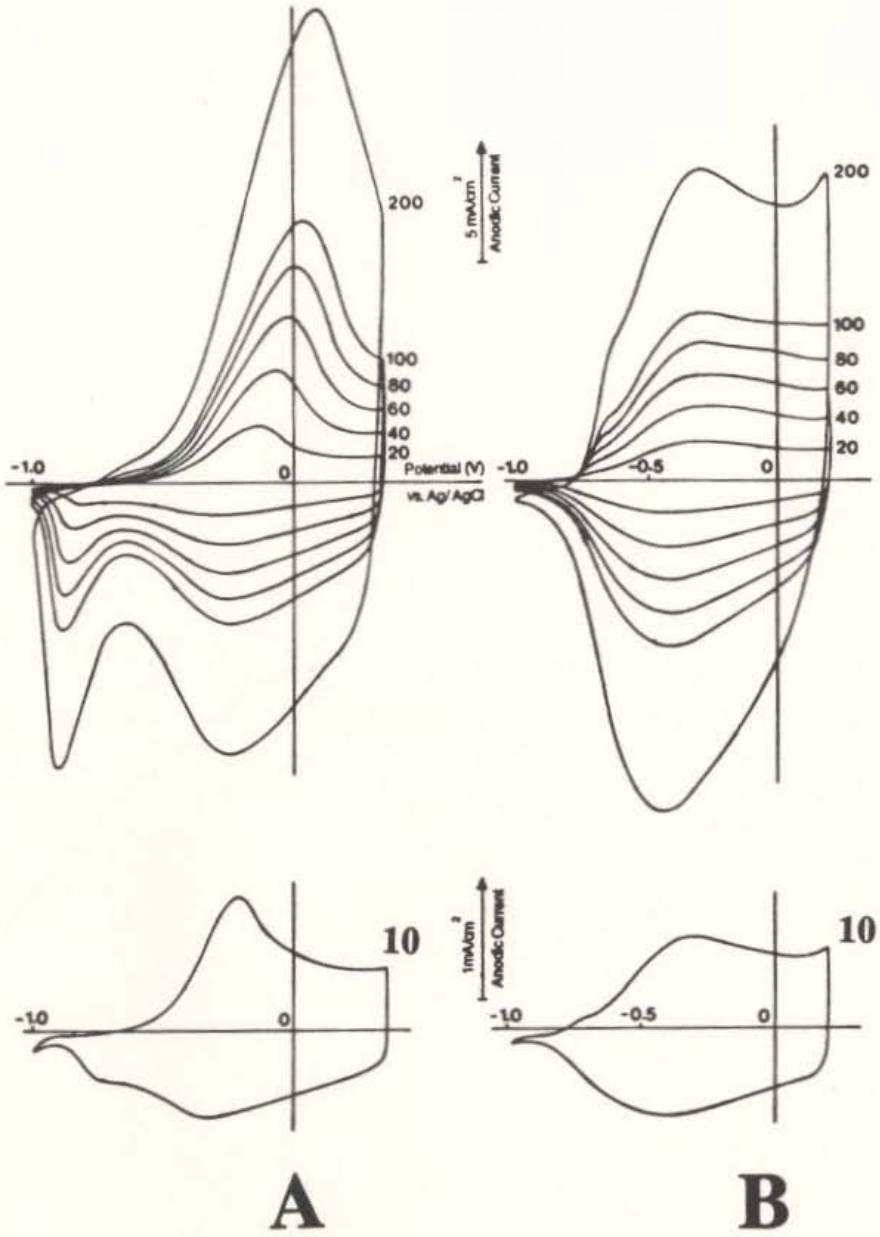

Figure 7.2.1 Cyclic voltammograms of 2 μm PPY/ClO_4^- (A) and 2 μm PPY/PSS (B) coated Pt electrodes in 0.2 M $NaClO_4$(aq). Scan rates in mV s^{-1} are indicated.

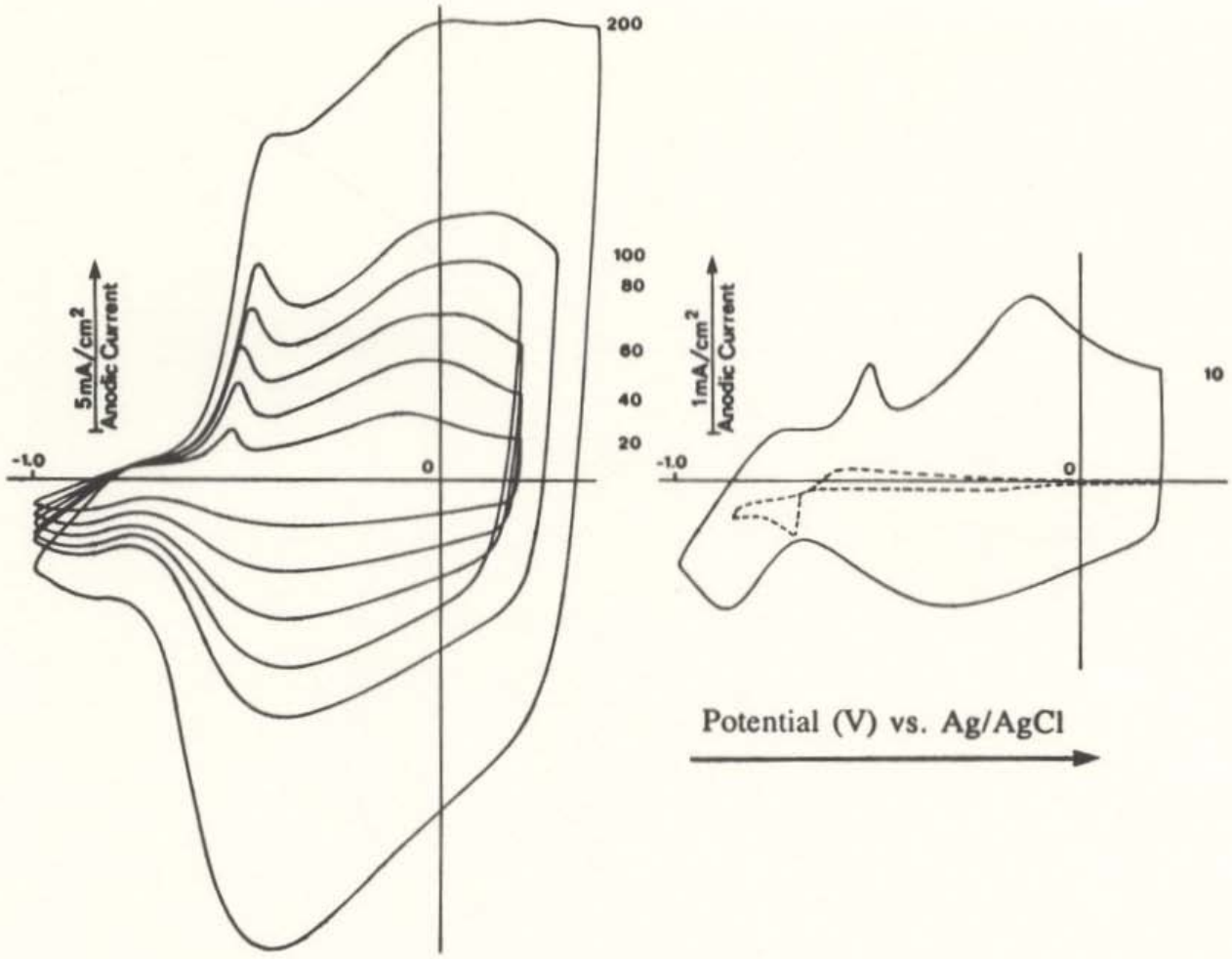

Figure 7.2.2 Cyclic voltammograms of a 2 μm PPY/PSS coated Pt electrode in 0.2M $NaClO_4$ (aq) containing 3 mM $MVCl_2$. Scan rates in mV s^{-1} are indicated. The dashed line is the voltammogram at the bare Pt electrode.

MV^{2+} cations and the sulphonate anions.

Plots of peak potentials and peak currents *vs.* scan rates for the voltammograms shown in Figs. 7.2.1 and 7.2.2 are shown in Figs. 7.2.3 and 7.2.4, respectively. For both PPY/ClO_4^- and PPY/PSS/MV^{2+} there is a significant peak separation which increases with increasing scan rate due to an positive shift of the anodic peak potential. For PPY/ClO_4^- the cathodic peak also shifts positively with increasing scan rate, although to a lesser degree. In contrast, the peak separation for PPY/PSS is smaller, and the cathodic peak is slightly more sensitive to increasing scan rate than the anodic peak. Table 7.2.1 lists peak potentials at various scan rates from Figs. 7.2.1. and 7.2.2.

At low scan rates the peak currents for all three types of film increase linearly with increasing scan rate indicating the absence of charge transport limitations. However, departure from this relationship occurs at scan rates below 200 mV s^{-1} for PPY/ClO_4^- and PPY/PSS/MV^{2+}, especially for the anodic peak. For PPY/PSS both peaks increase linearly up to at least 200 mV s^{-1}.

For both PPY/ClO_4^- and PPY/PSS the total anodic voltammetric charge (Q_{cv}) integrated to 0.2 V (the open circuit potential immediately after electrochemical polymerization) is *ca.* 52 mC cm^{-2}. Assuming 100% polymerization efficiency according to eq. [7.2.1],

$$Py^{\bullet} \rightarrow \cdots(\cdots Py^{\chi+}\cdots)\cdots + 2\ H^{+} + (2+\chi)\ e \qquad [7.2.1]$$

the degree of oxidation (χ) of the as formed film is given by

$$\frac{Q_{cv}}{Q_{prp}} = \frac{\chi}{2 + \chi} \qquad [7.2.2]$$

where Q_{prp} is the charge used to prepare the film. Thus χ is *ca.* 0.23, indicating that every four to five pyrrole units in the polypyrrole chain carries one positive charge at 0.2 V. This result is consistent with the measured composition of PPY/PSS (section 3.3.1).

Table 7.2.1 Cyclic voltammetric peak potentials for 2 μm film coated Pt electrodes in 0.2 M $NaClO_4$ (aq).

Scan rate mV s^{-1}	PPY/ClO_4^-		PPY/PSS		PPY/PSS/MV^{2+}	
	E_{pa} V	E_{pc} V	E_{pa} V	E_{pc} V	E_{pa} V	E_{pc} V
10	-0.22	-0.34	-0.31	-0.37	-0.14	-0.39
20	-0.14	-0.33	-0.30	-0.38	-0.08	-0.39
40	-0.07	-0.28	-0.29	-0.39	-0.02	-0.39
60	-0.02	-0.25	-0.29	-0.39	0.04	-0.39
80	0.01	-0.25	-0.29	-0.40	0.10	-0.39
100	0.04	-0.25	-0.29	-0.41	0.15	-0.39
200	0.11	-0.26	-0.29	-0.43	0.25	-0.42

X-ray emission analysis was performed on PPY/PSS films to determine the equilibrium ion contents of the oxidized and reduced states (Fig. 7.2.5). After

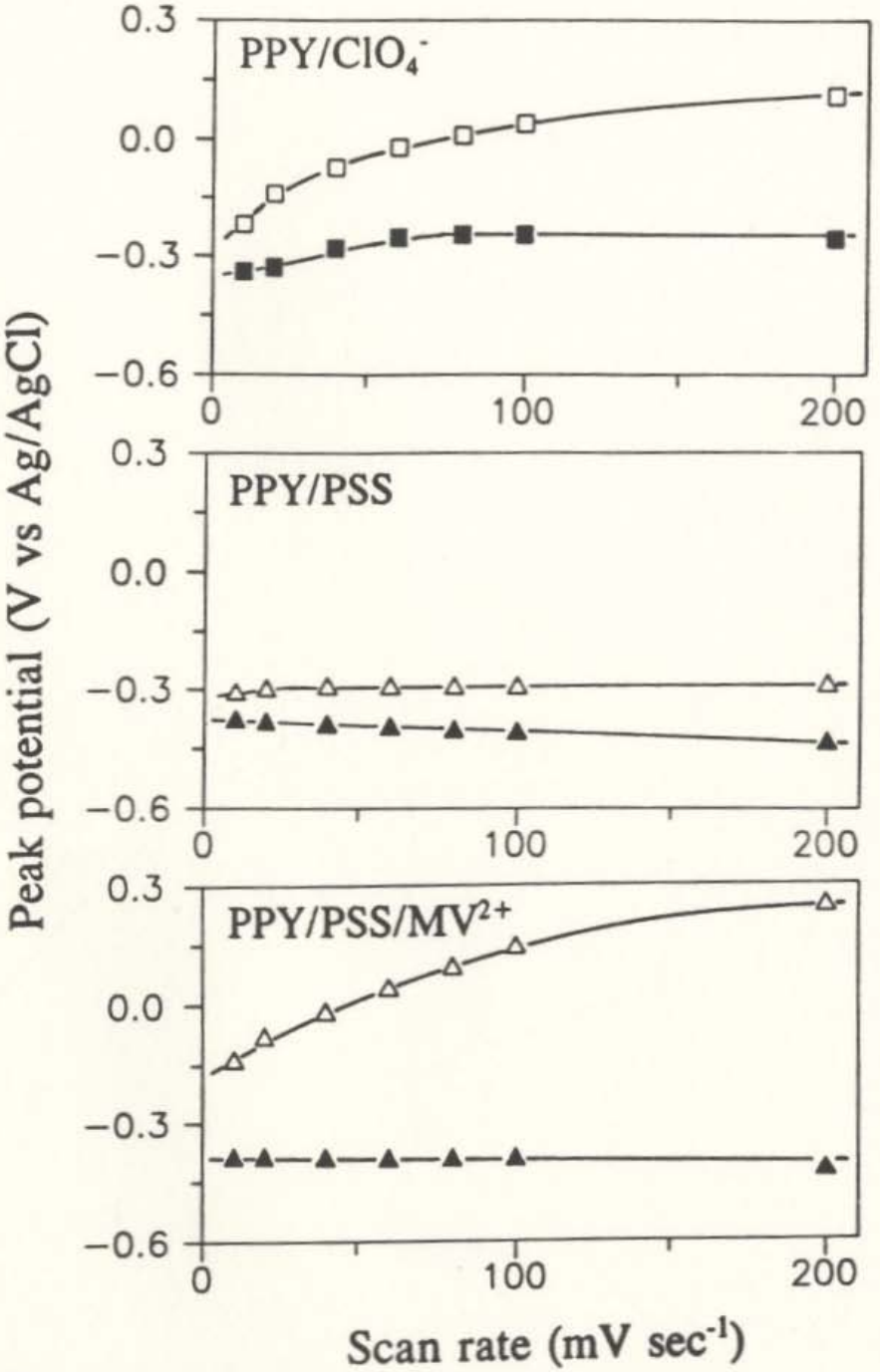

Figure 7.2.3 Plots of peak potential *vs.* scan rate for the cyclic voltammograms shown in Figs 7.2.1 and 7.2.2. Solid symbols are for the main cathodic peak, open symbols for the main anodic peak.

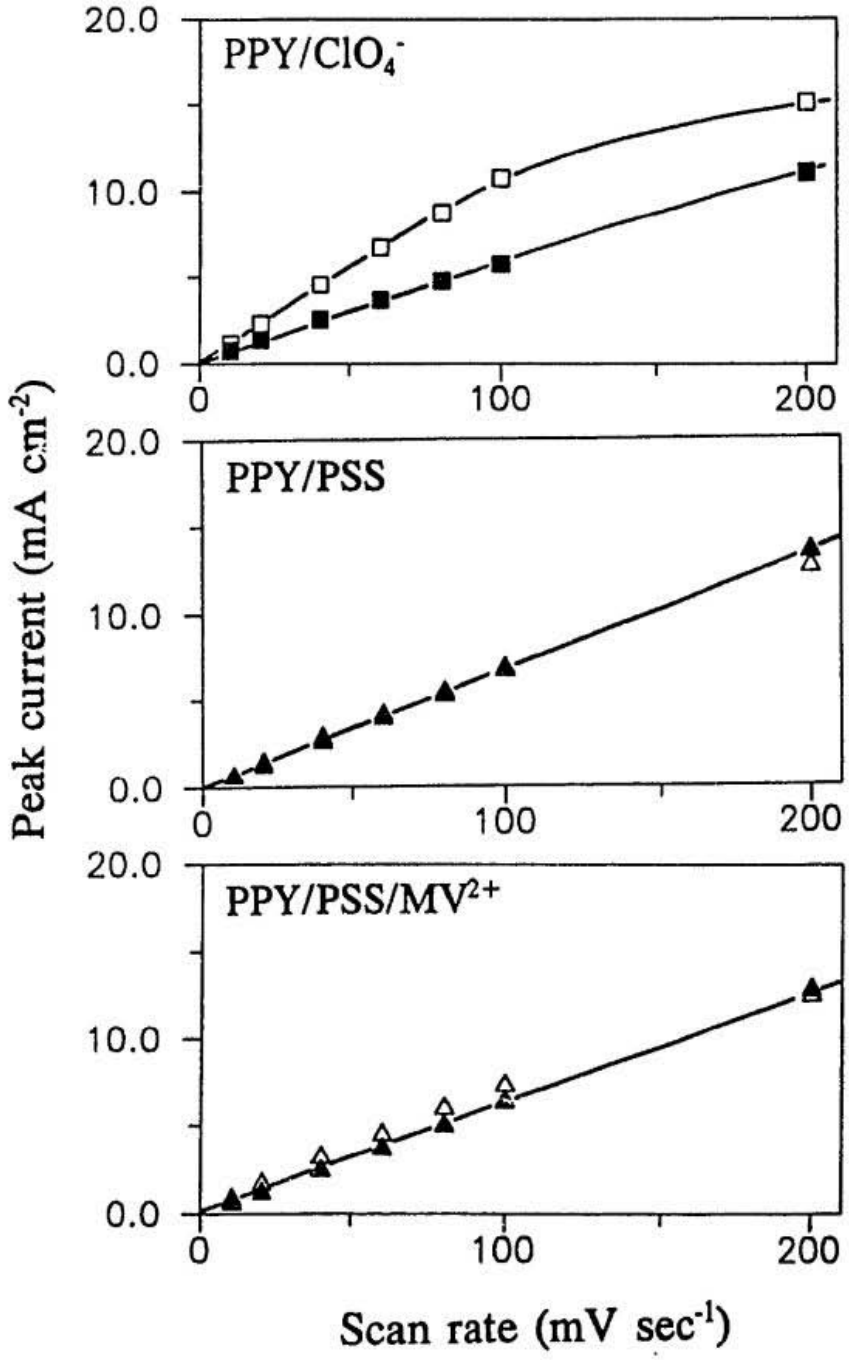

Figure 7.2.4 Plots of peak current *vs.* scan rate for the cyclic voltammograms shown in Figs 7.2.1 and 7.2.2. Solid symbols are for the main cathodic peak, open symbols for the main anodic peak.

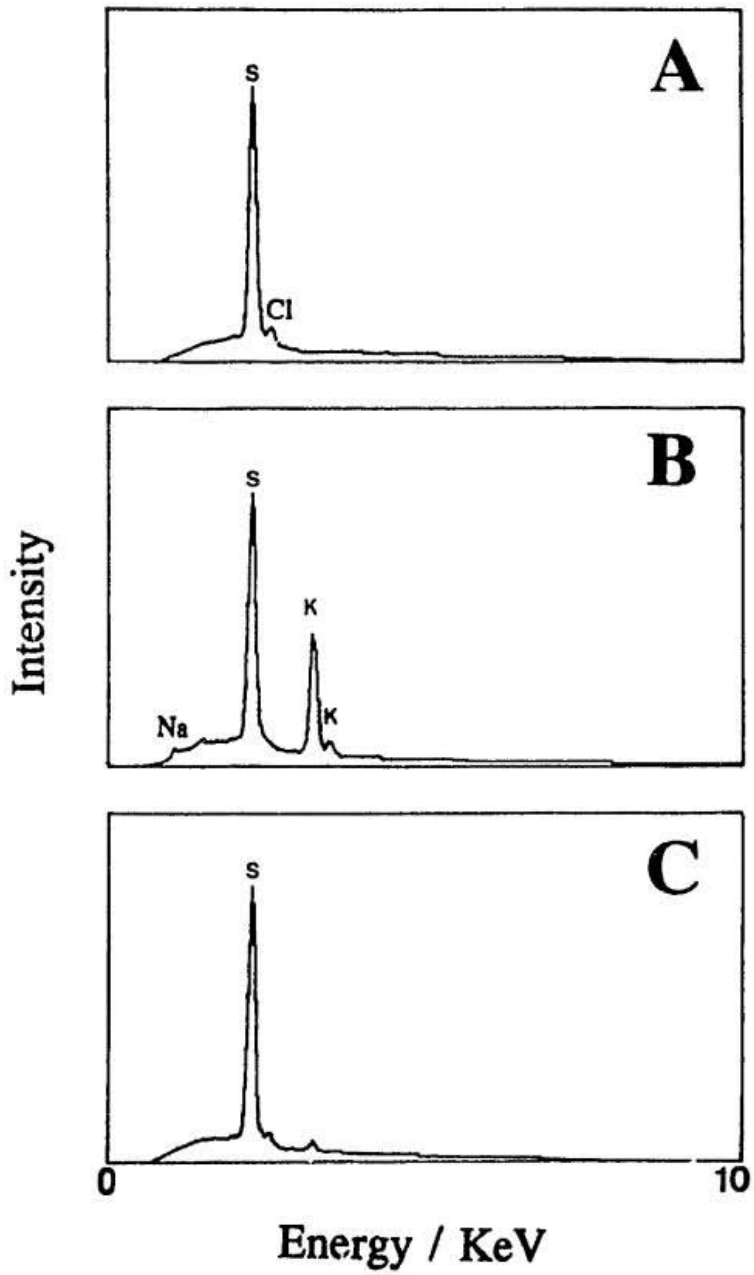

Figure 7.2.5 X-ray emission spectra of 2 μm free-standing PPY/PSS films. (A) as grown film; (B) following reduction at -1.0 V in 0.05 M $KClO_4$; and (C) following reduction at -1.0 V and reoxidation at 0.1 V in 0.05 M $KClO_4$.

their formation the films were immediately removed from the monomer solution and blotted dry with Kimwipe tissue paper to remove the adhering solution. Washing the films with deionized water can also effectively remove the adhering solution, and similar results were obtained. Fig. 7.2.5A shows the X-ray emission spectrum of a PPY/PSS film that was removed from the polymerization solution immediately after the polymerization current was turned off. No Na is detected, showing that all of the sulphonate anions incorporated during the electrochemical polymerization are used to compensate the positive charges on the oxidized polypyrrole chains. The small Cl peak is due to leakage of the Ag/AgCl reference electrode, since no Cl was detected in films prepared without using the reference electrode. Figs. 7.2.5B and 7.2.5C show X-ray spectra of PPY/PSS films that have been reduced and re-oxidized, respectively, in 0.05 M $KClO_4$ (aq). These spectra clearly show that electrolyte cations (K^+) are incorporated into the composite upon reduction and are expelled upon oxidation. Fig. 7.2.6A and 7.2.6B show X-ray spectra of the PPY/PSS/MV^{2+} films after oxidization and reduction, respectively, in 0.2 M $NaClO_4$ (aq) solution containing 3 mM methyl viologen dichloride. In this case, electrolyte perchlorate anions are incorporated into the polymer upon its oxidation and expelled upon reduction. Similar X-ray spectra were obtained for PPY/ClO_4^- films that had been oxidized and reduced in 0.2 M $NaClO_4$(aq).

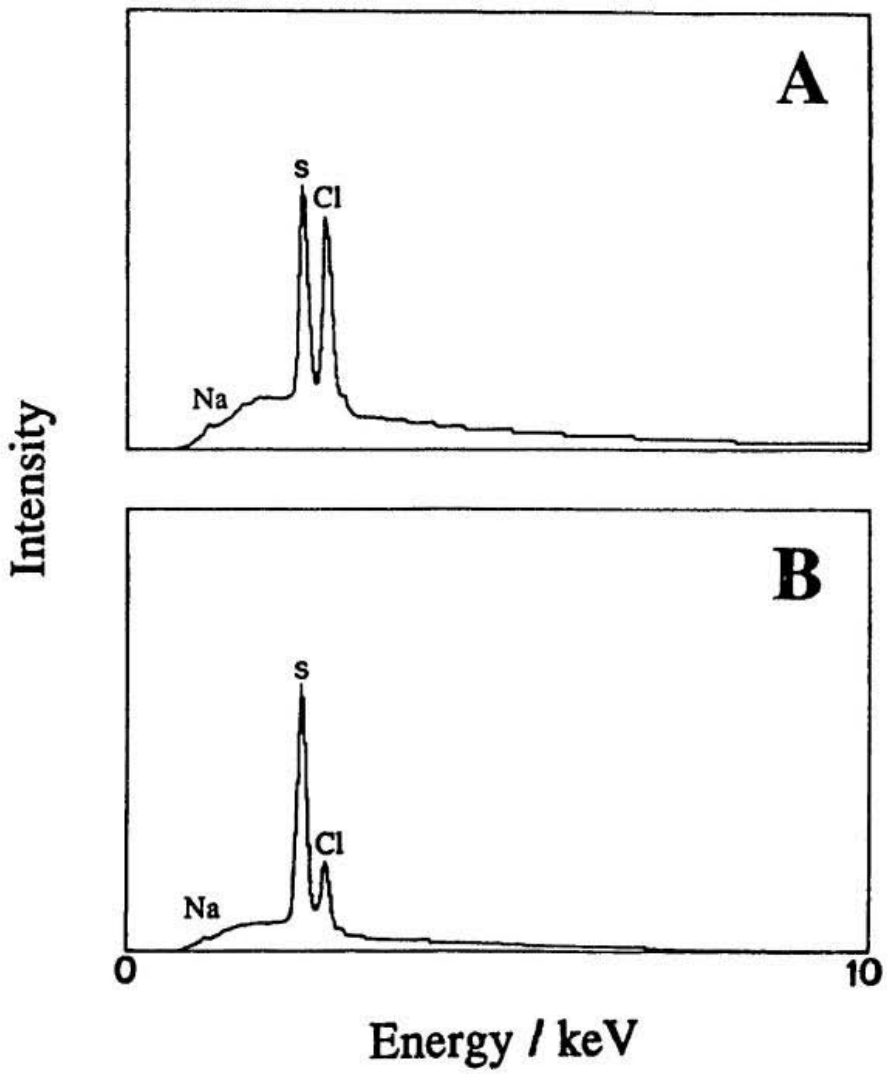

Figure 7.2.6 X-ray emission spectra of oxidized (A) and reduced (B) PPY/PSS/MV^{2+} films. Both films were equilibrated with 0.2 M $NaClO_4$ containing 3 mM $MVCl_2$ under potential cycling conditions (as in Fig.7.2.2) prior to the final reduction or oxidation before analysis.

7.2.2 Impedance studies

Complex plane impedance plots for PPY/ClO_4^-, PPY/PSS and PPY/PSS/MV^{2+} at selected potentials are shown in Figs. 7.2.7, 7.2.8 and 7.2.9, respectively. For all data considered here, the real axis intercept at high frequency is independent of the type of polymer film and electrode potential ($>$ -0.6 V), and coincides with the uncompensated resistance of the bulk electrolyte solution (R_s = 320 Ω, determined with the bare Pt electrode). Thus either the ionic or the electronic resistance of the polymer is negligible compared to the other[21]. It has been clearly established in section 5.1 that the impedance data can be modelled with the classical transmission line circuit (Fig. 4.2.3) to extract the polymer film ionic resistance[22,23].

The measured ionic conductivities for the three polymers depend to some extent on the order of potential change. For PPY/PSS, conductivities are higher when measured in the order of increasing potential than when measured in the order of decreasing potential (Figs. 7.2.8 and 7.2.10). In contrast, for PPY/ClO_4^- and PPY/PSS/MV^{2+}, conductivities are lower when measured in the order of increasing potential than those measured in the order of decreasing potential. This type of hysteresis is almost universally seen in the properties of conducting

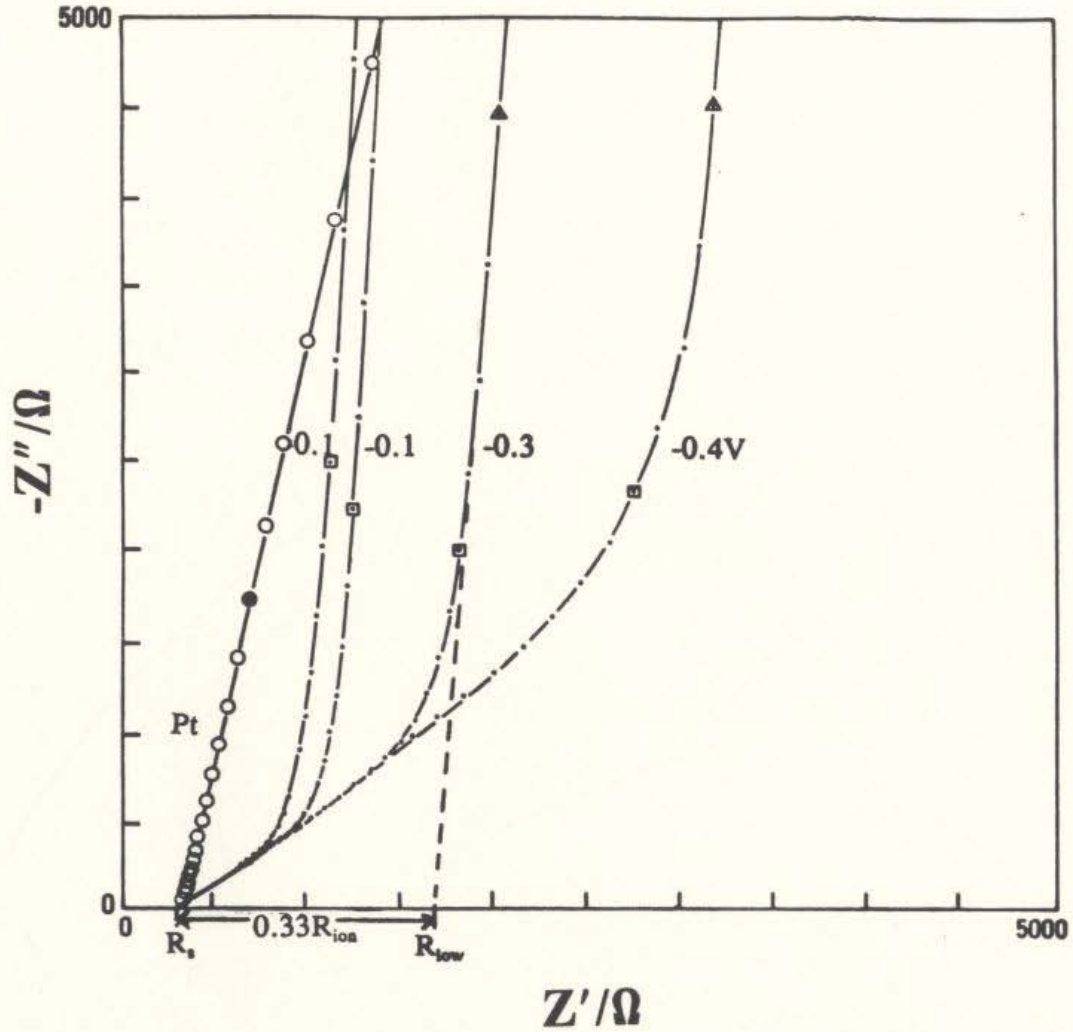

Figure 7.2.7 Complex plane impedance plots for a PPY/ClO_4^- coated Pt electrode at selected (indicated) potentials in 0.2M $NaClO_4$(aq). Circled points are for the bare Pt electrode at open circuit potential. Marked points correspond to frequencies of 1k (●); 0.5(□) and 0.2(▵) Hz.

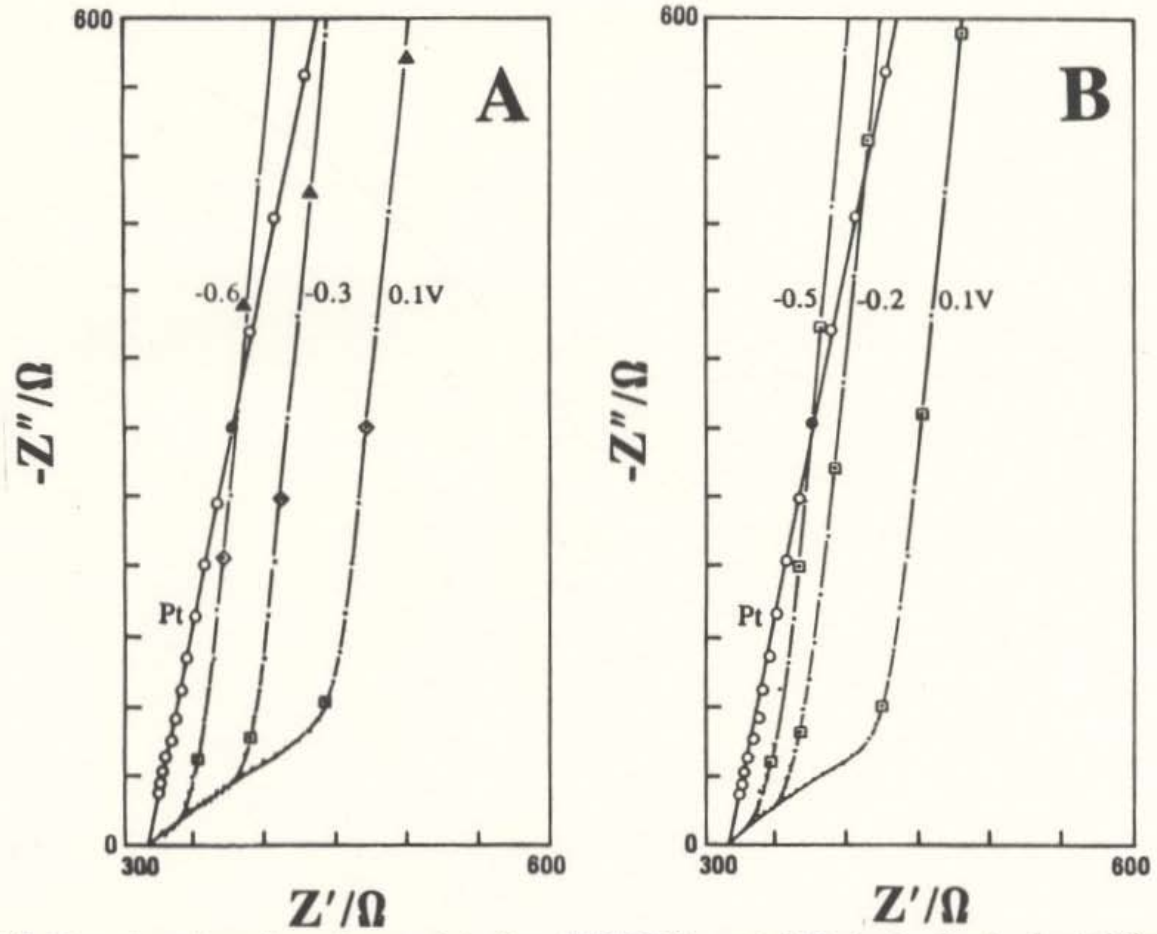

Figure 7.2.8 Complex plane impedance plots for a PPY/PSS coated Pt electrode at selected (indicated) potentials in 0.2M $NaClO_4$(aq). Data recorded in order of decreasing (A) or increasing (B) potential. Circled points are for the bare Pt electrode at open circuit potential. Marked points correspond to frequencies of 5.2k (●); 21(□) and 2.6(▵) Hz.

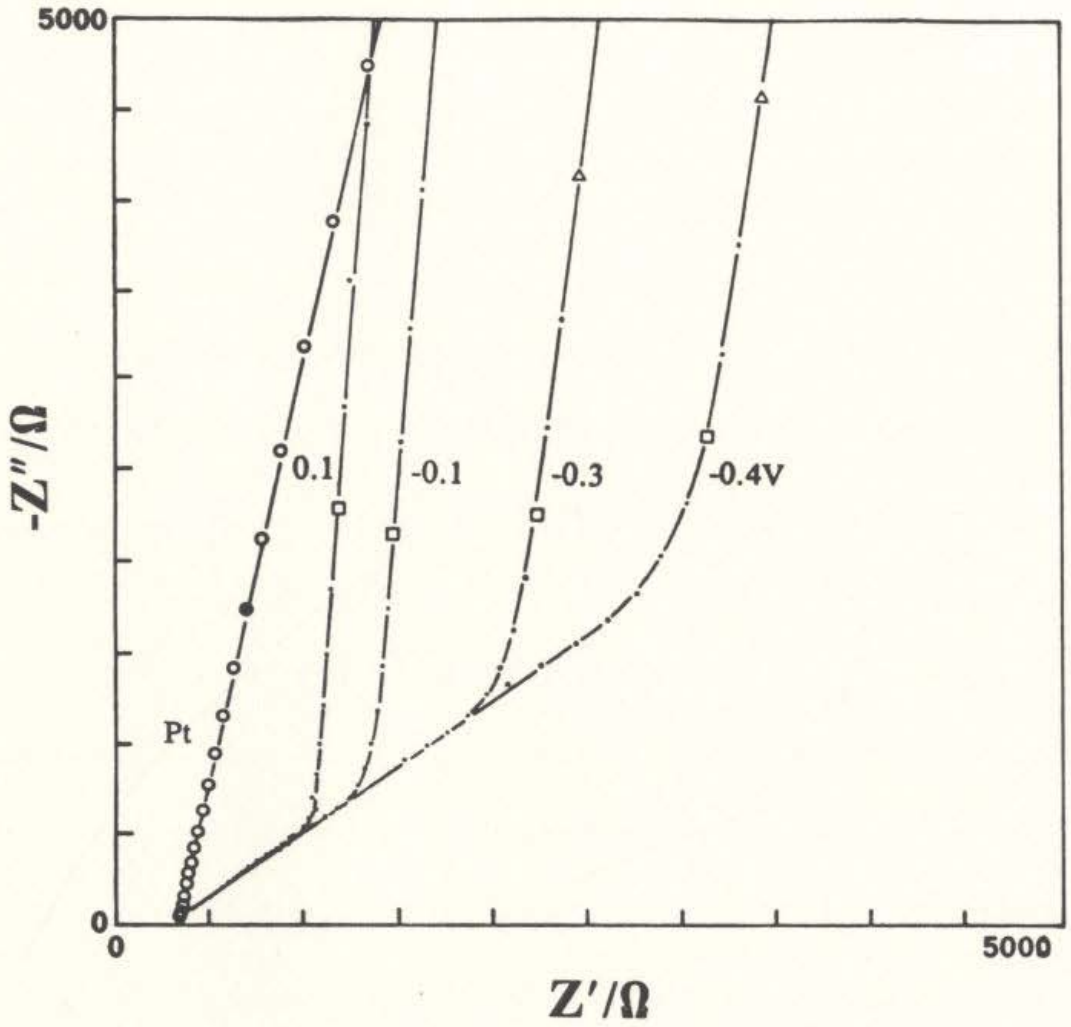

Figure 7.2.9 Complex plane impedance plots for a PPY/PSS/MV^{2+} coated Pt electrode at selected (indicated) potentials in 0.2 M $NaClO_4$(aq) containing 3 mM $MVCl_2$. Circled points are for the bare Pt electrode at open circuit potential. Marked points correspond to frequencies of 1k (●); 0.5(□) and 0.2(▵) Hz.

polymers. It has been attributed to N-shaped free energy curves[24] and conformation changes[25,26]. Unless otherwise stated, data in this chapter were recorded in the order of decreasing potential. As shown in Fig. 7.2.10, the ionic conductivities of PPY/ClO_4^- and PPY/PSS/MV^{2+} increase with increasing electrode potential, while ionic conductivity decreases with increasing potential for PPY/PSS. Plots of ionic conductivity *vs.* voltammetric charge are approximately linear for all three types of polymer films (Fig. 7.2.11).

Plotting the imaginary impedance (Z″) *vs.* 1/frequency for the data on the almost vertical line in the complex plane impedance plot forms a straight line. Low frequency capacitances (C_F) of polymer were calculated from the slopes (C_F = 1/(2π slope)) and are shown in Fig. 7.2.12, together with capacitances calculated from a slow scan rate cyclic voltammogram of PPY/PSS (C_{cv}=(anodic + cathodic current)/(2 scan rate)). For PPY/PSS vertical lines are obtained in the complex plane impedance plots for the whole potential range. For PPY/ClO_4^- and PPY/PSS/MV^{2+} at potentials below -0.6 V, low frequency capacitances cannot be determined with confidence since the 45° Warburg-type lines extend to very low frequency and no vertical lines are obtained.

The low frequency capacitance can also be obtained by examining the impedance data in the complex capacitance plane ($C_{ac}=1/(j\omega Z)$), which emphasizes the frequency dependence of charging processes at low frequency. The complex

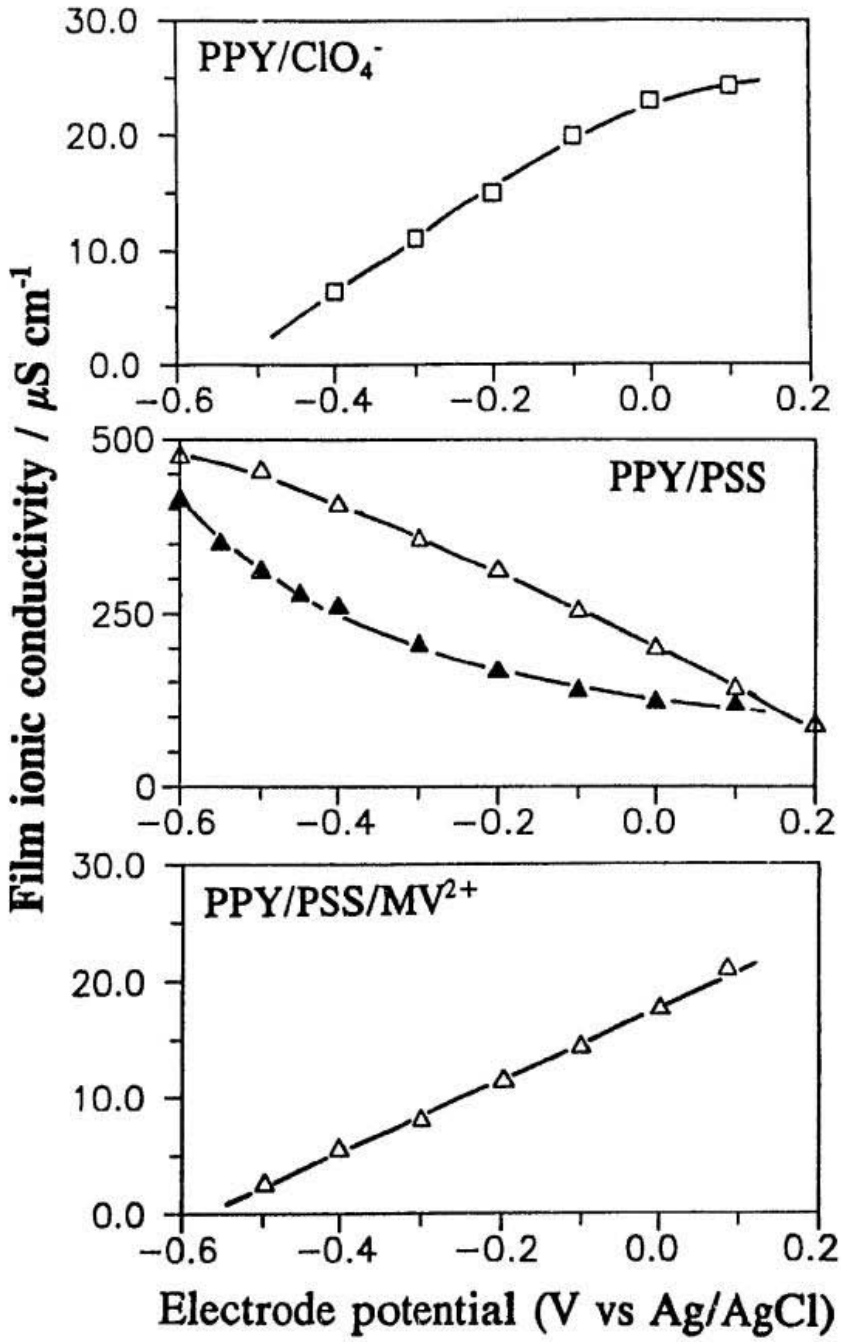

Figure 7.2.10 Plots of ionic conductivity *vs.* potential from the impedance plots (plus additional data) shown in Figs. 7.2.7-9. Conductivities were measured in the order of decreasing potential, except for the open points for PPY/PSS.

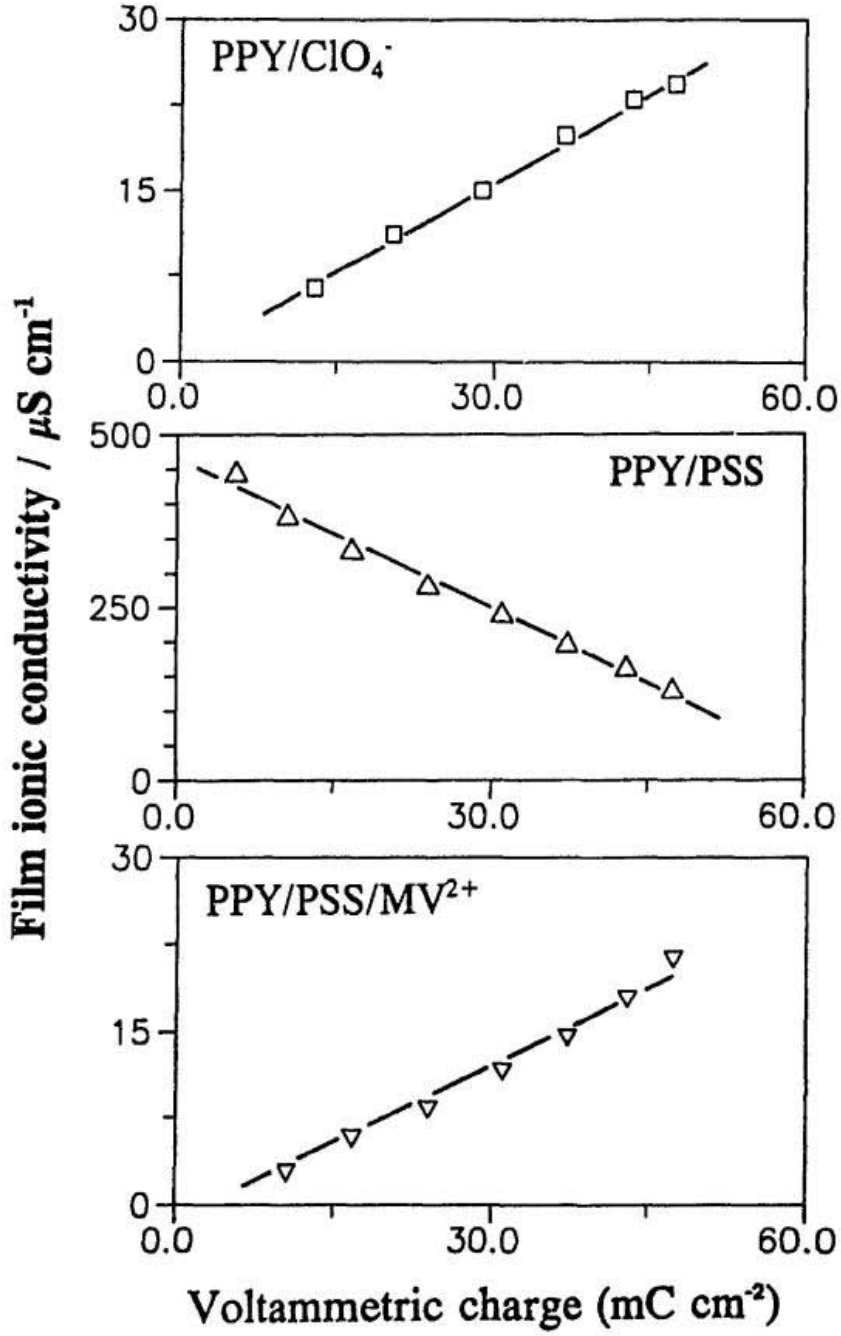

Figure 7.2.11 Plots of ionic conductivity *vs.* cyclic voltammetric charge (Q_{cv}) for PPY/ClO_4^-, PPY/PSS and $PPY/PSS/MV^{2+}$. Conductivities for PPY/PSS are averages of values measured in the order of decreasing and increasing potential.

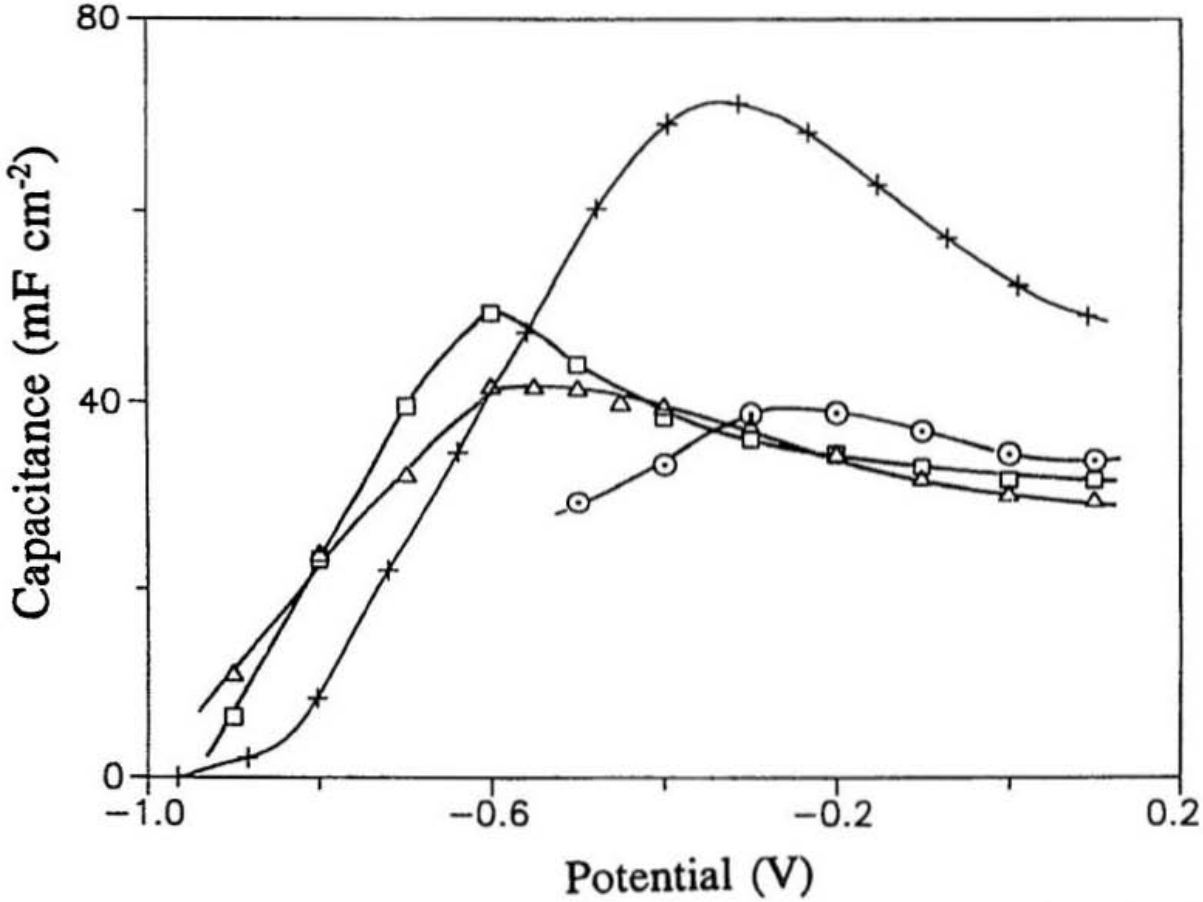

Figure 7.2.12 Plots of low frequency capacitances from impedance spectroscopy *vs.* electrode potential for 2 μm PPY/ClO_4^-(△), PPY/PSS (△) and PPY/PSS/MV^{2+} (⊙) films, and capacitances from cyclic voltammetry on a PPY/PSS film (+).

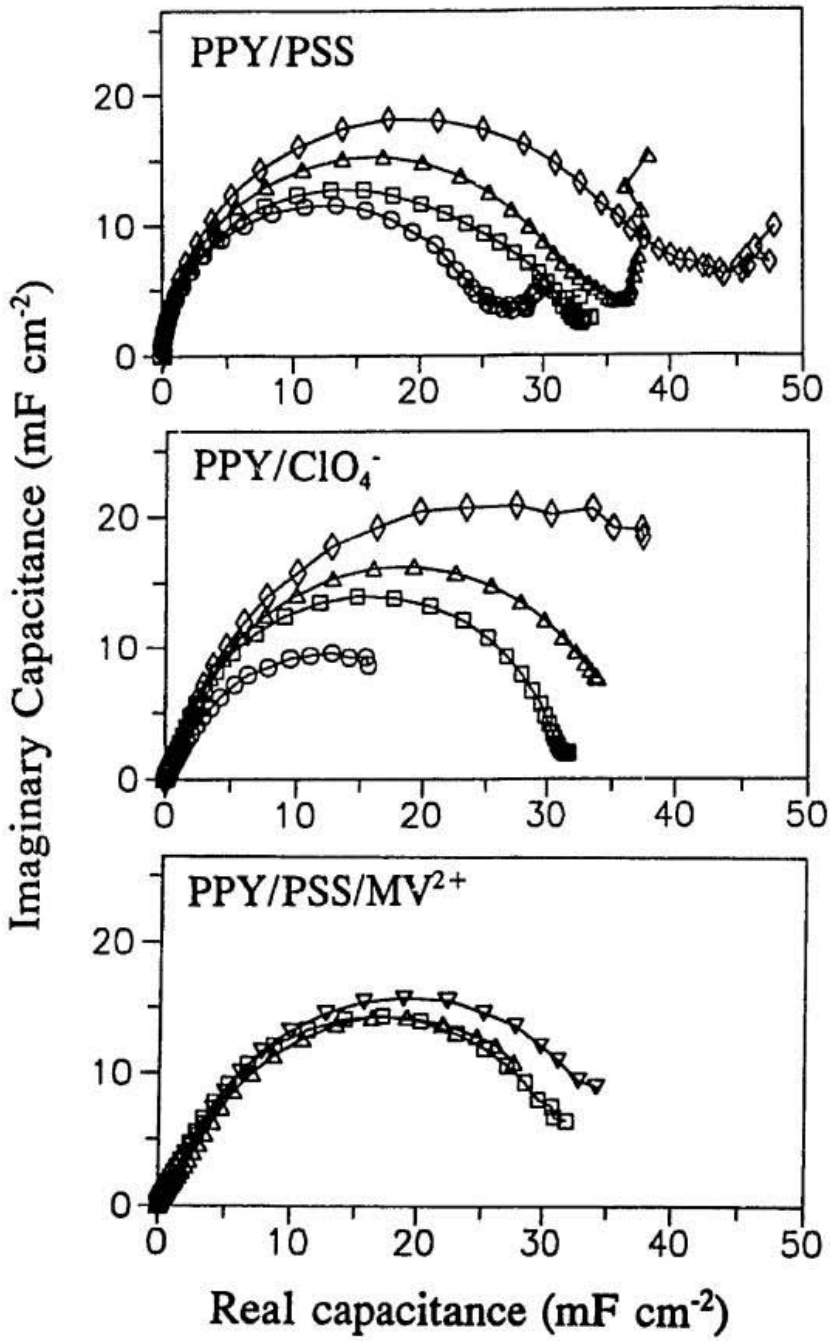

Figure 7.2.13 Complex capacitance plots at select electrode potentials, 0 V (□), -0.4 V (△), -0.5 V (▽), -0.6 V (◇), and -0.8 V (○) for PPY/ClO_4^-, PPY/PSS and PPY/PSS/MV^{2+}.

capacitance plots shown in Fig. 7.2.13 consist of a single semicircle indicating that the electrochemistry of each film involves a single ion transport process. Capacitances obtained from the diameter of the semicircles agree with those obtained from imaginary impedance (Z″) *vs.* 1/frequency plots. Capacitances from impedance measurements and cyclic voltammetry are compared in Fig. 7.2.12. The discrepancy is quite significant especially at high potentials and there is a mis-match in the peak potential. These differences are related to the hysteresis between anodic and cathodic potential scans seen in the properties (charge, conductivity, *etc.*) of the polymers (*e.g.*, Fig. 7.2.10). Conformation changes in the polymer accompanying oxidation and reduction[25] are thought to be responsible[27].

7.3 Discussion

It is clear from the x-ray emission analysis results in Fig. 7.2.5 that reduction and re-oxidation of PPY/PSS involves net uptake and expulsion of cations (*i.e.* cation transport). In contrast the electrochemistry of PPY/ClO_4^- in $NaClO_4$(aq) involves net anion transport. These different modes of ion transport are reflected in different potential dependencies of the ionic conductivities of the two materials. Thus the ionic conductivity of PPY/ClO_4^- increases with increasing potential (Fig. 7.2.10) as the amount of incorporated ClO_4^- is increased. Since the

ClO_4^- concentration in the polymer is proportional to its oxidation level, there is a linear relationship between the ionic conductivity and the voltammetric charge (Fig. 7.2.11).

In contrast, the ionic conductivity of PPY/PSS decreases with increasing potential (Fig. 7.2.10). In this polymer, the charge compensation is achieved by expulsion of cations as shown by x-ray emission spectra (Fig. 7.2.5). The concentration of cations in the film decreases proportionally to its degree of oxidation and so again there is a linear relationship between the polymer's ionic conductivity and its voltammetric charge (Fig. 7.2.11)

It can be concluded that in PPY/ClO_4^-, the ClO_4^- ions dominate the ionic transport process, while in PPY/PSS, Na^+ ion transport dominates. The reasonable linearity of the conductivity *vs.* charge plots (Fig. 7.2.11) suggests that these two processes are quite exclusive and that both materials are permselective under the conditions studied. The diffusion coefficient (D_{ion}) of the counterions (ClO_4^- or Na^+) in each material can be estimated from the slope of the conductivity *vs.* charge plot (Fig. 7.2.11) using eq. [4.3.2]. The c_{Ion} is the counterion concentration, which is proportional to the voltammetric charge. Diffusion coefficients of 2.8×10^{-9} $cm^2\ s^{-1}$ for ClO_4^- in PPY/ClO_4^-, 3.7×10^{-8} $cm^2\ s^{-1}$ for Na^+ in PPY/PSS, and 2.4×10^{-9} $cm^2\ s^{-1}$ for ClO_4^- in PPY/PSS/MV^{2+} were obtained.

Although ClO_4^- and Na^+ have similar mobilities in solution and they have

similar maximum concentrations in the PPY/ClO_4^- and PPY/PSS polymers, the maximum ionic conductivity of PPY/ClO_4^- is much less than that of PPY/PSS. The higher mobility of Na^+ ions in PPY/PSS relative to ClO_4^- ions in PPY/ClO_4^- is attributed to the relative strengths of ion-pairing between the mobile and fixed charges in the two systems. In PPY/ClO_4^-, ion pairs are presumably formed between oxidized polymer chain segments and ClO_4^-.[28] The following dissociation must occur before the ClO_4^- ions can move:

$$\text{-(-Py-)-}_n^+ClO_4^- \rightleftharpoons \text{-(-Py-)-}_n^+(aq) + ClO_4^-(aq) \qquad [7.4.1]$$

In PPY/PSS, ion pairs could be formed between the sulphonate anion and Na^+ ions and the following dissociation equilibrium could exist:

$$--SO_3^-Na^+ \rightleftharpoons --SO_3^-(aq) + Na^+(aq) \qquad [7.4.2]$$

The dissociation constant of eq. [7.4.2] should be very large, since both cation and anion are well solvated and thus stabilized. This is similar to a strong electrolyte in aqueous solution. However, the positive charges on a polypyrrole chain are diffuse due to their delocalization along the conjugated π-system. Thus -(-Py-)-$_n^+$ will not be stabilized effectively by solvation. In addition, the diffuse nature of the

positive charge of -(-Py-)-$_n^+$ makes it very polarizable so that it can form a strong interaction with ClO_4^-. If —(-Py-)—$SO_3^-Na^+$ is assumed to be completely dissociated in the PPY/PSS composite, a comparison of the diffusion coefficient of ClO_4^- ions in PPY/ClO_4^- with that of Na^+ ions in PPY/PSS suggests that the dissociation coefficient of -(-Py-)-$_n^+ClO_4^-$ is *ca.* 0.08. The interaction between ClO_4^- and oxidized polypyrrole is even stronger in acetonitrile, and can cause complete immobilization of the ClO_4^- ions when the polymer is poorly solvated[19].

Support for the ion-pairing hypothesis discussed above is provided by the results for PPY/PSS/MV^{2+} films. The charges on the methyl viologen dications (MV^{2+}) are to some extent delocalized over the conjugated π-orbital, as in oxidized segments of polypyrrole chains. MV^{2+} can therefore form tight ion pairs with the sulphonate anions in reduced PPY/PSS and becomes immobilized in the composite. Oxidation of the resulting PPY/PSS/MV^{2+} film involves ClO_4^- uptake (Fig. 7.2.6) and so the potential dependence of its ionic conductivity follows the pattern observed for PPY/ClO_4^- (Fig. 7.2.10). The ionic conductivity of PPY/PSS/MV^{2+} increases with increasing electrode potential and is proportional to the voltammetric charge. Remarkably, the ionic conductivities of PPY/PSS/MV^{2+} and PPY/ClO_4^- at each oxidation level are very similar. This is also reflected in the similar ClO_4^- diffusion coefficients in the two materials. This strongly suggests that the low mobility of ClO_4^- is due to an electrostatic

interaction with the polypyrrole, which will be similar in the two materials, rather than steric factors which will be quite different. When a PPY/PSS/MV^{2+} coated electrode was transferred to 0.2 M $NaClO_4$(aq) containing no MV^{2+} the potential dependence and magnitude of its ionic conductivity became slowly characteristic of PPY/PSS, indicating that MV^{2+} ions are slowly replaced by Na^+ ions.

The difference in the scan rate dependence of the cyclic voltammetric peak potentials between PPY/ClO_4^- (or PPY/PSS/MV^{2+}) and PPY/PSS can be explained by the difference in ion transport and its dependence on the degree of oxidation of the polypyrrole in these materials. In all cases the voltammetric peak corresponding to insertion of the mobile ions is most sensitive to scan rate (Fig. 7.2.3). Thus for PPY/ClO_4^- and PPY/PSS/MV^{2+}, the anodic peak, which corresponds to ClO_4^- insertion, shifts markedly to higher potential with increasing scan rate, while the cathodic peak remains at the same potential or shifts only slightly. For PPY/PSS, the cathodic peak, which corresponds to Na^+ insertion, shifts slightly to lower potential while the cathodic peak remains at the same potential. Clearly the insertion of the mobile ionic species from the solution into the polymer is associated with a larger ohmic potential drop than its expulsion. This can be attributed to the fact that at the beginning of the potential scan involving insertion, the ionic resistance of the film is at its maximum value. The fact that the ionic conductivity of PPY/PSS is higher than that of PPY/ClO_4^- (or

PPY/PSS/MV^{2+}) also explains the smaller peak potential separation of PPY/PSS relative to that of PPY/ClO_4^- (or PPY/PSS/MV^{2+})

7.4 Conclusions

Impedance measurements of ionic conductivity as a function of electrode potential give good evidence that the PPY/PSS composite is self-doped. The great enhancement in ionic conductivity shown by PPY/PSS over PPY/ClO_4^- is achieved by free mobile Na^+ ions in the film. For PPY/ClO_4^-, however, formation of a strong ion-pair between the positive charges on the polypyrrole chains and ClO_4^- ions decreases the mobility of ClO_4^- ions in the polymer.

Methyl viologen dication in the supporting electrolyte solution becomes immobilized in PPY/PSS by the formation of ion-pairs between MV^{2+} and $-SO_3^-$. For both PPY/PSS/MV^{2+} and PPY/ClO_4^-, the magnitude of the ionic conductivity and the way it changes with the oxidation level of the polypyrrole are similar. Changes in cyclic voltammetric peak potentials with increasing scan rate are also similar. In both materials, movement of ClO_4^- anions dominates ion transport.

The changes in the cyclic voltammetric peak potentials for PPY/ClO_4^- (or PPY/PSS/MV^{2+}) and PPY/PSS with increasing scan rate can be related to the difference in their mode of ion transport. Since the insertion of the mobile ions

into the polymer increases the ionic conductivity, the process that corresponds to the insertion of mobile ions starts from the most highly resistive form. Consequently, a large ohmic potential drop occurs which causes a large shift in peak potential. Such changes in peak potential with increasing scan rate can be used as a simple diagnostic means to determine the mode of ion transport in polypyrrole, and other similar materials, by cyclic voltammetry.

Comparing the cyclic voltammograms for the three types of polypyrrole films, increasing the polymer's ionic conductivity decreases its peak potential separation.

References

(1) Iyoda, T.; Ohtani, A.; Shimidzu, T.; Honda, K. *Chem. Lett.* 1986,,687.

(2) Shimidzu, T.; Ohtani, A.; Iyoda, T.; Honda, K. *J. Electroanal. Chem.* 1987,*224*,123.

(3) Shimidzu, T.; Ohtani, A.; Iyoda, T.; Honda, K. *J. Chem. Soc., Chem. Commun.* 1986,,1415.

(4) Iyoda, T.; Ohtani, A.; Shimidzu, T.; Honda, K. *Synth. Met.* 1987,*18*,747.

(5) Shimidzu, T.; Ohtani, A.; Honda, K. *J. Electroanal. Chem.* 1988,*251*,323.

(6) Ohtani, A.; Abe, M.; Higuchi, H.; Shimidzu, T. *J. Chem. Soc., Chem. Commun.* 1988,,1545.

(7) Zhou, Q.-X.; Miller, L.L.; Valentine, J.R. *J. Electroanal. Chem.* 1989,*261*,147.

(8) Baker, C.K.; Qiu, Y.J.; Reynolds, J.R. *J. Phys. Chem.* 1991,*95*,4446.

(9) Prezyna, L.A.; Qiu, Y.J.; Reynolds, J.R.; Wnek, G.E. *Macromolecules* 1991,*24*,5283.

(10) Li, F.; Albery, W.J. *J. Chem. Soc., Faraday. Trans.* 1991,*87*,2949.

(11) Elliott, C.M.; Kopelove, A.B.; Albery, W.J.; Chen, Z. *J. Phys. Chem.* 1991,*95*,1743.

(12) Gieselman, M.B.; Reynolds, J.R. *Macromolecules* 1990,*23*,3118.

(13) Reynolds, J.R.; Baker, C.K.; Gieselman, M. *Polym. Prepr. (Am. Chem. Soc., Div. Polym. Chem.)* 1989,*30*,151.

(14) Wang, J.; Sun, Z.; Lu, Z. *J. Electroanal. Chem.* 1991,*310*,269.

(15) Hyodo, K.; Omae, M. *Electrochim. Acta* 1990,*35*,1245.

(16) Naoi, K.; Lien, M.; Smyrl, W.H. *J. Electrochem. Soc.* 1991,*138*,440.

(17) Nagasubramanian, G.; Di Stefano, S.; Moacanin, J. *J. Phys. Chem.* 1986,*90*,4447.

(18) Zhou, Q.-X.; Kolaskie, C.J.; Miller, L.L. *J. Electroanal. Chem.* 1987,*223*,283.

(19) Duffitt, G.L.; Pickup, P.G. *J. Chem. Soc., Faraday. Trans.* 1992,*88*,1417.

(20) Lien, M.; Smyrl, W.H.; Morita, M. *J. Electroanal. Chem.* 1991,*309*,333.

(21) Albery, W.J.; Elliott, C.M.; Mount, A.R. *J. Electroanal. Chem.* 1990,*288*,15.

(22) Pickup, P.G. *J. Chem. Soc., Faraday. Trans.* 1990,*86*,3631.

(23) Ren, X.; Pickup, P.G. *J. Chem. Soc., Faraday. Trans.* 1993,*89*,321.

(24) Feldberg, S.W.; Rubinstein, I. *J. Electroanal. Chem.* 1988,*240*,1.

(25) Heinze, J.; Bilger, R.; Meerholz, K. *Ber. Bunsenges. Phys. Chem.* 1988,*92*,1266.

(26) Albery, W.J.; Chen, Z.; Horrocks, B.R.; Mount, A.R.; Wilson, P.J.; Bloor, D.; Monkman, A.T.; Elliott, C.M. *Faraday. Discuss. Chem. Soc.* 1989,*88*,247.

(27) Ren, X.; Pickup, P.G. *J. Electroanal. Chem.* 1993,,submitted.

(28) Kaufman, J.H.; Kanazawa, K.K.; Street, G.B. *Phys. Rev. Lett.* 1984,*53*,2461.

Chapter 8

The Structure of Polypyrrole

Many fundamental properties of a conducting polymer such as the mechanical stability[1], solvent and salt transfer upon redox switching[2], electronic/ionic conductivity[3], and permselectivity[4] are closely related to its structure. Structure becomes an important issue when considering many practical applications such as gas separation[5], separation of neutral solution species[6], sensors based on charge and size separation[4,7,8], ion-gate devices[9,10], the switching speed of electrochromic devices[11-14], charging/discharging rates of battery electrodes[15,16] and support for electrocatalytic materials[17,18]. Early studies by Diaz *et al*[19,20] implied that polypyrrole (PPY) is a densely packed, non-porous material. However, this view has not been shared by many other researchers. Noufi *et al*[21] demonstrated both the incorporation and mobility of $Fe(CN)_6^{3-}$ ions in PPY. From the cyclic voltammetry and impedance studies of oxidized PPY film coated electrodes, Bull *et al*[22] concluded that PPY is permeable to solvent and electrolyte and that a PPY coated electrode behaves as a porous electrode. Burgmayer and Murray[23] measured the ac/dc ionic conductivities and permeation rates of

electrolyte cations and anions in thick (*ca.* 10 μm) free-standing PPY membranes. They found that the oxidized form is highly permeable to anions, while cations also transport, although at a much lower rate, through the pore-channels of the polymer.

The studies on the ionic conductivity of poly-MPCA reported in chapter 6 have indicated that the polymer film has a two-phase structure consisting of a polymer phase and a pore solution phase[24]. The polymer phase consists of polymer aggregates joined at contacting points to form a continuous network, through which electronic current flows across the polymer film thickness during the impedance measurement. Ionic conduction in the polymer aggregates occurs mainly by hopping of the counterions between neighbouring ion-exchanging sites. The contribution to the ionic conductivity of the polymer aggregates by the supporting electrolyte salt is negligible. This is perhaps due firstly to the low solubility and low dissociation constant of the electrolyte in the hydrophobic polymer phase and secondly, to the Donnan exclusion of co-ions, which further reduces the concentration of salt in the polymer aggregates. The ionic conduction mechanism in the pore solution is the same as that in the bulk electrolyte solution, where both free mobile electrolyte cations and anions are charge carriers. At equilibrium the composition and ionic conductivity of the pore solution appears to

be the same as those of the bulk electrolyte solution.

The experimental results for poly-MPCA have also shown that the ionic conduction paths in the polymer film include both pore solution and polymer aggregates, suggesting that the pores are discontinuous. Since the ionic conductivity of the pore solution is about 1000 times higher than that of the polymer aggregates for poly-MPCA, ion conduction will preferentially follow the pore solution with a minimum number of polymer aggregates blocking the pore channels. The diversity of ionic current paths in the polymer film has been invoked to explain the deviation of the experimental impedance data at low frequency from an ideal vertical line in the complex plane impedance plot[24]. Another factor that may cause such deviation and must be considered is charging of the polymer aggregates themselves. The redox reaction layer starts at the surface of the polymer aggregates and spreads into the centre as the frequency is decreased. Consequently, the ion conduction paths at a lower frequency include more polymer phase and become more resistive.

In this chapter, similar experimental strategies to those applied to poly-MPCA are used to study polypyrrole, both PPY/ClO_4^- and PPY/PSS polymer films. The fact that these two types of polymers have different ion transport mechanisms opens a new opportunity to investigate their structure. Also, since polypyrrole has been one of the most widely studied conducting polymers, the

results are more relevant than those obtained for poly-MPCA.

8.1 Factors Affecting Film Ionic Conductivity

The PPY/PSS and PPY/ClO_4^- films studied in this section were all 2 μm thick and all the impedance measurements were carried out in aqueous electrolyte solutions. Figs. 8.1.1 and 8.1.2 show complex plane impedance plots for PPY/PSS film coated Pt electrodes in $NaClO_4$ and NaPSS solutions respectively. Ionic conductivities for these films were obtained from their impedance data using the porous electrode model as was applied for the polypyrrole films in section 5.1. Tables 8.1.1 and 8.1.2 list the solution and film ionic conductivities. Film ionic conductivities are plotted as a function of solution conductivity in Figs. 8.1.3 and 8.1.4 for the two electrolyte solutions respectively.

In both electrolyte solutions, decreasing the electrode potential increases the ionic conductivity of the PPY/PSS film. As has been discussed in chapter 7, this is due to the self-doping of the polymer composite[25-29]. In this material, ion conduction in the polymer aggregates occurs by the hopping of the mobile cations between neighbouring fixed cation-exchanging sites ($-SO_3^-$)[29]. Clearly the polymer

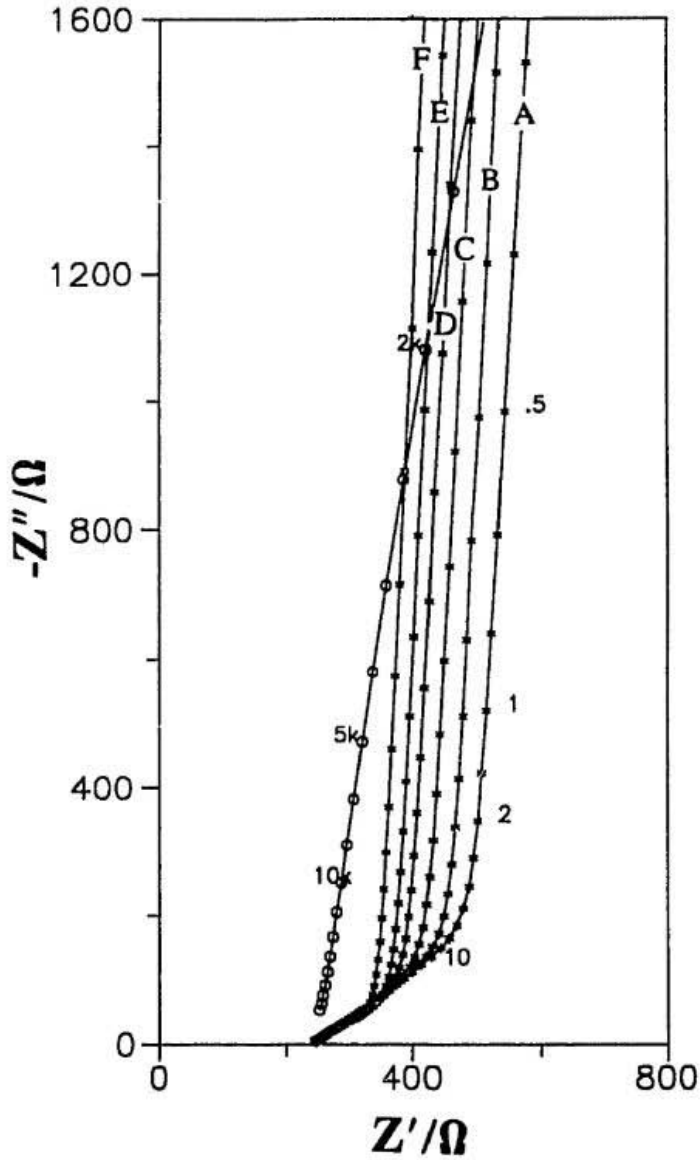

Figure 8.1.1A Complex plane impedance plots for a 2 μm PPY/PSS film coated Pt electrode in 0.25 M $NaClO_4$(aq) solution at selected potentials (A: 0.1; B: 0.0; C: -0.1; D: -0.2, E: -0.3 and F: -0.4 V *vs.* Ag/AgCl). Circled points are for the bare Pt electrode at the open circuit potential. Frequencies at selected points are marked in Hz.

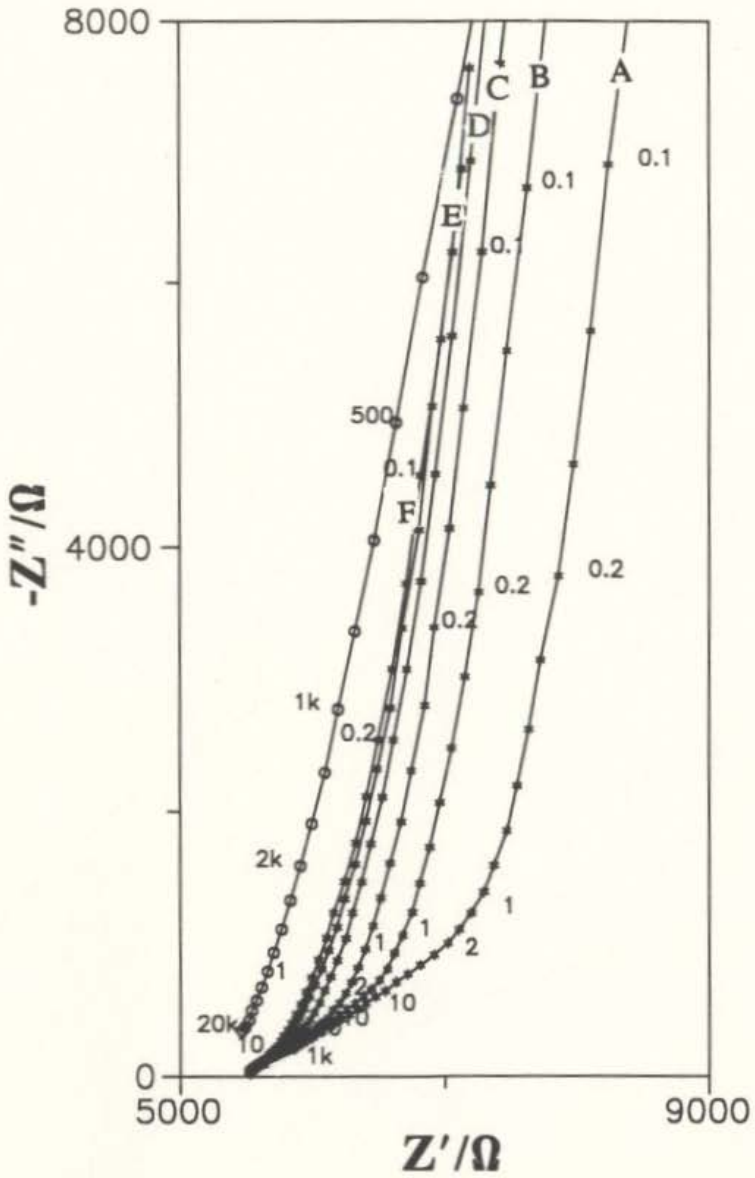

Figure 8.1.1B Complex plane impedance plots for a 2 μm PPY/PSS film coated Pt electrode in 0.01 M $NaClO_4$(aq) solution at selected potentials (A: 0.1; B: 0.0; C: -0.1; D: -0.2, E: -0.3 and F: -0.4 V *vs.* Ag/AgCl). Circled points are for the bare Pt electrode at the open circuit potential. Frequencies at selected points are marked in Hz.

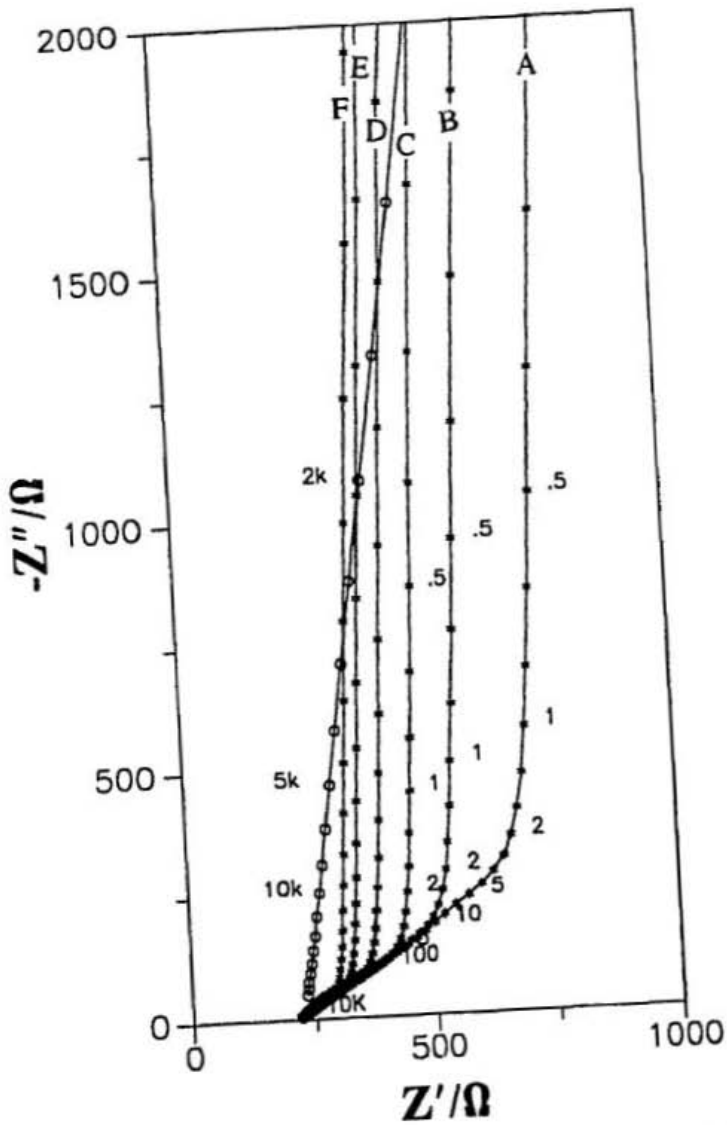

Figure 8.1.2A Complex plane impedance plots for a 2 μm PPY/PSS film coated Pt electrode in 0.5 M NaPSS(aq) solution at selected potentials (A: 0.1; B: 0.0; C: -0.1; D: -0.2, E: -0.3 and F: -0.4 V *vs.* Ag/AgCl). Circled points are for the bare Pt electrode measured at the open circuit potential. Frequencies at selected points are marked in Hz.

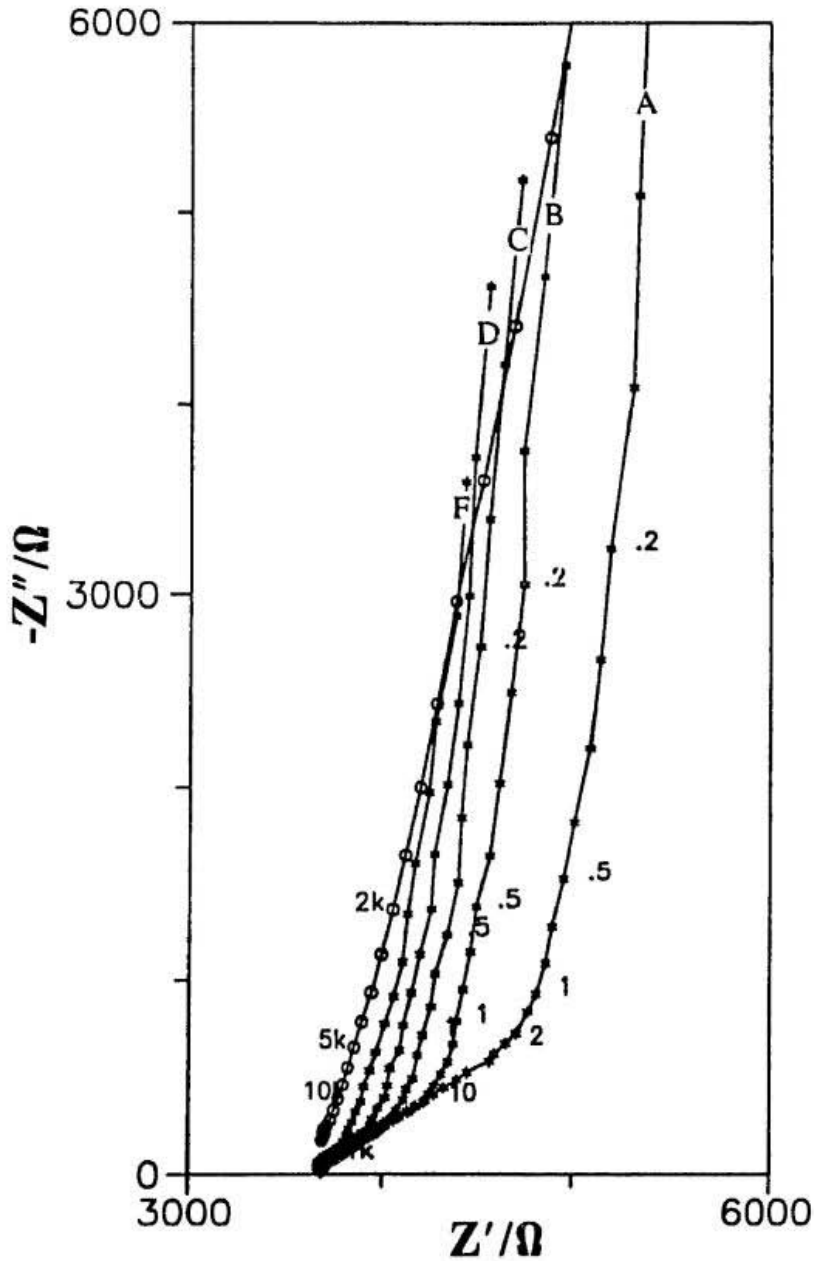

Figure 8.1.2B Complex plane impedance plots for a 2 μm PPY/PSS film coated Pt electrode in 0.025 M NaPSS(aq) solution at selected potentials (A: 0.1; B: 0.0; C: -0.1; D: -0.2, E: -0.3 and F: -0.4 V *vs.* Ag/AgCl). Circled points are for the bare Pt electrode at the open circuit potential. Frequencies at selected points are marked in Hz.

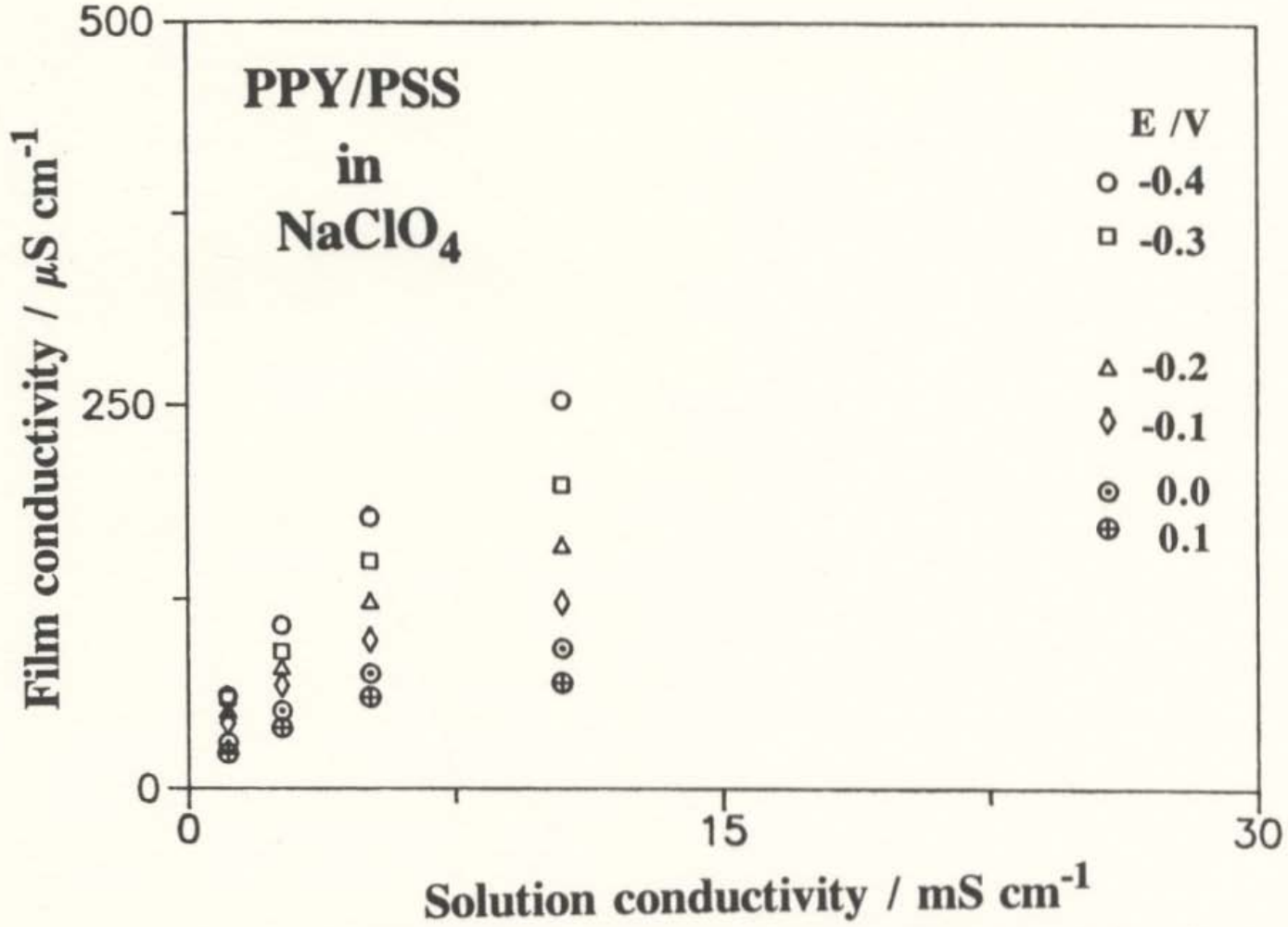

Figure 8.1.3 Plots of PPY/PSS film ionic conductivity in $NaClO_4$(aq) solution at indicated potential as a function of the solution conductivity.

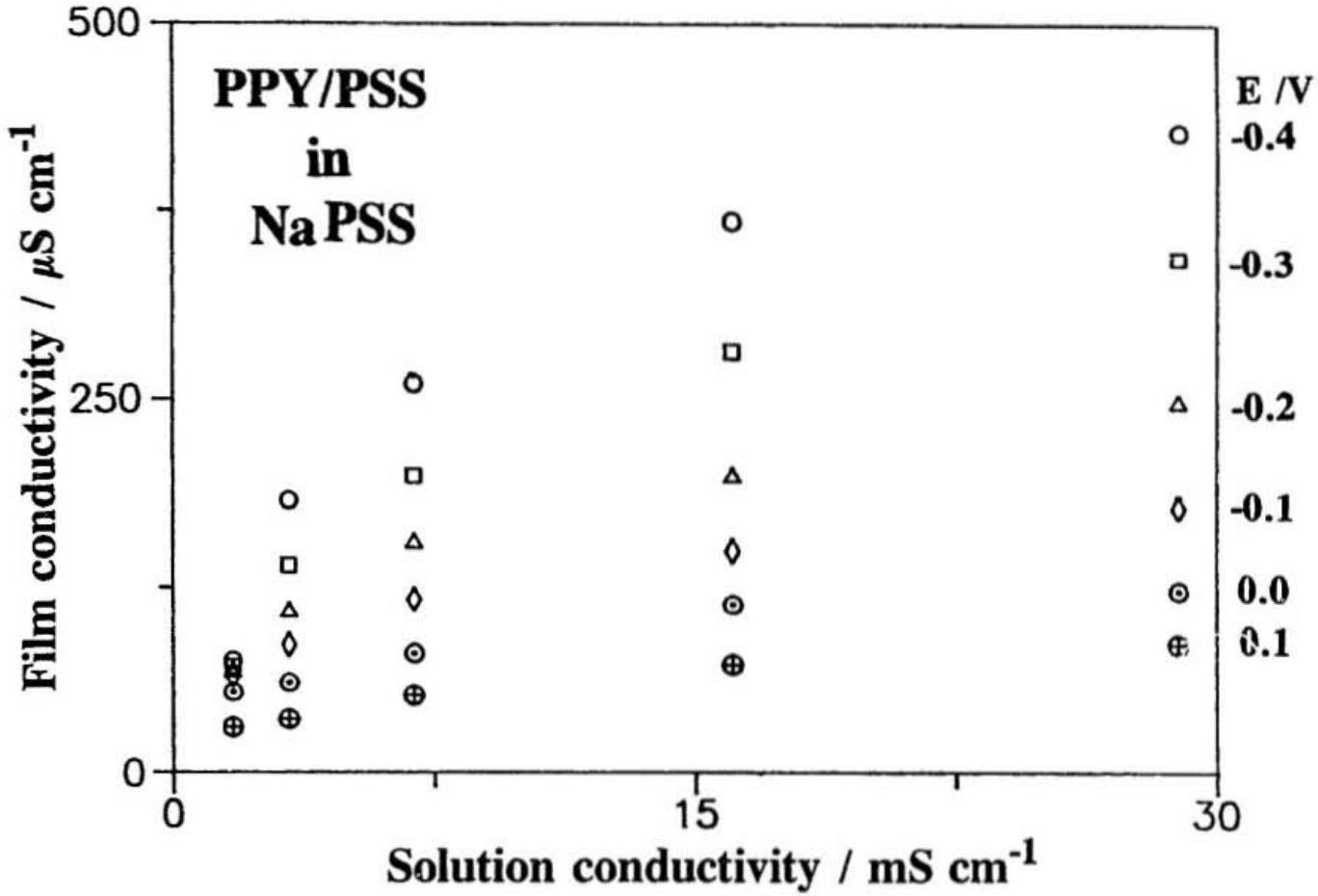

Figure 8.1.4 Plots of PPY/PSS film ionic conductivity in NaPSS(aq) solution at indicated potential as a function of solution conductivity.

aggregates are permselective and the concentration of anions is low. However, it is also observed that in both electrolyte solutions increasing the concentration of supporting electrolyte increases the polymer film ionic conductivity (Tables 8.1.1 and 8.1.2). This effect may be due to an increase in the ionic conductivity of the solution in pores. Thus since both electrode potential and the conductivity of the supporting electrolyte solution affect the polymer film ionic conductivity, the two-phase model proposed for poly-MPCA may also apply to PPY/PSS films.

Using a uniform polymer phase model (one-phase model) may give an alternative explanation of the above experimental observations. Increasing the supporting electrolyte concentration may increase the salt content in the polymer phase and thus increase the polymer film ionic conductivity. Changing the electrode potential may change the mobilities of ionic species in the polymer film and thus change the film ionic conductivity. However, comparing Figs. 8.1.3 and 8.1.4 it can be seen that at the same solution conductivity the film ionic conductivity is similar despite of the great difference in the size of the ClO_4^- and PSS anions. Such a great difference in anion size should cause a great difference in salt content of the polymer phase and thus the film ionic conductivity, according to the one-phase model. The two-phase model provides a more logical explanation that increasing the pore solution ionic conductivity by increasing the concentration of either $NaClO_4$ or NaPSS increases the film ionic conductivity.

Table 8.1.1 PPY/PSS film ionic conductivity in aqueous $NaClO_4$ solution.

Electrolyte solution		Film ionic conductivity at the indicated potential / $\mu S\ cm^{-1}$					
Conc. M	Cond. $mS\ cm^{-1}$	-0.4 V	-0.3 V	-0.2 V	-0.1 V	0.0 V	0.1 V
saturated	105	315	237	166	119	119	
0.25	25.8	398	363	277	241	196	173
0.10	10.5	253	199	160	122	92.2	70.1
0.050	5.11	178	149	124	97.9	75.6	60.5
0.025	2.63	108	90.3	80.1	68.2	51.4	40.4
0.010	1.11	61.3	59.6	51.6	43.4	30.1	23.2

The view that polypyrrole has a porous structure was supported by studying the ionic conductivity of PPY/ClO_4^- films in the two electrolyte solutions. Fig. 8.1.5A and B show complex plane impedance plots for a PPY/ClO_4^- film in two $NaClO_4$ solutions. Table 8.1.3 lists ionic conductivities from these plots and at other electrolyte concentrations against the electrode potential and the solution conductivity. The film ionic conductivity as a function of the solution conductivity is plotted in Fig. 8.1.6.

Table 8.1.2 PPY/PSS film ionic conductivity in aqueous NaPSS solution.

Electrolyte solution		Film ionic conductivity at the potential $\mu S\ cm^{-1}$					
Conc. M	Cond. $mS\ cm^{-1}$	-0.4 V	-0.3 V	-0.2 V	-0.1 V	0.0 V	0.1 V
0.50	28.9	427	344	249	178	122	86.7
0.25	16.1	368	281	201	149	113	73.5
0.10	6.91	260	199	155	117	80.3	52.5
0.050	3.33	183	139	109	86.3	60.8	36.4
0.025	1.72	75.9	72.0	69.6	65.5	54.1	30.8

As has been discussed in chapter 7, the ionic conductivity of a PPY/ClO_4^- film increases with increasing electrode potential. This has been explained in terms of the normal anion-doping mechanism[29]. For this polymer, increasing the concentration of the supporting electrolyte solution also increases the polymer film ionic conductivity. Again, the simultaneous variation of polymer film ionic conductivity with both electrode potential and the conductivity of the supporting electrolyte solution may be attributed to ionic conductivity changes in a polymer phase and a pore solution phase respectively.

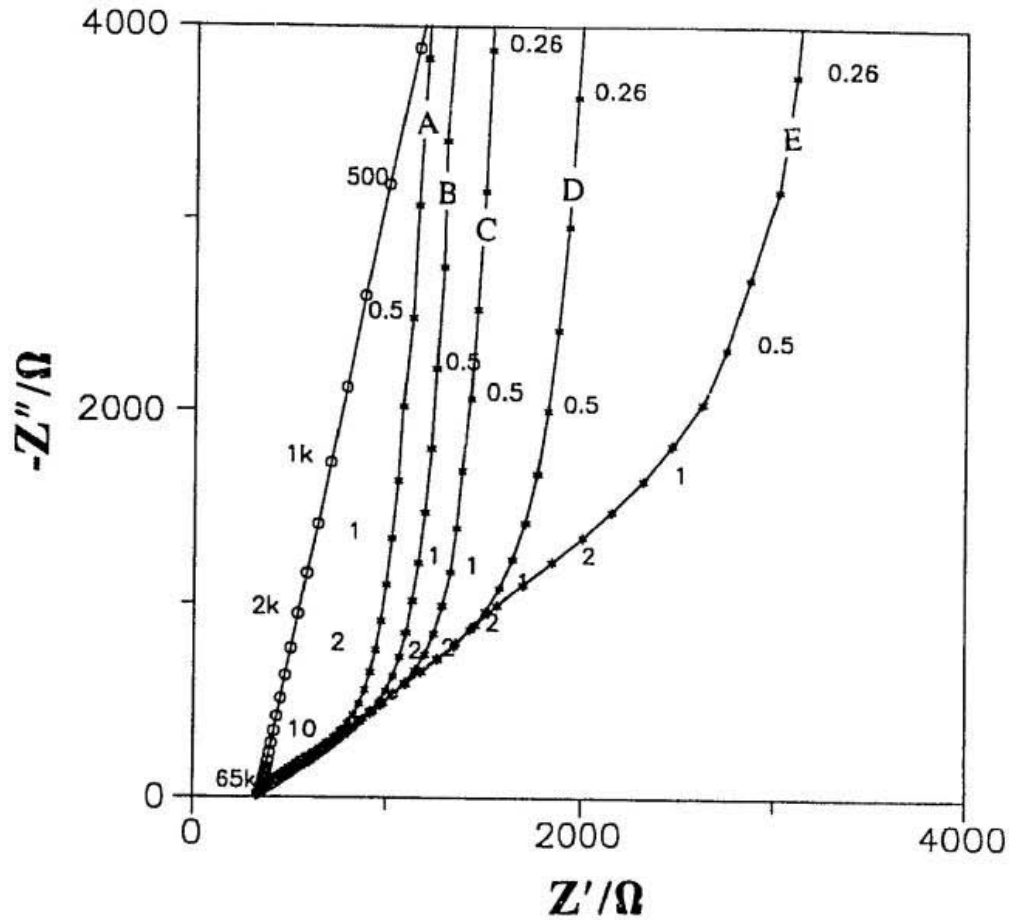

Figure 8.1.5A Complex plane impedance plots for a 2 μm PPY/ClO_4^- film coated Pt electrode at 0.1(A), -0.1(B), -0.2(C), -0.3(D) and -0.4(E) *vs.* Ag/AgCl in 0.20 M $NaClO_4$(aq) solution. Circled points are for the bare Pt electrode at the open circuit. Frequencies at selected points are marked in Hz.

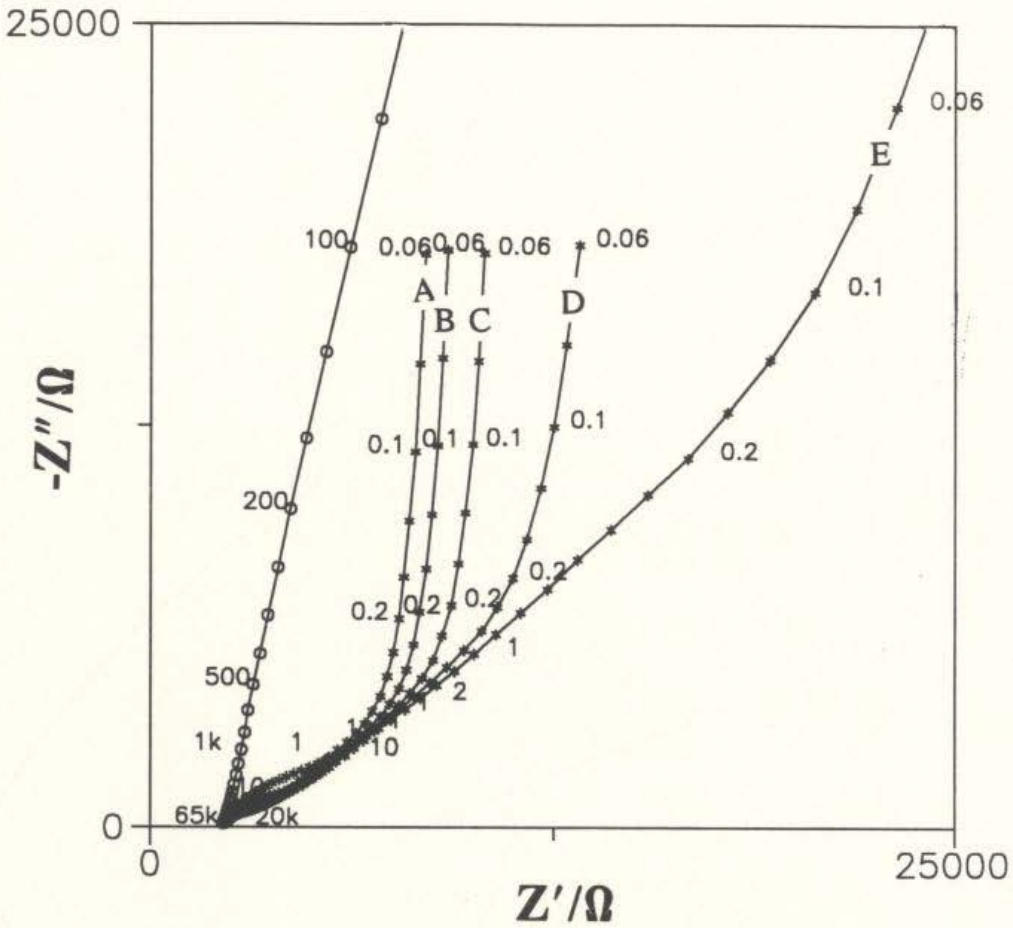

Figure 8.1.5B Complex plane impedance plots for a 2 μm PPY/ClO_4^- film coated Pt electrode at 0.1 (A), 0.0(B), -0.1(C), -0.2(D) and -0.3(E) V *vs.* Ag/AgCl in 0.025 M $NaClO_4$(aq) solution. Circled points are for the bare Pt electrode at the open circuit. Frequencies at selected points are marked in Hz.

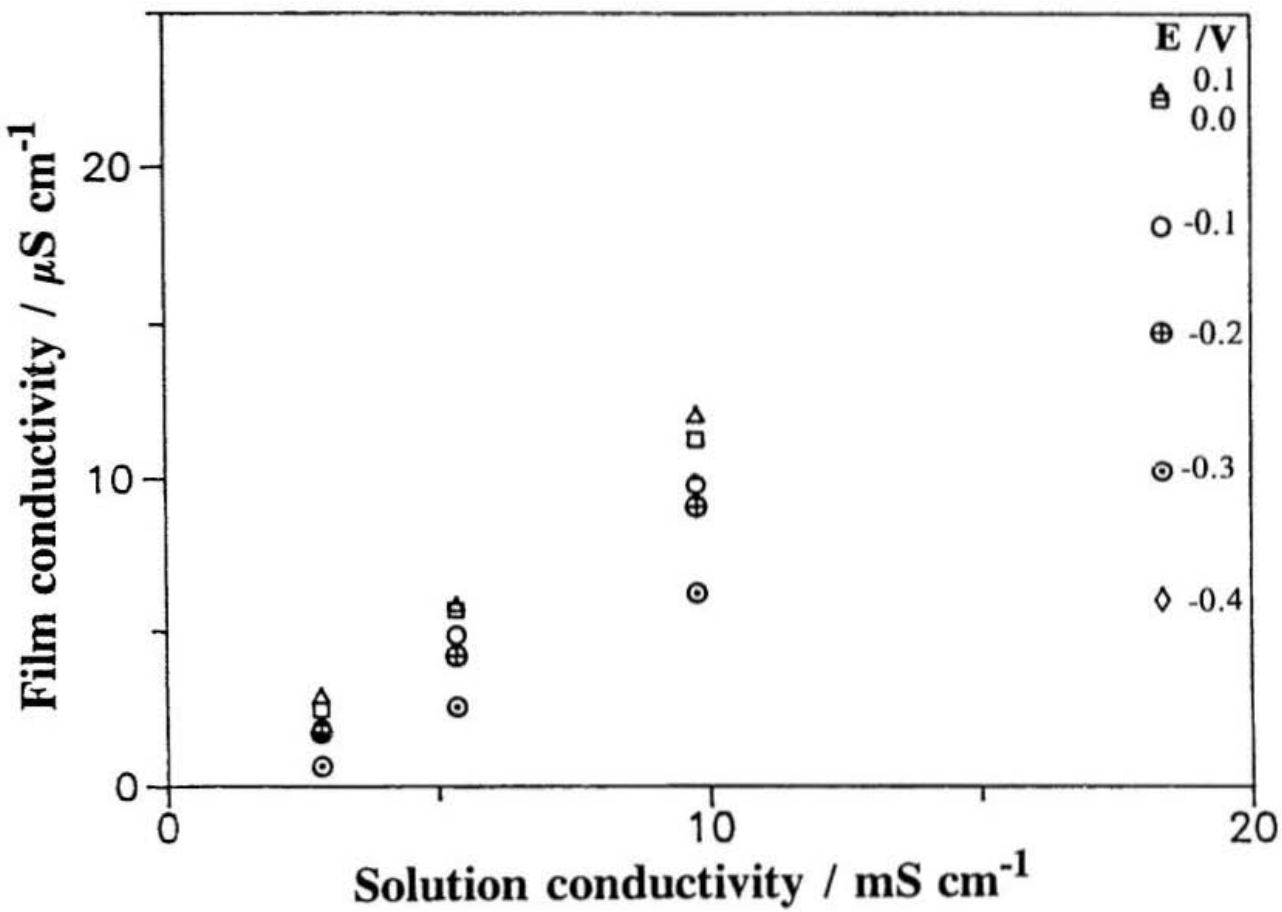

Figure 8.1.6 Plot of PPY/ClO_4^- film ionic conductivity in aqueous $NaClO_4$ solution as a function of solution ionic conductivity.

Table 8.1.3 PPY/ClO_4^- film ionic conductivity in aqueous $NaClO_4$ solution.

Electrolyte solution		Film ionic conductivity at the indicated potential / $\mu S\ cm^{-1}$					
Conc. M	Cond. $mS\ cm^{-1}$	-0.4 V	-0.3 V	-0.2 V	-0.1 V	0.0 V	0.1 V
0.20	18.4	6.01	10.2	14.8	18.1	22.2	22.5
0.10	9.77	-*	6.23	9.08	9.78	11.3	12.1
0.050	5.33	-*	2.57	4.19	4.85	5.67	5.87
0.025	2.84	-*	0.64	1.74	1.86	2.49	2.95

* A high frequency semicircle appeared in the complex plane impedance plot so that the ionic conductivity was indeterminate.

When impedance measurements on a PPY/ClO_4^- coated electrode were carried out in NaPSS solutions, the film ionic resistance increased dramatically as shown in Fig. 8.1.7 by the length of the Warburg-type line, indicating a very low mobility of the PSS anions in the film. Fig. 8.1.8 shows cyclic voltammograms of a freshly prepared (oxidized) PPY/ClO_4^- film in NaPSS solution. A large reduction wave was observed in the first cathodic scan, but on subsequent scans, the polymer film showed little electrochemical activity. Energy dispersive X-ray analysis (Fig. 8.1.9) revealed that the initial reduction was accompanied by loss of almost all incorporated ClO_4^- ions during polymerization. Clearly, the

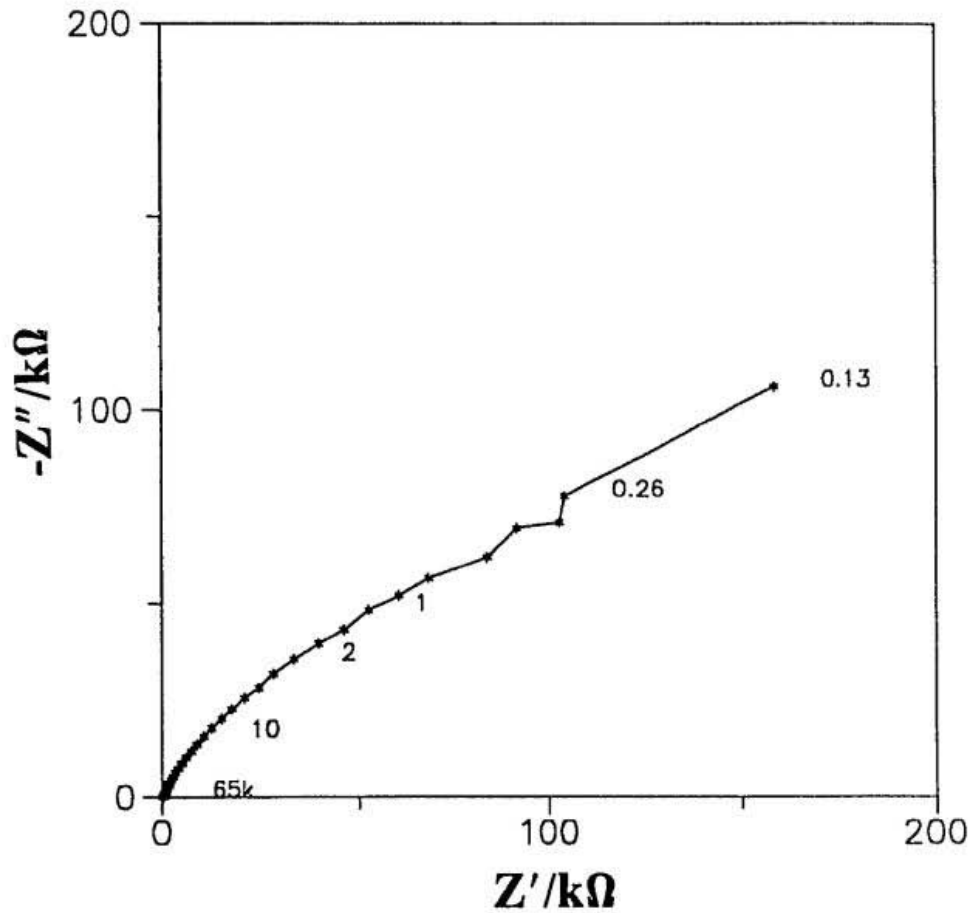

Figure 8.1.7 Complex plane impedance plots for a 2 μm PPY/ClO_4^- film coated Pt electrode in 0.5 M NaPSS(aq) solution at 0.0 V *vs.* Ag/AgCl. Frequencies at selected points are marked in Hz.

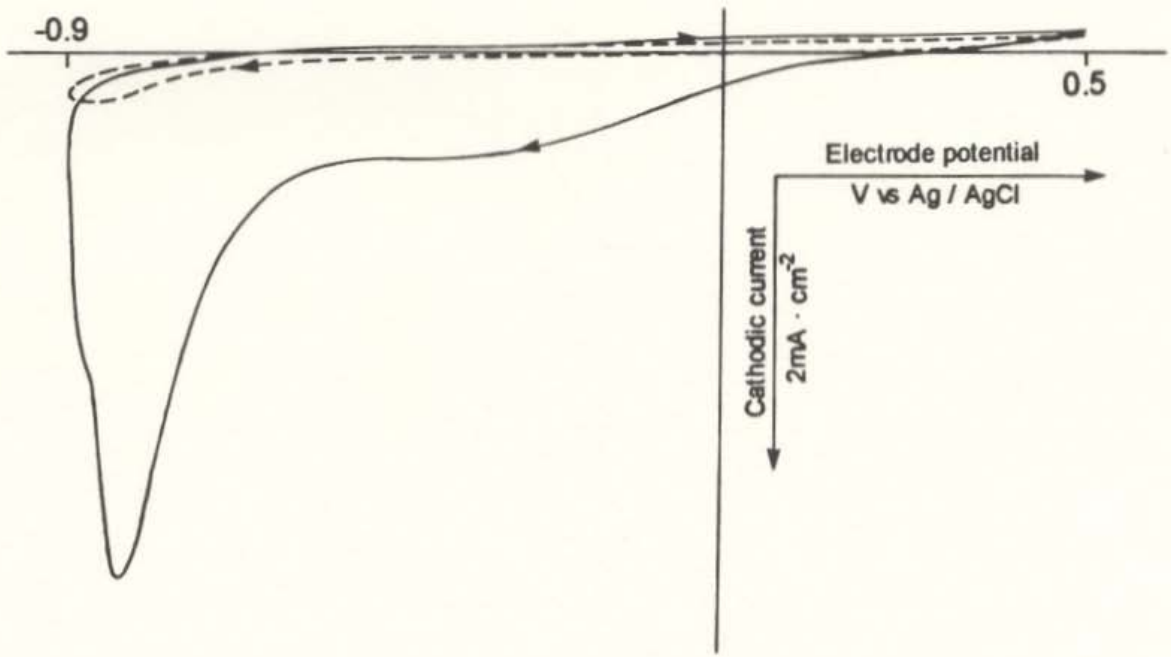

Figure 8.1.8 Cyclic voltammograms of a 4 μm PPY/ClO_4^- film coated Pt electrode in 0.5 M NaPSS aqueous solution at a scan rate of 60 mV s^{-1}. The solid line indicates the first cycle and the dashed line the second cycle.

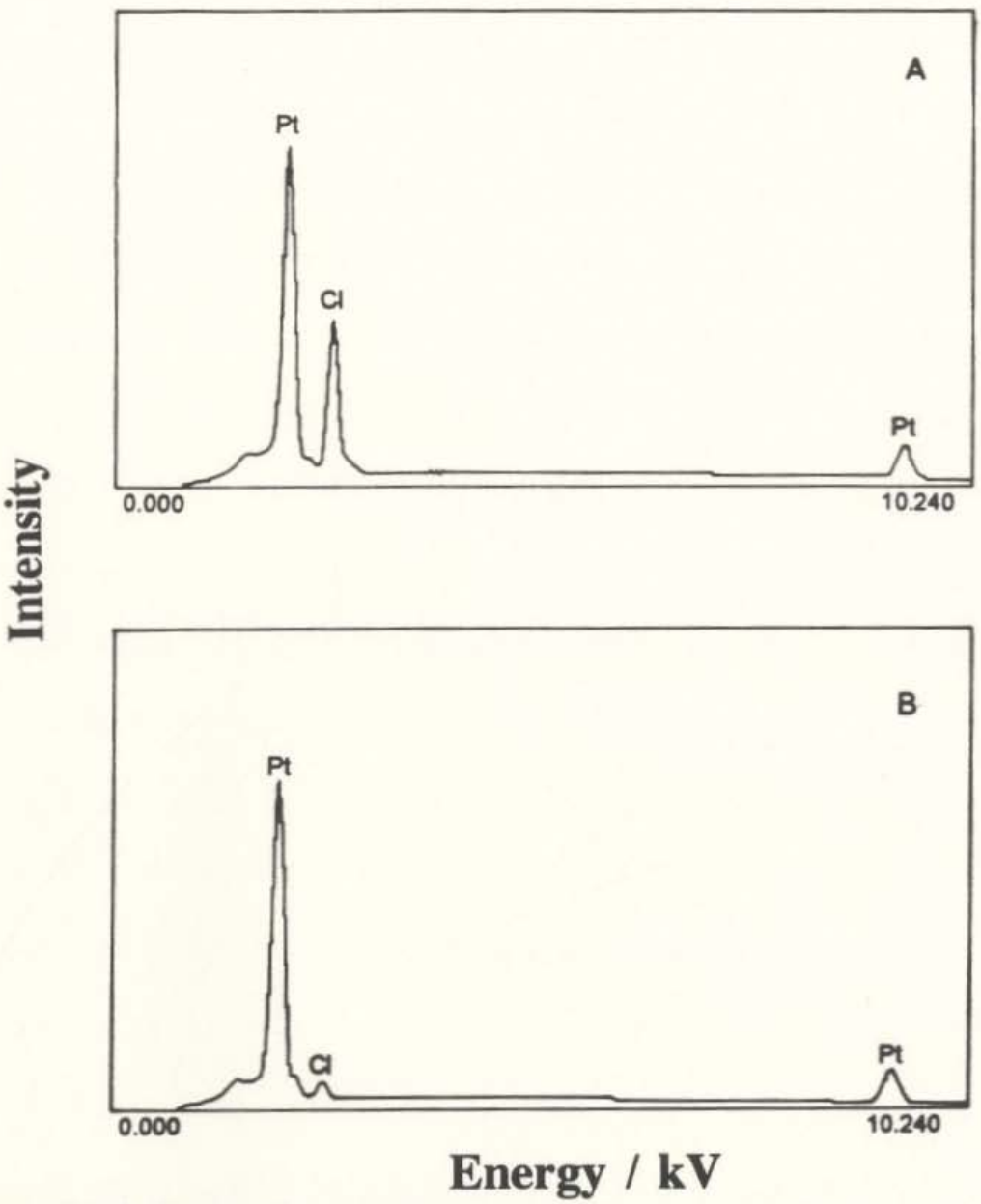

Figure 8.1.9 Energy dispersive X-ray spectra of a 2 μm PPY/ClO_4^- film coated Pt electrode. A -- original film, B -- after reduced at -0.8 V *vs.* Ag/AgCl in 0.5 M aqueous NaPSS solution.

electrochemical inactivity of the polymer film in the NaPSS solution is due to the fact that the PSS^- anions are too large to enter the polymer aggregates to re-dope the film. This is in contrast with the dependence of PPY/PSS film ionic conductivity (Table 9.2.2) on the NaPSS concentration, which shows that the poly-anions can enter pores of the polymer film.

As shown in Figs. 8.1.3, 8.1.4, and 8.1.6, it is clear that ion transport in the polymer films is strongly influenced by the ion-exchanging process. The difference in the polymer ionic conductivity at different potentials is most pronounced as the concentration of electrolyte increased. If the one-phase model were applicable, the increase in the electrolyte concentration would cause an increase in the salt content in the polymer. For both type of polymers, the salt (both cations and anions) would dominate ionic conduction. Consequently, the variation in film ionic conductivity due to the difference in the mode of ion transport (cations in PPY/PSS *vs.* anions in PPY/ClO_4^-) as well as in electrode potential would become less and less significant. The two-phase model gives a more logical explanation. Since the film ionic resistance is the sum of polymer aggregate (R_{aggr}) and pore (R_{pore}) resistances. R_{aggr}, which is greatly influenced by mode of ion transport and electrode potential, becomes important only when R_{pore} is small.

Figs. 8.1.10 and 8.1.11 are plots of film ionic conductivity as a function of

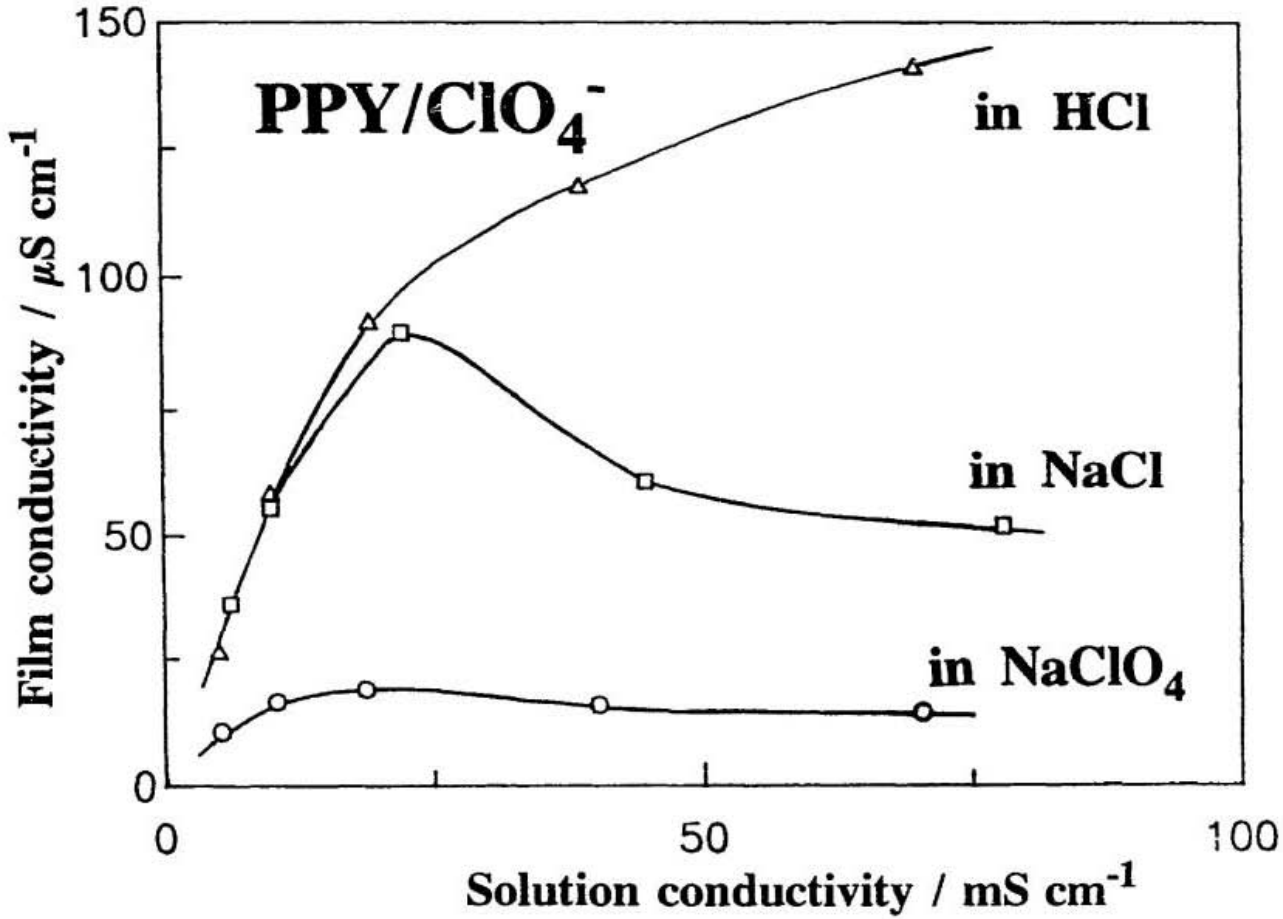

Figure 8.1.10 Plots of PPY/ClO_4^- film ionic conductivity at 0.0 V *vs.* Ag/AgCl as a function of solution conductivity in NaCl, $NaClO_4$ and HCl electrolyte solutions.

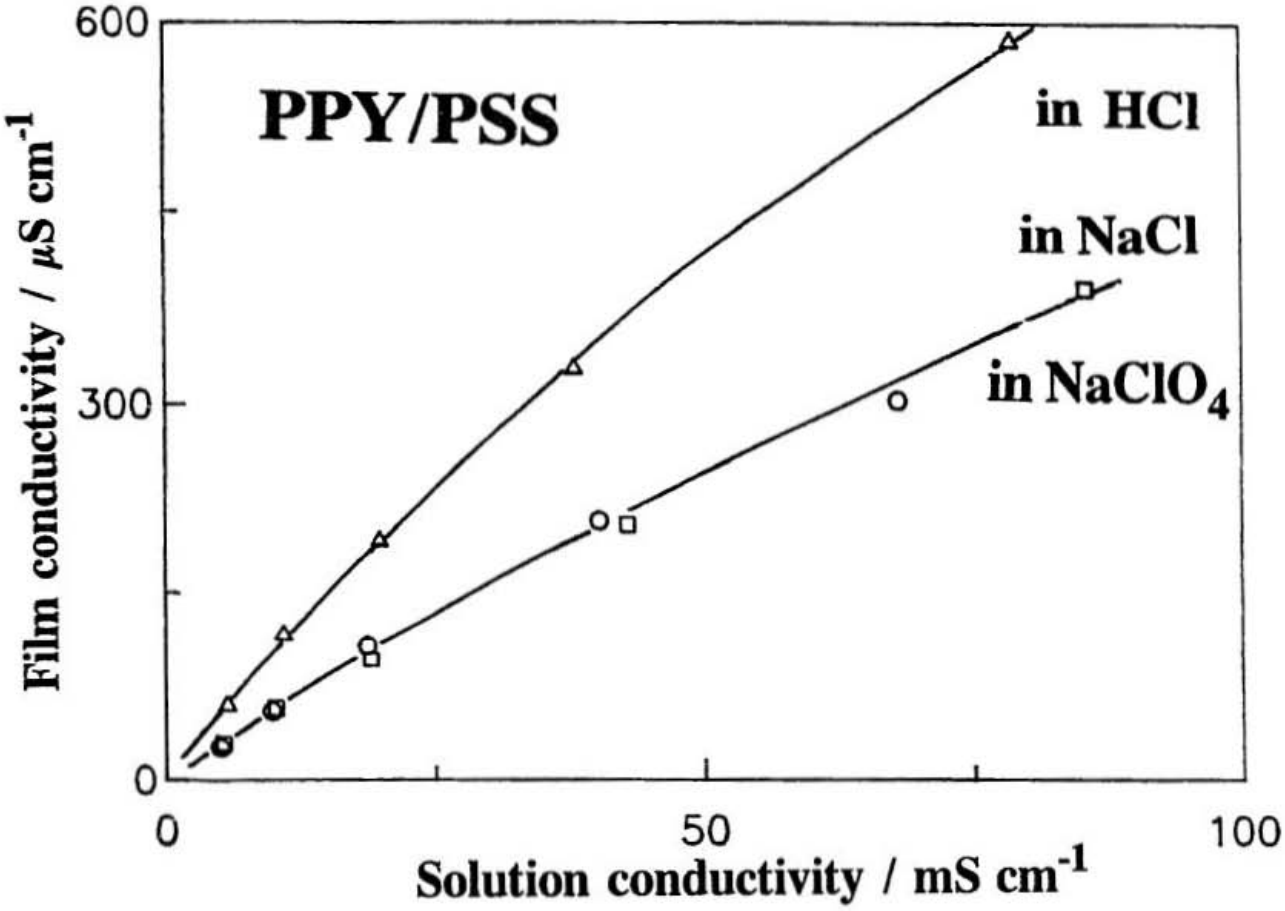

Figure 8.1.11 Plots of PPY/PSS film ionic conductivity at 0.0 V *vs.* Ag/AgCl as a function of solution conductivity in NaCl, $NaClO_4$ and HCl electrolyte solutions.

solution conductivity in aqueous NaCl, $NaClO_4$ and HCl solutions for PPY/ClO_4^- and PPY/PSS films, respectively.

At the same solution conductivity, the PPY/ClO_4^- film immersed in different electrolyte solutions has the same ionic conductivity when the anions are the same (Cl^-) and the electrolyte concentrations are low. However, film conductivities are quite different when the anions are different. The higher film ionic conductivity in the chloride solution relative to the perchlorate solution has been attributed to a lower extent of ion-pairing between the chloride anions and the positive charges on the oxidized polypyrrole c..ains[29,30]. The film ionic conductivity starts to decrease at concentrations above 0.2 M for both NaCl and $NaClO_4$ solutions but not for HCl solution. This phenomenon is attributed to dehydration of the polymer film caused by the high electrolyte concentration in the bathing solution. The high mobility of H^+ means that for the same solution conductivity the HCl concentration is much lower than those of $NaClO_4$ and NaCl. Thus, for a solution conductivity of 70 mS cm^{-1}, the concentration of HCl is 0.2 M while the NaCl and $NaClO_4$ concentrations are about 1 M.

When comparing PPY/PSS film ionic conductivities at the same solution conductivity in the three electrolyte solutions, the polymer film exhibits the same film conductivity when the cations are the same (Na^+). The equivalent ionic

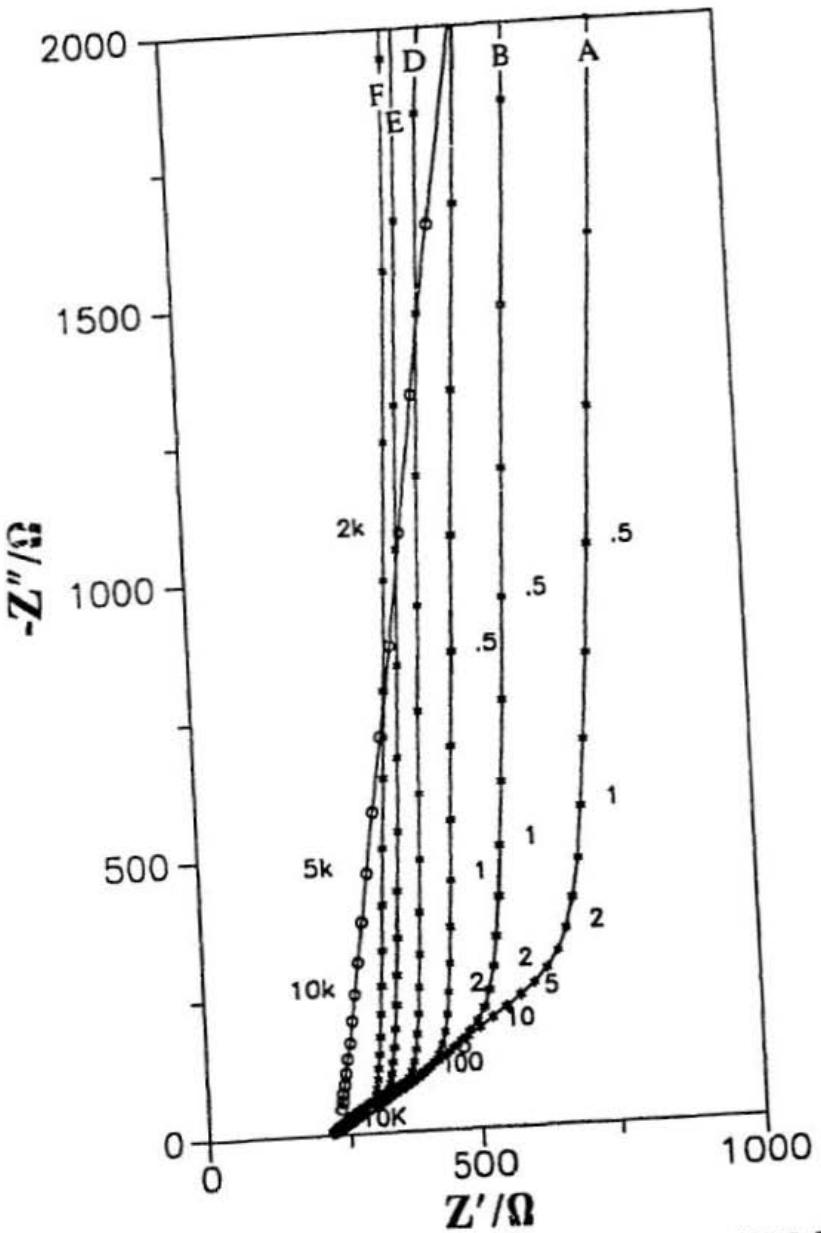

Figure 8.1.12 Complex plane impedance plots for a 2 μm PPY/PSS film coated Pt electrode in saturated $NaClO_4$ solution at selected potentials (A: 0.1; B: 0.0; C: -0.1; D: -0.2, E: -0.3 and F: -0.4 V *vs.* Ag/AgCl). Circled points are for the bare Pt electrode at the open circuit potential. Frequencies at selected points are marked in Hz.

conductivity of H^+ at infinite dilution in aqueous solution is about six times that of Na^+. The high mobility of H^+ is due to proton hopping from the hydronium ion (H_3O^+) to a neighbouring water molecule with the aid of hydrogen bonding between the two molecules. In the polymer phase, the mobility of H^+ is only about 68% greater than that of Na^+. Clearly the significance of the fast proton relay mechanism (Grotthus mechanism) that functions well in aqueous solution is greatly reduced in the polymer aggregates, where ion conduction occurs by hopping of the cations between neighbouring ion-exchanging sites ($-SO_3^-$). For PPY/PSS, the dehydration effect is much less pronounced than for PPY/ClO_4^-. This may be due to the high concentration of the immobilized ionic species within PPY/PSS. Dehydration of this polymer film only occurs with a highly concentrated bathing electrolyte solution such as saturated $NaClO_4$ solution (Table 8.1.2). Fig. 8.1.12 shows complex plane impedance plots of a 2 μm PPY/PSS film coated Pt electrode in a saturated aqueous $NaClO_4$ solution. In spite of the high concentration of electrolyte in the bathing solution, the film ionic conductivity still decreases with increasing potential, indicating that the predominant mobile ionic species in the polymer aggregates are still the electrolyte cations (Na^+).

8.2 Conclusions

Ionic conductivity measurements on polypyrrole have shown that, like poly-MPCA, it has a two-phase porous structure. The solution in the pores is discontinuous so that ion conduction paths must contain both the pore solution and polymer aggregates. The envisaged structure of the polymer film is shown schematically in Fig. 8.2.1. Such a structure causes the ionic conductivity of the polymer film to exhibit behaviour characteristic of both pore solution and polymer aggregates.

The ion conduction mechanism in the pore solution is the same as that in the bulk electrolyte solution, where both cations and anions are the charge carriers. Since the ionic conductivity of the pore solution is the same as that of the bulk electrolyte solution, differences in the ionic conductivity of the polymer aggregates can best be detected by measuring the film ionic conductivity in electrolyte solutions with identical conductivity.

The polymer aggregates can be regarded as an ion-exchanging resin, where only the cations (for a cation-exchanging resin) or anions (for an anion-exchanging resin) serve as charge carriers. This conclusion is substantiated by the fact that in

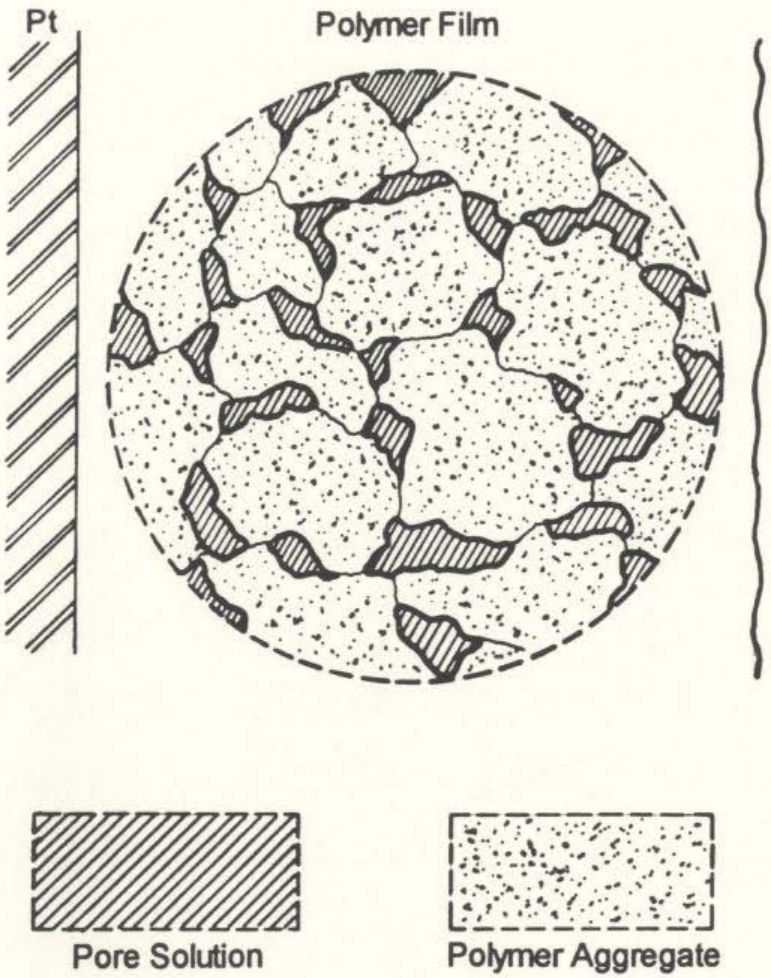

Figure 8.2.1 Sketch of the proposed structure of a poly-MPCA or polypyrrole film.

PPY/ClO_4^- film the electrolyte anions are the predominant mobile ions and in PPY/PSS film the electrolyte cations. The ionic conductivity of the polymer aggregates changes with the electrode potential, the mobility of the mobile ionic species, and the hydration level of the polymer film. Varying the electrode potential changes the oxidation level of the polymer film, which changes the concentration of the fixed ion-exchanging sites. There are reasonably linear relationships between the film ionic conductivity and oxidation level for both poly-MPCA and polypyrrole films[29]. The mobility of the mobile ionic species in the polymer aggregates depends on their sizes and their interactions with the oppositely charged fixed ion-exchanging sites in the polymer aggregates. Dehydration of the polymer film occurs at high bathing electrolyte concentrations, which decreases the ionic conductivity of polymer aggregates.

By using the poly(styrene sulphonate) anions as size probes, it was concluded that the pores in polypyrrole are sufficiently large to allow the entry of the polyanions. But the ion conduction channels in the polymer aggregates are too small to allow the polyanions to dope the polymer.

References

(1) Sun, B.; Jones, J.J.; Burford, R.P.; Skyllas-Kazacos, M. *J. Mater. Sci.* 1989,*24*,4024.

(2) Bruckenstein, S.; Hillman, A.R. *J. Phys. Chem.* 1991,*95*,10748.

(3) Martin, C.R.; Van Dyke, L.S.; Cai, Z. *Electrochim. Acta* 1992,*37*,1611.

(4) Centonze, D.; Guerrieri, A.; Malitesta, C.; Palmisano, F.; Zambonin, P.G. *Fresenius J. Anal. Chem.* 1992,*342*,729.

(5) Walker, D.R.B.; Koros, W.J. *J. Membr. Sci.* 1991,*55*,99.

(6) Feldheim, D.L.; Elliott, C.M. *J. Membr. Sci.* 1992,*70*,9.

(7) Josowicz, M.; Janata, J.; Ashley, K.; Pons, S. *Anal. Chem.* 1987,*59*,253.

(8) Zotti, G. *Synth. Met.* 1992,*51*,373.

(9) Burgmayer, P.; Murray, R.W. *J. Phys. Chem.* 1984,*88*,2515.

(10) Burgmayer, P.; Murray, R.W. *J. Am. Chem. Soc.* 1982,*104*,6139.

(11) Chiu, H.T.; Lin, J.S.; Shiau, J.N. *J. Appl. Electrochem.* 1992,*22*,522.

(12) Mastragostino, M.; Arbizzani, C.; Bongini, A.; Barbarella, G.; Zambianchi, M. *Electrochim. Acta* 1993,*38*,135.

(13) Ikenoue, Y.; Tomozawa, H.; Saida, Y.; Kira, M.; Yashima, H: *Synth. Met.* 1991,*40*,333.

(14) Mastragostino, M.; Marinangeli, A.M.; Corradini, A.; Giacobbe, S. *Synth. Met.* 1989,*28*,C501.

(15) Scrosati, B. *J. Electrochem. Soc.* 1989,*136*,2774.

(16) Naegele, D.; Bittihn, R. *Solid State Ionics* 1987,*28-30*,983.

(17) Curran, D.; Grimshaw, J.; Perera, S.D. *Chem. Soc. Rev.* 1991,*20*,391.

(18) Cosnier, S.; Deronzier, A.; Roland, J.F. *J. Mol. Catal.* 1992,*71*,303.

(19) Diaz, A.F.; Castillo, J.I.; Logan, J.A.; Lee, W.-Y. *J. Electroanal. Chem.* 1981,*129*,115.

(20) Diaz, A.; Vasquez Vallejo, J.M.; Martinez Duran, A. *IBM J. Res. Develop.* 1981,*25*,42.

(21) Fan, F.R.F.; Wheeler, B.; Bard, A.J.; Noufi, R. *J. Electrochem. Soc.* 1981,*128*,2042.

(22) Bull, R.A.; Fan, F.-R.F.; Bard, A.J. *J. Electrochem. Soc.* 1982,*129*,1009.

(23) Feldman, B.J.; Burgmayer, P.; Murray, R.W. *J. Am. Chem. Soc.* 1985,*107*,872.

(24) Ren, X.; Pickup, P.G. *J. Electrochem. Soc.* 1992,*139*,2097.

(25) Shimidzu, T.; Ohtani, A.; Iyoda, T.; Honda, K. *J. Electroanal. Chem.* 1987,*224*,123.

(26) Shimidzu, T.; Ohtani, A.; Honda, K. *J. Electroanal. Chem.* 1988,*251*,323.

(27) Baker, C.K.; Qiu, Y.J.; Reynolds, J.R. *J. Phys. Chem.* 1991,*95*,4446.

(28) Naoi, K.; Lien, M.; Smyrl, W.H. *J. Electrochem. Soc.* 1991,*138*,440.

(29) Ren, X.; Pickup, P.G. *J. Phys. Chem.* 1993,*97*,5356.

(30) Ren, X.; Pickup, P.G. *unpublished. results.* 1993.

Chapter 9

Charge Transport in Polypyrrole/perchlorate and Polypyrrole/poly(styrene sulphonate) Bilayers

Despite a great deal of recent work[1], there is still no consensus on how the impedance response of a polymer coated electrode should be modelled and interpreted. The various treatments of polymer coated electrodes (discussed in Chapter 4) give different predictions of the location of the initial redox reaction. The porous electrode model[2,3], and Albery's redox polymer model[4,5] predict that oxidation and reduction of a highly conducting polymer will begin at the polymer/solution interface. The tungsten oxide[6] and redox polymer model proposed by Gabrielli *et al*[7,8] assumes that these reactions begin at the polymer/electrode interface, while Buck in the treatment of thin layer and membrane cells predicts that they begin simultaneously at both interfaces[9,10]. Clearly, finding the location of the initial electrochemical reaction in a conducting polymer coated electrode submerged in an electrolyte solution is important to the understanding of charge transport in the polymer.

Previous studies on this subject have been reported by Bard and coworkers[11]. Using ellipsometry, they studied the spatial distribution of oxidized and reduced states of an electrochemically polymerized polypyrrole film on a Pt electrode when potential steps were applied. The experimental ellipsometric conversion data were simulated by a multilayer film model. Their results show that the electrochemistry of polypyrrole begins at the polymer/solution interface. However, similar experiments on polyaniline[12,13] indicate that oxidation and reduction occur uniformly throughout the film during potential cycling. The discrepancy appears to arise from the large changes in the electronic conductivity of the polymer that occur when a large amplitude potential perturbation is applied. Aoki and coworkers have shown that the oxidation of polypyrrole[14] and polyaniline[15] strips starts at the metallic contact. However, these results were obtained when insertion/expulsion of bulk ionic species was perpendicular to the propagation direction of the polymer reaction zone. Clearly this is not the case for a polymer film on a flat electrode.

In this chapter, results of impedance studies on conducting polypyrrole bilayers at steady state conditions are reported. It is clearly shown that the redox reaction of the polymer spreads from the polymer/solution interface. The bilayer films consist of partially oxidized polypyrrole (PPY) doped with perchlorate (PPY/ClO_4^-) and PPY doped with sodium poly(styrene sulphonate) (PPY/NaPSS)

layers. Previous work (Chapter 7) has shown that these two polymers are different in their mode of ion conduction as well as in the magnitude of their ionic conductivity[16]. In PPY/ClO_4^- the perchlorate anions dominate ion transport, and increasing the electrode potential increases the polymer's ionic conductivity. While in PPY/PSS cation transport dominates and increasing the electrode potential decreases the polymer's ionic conductivity. This forms the basis for discrimination between the electrochemistry of the two layers in the bilayer films.

9.1 Polymer Film Electrode Preparation

Bilayer films were deposited on Pt disc electrodes (0.0045 cm^2) by anodic oxidation of pyrrole (0.5 M) at a constant current density of 0.88 mA cm^{-2} in 0.5 M $NaClO_4$ (aq) to form the PPY/ClO_4^- layer, and in 0.5 M NaPSS (aq) to form the PPY/PSS layer. The thickness of each polymer layer was controlled by the deposition time. For both polymers, deposition of 1 μm requires a charge density of *ca.* 0.24 C cm^{-2} (section 3.2). A bilayer electrode with a PPY/ClO_4^- inner layer and a PPY/PSS outer layer is denoted as ‖ PPY/ClO_4^- | PPY/PSS, where "‖" represents the substrate Pt electrode, and "|" the visualized plane that separates the two contacting polymer layers.

9.2 Impedance

Fig. 9.2.1A shows complex plane impedance plots for a bare Pt electrode and a ‖ PPY/ClO_4^-(1 μm) | PPY/PSS (1 μm) bilayer electrode at 0.1 V in 0.2 M $NaClO_4$ (aq). At high frequency the bilayer shows a Warburg-type (45° linear region) impedance response starting at a real axis intercept corresponding to the uncompensated solution resistance (given by the intercept for the bare Pt electrode). At lower frequencies a second, steeper linear region (Warburg-type line at low frequency) appears in the impedance plot, followed by the normal capacitive response, which forms an almost vertical line. Similar dual time constant responses are observed at other potentials (Fig. 9.2.1B). Adequate separation of the two charging processes is obtained by plotting the impedance data in the complex capacitance plane (Fig. 9.2.2).

The Warburg-type line at high frequency is characterized by a decreasing length as the electrode potential is decreased (Figs. 9.2.1B and C), while the length of the Warburg-type line at low frequency increases as the electrode potential is decreased (Fig. 9.2.1B). Thus, at high frequency, the impedance response of the bilayer electrode is characteristic of PPY/PSS, while the lower frequency response is characteristic of PPY/ClO_4^-. This result shows that high frequency potential stimulation causes only the PPY/PSS outer layer to be oxidized

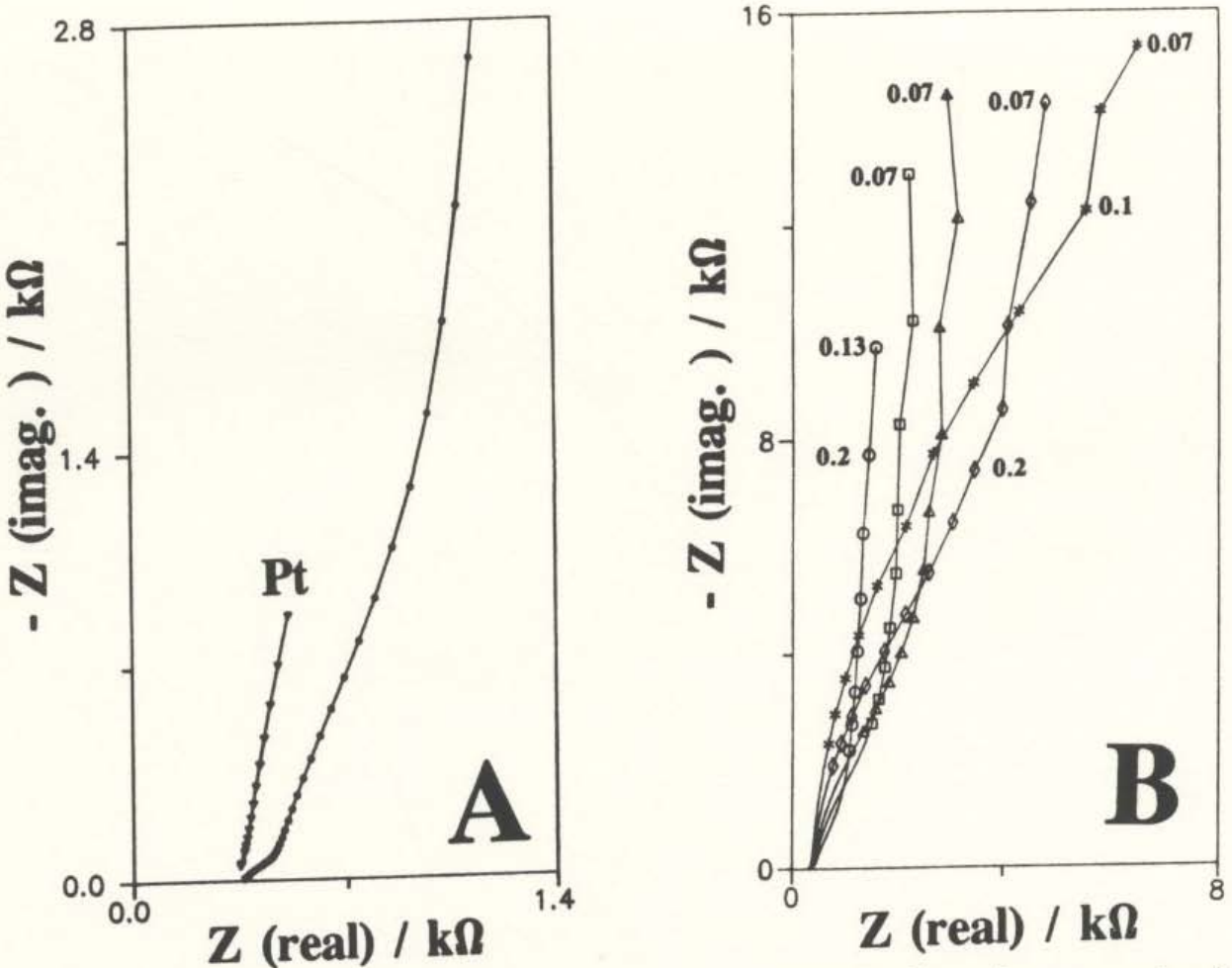

Figure 9.2.1 A & B Complex plane impedance plots for a bare Pt electrode at open circuit (▽ in A) and a ‖PPY/ClO_4^-(1 μm)| PPY/PSS(1 μm) bilayer electrode in 0.2 M $NaClO_4$ (aq). Electrode potentials are indicated as follows ○ 0.1 V, □ -0.2 V, △ -0.3 V, ◇ -0.4 V, * -0.5 V. Frequencies in Hz are indicated for selected points.

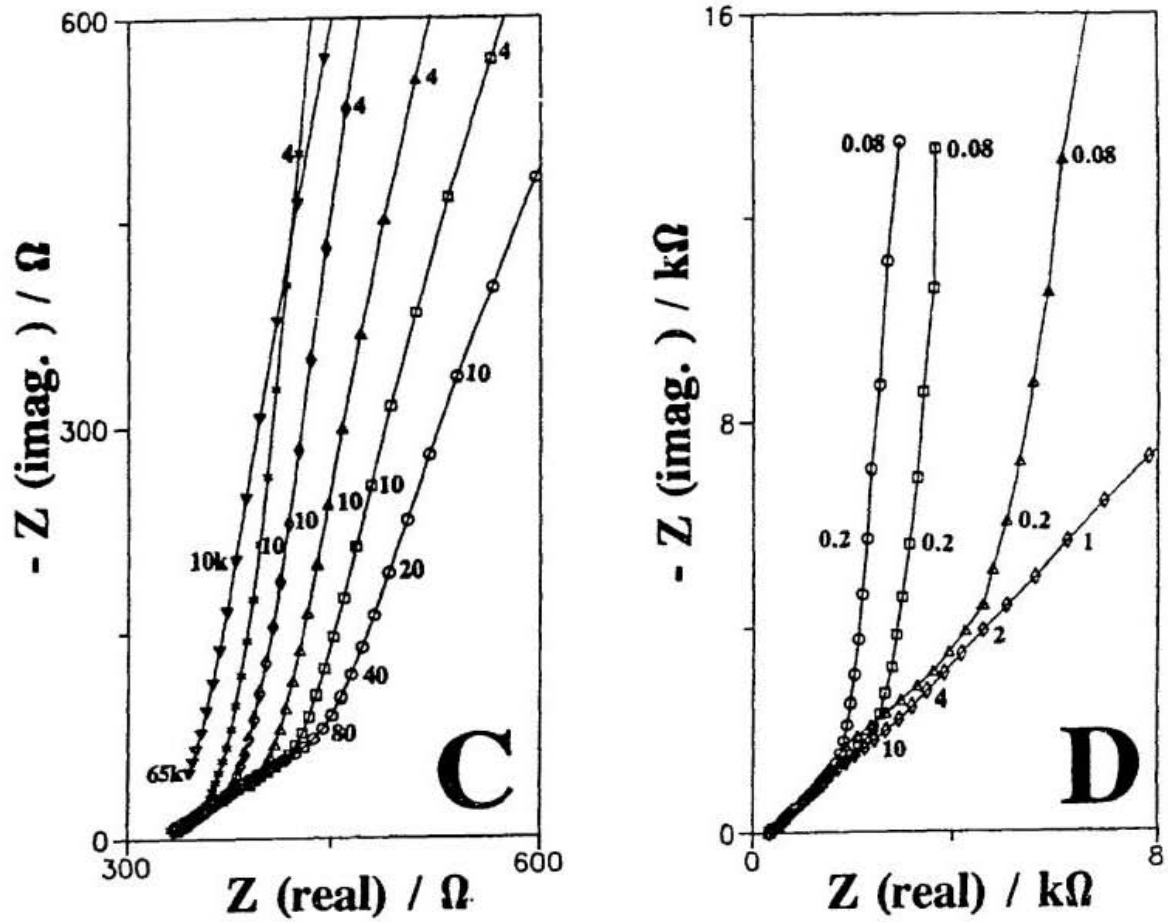

Figure 9.2.1 C & D Complex plane impedance plots for a bare Pt electrode at open circuit (▽ in C), a ‖PPY/ClO_4^-(1 μm)| PPY/PSS(1 μm) bilayer electrode (C) and a ‖PPY/PSS(1 μm) |PPY/ClO_4^-(1 μm) bilayer electrode (D) in 0.2 M $NaClO_4$ (aq). Electrode potentials are indicated as follows ○ 0.1 V, □ -0.2 V, △ -0.3 V, ◇ -0.4 V, * -0.5 V. Frequencies in Hz are indicated for selected points.

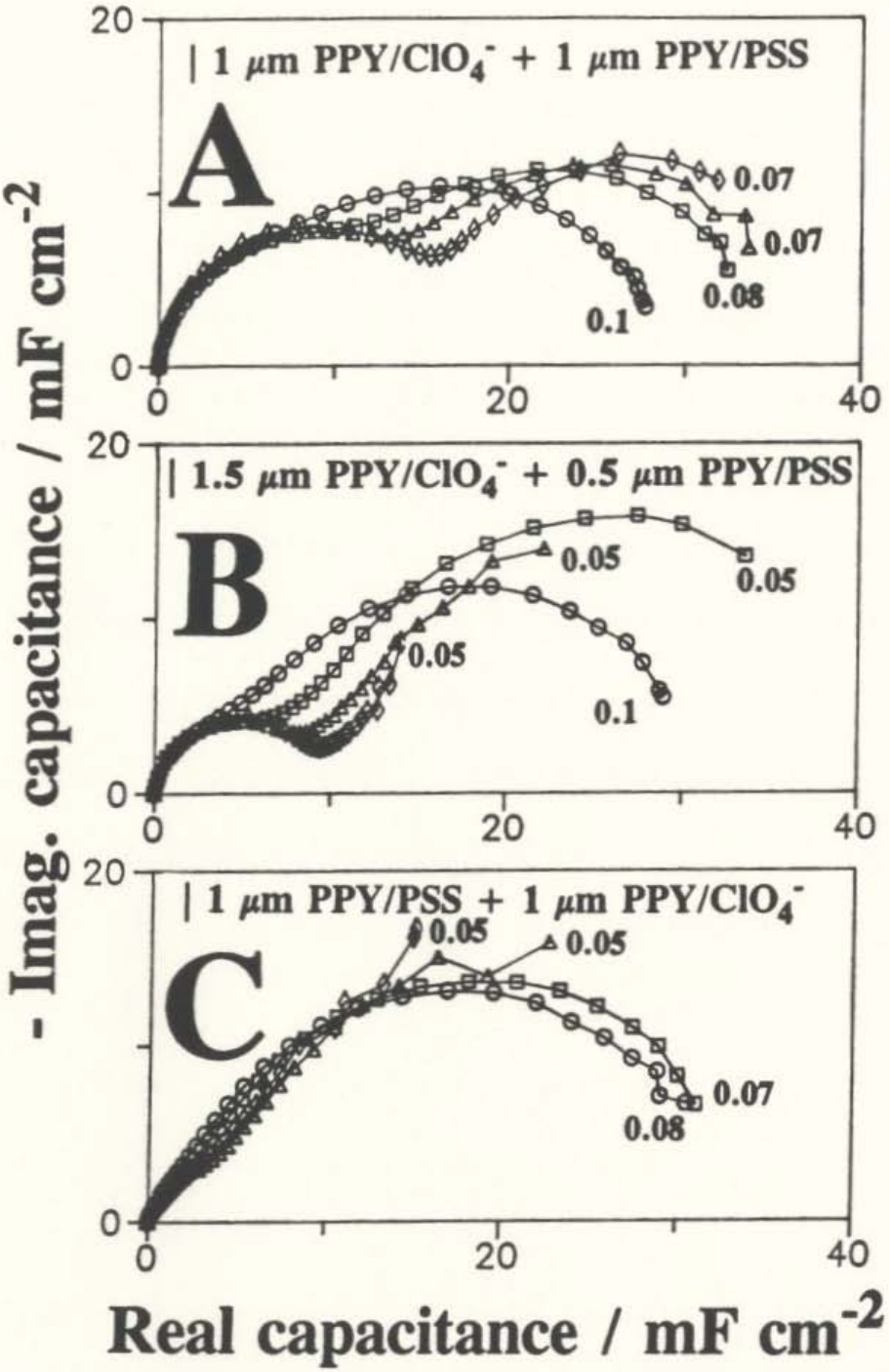

Figure 9.2.2 Complex plane capacitance plots for the bilayer electrode data shown in Fig.9.2.1 and for a ‖PPY/ClO_4^-(1.5 μm)| PPY/PSS(0.5 μm) bilayer electrode. See Fig.9.2.1 for electrode potential symbols.

and reduced. As the frequency is decreased, the redox reaction spreads into the PPY/ClO_4^- inner layer.

Fig. 9.2.2A shows complex capacitance plots for the data in Fig. 9.2.1. The two semicircles correspond to two charge transport processes with different time constants. They are of similar diameters, indicating that the two processes involve similar capacitances (*i.e.*, the two equal thickness layers of the bilayer). A bilayer with a thinner (0.5 μm) outer PPY/PSS layer and a thicker (1.5 μm) inner PPY/ClO_4^- layer gave a correspondingly smaller semicircle at high frequency and a larger semicircle at low frequency (Fig. 9.2.2B). This confirms the assignment of the high frequency response to the outer PPY/PSS layer.

The low frequency capacitances were also calculated from the slopes of plots of imaginary impedance *vs.* 1/frequency for the impedance data following the Warburg-type line in the complex plane impedance plots. The capacitances obtained from the data immediately after the Warburg type-line at high frequency are for the outer layer while those obtained from the data after the Warburg-type line at low frequency are for the whole bilayer. Table 9.2.1 lists the capacitances obtained for three bilayer electrodes, together with those for a ‖ PPY/ClO_4^-(2 μm) and a ‖ PPY/PSS (2 μm) electrode. Clearly, for a ‖ PPY/ClO_4^-| PPY/PSS bilayer the redox reaction of the PPY/ClO_4^- layer is not initiated until all of the PPY/PSS layer is oxidized/reduced by the ac potential perturbation (at low enough

Table 9.2.1 Capacitances (mF cm^{-2}) from the slopes of Z″ *vs.* $1/\omega$ for three bilayer and two single layer electrodes.

Electrode Potential V *vs.* Ag/AgCl	‖PPY/ClO_4^- (1 μm) |PPY/PSS (1 μm)		‖PPY/ClO_4^- (1.5 μm) |PPY/PSS (0.5 μm)		‖PPY/PSS (1 μm)| PPY/ClO_4^- (1 μm)	‖PPY/PSS (2 μm)	‖PPY/ClO_4^- (2 μm)
	High ω	Low ω	High ω	Low ω			
0.1	14.5	28.3	8.9	32.9	32.9	29.6	31.7
0.0	14.6	31.1	9.2	34.2	34.2	30.2	31.7
-0.1	15.3	32.2	9.2	34.3	34.3	32.0	33.2
-0.2	16.1	34.5	12.3	46.8	41.4	34.7	34.5
-0.3	18.0	37.6	10.3	42.9	53.1	37.6	36.1
-0.4	18.0	40.5	9.9	40.0	46.7	39.6	38.4
-0.5	18.6	42.2	8.9	31.3	48.7	41.5	44.1

frequency). Impedance responses similar to Fig. 9.2.1A, B, C have been observed on bilayer electrodes with a very thin (down to 0.2 μm) PPY/PSS outer layer.

The conclusion that the redox reaction in conducting polypyrrole films begins at the polymer/solution interface is reaffirmed by the response of bilayers with PPY/PSS as the inner layer. Figs. 9.2.1D and 9.2.2C show complex plane impedance and capacitance plots for a ‖PPY/PSS(1 μm) |PPY/ClO_4^-(1 μm) bilayer electrode. In this case, only one long Warburg-type line is obtained and its length decreases with increasing electrode potential. This behaviour is characteristic of the PPY/ClO_4^- layer. The almost vertical impedance response at low frequency corresponds to the full capacitance of both layers. The absence of a second Warburg-type line for the PPY/PSS inner layer is due to the fast charging rate of PPY/PSS relative to PPY/ClO_4^-. Thus the time required to oxidize/reduce the whole PPY/ClO_4^- outer layer is by far enough to charge the PPY/PSS inner layer. Consequently, no Warburg-type line corresponding to oxidizing/reducing the inner PPY/PSS layer is observed. The fast charging rate of the PPY/PSS is due to the rapid cation transport in this polymer (Chapter 7).

9.3 Simulation of Impedance Response

The impedance responses of bilayer electrodes are simulated based on the electrical circuit shown in Fig. 9.3.1. The circuit contains a conducting rail connected to the substrate Pt electrode and a resistive rail connected to the conducting rail through the distributed capacitances. The conducting rail models the fast electron movement in the conducting polypyrrole film and the resistive rail models the slow ion movement. The ionic resistances of the inner layer and outer layer are represented by $R_{I,inner}$ and $R_{I,outer}$ in series across the polymer film thickness. The impedance response of the modelling circuit is calculated using the systematic reduction method described in section 5.2. For a bilayer electrode with equal thickness inner and outer layers, $R_{I,inner}$ and $R_{I,outer}$ are each divided into 500 resistors, and the total film capacitance which is calculated from the low frequency data (Table 9.2.1), is divided into 1000 capacitors.

Figs. 9.3.2 and 9.3.3 show complex plane impedance plots of the experimental and simulated data. For a $\|$PPY/ClO_4^-(1 μm) | PPY/PSS (1 μm) bilayer electrode at -0.2 V in 0.2 M $NaClO_4$, the experimental data are simulated with $\| R_{I,inner}$ = 12.8 kΩ $| R_{I,outer}$ = 310 Ω. The simulated impedance response closely resembles the experimental one, giving a high frequency Warburg-type line

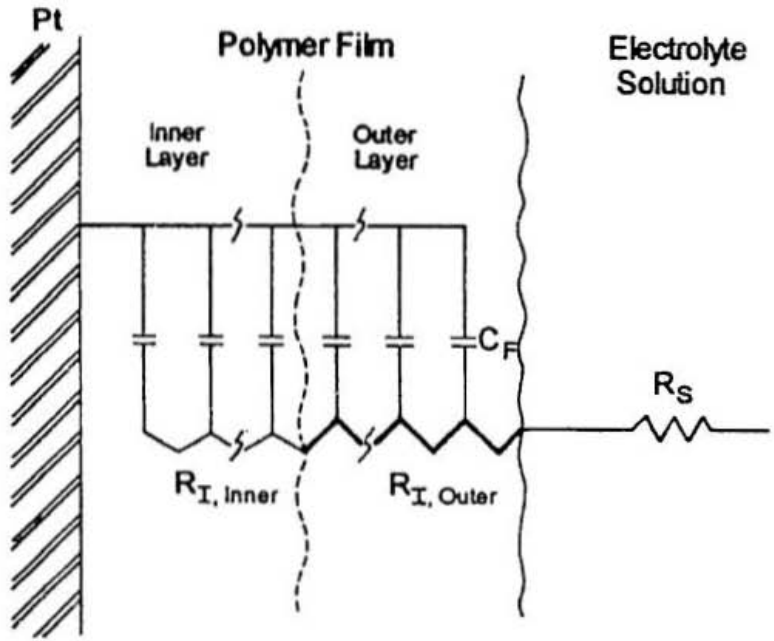

Figure 9.3.1 Electrical circuit used to simulate the experimental impedance responses of bilayer electrodes.

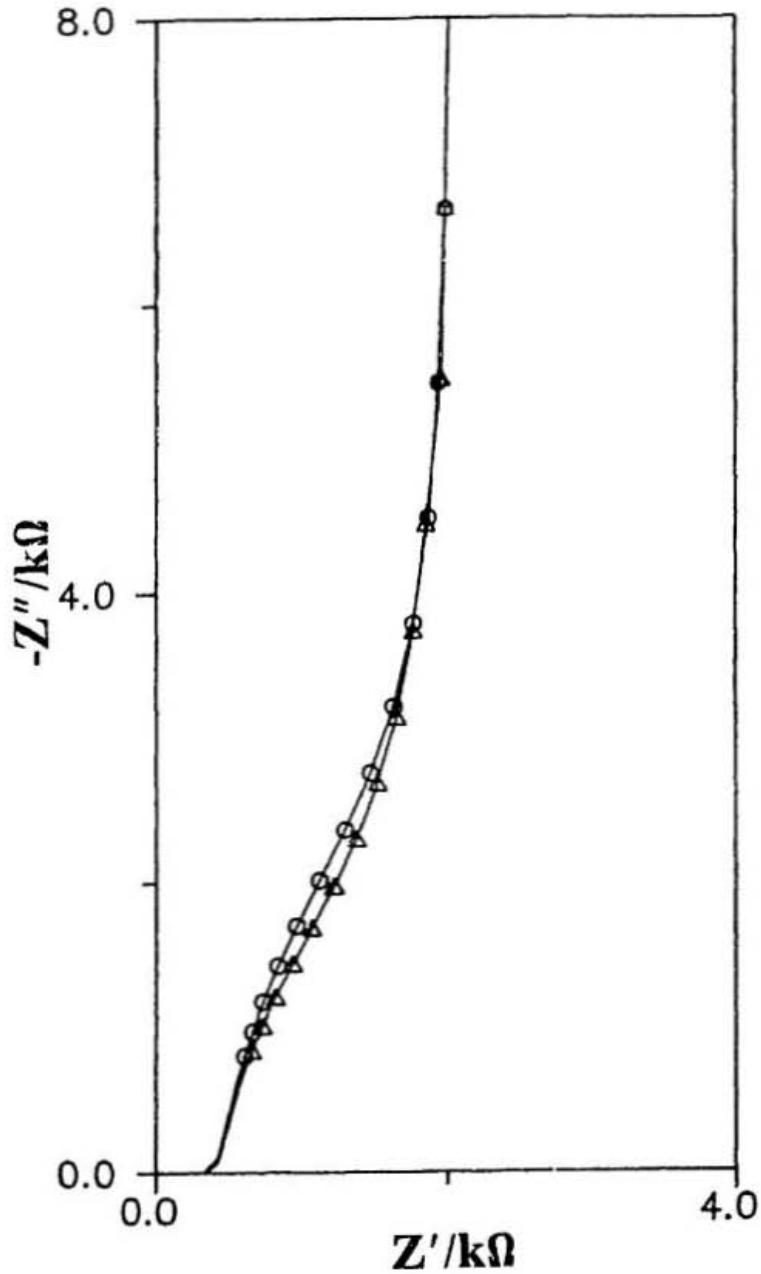

Figure 9.3.2 Complex plane impedance plots of the experimental (△) and simulated (○) data for the ‖ PPY/ClO_4^-(1 μm)| PPY/PSS(1 μm) bilayer electrode at -0.2 V in 0.2 M $NaClO_4$(aq). The ionic resistance $R_{I,inner}$ and $R_{I,outer}$ used to simulate the experimental data are 12.8 kΩ and 310 Ω respectively.

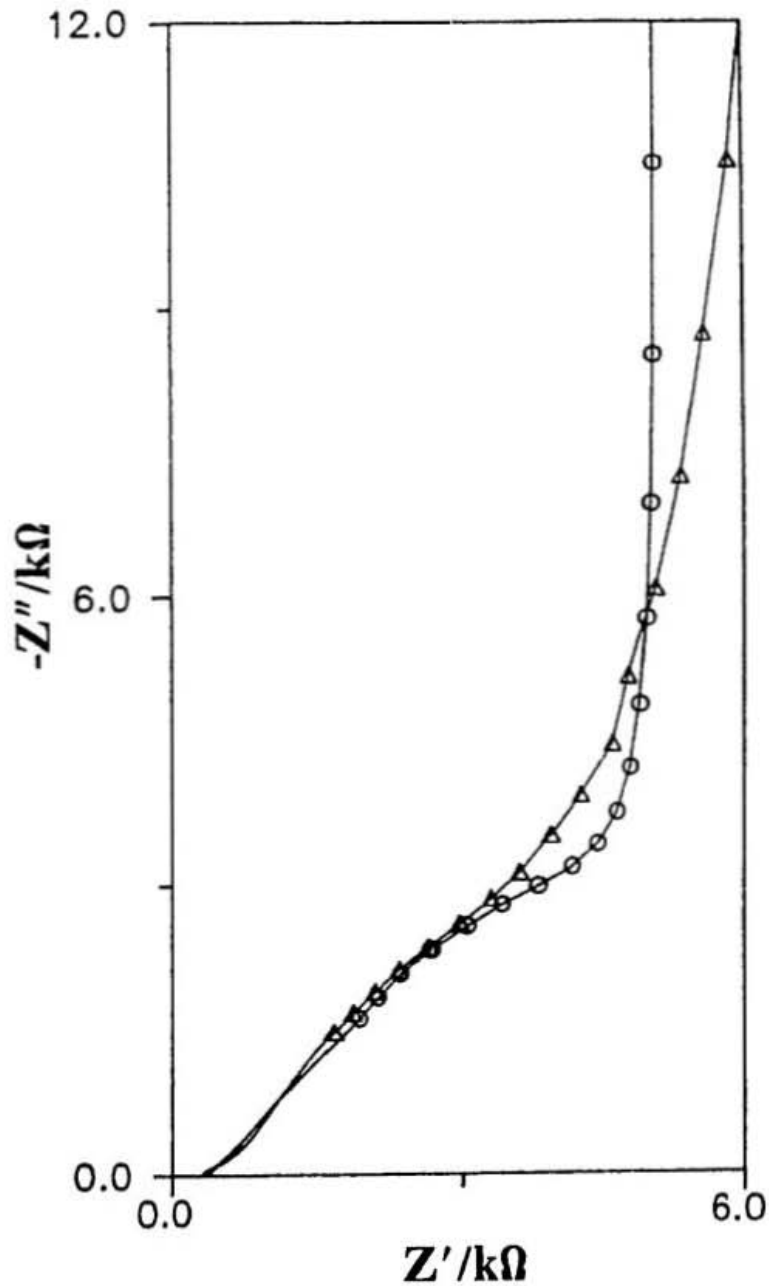

Figure 9.3.3 Complex plane impedance plots of the experimental (△) and simulated (○) data for the ‖ PPY/PSS(1 μm) | PPY/ClO_4^-(1 μm) bilayer electrode at -0.1 V in 0.2 M $NaClO_4$(aq). The ionic resistance $R_{I,inner}$ and $R_{I,outer}$ used to simulate the experimental data are 300 Ω and 8 kΩ respectively.

at 45° angle to the real axis, a second steeper Warburg-type line at lower frequency and a vertical line at very low frequency. For a ‖PPY/PSS (1 μm) | PPY/ClO_4^- (1 μm) bilayer electrode at -0.1 V in 0.2 M $NaClO_4$, the experimental data are simulated with ‖ $R_{I,inner}$ = 250 Ω | $R_{I,outer}$ =8 kΩ. The simulated impedance response, like the experimental one, gives a single Warburg-type line at high frequency and a vertical line at low frequency. The simulated impedance response is insensitive to the choice of $R_{I,inner}$ as long as $R_{I,outer}/R_{I,inner} > 10$. This situation is expected since the fast charging process of the inner layer is not resolved from the slow preceding charging process of the outer layer.

9.4 Cyclic Voltammetry

Fig. 9.4.1 shows cyclic voltammograms of the two types of bilayer electrodes in 0.2 M $NaClO_4$(aq). The single charging process of the ‖PPY/PSS (1 μm)| PPY/ClO_4^-(1 μm) bilayer electrode is clearly reflected by the single pair of redox peaks. The voltammogram (Fig. 9.4.1A) closely resembles that of a 2 μm PPY/ClO_4^- film (Fig. 7.2.1A), as marked by the large potential shift of the anodic peak with increasing scan rate. In Fig. 9.4.1B the two pairs of redox peaks correspond to the two well resolved charging processes of the outer and inner

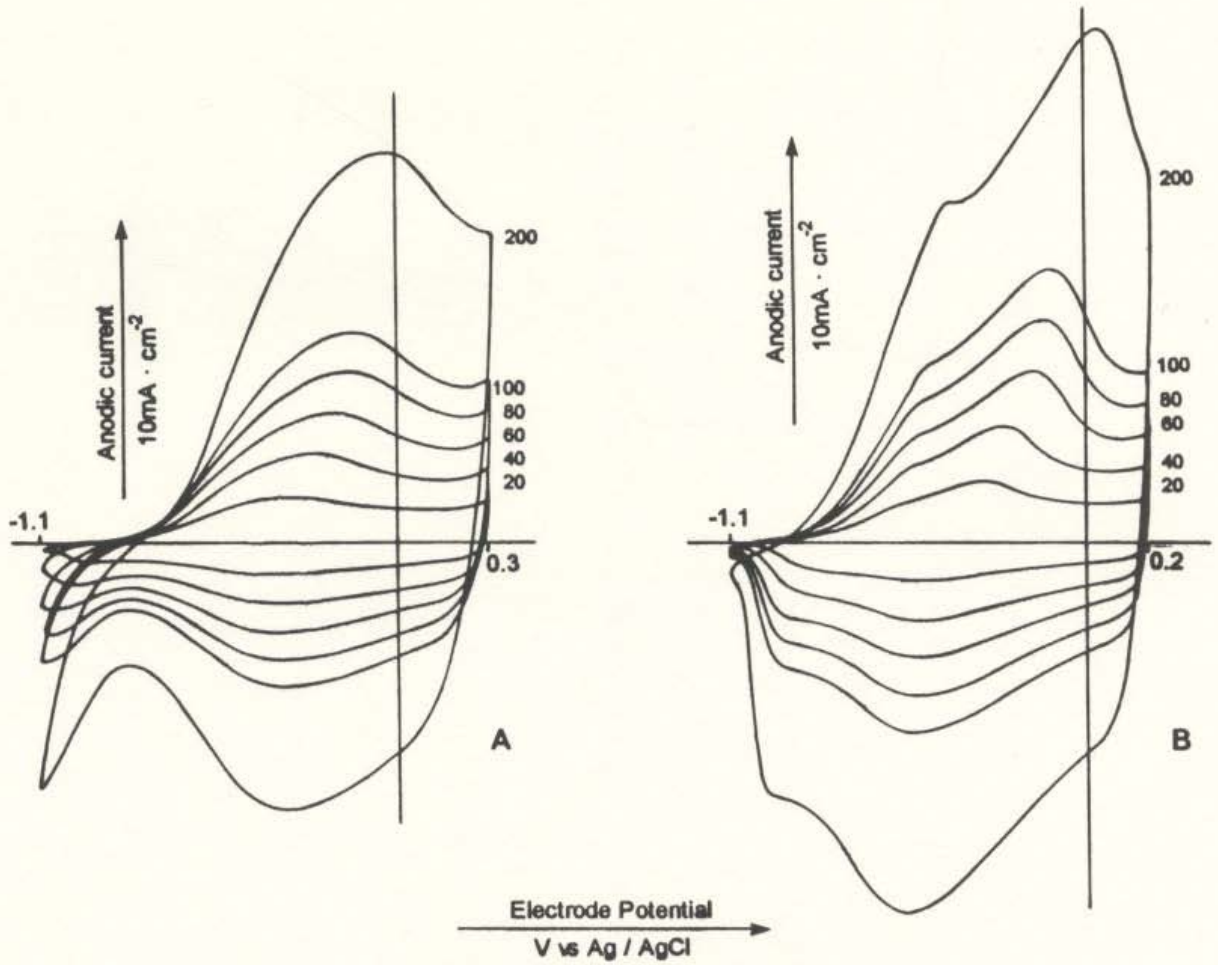

Figure 9.4.1 Cyclic voltammograms of ‖ PPY/PSS(1 μm) | PPY/ClO_4^-(1 μm) (A) and ‖ PPY/ClO_4^- (1 μm)| PPY/PSS(1 μm) (B) bilayer electrodes in 0.2 M $NaClO_4$(aq). Scan rates in mV s^{-1} are indicated.

layers for the ‖PPY/ClO_4^-(1 μm) | PPY/PSS (1 μm) bilayer electrode.

9.5 Usefulness in Immobilization of Ionic Species

The immobilization of catalytic species within a polymer film is crucial to many applications of modified electrodes, such as in electrocatalysis[17-22], electroanalysis and sensors[23]. Electrostatic binding of electroactive counter-ions in ion-exchange polymer coating on electrodes was first studied by Oyama *et al*[24,25]. Immobilization of anionic species in oxidized polypyrrole by electrostatic binding has been demonstrated[26]. However, such immobilization in a conducting polymer is unstable due to the anion-exchange process when the electrode is immersed in an electrolyte solution. Also, the anionic species will be lost when the electrode is reduced[26]. Immobilization by forming a covalent bond between the catalytic species and the polymer backbone has also been reported[27]. Although this type of immobilization is physically stable, loss of catalytic activity generally occurs due to the decreased mobility of the catalytic centres.

An alternative method of increasing stability is to use multiple layer electrodes. Rubinstein *et al*[28,29] have reported an electrostatic encapsulation using bilayer films with an ion exchanger as the outer layer. The anionic species is

confined within the inner layer due to the Donnan co-ion exclusion of the outer layer.

Bilayer electrodes are potentially useful for confinement of anionic or cationic catalytic species in conducting polymers. For example, in Fig. 9.5.1A, an anionic species (A^-) is initially immobilized in polypyrrole during the electrochemical polymerization of the inner layer. The electrode is then coated with a PPY/PSS outer layer. Decreasing the electrode potential causes the outer PPY/PSS layer to be reduced first. Reducing PPY/A^- at a later stage would normally be accompanied by the expulsion of A^-, which now should not be able to pass through the outer layer due to Donnan co-ion exclusion. Electroneutrality in the inner layer is therefore achieved by the insertion of electrolyte cations, which travel through the outer layer (Fig. 9.5.1B). Upon oxidation, the reverse process occurs. In any event, the anionic species (A^-) initially incorporated in the inner layer are preserved in the bilayer electrode.

Similarly, a bilayer electrode with PPY/ClO_4^- as the outer layer is useful for confinement of cationic species (C^+) in the inner PPY/PSS layer. The C^+ is inserted into the inner PPY/PSS layer during the first cathodic potential scan by transport through the already reduced PPY/ClO_4^- outer layer (Fig. 9.5.2B). During the anodic potential scan, oxidation of the PPY/ClO_4^- outer layer occurs initially. Oxidizing the PPY/PSS inner layer at a later stage would normally cause the

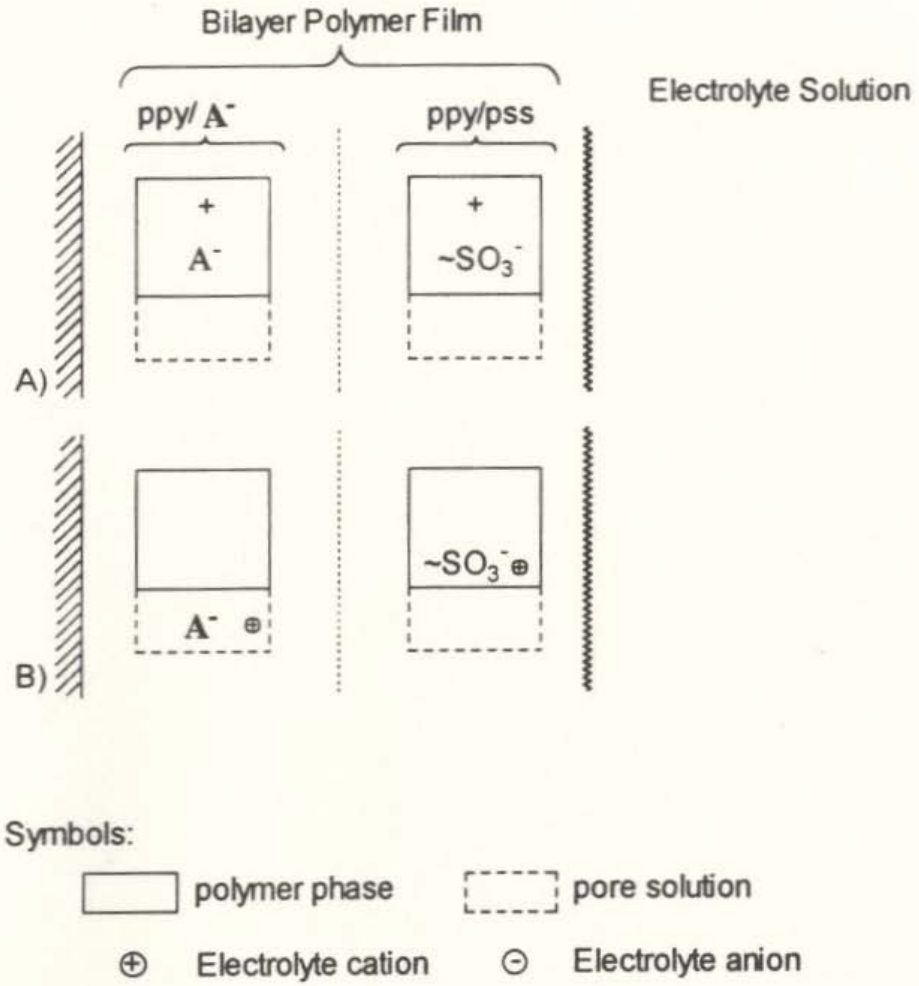

Figure 9.5.1 Schematic illustration of the confinement of an anionic species (A^-) in a ‖ PPY/A^- | PPY/PSS bilayer electrode. A - newly prepared bilayer electrode; B - after reduction.

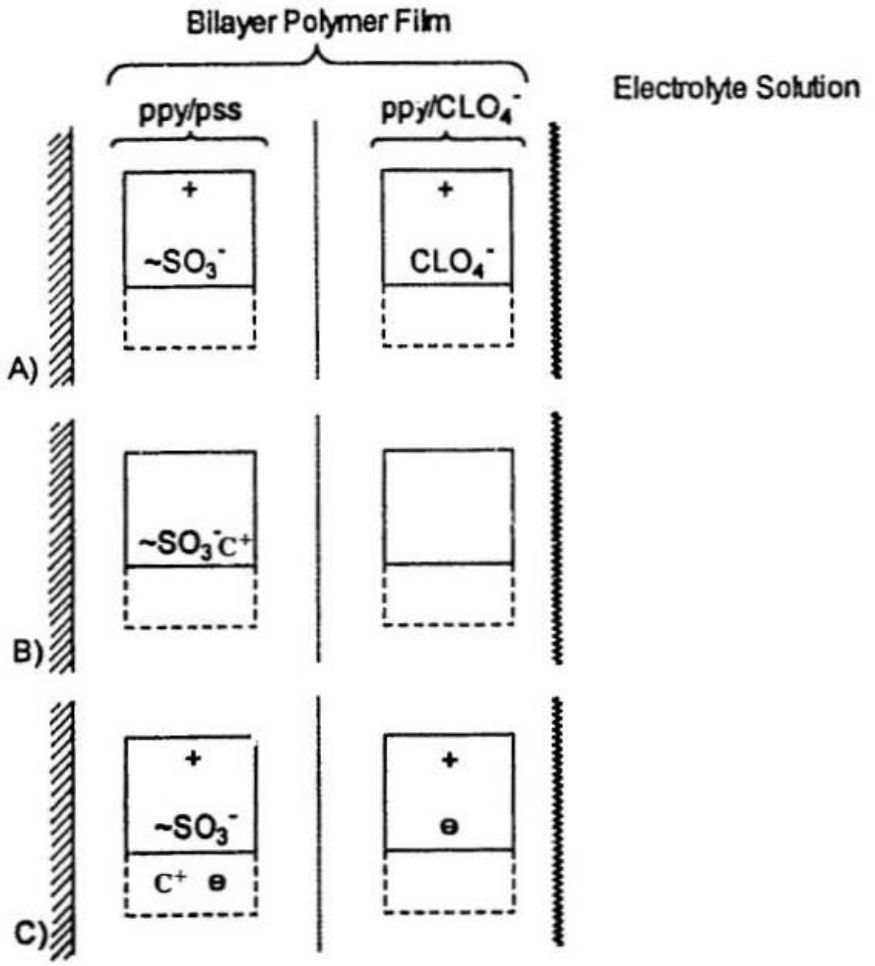

Figure 9.5.2 Schematic illustration of the confinement of a cationic species (C^+) in a ‖PPY/PSS|PPY/ClO_4^- bilayer electrode. A - newly prepared bilayer electrode; B - after first cathodic potential scan in electrolyte solution containing C^+, and C - after oxidation.

expulsion of the C^+, which now should not be able to pass through the outer layer due to Donnan co-ion exclusion. Electroneutrality in the inner layer is preserved by the insertion of electrolyte anions, which travel through the outer layer (Fig. 9.5.2C). Upon reduction, the reverse process occurs (Fig. 9.5.2C to Fig. 9.5.2B). In any event, the cationic species incorporated in the inner layer during the first cathodic potential scan are preserved in the bilayer electrode.

9.6 Conclusion

The impedance responses observed for conducting polypyrrole bilayer electrodes clearly show that the electrochemical reaction begins at the polymer/solution interface. This is consistent with the prediction from Albery's dual rail transmission line model and the porous electrode model. These models also predict that under some circumstances the redox reaction of a conducting polymer will begin either at the electrode/polymer interface or simultaneously at both interfaces. The former will occur when ion transport in the polymer is faster than electron transport. The latter occurs when electron and ion transports occur at similar rates. Studies on a pyrrole based ion exchange polymer (Section 5.3) and PPY/PSS (Section 5.4) have revealed the impedance responses corresponding to

all three cases.

References

(1) Musiani, M.M. *Electrochim. Acta* 1990,*35*,1665.

(2) DeLevie, R.; in *Advances in Electrochemistry and Electrochemical Engineering*, Vol.6, Delahay, P.; Tobias, C.W. (Eds.); John-wiley & Sons: New York,1967;p.329.

(3) Raistrick, I.D. *Electrochim. Acta* 1990,*35*,1579.

(4) Albery, W.J.; Chen, Z.; Horrocks, B.R.; Mount, A.R.; Wilson, P.J.; Bloor, D.; Monkman, A.T.; Elliott, C.M. *Faraday. Discuss. Chem. Soc.* 1989,*88*,247.

(5) Albery, W.J.; Elliott, C.M.; Mount, A.R. *J. Electroanal. Chem.* 1990,*288*,15.

(6) Ho, C.; Raistrick, I.D.; Huggins, R.A. *J. Electrochem. Soc.* 1980,*127*,343.

(7) Gabrielli, C.; Haas, O.; Takenouti, H. *J. Appl. Electrochem.* 1987,*17*,82.

(8) Mathias, M.F.; Haas, O. *J. Phys. Chem.* 1992,*96*,3174.

(9) Buck, R.P. *J. Electroanal. Chem.* 1986,*210*,1.

(10) Kotz, R.; Neff, H.; Stucki, S. *J. Electrochem. Soc.* 1984,*131*,72.

(11) Lee, C.; Kwak, J.; Bard, A.J. *J. Electrochem. Soc.* 1989,*136*,3720.

(12) Gottesfeld, S.; Redondo, A.; Feldberg, S.W. *J. Electrochem. Soc.* 1987,*134*,271.

(13) Gottesfeld, S. in *Electroanalytical Chemistry,V15*, Bard,AJ (Ed.), 1988, Marcel Dekker: New York.

(14) Tezuka, Y.; Ohyama, S.; Ishii, T.; Aoki, K. *Bull. Chem. Soc. Jpn.* 1991,*64*,2045.

(15) Aoki, K.; Aramoto, T.; Hoshino, Y. *J. Electroanal. Chem.* 1992,*340*,127.

(16) Ren, X.; Pickup, P.G. *J. Phys. Chem.* 1993,*97*,5356.

(17) Bedioui, F.; Bongars, C.; Devynck, J.; Bied-Charreton, C.; Hinnen, C. *J. Electroanal. Chem.* 1986,*207*,87.

(18) Mizutani, F.; Iijima, S.; Tanabe, Y.; Tsuda, K. *Synth. Met.* 1987,*18*,111.

(19) Daire, F.; Bedioui, F.; Devynck, J.; Bied-Charreton, C. *J. Electroanal. Chem.* 1987,*224*,95.

(20) Bedioui, F.; Granados, S.G.; Devynck, J.; Biedcharreton, C. *New J. Chem.* 1991,*15*,939.

(21) Deoliveira, I.M.F.; Moutet, J.C.; Hamarthibault, S. *J. Mater. Chem.* 1992,*2*,167.

(22) Potjekamloth, K.; Josowicz, M. *Berichte der Bunsen Gesellschaft Fur Physikalische Chemie* 1992,*96*,1004.

(23) Labuda, J. *Selective Electrode Reviews* 1992,*14*,33.

(24) Oyama, N.; Anson, F.C. *J. Am. Chem. Soc.* 1979,*101*,3450.

(25) Oyama, N.; Shimomura, T.; Shigehara, K.; Anson, F.C. *J. Electroanal. Chem.* 1980,*112*,271.

(26) Pickup, P.G. *J. Electroanal. Chem.* 1987,*225*,273.

(27) Ochmanska, J.; Pickup, P.G. *J. Electroanal. Chem.* 1989,*271*,83.

(28) Rubinstein, I. *J. Electroanal. Chem.* 1985,*195*,431.

(29) Rubinstein, I.; Rubinstein, I. *J. Phys. Chem.* 1987,*91*,235.

Chapter 10

Polypyrrole Having Two Types of Ion Transport

Previous impedance studies[1] on polypyrrole doped with perchlorate (PPY/ClO_4^-) and polypyrrole doped with poly(styrene sulphonate) (PPY/PSS) have shown that ion transport in the former is dominated by anion movement and in the latter by cation movement (chapter 7). These types of ion transport differ in their potential dependence and rate. In this chapter, polypyrrole films having both two types of ion transport are studied with impedance spectroscopy and cyclic voltammetry.

The shapes of cyclic voltammograms of polypyrrole have been noted by Diaz and coworkers to be sensitive to the anions in the polymer[2], indicating that the limiting process in charge transport for the polypyrrole redox reaction is slow ion transport. The polymer films studied in this chapter offer a new opportunity to study the relationship between ion transport and the shape of cyclic voltammograms.

10.1 Polymer Preparation And Characterization

The monomer solutions contained 0.5 M pyrrole in water plus the two electrolytes ($NaClO_4$ and NaPSS) with a total electrolyte concentration of 0.5 M. The polymer films were prepared by anodic oxidation of pyrrole at a constant current density of 0.88 mA cm^{-2} on Pt (area = 0.0045 cm^{-2}), each with a charge density of 0.48 mC cm^{-2}. This charge density will produce a dry film thickness of 2 μm PPY/ClO_4^- or PPY/PSS film as measured with SEM (Chapter 3). It is assumed here that the same charge density will also produce a 2 μm polypyrrole /perchlorate + poly(styrene sulphonate) (PPY/ClO_4^-+PSS) composite film. All ionic conductivities for the polymer films are calculated using the dry film thickness. In the following discussion, a polymer film polymerized from a monomer solution containing $NaClO_4$ and NaPSS (in $-SO_3^-$ unit) in the molar ratio of m/n will be referred to as a [m/n] film alone. An Ag/AgCl electrode was used as the reference electrode and the electrode potentials reported are quoted with respect to this reference electrode.

The molar ratios of ClO_4^-/$-SO_3^-$ in the newly prepared (oxidized) polymer films were determined by energy dispersive x-ray analysis (EDXA) on free standing films fixed on the sample stage using Scotch tape. The films were peeled

from the Pt electrode by following procedures. After the polymerization, the polymer coated Pt electrode was removed immediately from the monomer solution, then washed with water to remove the adhering solution and then with acetone, and dried in air. Free standing PPY/4-chlorobenzene sulphonate films (2 μm) which contain Cl and S in one to one molar ratio were prepared similarly. These films closely match the matrix of the PPY/PSS+ClO_4^- films, and were used as a standard to correct the Cl and S molar ratio calculated from the x-ray emission counts of the two elements using Tracor Northern's Standardless Quantitative Analysis (SQ) software. X-ray emission analysis using SQ on four standard PPY/4-chlorobenzene sulphonate films gave an average Cl:S ratio of 0.92 ($\pm$ 0.01), which is duly corrected to the value of 1 with a correction factor of 1.09. This correction factor was used to correct all SQ results for PPY/ClO_4^-+PSS films. Fig. 10.1.1 shows x-ray emission spectra for a standard and five PPY/PSS+ClO_4^- films. The corrected ClO_4^-/-SO_3^- molar ratios in the freshly formed (oxidized) PPY/ClO_4^-+PSS films are listed in Table 10.1.1.

It is interesting to note that polypyrrole preferentially incorporates PSS over ClO_4^-. This may be explained by the large entropy gain ($\Delta S > 0$) when many small ClO_4^- anions (*ca.* 340) are replaced by a large PSS poly-anion. Stronger interaction between the positive charges on the oxidized polypyrrole chains and $-SO_3^-$ ions may also favour the incorporation of PSS.

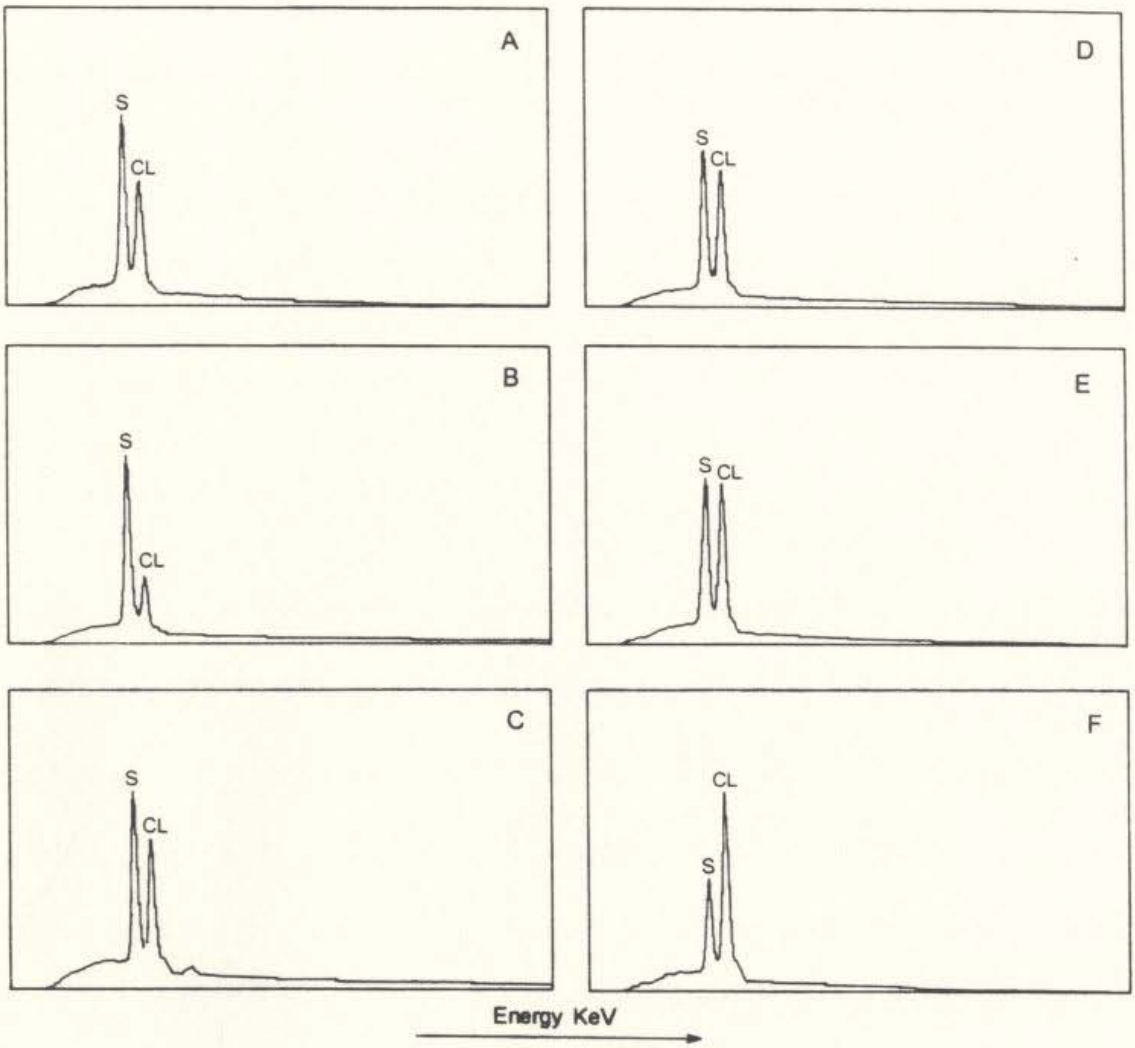

Figure 10.1.1 Energy dispersive x-ray spectra of a PPY/4-chlorobenzesulphonate standard (A), and [1/3](B), [3/1] (C), [6/1] (D), [20/1] (E), [40/1] (F) PPY/PSS+ClO_4^- polymer films.

Table 10.1.1 Energy dispersive X-ray analysis of $ClO_4^-/-SO_3^-$ molar ratios in freshly formed (oxidized) PPY/ClO_4^-+PSS composite films.

$ClO_4^-/-SO_3^-$ ratios in the monomer solution	$ClO_4^-/-SO_3^-$ ratios in the polymer films
50	2.67
40	2.45
20	1.40
6	1.28
3	1.11
1	0.82
0.333	0.31

X-ray emission analysis was used to measure the K^+ and ClO_4^- contents of some [3/1] PPY/ClO_4^-+PSS films ($ClO_4^-/-SO_3^-$ ratio in film ~ 1.1) after equilibration at various potentials in 0.2 M $KClO_4$ (aq). Using $KClO_4$ instead of $NaClO_4$ enhances the sensitivity of this method to detect cations in the film. Fig. 10.1.2 shows x-ray emission spectra of the polymer films after equilibration at various potentials. X-ray emission analysis results for PPY/PSS films after full reduction (-1.0 V) in $KClO_4$ were used to correct the K/S molar ratios obtained using SQ. Corrected $ClO_4^-/—SO_3^-$ and $K^+/—SO_3^-$ molar ratios are listed in Table 10.1.2. These results show that the ClO_4^- anions are the dominant mobile ions in

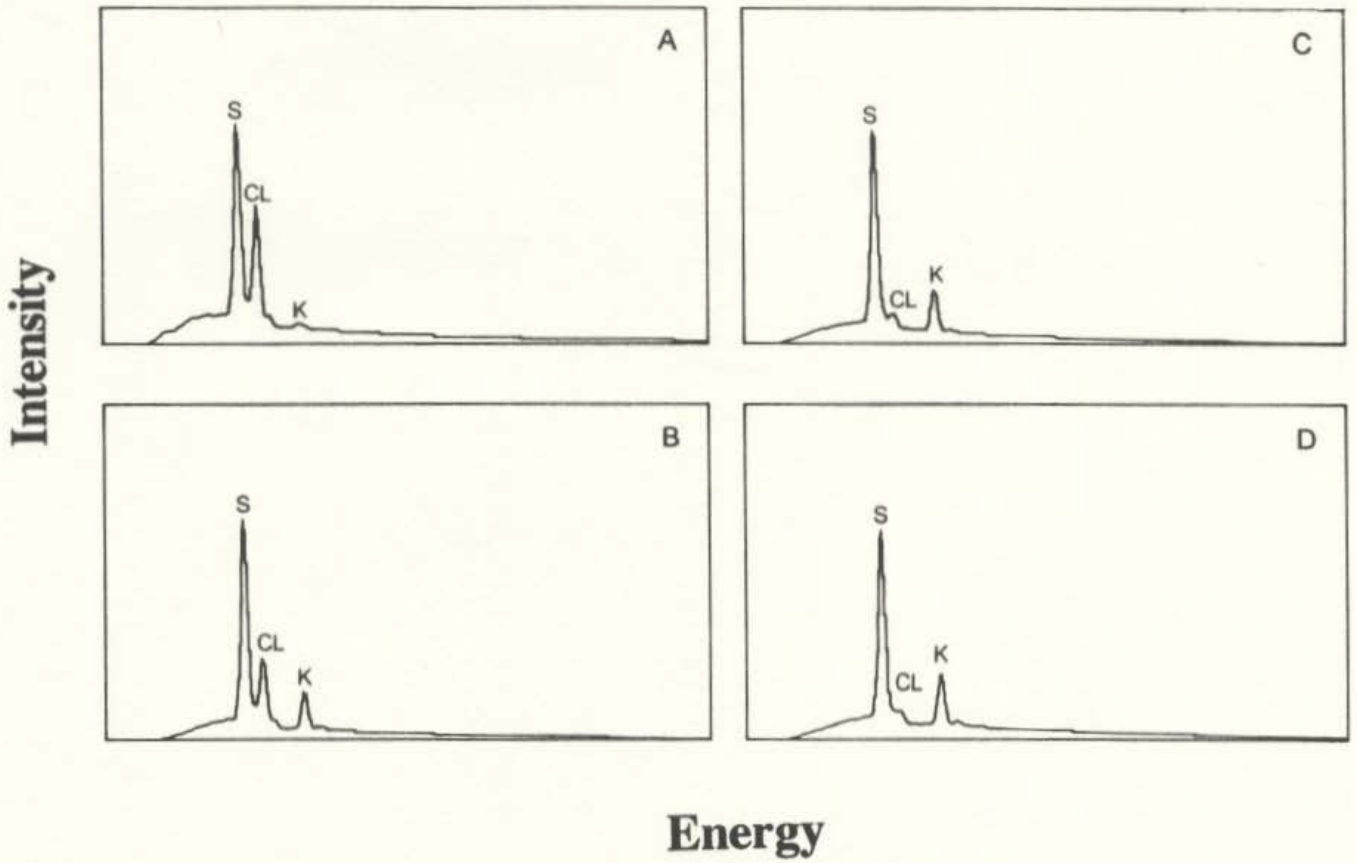

Figure 10.1.2 Energy dispersive x-ray spectra of free standing [3/1] PPY/PSS+ClO_4^- polymer films after polarization at 0.0(A), -0.3(B), -0.5(C) and -0.7(D) V *vs.* Ag/AgCl in 0.05 M $KClO_4$(aq).

the oxidized polymer while K^+ cations are the dominant mobile ions in the reduced polymer. Decreasing the electrode potential causes some expulsion of ClO_4^- and some intercalation of K^+ ions to reach the equilibrium composition of the polymer at the lower potential.

Table 10.1.2 EDXA analysis of $ClO_4^-/-SO_3^-$ and $K^+/-SO_3^-$ molar ratios in [3/1] films after equilibration in 0.2 M $KClO_4$ (aq) at various potentials.

Potential V. *vs* Ag/AgCl	$ClO_4^-/-SO_3^-$ molar ratio	$K^+/-SO_3^-$ molar ratio
0.1	1.11	0.00
0.0	0.96	0.18
-0.3	0.50	0.58
-0.5	0.14	0.69
-0.7	0.09	0.84
-0.9	0.00	1.00

10.2 Impedance

The impedances of the polymer film coated Pt electrodes were all measured in 0.2 M $NaClO_4$ (aq). For each film the electrode potential was decreased by increments of 100 mV from 0.1 to -0.8 V. The polymer film coated electrode was held at the measuring potential for 5 min. before impedance measurements.

Fig. 10.2.1 shows complex plane impedance plots for a [45/1] PPY/ClO_4^- +PSS film coated Pt electrode in 0.2 M $NaClO_4$ (aq). The high frequency data form a Warburg-type line, which intersects the real axis at the uncompensated solution resistance (R_s). Based on the previous discussion of the impedance behaviour of polypyrrole film coated electrodes (Section 5.1) as well as the known high electronic conductivity of even slightly oxidized PPY, the projected length of the Warburg-type line on the real axis is therefore related to the polymer's ionic resistance. As the electrode potential is decreased, the length of the Warburg-type line for the nearly fully oxidized polymer (*ca.* 0.1 to -0.1 V) increases, while that for the nearly fully reduced polymer (*ca.* -0.7 to -0.8 V) decreases. Comparison with the results for PPY/ClO_4^- and PPY/PSS reported in Chapter 7 shows that the oxidized polymer is mainly doped with ClO_4^-, while the reduced polymer with PSS. The impedance spectra in the complex capacitance plane (Fig. 10.2.2A) show that for the fully oxidized or fully reduced forms there is one nearly perfect semicircle, indicating a single dominant charging process. At intermediate potentials (*e.g.* -0.4 V) there are two distinguishable semicircles, indicating that there are a fast and a slow charging processes. These two processes involve nearly equal amount of the polymer at -0.4 V as shown by the similar diameters of the two semicircles. In the complex plane impedance plots (Fig. 10.2.1), the slow charging process corresponds to a second steeper Warburg-type line at low

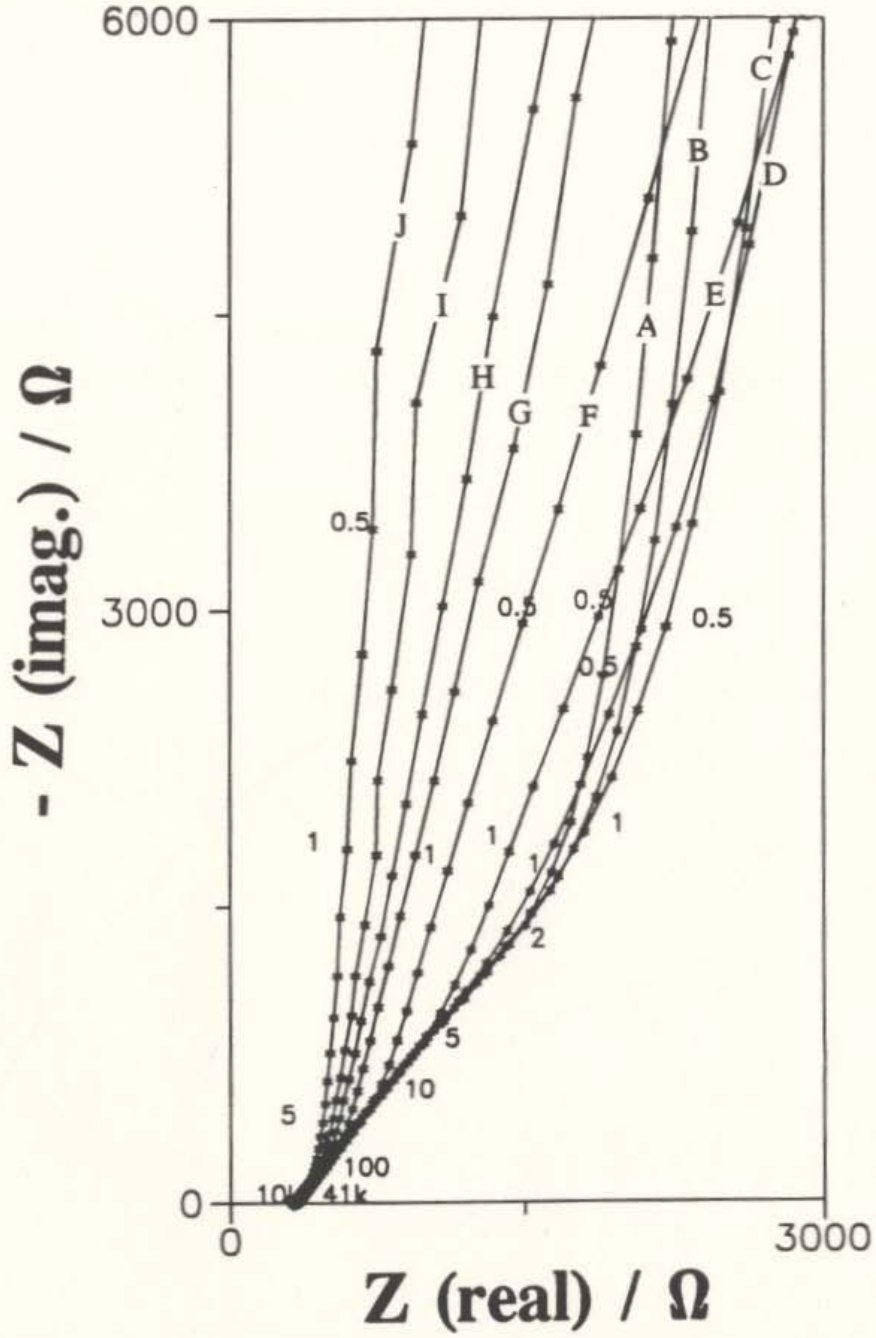

Figure 10.2.1 Complex plane impedance plots for a 2 μm [45/1] film covered Pt electrode at 1.0 (A), 0.0 (B), -0.1(C), -0.2(D), -0.3(E), -0.4(F), -0.5(G), -0.6(H), -0.7(I) and -0.8 V (J) *vs.* Ag/AgCl in 0.20 M $NaClO_4$(aq) solution. Frequencies at selected points are marked in Hz.

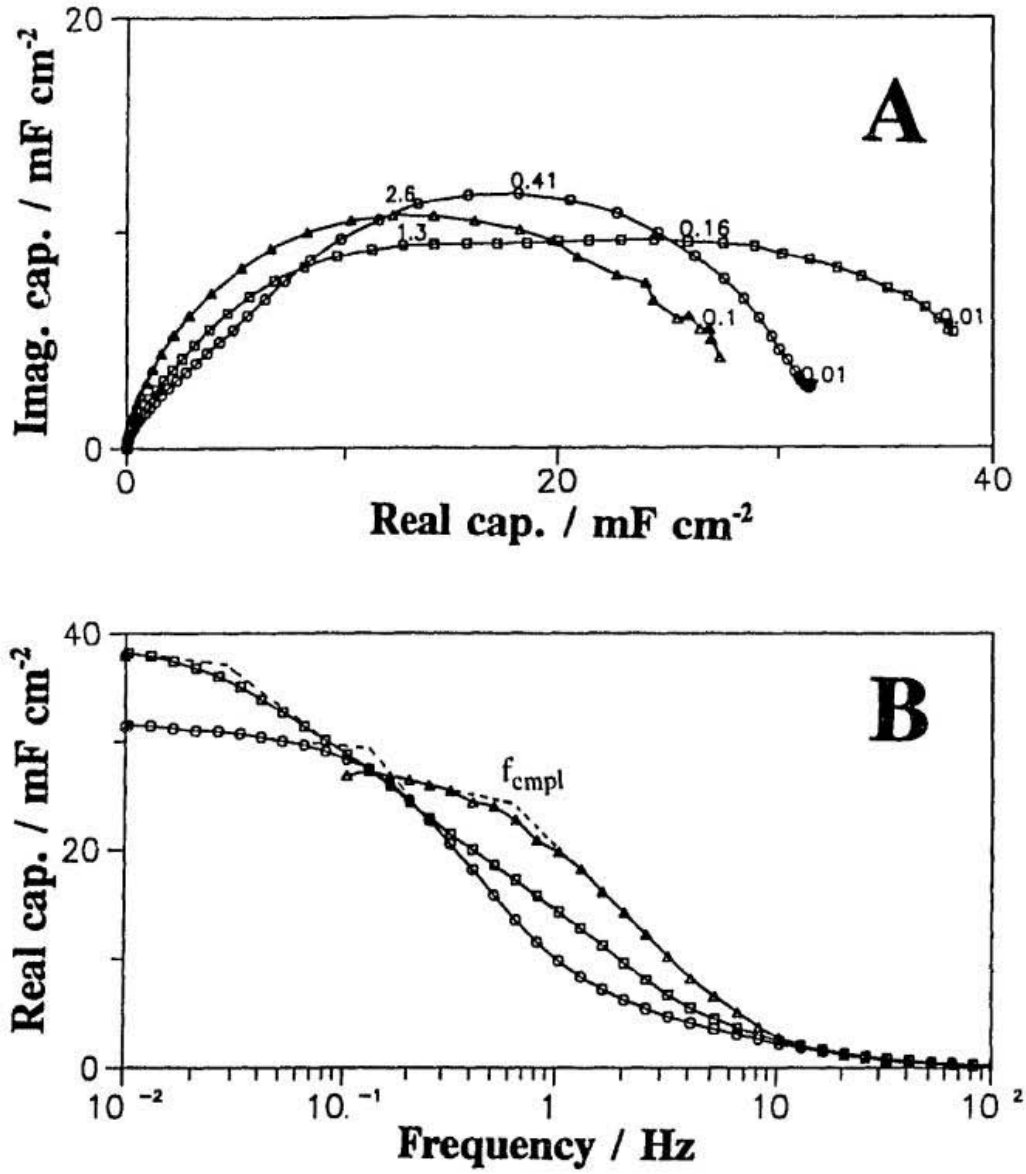

Figure 10.2.2 (A) Complex plane capacitance plots for some of the impedance data shown in Fig.10.2.1. (B) Plots of the film capacitance as a function of frequency. Electrode potentials are indicated as follows ○ 0.0 V, □ -0.4 V and ▵ -0.7 V *vs.* Ag/AgCl.

frequency shown by the curves for potentials from *ca.* -0.2 to -0.6 V. Decreasing the electrode potential causes a gradual transition from the dominant ClO_4^- doping in the oxidized form to the dominant $-SO_3^-$ doping in the reduced form. Fig. 10.2.2B shows the variation of the polymer film capacitance with the frequency of potential perturbation. The frequency at which the charging process is considered nearly completed (f_{cmpl}) is estimated as shown in Fig. 10.2.2B. For the reduced, oxidized and intermediate states this frequency was *ca.* 0.6, 0.12, and 0.025 Hz, respectively. The fast charging of the reduced polymer is due to the rapid movement of mobile Na^+ ions. The low mobility of ClO_4^- ions in the oxidized polymer results in a low charging rate. The very low charging rate of the intermediate state is due to the low number of mobile ions (both Na^+ and ClO_4^-) in the polymer.

Fig. 10.2.3 shows complex plane impedance plots for a [40/1] PPY/PSS+ClO_4^- polymer film coated Pt electrode. The dominant normal doping process is now observed in a narrower potential region (*ca.* 0.1 to 0.0 V), while the self-doping process is observed in a wider potential region (*ca.* -0.1 to -0.8 V) as compared to the [45/1] polymer. For both the fully oxidized and fully reduced forms the complex plane capacitance plots (Fig. 10.2.4A) show a single dominant charging process. At intermediate potentials (*ca.* -0.4 V), there are two semicircles with the larger one at the high frequency representing the fast self-doping process.

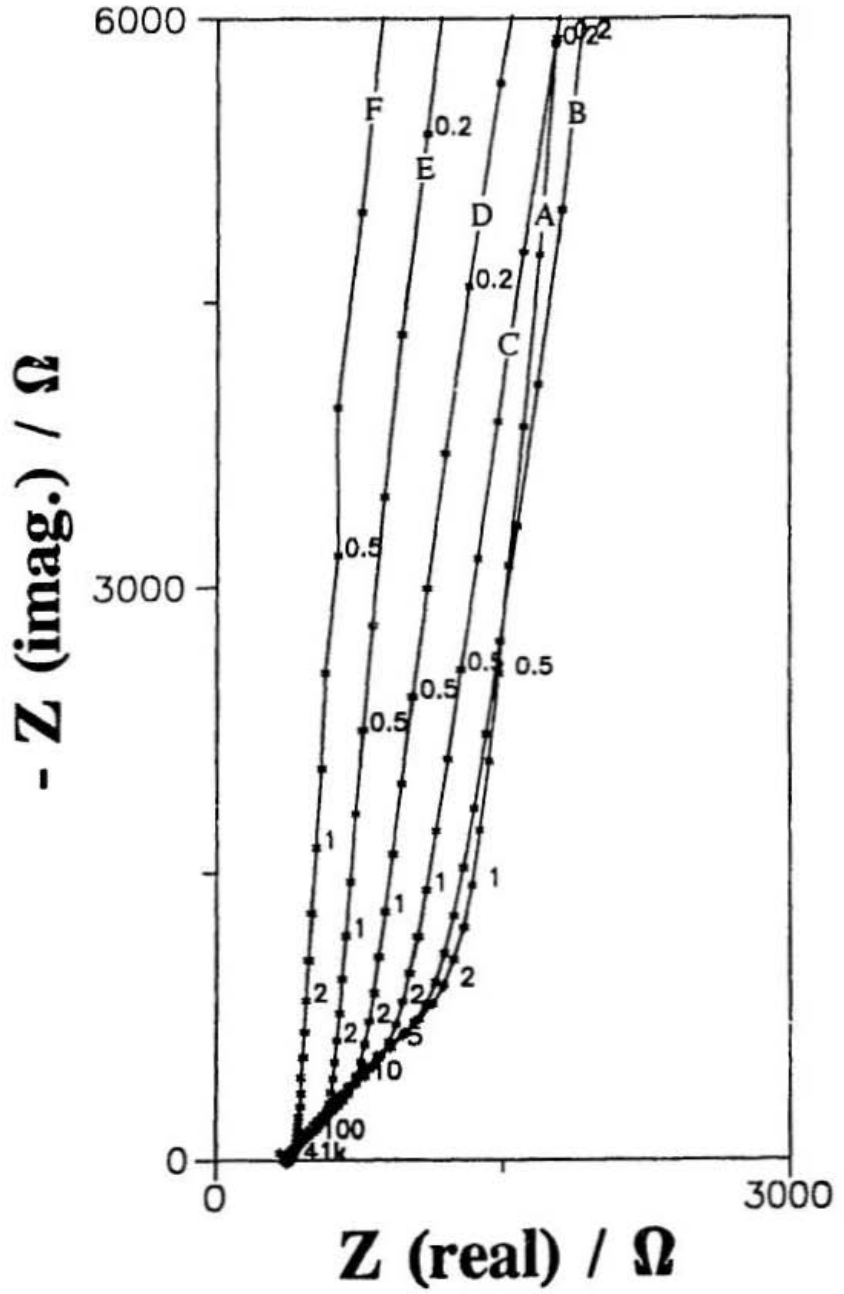

Figure 10.2.3 Complex plane impedance plots for a 2 μm [40/1] film covered Pt electrode at 0.1 (A), -0.1 (B), -0.2(C), -0.3(D), -0.4(E) and -0.8(F) *vs.* Ag/AgCl in 0.20 M $NaClO_4$(aq) solution. Frequencies at selected points are marked in Hz.

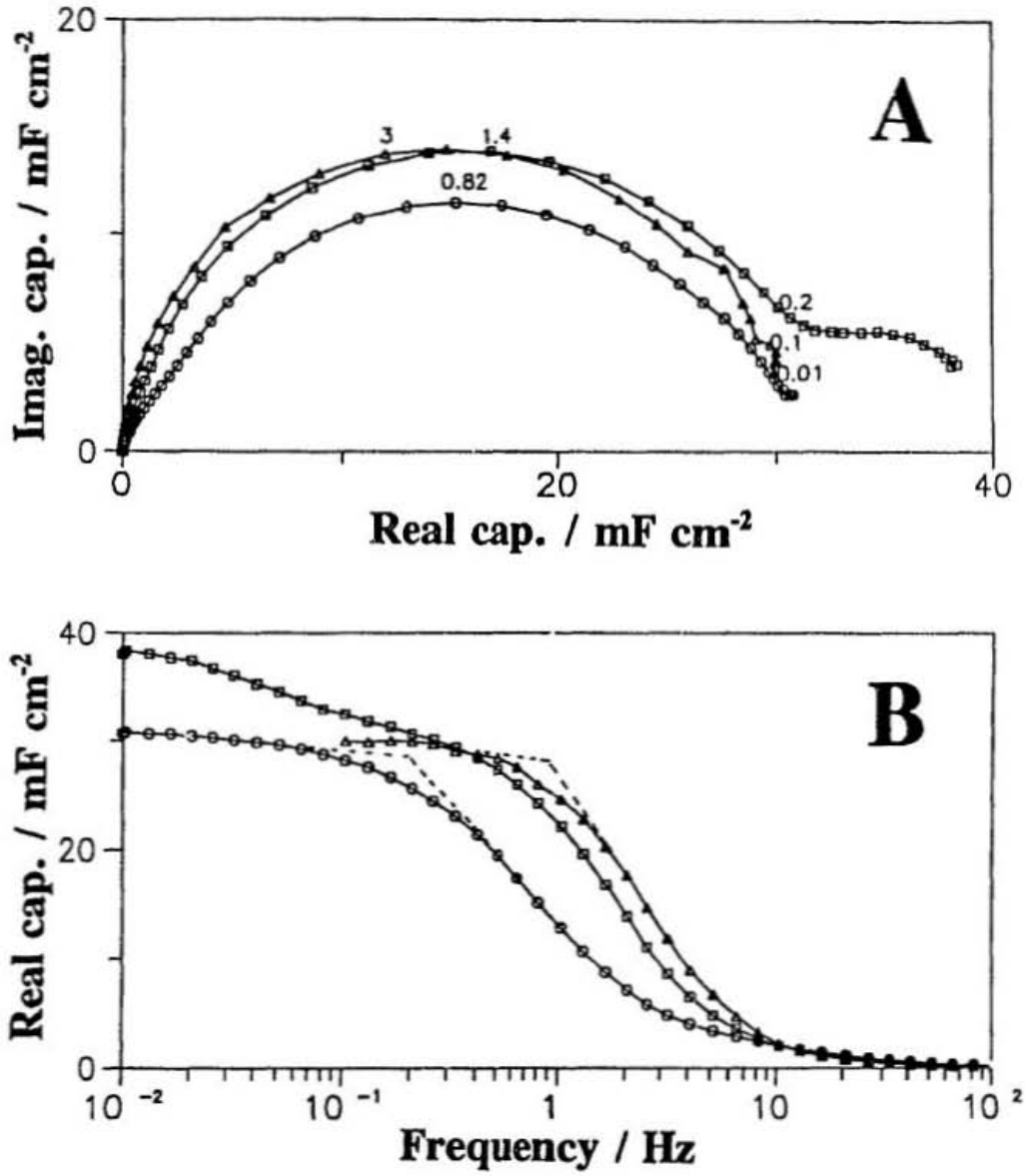

Figure 10.2.4 (A) Complex plane capacitance plots for some of the impedance data shown in Fig.10.2.3. (B) Plots of the film capacitance as a function of frequency. Electrode potentials are indicated as follows ○ 0.0 V, □ -0.4 V and ▵ -0.7 V *vs.* Ag/AgCl.

Fig. 10.2.4B shows the variation of the polymer film capacitance with the frequency of potential perturbation. The relative charging rates for the above three oxidization states of this polymer were similar to those discussed for the [45/1] film in Fig. 10.2.2B.

Fig. 10.2.5 shows complex plane impedance plots for a [50/1] polymer film coated Pt electrode. Compared with a [45/1] film, a [50/1] film contains a greater proportion of polymer doped with ClO_4^-. The ClO_4^- dominated doping process of this polymer is observed in the potential region of 0.1 to -0.2 V. The transition from normal doping to self-doping occurs in the potential region of -0.3 to -0.6 V. For both the fully oxidized and fully reduced forms there is a single dominant charging process as shown in the complex plane capacitance plots (Fig. 10.2.6A). At intermediate potentials (*e.g.* -0.4 V), there are two semicircles with the smaller one at high frequency representing the fast self-doping process. Fig. 10.2.6B shows the variation of the polymer film capacitance with the frequency of the potential perturbation, and the relative charging rates for the above three oxidization states of this polymer were similar to those discussed for Fig. 10.2.2B.

Table 10.2.1 lists apparent film ionic conductivities, which will be defined in next section, obtained from impedance measurements. For PPY/PSS and PPY/ClO_4^- films, the apparent ionic conductivities equal the true film ionic conductivities since there is only one charge transport process involved. The data

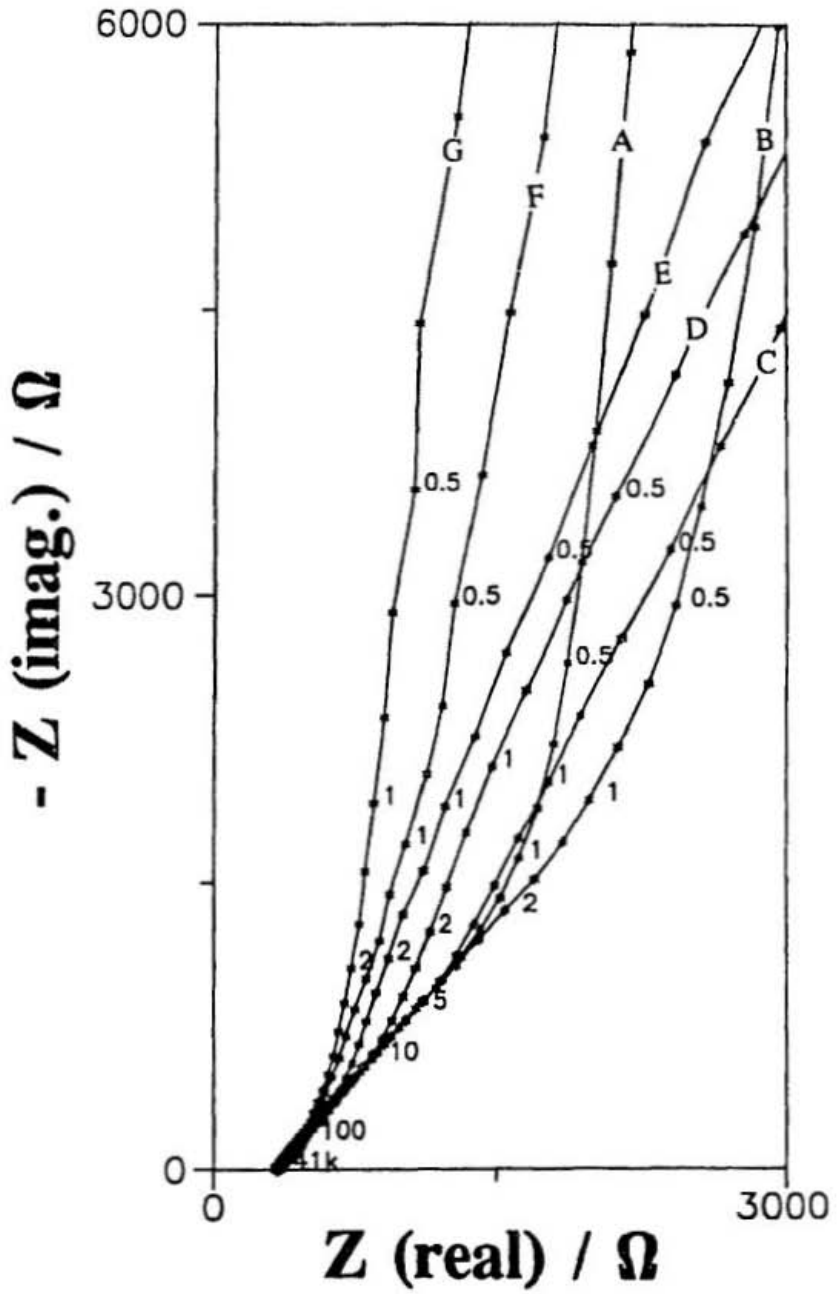

Figure 10.2.5 Complex plane impedance plots for a 2 μm [45/1] film covered Pt electrode at 0.1 (A), -0.2 (B), -0.3(C), -0.4(D), -0.6(E), -0.7(F) and -0.8 V(G) *vs.* Ag/AgCl in 0.20 M $NaClO_4$(aq) solution. Frequencies at selected points are marked in Hz.

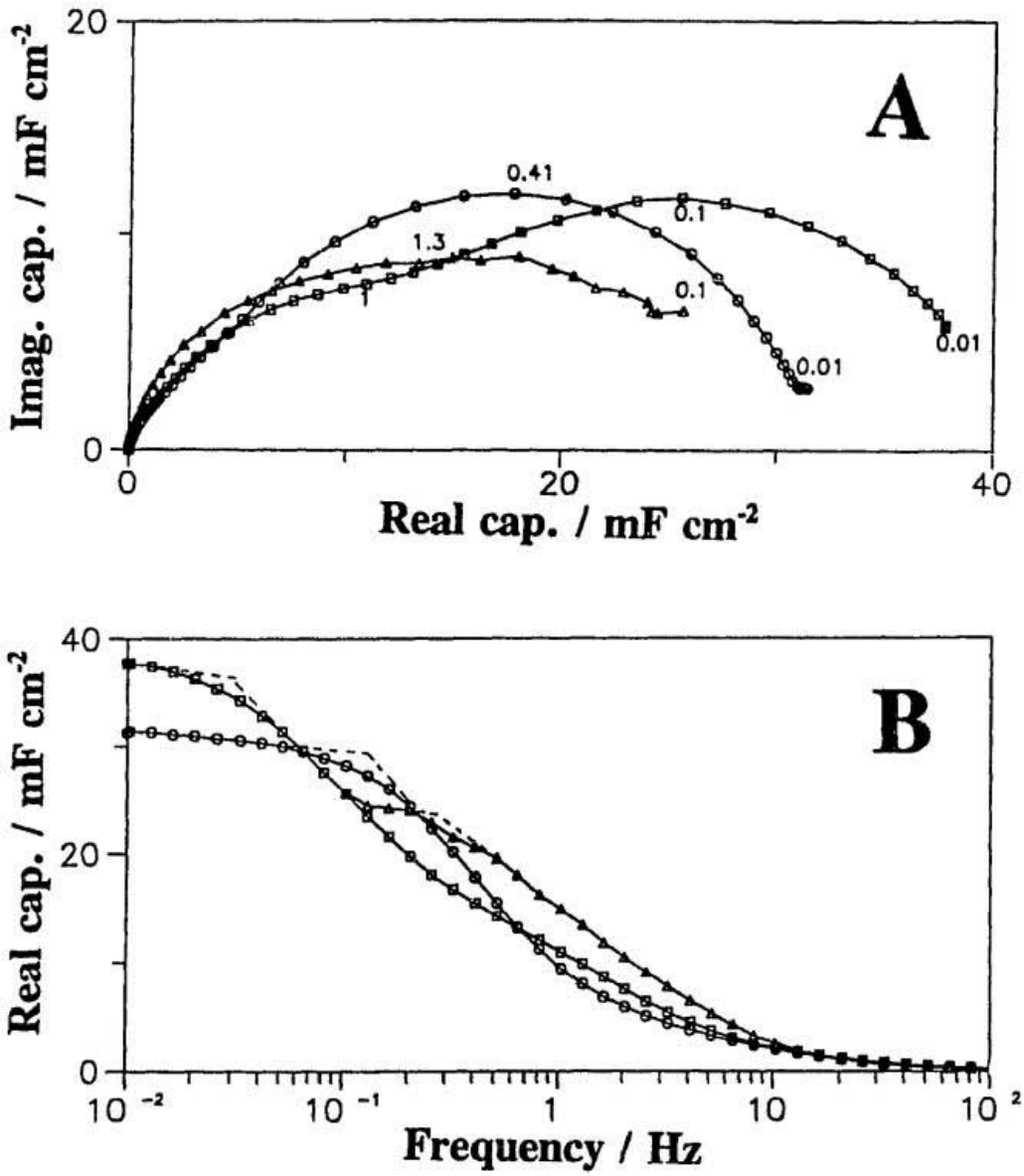

Figure 10.2.6 (A) Complex plane capacitance plots for some of the impedance data shown in Fig.10.2.5. (B) Plots of the film capacitance as a faction of frequency. Electrode potentials are indicated as follows ○ 0.0 V, □ -0.4 V and ▵ -0.7 V *vs.* Ag/AgCl.

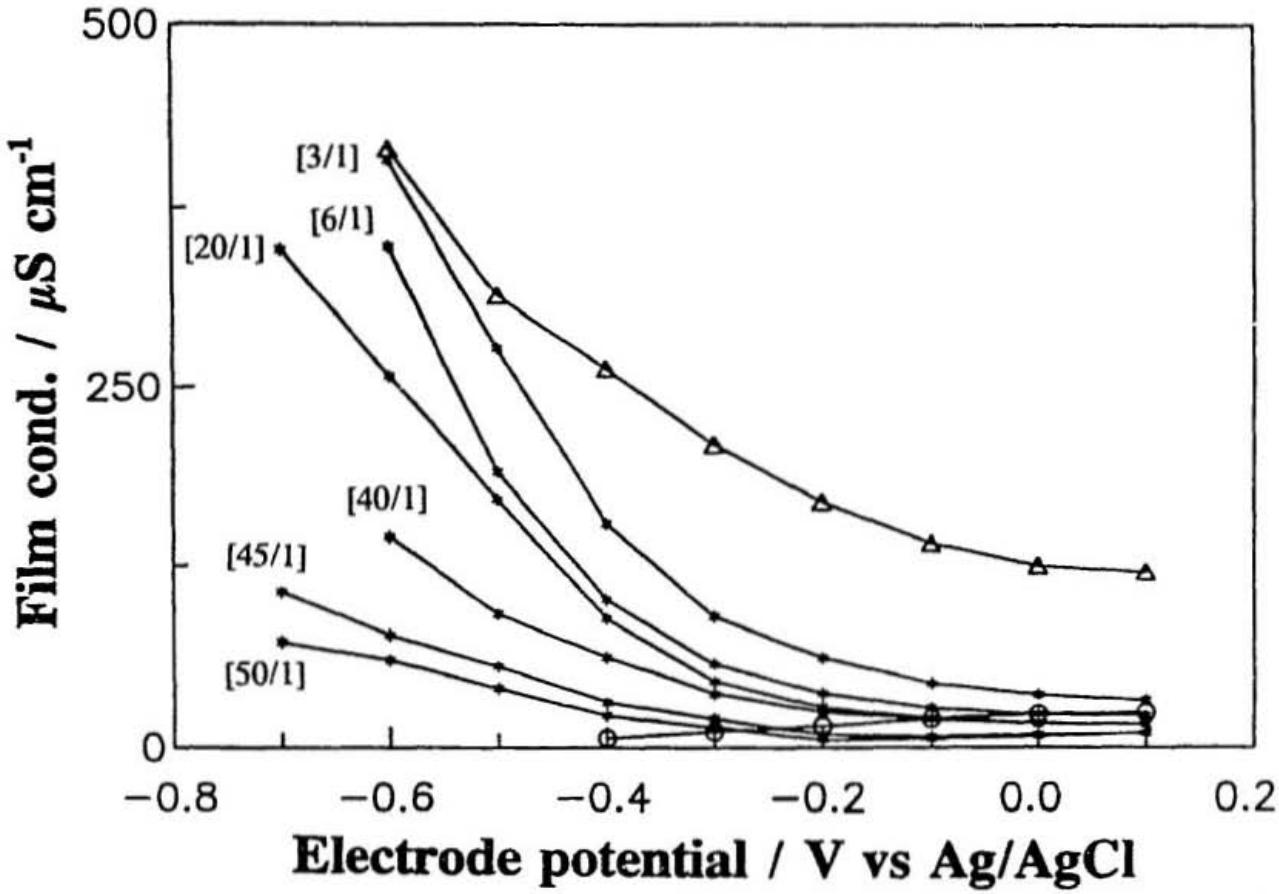

Figure 10.2.7 Plots of the apparent film ionic conductivity *vs.* electrode potential. Curves for PPY/ClO_4 and PPY/PSS films are marked by ○ and ▵ respectively, and curves for PPY/PSS+ClO_4^- are labelled.

listed in Table 10.2.1 are also plotted in Fig. 10.2.7 as a function of electrode potential. The ionic conductivities of the polymer films change continuously and smoothly with electrode potential as well as with the $ClO_4^-/-SO_3^-$ molar ratio in the freshly prepared polymer film.

Table 10.2.1 Apparent ionic conductivities of PPY/ClO_4^-+PSS films on Pt in 0.2 M $NaClO_4$ (aq) at various electrode potentials.

E/V	Apparent ionic conductivity / $\mu S\ cm^{-1}$							
	PPY/ ClO_4^-	[50/1][a]	[45/1][a]	[40/1][a]	[20/1][a]	[6/1][a]	[3/1][a]	PPY/ PSS
0.1	24.3	10.2	9.98	16.4	16.0	22.2	32.5	121
0.0	23.0	7.78	9.00	16.4	16.9	22.9	36.2	125
-0.1	19.9	6.23	7.84	19.5	20.4	27.1	44.1	141
-0.2	15.0	5.53	9.22	24.4	27.6	37.0	61.9	169
-0.3	11.1	14.1	20.1	36.9	45.2	57.5	90.6	208
-0.4	6.40	22.1	31.1	62.4	89.1	102	154	263
-0.5	[b]	40.4	55.7	92.0	170	189	277	314
-0.6	[b]	60.2	77.5	145	258	348	408	416
-0.7	[b]	72.6	107		346			

[a] $ClO_4^-/-SO_3^-$ molar ratio in the polymerization solution.

[b] High frequency data form a semicircle, which is superimposed on the Warburg-type line.

PPY/ClO_4^-+PSS films are potentially useful for the construction of an ion-

gate device, in which selective control of the passage of cations or anions across the polymer film is possible by varying the electrode potential. Burgmayer and Murray have shown that a polypyrrole membrane formed on a gold minigrid electrode can be used to selectively allow anions to pass through[3,4]. Feldheim and Elliott have shown that conducting polymer films can also be used as a "gate" for the separation of neutral solutes[5]. Now this study shows that oxidized PPY/ClO_4^- +PSS films are anion exchangers which allow the passage of electrolyte anions, while the reduced films are cation exchangers which let the electrolyte cations pass through. Similar polymer films that can be electrochemically switched between the anion and cation exchanger states are poly-pyrrole/N-methylpyrrole copolymer polymerized in sodium dodecylsulphonate electrolyte[6] and poly-N-methylpyrrole/N-sulfopropylpyrrole copolymer polymerized in KCl[7].

10.3 Simulation of Impedance Responses

The impedance responses of PPY/ClO_4^-+PSS films can be modelled with the electrical circuit shown in Fig. 10.3.1. The two parallel resistive rails, $R_{Ion,A}$ and $R_{Ion,B}$, model the movement of Na^+ and ClO_4^- ions across the polymer film thickness respectively. The distributed capacitances, $C_{F,A}$ and $C_{F,B}$, represent the

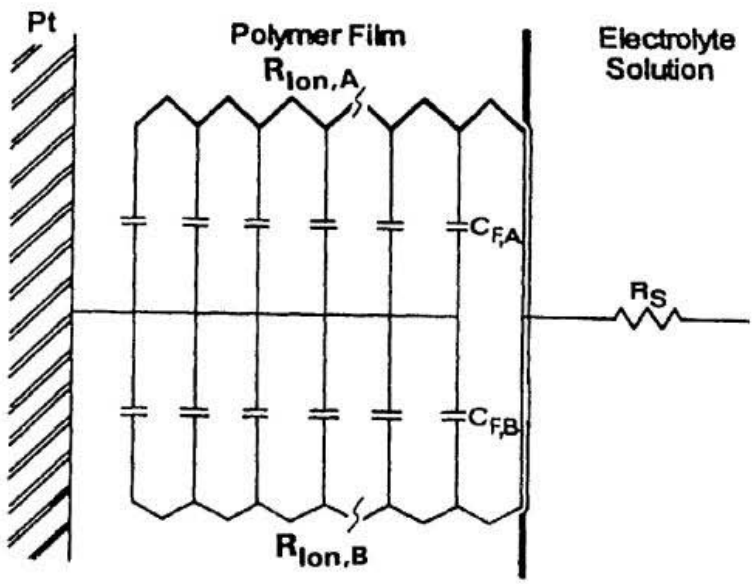

Figure 10.3.1 Electrical circuit used to simulate the experimental impedance response of a PPY/PSS+ClO_4^- film coated Pt electrode.

doping of the polymer with $-SO_3^-$ and ClO_4^- respectively. The impedance response of the model circuit which contains in total 2000 resistors and 2000 capacitors was calculated using the successive reduction method discussed in section 5.2. Fig. 10.3.2 shows the complex plane impedance plots of simulated impedance responses calculated from the model circuit with $C_{F,A} = C_{F,B}$ and different $R_{Ion,A}/R_{Ion,B}$ ratios. When $R_{Ion,A}$ equals $R_{Ion,B}$ (curve A), the curve has the shape for the classical transmission line (Fig. 4.2.3) calculated with $R_{ion} = R_{Ion,A}/2$ and $C_F = 2C_{F,A}$. With $R_{Ion,A}$ and $R_{Ion,B}$ unequal, a second steeper Warburg-type line appears at low frequency. However, the normalized length of the high frequency Warburg-type line remains unchanged. Thus despite the various shapes of the second Warburg-type line (which depends on the $R_{Ion,A}/R_{Ion,B}$ ratio), a film ionic resistance (called the apparent film ionic resistance, $R_{appr} = (R_{Ion,A} \times R_{Ion,B})/(R_A + R_{Ion,B})$) can be quite accurately obtained. The projected length of the high frequency Warburg-type line on the real axis equals one third of R_{appr} (Fig. 10.3.2). When one of the two ion transport processes dominates, R_{appr} approaches the (smaller) resistance of the dominant transport process. Fig. 10.3.3A shows complex plane capacitance plots for the simulated impedance data shown in Fig. 10.3.2. Adequate separation of the two charging processes occurs when $R_{Ion,A} > 10\ R_{Ion,B}$. The variation of the capacitance with the frequency of the potential perturbation is shown in

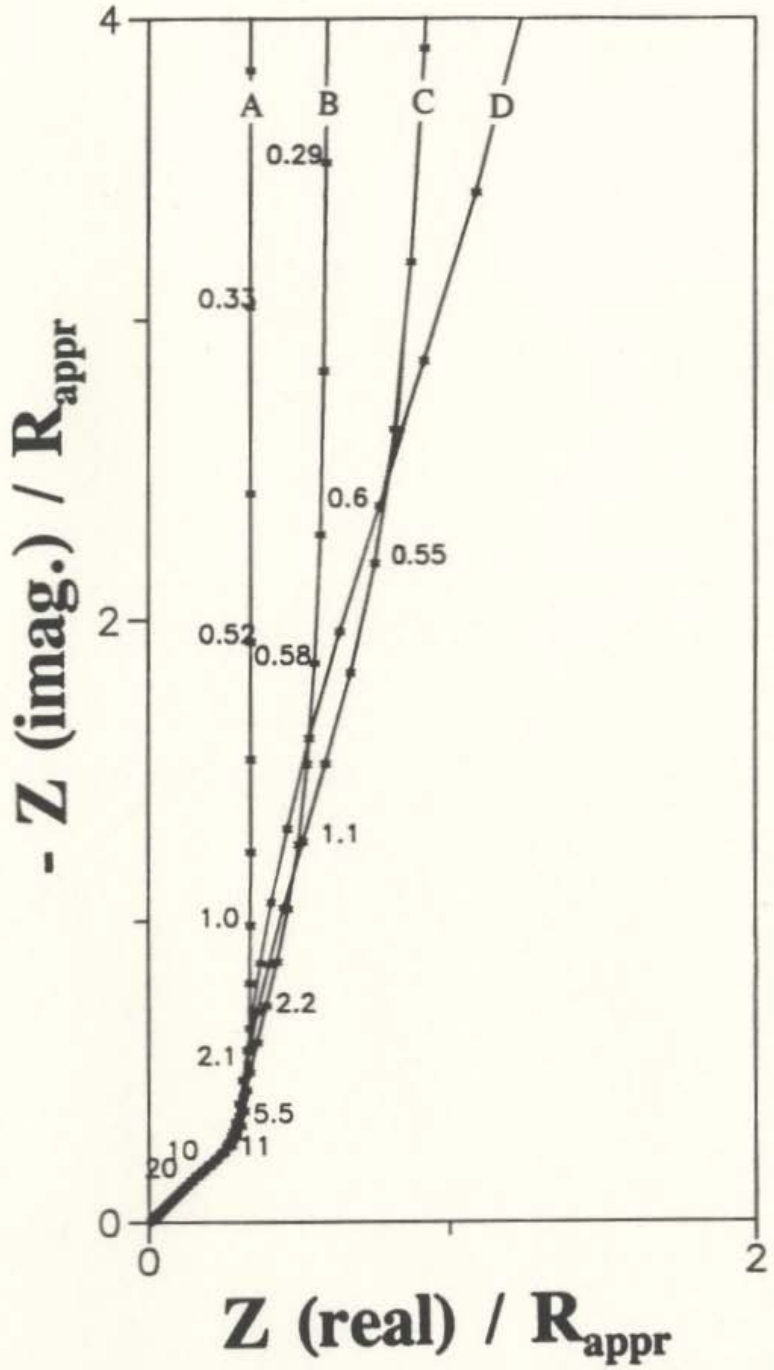

Figure 10.3.2 Simulated impedance responses presented as complex plane impedance plots. The simulation conditions were that $C_{F,A}$ equals $C_{F,B}$ for all curves, and $R_{Ion,A}/R_{Ion,B}$ equals 1 (A), 5 (B), 10 (C) and 20 (D). Normalized frequencies [$f_N = 2\pi f R_{appr}(C_{F,A}+C_{F,B})$] are marked for selected points.

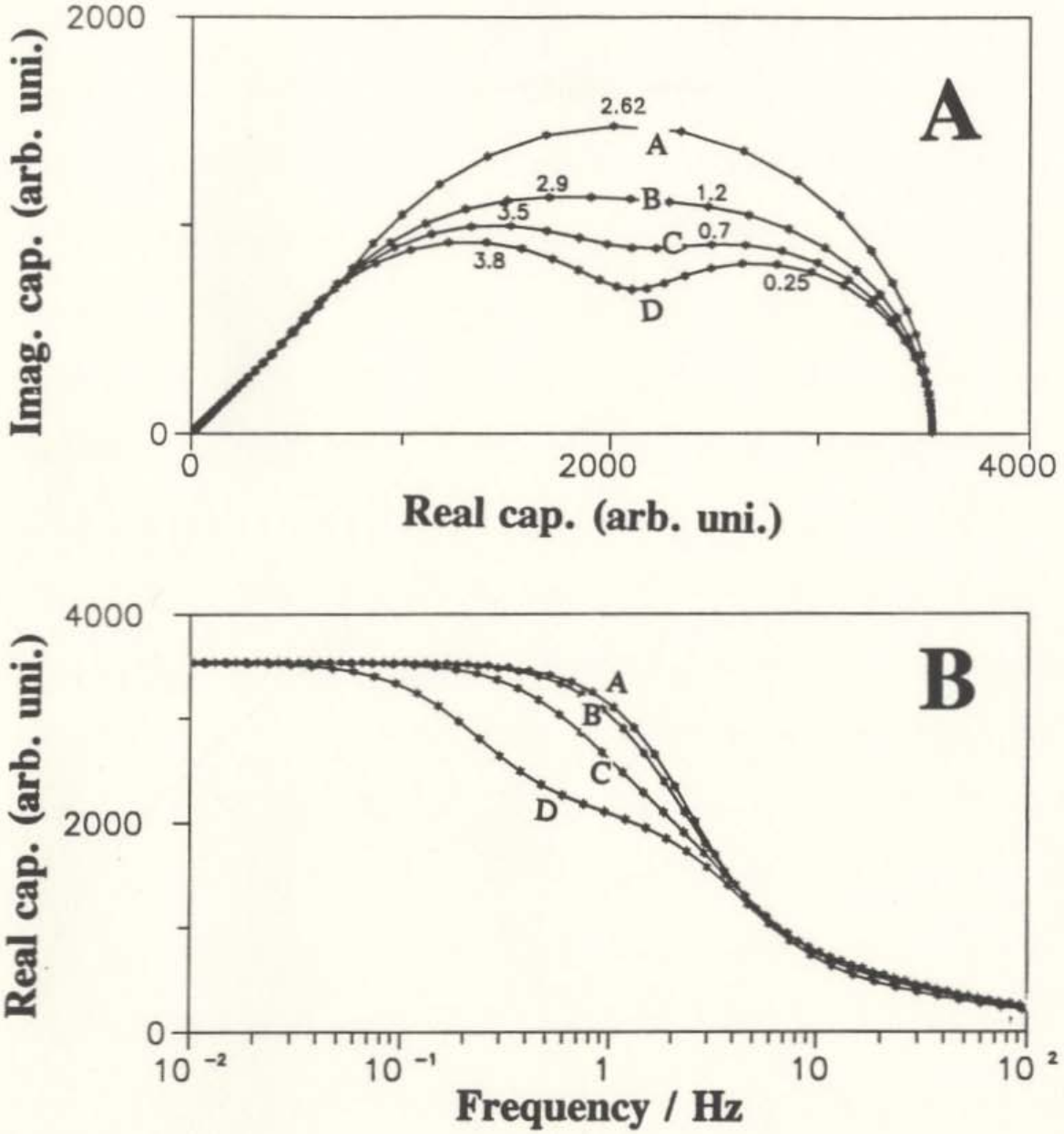

Figure 10.3.3 (A) Complex plane capacitance plots for the simulated impedance data shown in Fig.10.3.2. (B) Plots of the film capacitance as a function of the normalized frequency.

Fig .10.3.3B.

A polymer film may have multiple ion conduction paths across its thickness due to its porous structure. Each of the different ion conduction paths can be modelled with a transmission line in parallel with the others. Simulations of such model circuits show that as long as all the transmission lines are uniformly distributed across the polymer film thickness, the Warburg-type line at high frequency will be at 45° to the real impedance axis. The line at low frequency will deviate from the ideal vertical line with a slope depending on the relative values of the transmission line resistances. A polymer film which has multiple ion conduction paths can be regarded as non-uniform across the polymer surface. Simulated results in Section 5.2 show that the non-uniform distribution of the transmission line elements across the polymer film thickness causes the deviation of the high frequency Warburg-type line from the ideal 45° angle, but the low frequency line is still vertical.

Fig. 10.3.4 shows a comparison of complex plane impedance plots of experimental and simulated data. The parameters used in the simulation were estimated from the experimental data; R_{appl} from the complex plane impedance plot and $C_{F,A}$, $C_{F,B}$, and $R_{Ion,A}/R_{Ion,B}$ from the complex plane capacitance plot. The simulated impedance response closely matched the experimental one with no further optimization of the simulation parameters. The experimental data shows a

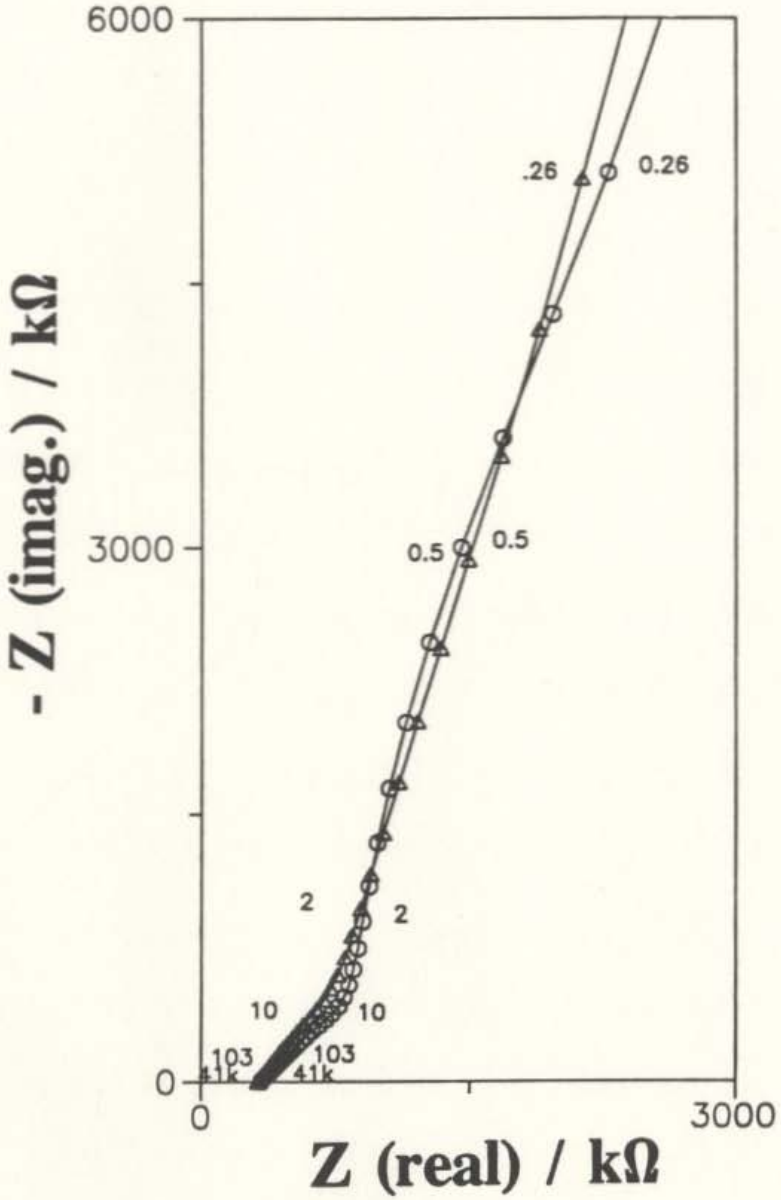

Figure 10.3.4 Complex plane impedance plots of the experimental (△) and simulated (○) data for the [45/1] film coated Pt electrode at -0.4 V *vs.* Ag/AgCl in 0.2 M $NaClO_4$(aq). The simulation parameters are $C_{F,A}$ = 16 and $C_{F,B}$ = 19 mF cm^{-2}, and $R_{Ion,A}$ = 1.8 and $R_{Ion,B}$ = 18 kΩ.

slight deviation of the high frequency Warburg-type line from 45°, indicating a non-uniformity across the polymer film thickness.

10.4 Cyclic Voltammetry

The above discussion of impedance measurements helps to understand the ion transport processes occurring during potential cycling. Cyclic voltammograms of the PPY/ClO_4^-+PSS films (Fig. 10.4.1) show two oxidation peaks, which separate from each other with increasing scan rate. The oxidation peak at lower potential (first oxidation peak) exhibits a smaller peak potential shift than the one at higher potential (second oxidation peak). As the ClO_4^-/PSS molar ratio in the freshly formed polymer is increased, the size of the first oxidation peak deceases while that of the second oxidation peak increases. These facts indicate that the first oxidation peak involves the self-doping process (expulsion of the electrolyte cations) while the second oxidation peak involves normal doping (insertion of electrolyte anions). Separation of these two processes occurs only when the polymer is subjected to a fast potential scan. When the polymer is reduced, the self-doped polymer reaches its highest ionic conductivity while the normally doped polymer has its lowest ionic conductivity. This difference in ionic conductivity

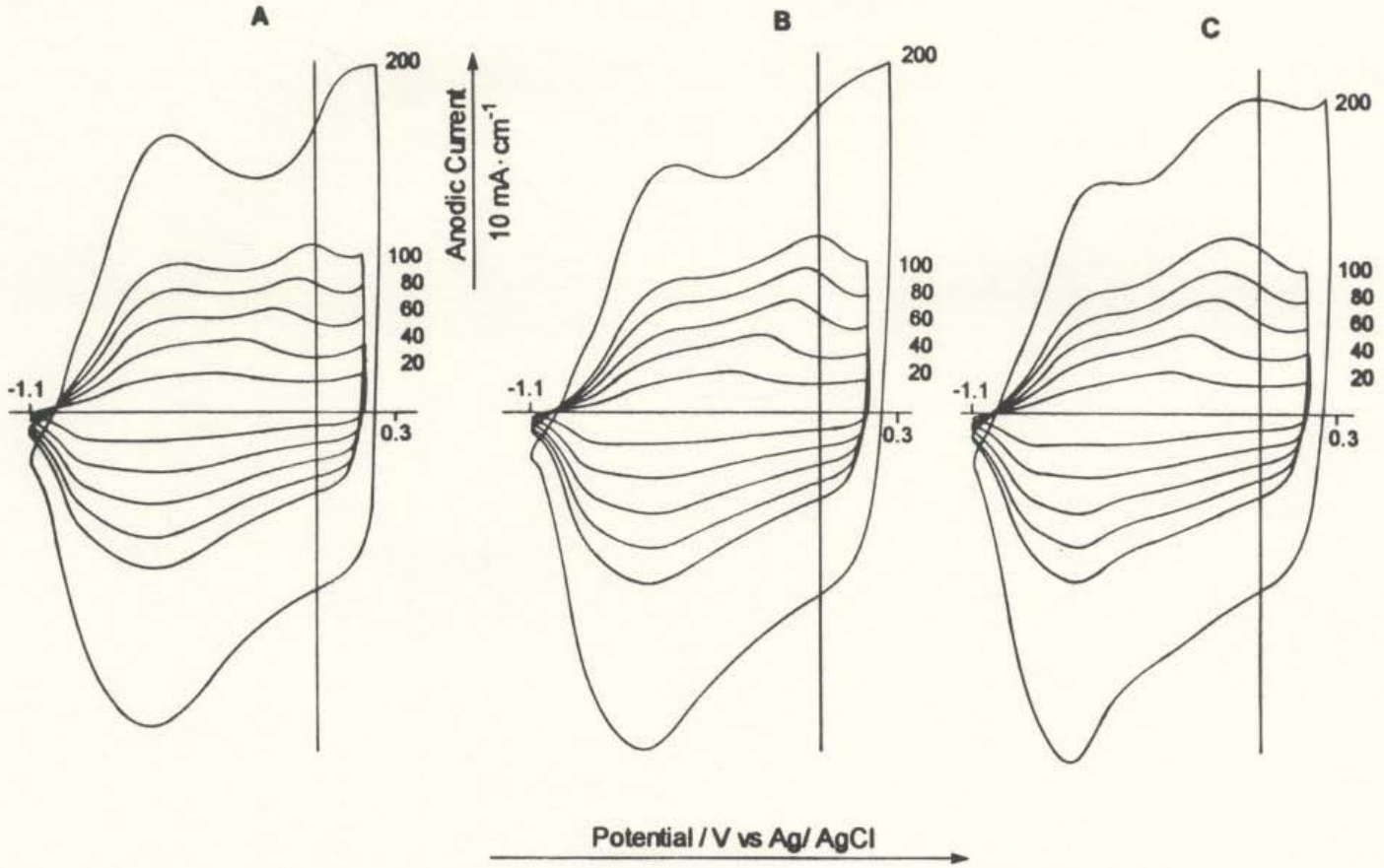

Figure 10.4.1 Cyclic voltammograms of [40/1] (A), [45/1] (B) and [50/1] (C) film coated Pt electrodes in 0.2 M $NaClO_4$(aq). Scan rates in mV s^{-1} are indicated.

makes it possible to separate the two charging processes with simple cyclic voltammetry. On the other hand, the difference in the ionic conductivity between the two differently doped polymer chains in the oxidized state is much smaller. Subsequently, no peak separation is observed during the cathodic potential scan. It is also observed that as the ClO_4^-/PSS molar ratio in the freshly formed polymer is increased the peak potential shift for the second anodic peak decreases. This is due to the increased ClO_4^- ions transport as its concentration in the polymer is increased.

10.5 Conclusions

Anodic oxidation of pyrrole in a solution containing both $NaClO_4$ and NaPSS forms polypyrrole which is doped partially with ClO_4^- and partially with PSS. The oxidized polypyrrole preferentially incorporates PSS over ClO_4^- during polymerization. The composition of a PPY/ClO_4^-+PSS film after equilibration in $KClO_4$ (aq) shows the gradual increase of K^+ ions and decrease of ClO_4^- ions as the electrode potential is decreased. The impedance of a PPY/ClO_4^-+PSS film coated Pt electrode in 0.2 M $NaClO_4$ (aq) shows simultaneously ion transport behaviours of PPY/ClO_4^- and PPY/PSS. As the electrode potential is decreased, the ionic conductivity of the nearly fully oxidized polymer deceases, while that of

the nearly fully reduced polymer increases. This is explained by the observation that the oxidized polymer film (ca. +0.1 V) contains ClO_4^- as the dominant mobile ionic species, and decreasing the electrode potential decreases the number of ClO_4^- ions in the polymer. The reduced polymer (*ca.* -0.7 V) film contains Na^+ as the dominant mobile ionic species, and decreasing the electrode potential increases the number of Na^+ ions in the polymer. At intermediate oxidation states (*ca.* -0.4 V), both mobile ionic species are present and contribute to ion conduction in polymer. Complex impedance plots as well as capacitance plots show the separation of the two charging processes corresponding to transport of two types of ions.

The observed impedance responses can be modelled with an electrical circuit containing two parallel transmission lines. When the two transmission lines have different resistances, a second steeper Warburg-type line appears at low frequency, corresponding to the slower charging process of the more resistive line. A polymer film with multiple ion transport paths across the film thickness is regarded as non-uniform across the film surface. The simulated impedance response of such a polymer film shows a deviation from the ideal vertical line at low frequency. Deviation from the ideal 45° angle at high frequency occurs only when the polymer film is non-uniform across its thickness.

Cyclic voltammograms of PPY/ClO_4^-+PSS films can be explained by the ion transport processes elucidated in the impedance study. The voltammograms

exhibit two oxidation peaks; the one at lower potential corresponding to insertion of Na^+ ions and the one at higher potential to expulsion of ClO_4^- ins. Separation of the two peaks is due to the two charging processes having different rates, which are limited by the transport rate of Na^+ and ClO_4^- ions respectively. Peak separation occurs only at high potential scan rates. Since the difference in the ionic conductivity between the two differently doped polymers is small in the oxidized state, no peak separation occurs during the cathodic potential scan. This result shows that the shape of a cyclic voltammogram of polypyrrole is sensitive to the dynamics of ion transport in the film.

References

(1) Ren, X.; Pickup, P.G. *J. Phys. Chem.* 1993,*97*,5356.

(2) Diaz, A.F.; Castillo, J.I.; Logan, J.A.; Lee, W.-Y. *J. Electroanal. Chem.* 1981,*129*,115.

(3) Burgmayer, P.; Murray, R.W. *J. Am. Chem. Soc.* 1982,*104*,6139.

(4) Burgmayer, P.; Murray, R.W. *J. Phys. Chem.* 1984,*88*,2515.

(5) Feldheim, D.L.; Elliott, C.M. *Journal of Membrane Science* 1992,*70*,9.

(6) Zhong, C.; Doblhofer, K. *Electrochim. Acta* 1990,*35*,1971.

(7) Zhong, C.; Doblhofer, K. *Synth. Met.* 1991,*43*,3013.

Chapter 11

Summary

The purpose of this research was to achieve better understanding of the charge transport in polypyrrole-based conducting polymer films by using impedance spectroscopy (IS) as the major instrument. After studying the factors that affect electrochemical polymerization, polymer films of high quality were obtained by using the constant current polymerization method under optimized conditions. The impedance responses of these polymer films were simple and easy to understand. Various theoretical models have been tested by comparing the derived transport parameters from the polymer's impedances with those obtained from other independent methods.

For conducting films of polypyrrole (PPY) and poly-(3-methyl-pyrrole-4-carboxylic acid) (poly-MPCA), the porous electrode model[1] is adequate to derive the ionic conductivity of the polymer films. However, even for these simple systems, the experimental impedances may deviate from the model's ideal response. Two types of deviations were observed in the study of conducting polymers, namely, the high frequency deviation from the ideal 45° Warburg-type line and the low frequency deviation from the ideal vertical line in the complex impedance plane. A thick poly-MPCA film (> 0.6 μm) was shown by the

scanning electron microscope to have a dendritic structure over a dense bottom layer. Such film structure non-uniformity is responsible for the high frequency deviation observed for this polymer. In contrast, the impedance response of a polypyrrole film doped with perchlorate (PPY/ClO_4^-) has the nearly ideal high frequency line because of its structural uniformity. The high frequency deviation has also been simulated by varying the ionic resistance and capacitance distribution across the polymer film thickness in the classical transmission line electrical circuit.

The origin of the low frequency deviation has been studied by examining the impedance responses of polypyrrole films polymerized in perchlorate and poly(styrene sulphonate) solutions (PPY/ClO_4^-+PSS). The polymer film in oxidized form is an anion-exchanger and the electrolyte anions are the dominant ion transport carriers, while the polymer in reduced form is a cation-exchanger and the electrolyte cations are thus the dominant carriers. The impedance responses of both fully oxidized and fully reduced polymer films are close to the ideal vertical line in the low frequency region. However, for a PPY/ClO_4^-+PSS film in an intermediate redox state, both ion transport mechanism operate. Correspondingly, the film impedance response exhibits an obvious deviation in the low frequency region, which can thus be attributed to the multiple ion conduction paths in the film. Such multiple ion conduction paths are thought to exist when the polymer

film has variable thickness, porous structure, or multiple ionic charge carriers. These factors on the impedance responses can be simulated with a transmission line circuit containing multiple ionic resistance rails in parallel combination. Both types of deviations are attributed to the non-uniformity of the polymer films.

Experimental conditions that affect the polymer film's ionic conductivity have been studied on PPY and poly-MPCA. The ionic conductivity of these polymer films was found to change with the identity of the mobile ionic species and its population in the films, the hydration level of the polymer film, and the conductivity of bathing electrolyte solution. The mobility of the mobile ionic species in the polymer film depends on their sizes and their interactions with the oppositely charged fixed ion-exchanging sites in the films. Using the film ionic conductivity as a probe, it was found that both PPY and poly-MPCA films have a porous structure. The changes of the polymer film's ionic conductivity with the experimental conditions can be best explained by the combined ionic conductivity changes in the polymer phase and in the pore solution phase. Ionic conduction in the polymer phase occurs mainly through the movement of mobile counterions *via* an ion-exchanging process, while in the pore solution phase migration of both electrolyte cations and anions contributes to conduction.

The impedance responses of polypyrrole/poly(styrene sulphonate) (PPY/PSS) and poly-[1-methyl-3-(pyrrol-1-ylmethyl)pyridinium] (poly-MPMP)

have been used to thoroughly test Albery's redox polymer model[2], which can also be considered as a logical extension of the classical porous electrode model by including the electronic resistance of the electrode[3]. Changing the polymer film's oxidation state from a highly oxidized state to a nearly neutral state by varying the electrode potential produces three different types of impedance responses, corresponding to three situations where $\sigma_{Ion} < \sigma_E$, $\sigma_{Ion} \approx \sigma_E$ and $\sigma_{Ion} > \sigma_E$. The experimental results generally support Albery's model, where the mobilities of charge carriers in the polymer phase and in the pore solution phase are each modelled with a uniformly distributed resistance rail.

The location of the initial redox reaction layer in the polymer film induced by a potential perturbation has been found to be determined by the relative magnitudes of the polymer film's electronic and ionic conductivities, as theoretically predicted. An independent investigation of PPY/ClO_4^- and PPY/PSS bilayers using IS has also proved that for a conducting PPY film the initial redox reaction layer is located at the polymer/solution interface[4].

When either one of the electronic or ionic resistance is much larger than the other, the complex plane impedance plots exhibit a well defined 45° Warburg-type region. However, as the two resistances approach each other, the length of the Warburg-type region decreases and the polymer reaches the finite thickness-limited charging/discharging region at a higher frequency than predicted by Albery's

model. No real solutions were found for eqs. [4.2.9] and [4.2.10] when the two resistances were very similar. Such abnormal behaviour suggests that electron transport in the polymer phase is coupled with dopant ion transport in the solution phase[5]. This coupling effect deserves more detailed investigation in the future.

In some cases, a charge transfer process at either the polymer/solution interface or the Pt electrode/polymer interface was involved in the charge transport study of conducting polymers. IS has been proved to be a powerful tool in decoupling the interfacial charge transfer process from the bulk charge transport process. Whereas for techniques such as chronoamperometry or chronopotentiometry, the two processes are not well resolved. Consequently, the involvement of such charge transfer process is not easily recognized when using these techniques. Consequently, extracting charge transport parameters from these experimental data using a simple model may give erroneous results.

References

(1) DeLevie, R.; in *Advances in Electrochemistry and Electrochemical Engineering*, Delahay, P.; Tobias, C.W. (Eds.), Vol.6, John-wiley & Sons: New York,1967;p329.

(2) Albery, W.J.; Elliott, C.M.; Mount, A.R. *J. Electroanal. Chem.* 1990,*288*,15.

(3) Fletcher, S. *J. Chem. Soc., Faraday. Trans.* 1993,*89*,311.

(4) Ren, X.; Pickup, P.G. *J. Phys. Chem.* 1993,*97*,3941.

(5) Ren, X.; Pickup, P.G. *J. Chem. Soc., Faraday. Trans.* 1993,*89*,321.